The role of cerebellar GABA in visuomotor adaptation



Caroline R. Nettekoven

Jesus College

University of Oxford

A thesis submitted for the degree of

Doctor of Philosophy

Trinity 2020

Abstract

In daily life we must constantly adapt our movements to changes in the environment or changes in our body. Adaptation is a fundamental property of the central nervous system and involves plastic changes across a network of brain regions, in particular in the cerebellum. These changes likely involve the major inhibitory neurotransmitter GABA. How cerebellar GABA changes during adaptation and how these changes are linked to behaviour is currently not well understood. By combining brain imaging (Magnetic Resonance Spectroscopy and Magnetic Resonance Imaging) and brain stimulation (transcranial direct current stimulation; tDCS) with computational modelling of behaviour, this thesis investigates the relationship between GABA, plasticity and motor adaptation.

First, the effects of stimulating the cerebellum with anodal tDCS were investigated. We found no effect of tDCS on adaptation, but an effect of session. We then studied the relationship between M1 GABA concentration and adaptation. We found that GABA concentration at baseline measured from left M1 hand area predicted retention of an adapted movement of the right hand. Next we investigated changes in functional connectivity elicited by adaptation. After performing an adaptation task, cerebellar resting-state functional connectivity was increased. Further, the change in a cerebellar network correlated with adaptation performance. Finally, we explored changes in cerebellar GABA during adaptation. During adaptation, cerebellar GABA decreased in the right compared to the left cerebellar hemisphere, controlling for GABA changes during movement execution.

This work provides first evidence that GABA decreases during adaptation in the right compared to the left cerebellar hemisphere. It strengthens the theory of cerebellar involvement in adaptation and suggests that cerebellar GABA plays an important role during adaptation. It also highlights the importance of M1 GABA in retaining the adaptive movement. Taken together, these results demonstrate a potential mechanism by which adaptation may be achieved in the cerebellum. In order to develop interventions that successfully and reliably enhance adaptation, it is crucial to understand the factors that influence these changes in the cerebellum and across the motor network.

This thesis is 48, 538 words.

Acknowledgements

My thesis would not have been possible without the invaluable help of my mentors, friends and family and I would like to thank everyone who has supported me on this journey. The list of people that supported me along the way is endless, but I would like to name a few to whom I owe special thanks.

To Charlie, my primary supervisor, for so many things - they alone could fill another thesis. You did not only teach me how to do science, you shaped me into a scientist. Thank you for letting me trail off into analysis land and guiding me back at the right time. Thank you for creating a lab culture in which I could thrive. And thank you for being a never-tiring source of inspiration, creativity and outstanding support. I could not have asked for a better supervisor.

To Ned, my second supervisor, for teaching me all things cerebellar and always extending a helping hand when I needed it. I really valued our discussions and benefited a lot from them. You showed me new perspectives and pushed me further.

Thank you to the past and present members of the Physiological Neuroimaging Group and the Plasticity Group for constant support. To Sinead Brady, who collected the data presented in chapter 4 and 5 and to Muriel Panouilleres, who helped me get to grips with the behavioural data. To my two fantastic Final Honours School students, Rebecca Jurdon and Leah Mitchell, who helped collect the data in chapter 3 and in chapter 6, respectively, as part of their undergraduate thesis projects. Rebecca, thank you for spending countless hours entertaining our participants with me while we layered gel into their hair. You made all my dreams of supervising and none of my nightmares come true and just as I inspired a love for statistics in you, you inspired a love for supervising in me. Leah, thank you for getting me through the weeks of early mornings and late evenings in the scanner control room. We may not be the same chronotype, but together we work like clockwork. Thanks to Will for helping me analyse the Spectroscopy data in chapter 4 and 6. You told me everything I ever wanted to know about Spectroscopy analysis but was afraid to ask.

To my incredible labmates and colleagues for sharing their time and expertise with me and providing feedback, advice and a receptive audience for my science memes. Thank you to Ioana for always being there when I needed anything from a rubber duck for debugging to a hug. To Alberto for picking me back up when I was knocked down and believing in me, for being a true friend and a rigorous sparring partner for my ideas. Thank you to Catha for asking the hard questions, to Emily for helping me bring order into the chaos and to Jake for answering all my questions and questioning all my answers. To Adam, Ainslie, Evan, Marleen, Andrew, Pierre, PG, Gershon, Tulika, Mel, Ximena, James, Ding-lan, Tom, Zeena, Marilien and all the FMRIB and WIN people for saving me at one point or another. You all kept me sane.

To my friends who made Oxford my home. To Tanaya, for endless love and support and championing my success. To Priyav, Santiago and Peter for the days and nights at Santiago's kitchen. To Charles, my College advisor, who provided me with wise words when I needed it the most. To Bruno, Maria, Richard and and everyone else at Jesus College who made me feel so welcome.
Thank you to my Exeter College family for accepting me as their own. To Sandy, Lindsey, Ari and all the other Exonians who put up with me working nights in the MCR. And of course to Maxwell and Hank for the good times.

Thank you to Mariele for always being there for me and knowing me better than anyone. I do not think anyone deserves a friend as good as you.
Thank you to Maja, Melli and Anna for making me feel as though I never left when I come back.

Finally, to my family. To my brother for being a role model in true grit. To my Mom for teaching me what is really important. And to my Dad for everything. I could not have done this without you.

Contents

Abstract i

Acknowedlegments ii

Contents iii

List of Figures x

List of Tables xii

Acronyms xiii

Chapter 1 Introduction 1

1.1 Adaptation . . . 1

1.1.1 Adaptation paradigms . . . 2

1.1.2 Internal models . . . 3

1.1.3 Features and terminology of adaptation . . . 4

1.1.4 Explicit and implicit contributions to adaptation . . . 6

1.1.5 State-space models of adaptation . . . 7

1.2 Adaptation and the brain . . . 8

1.2.1 Cerebellum . . . 9

1.2.1.1 Cerebellar connectivity . . . 11

1.2.1.2 Plasticity in the cerebellum . . . 12

1.2.2 Primary motor cortex . . . 12

1.2.2.1 Plasticity in the primary motor cortex . . . 14

1.2.2.2 Primary motor cortex and adaptation . . . 14

1.2.3 Premotor cortex and supplementary motor areas . . . 15

1.2.4 Posterior parietal cortex . . . 16

1.2.5 Basal ganglia . . . 16

1.3 GABA and motor learning . . . 17

1.4 Aims of this thesis . . . 18

Chapter 2 Methods **20**

2.1 Measuring brain function . . . 20

2.1.1 Principles of magnetic resonance imaging . . . 20

2.1.1.1 T1 and T2 . . . 21

2.1.1.2 Localization . . . 22

2.1.1.3 Pulse sequence parameters . . . 23

2.1.1.4 Image Contrast . . . 23

2.1.1.5 T1-weighted images . . . 23

2.1.1.6 T2 and T2*-weighted images . . . 23

2.1.2 Functional MRI . . . 24

2.1.2.1 BOLD Contrast . . . 24

2.1.2.2 Imaging the cerebellum . . . 25

2.1.3 Resting-state fMRI . . . 26

2.1.3.1 Preprocessing . . . 28

2.1.3.2 Group-level analysis . . . 31

2.2 Measuring neurochemistry . . . 32

2.2.1 Principles of magnetic resonance spectroscopy . . . 32

2.2.1.1 Localization . . . 33

2.2.1.2 J-coupling and Spectral editing . . . 34

2.2.1.3 Water Suppression . . . 34

2.2.1.4 Magnetic Resonance Spectroscopic Imaging . . . 35

2.2.2 Quantifying metabolites . . . 36

2.2.2.1 Quality Control . . . 37

2.2.3 Studying GABA with MRS . . . 38

2.2.3.1 Interpreting MRS-measured GABA concentrations . . . 39

2.2.4 Studying cerebellar neurochemistry . . . 40

2.3 Modulating brain function using NIBS . . . 40

2.3.1 Principles of tDCS . . . 41

2.3.2 Cerebellar tDCS . . . 42

2.4 Visuomotor adaptation task . . . 43

2.4.1 Features of the adaptation task . . . 44

2.4.2 Tailoring the task to maximize adaptation . . . 45

2.5 Quantifying adaptation . . . 49

2.5.1 Single-state state-space model . . . 49

2.5.2 Dual-state state-space model . . . 50

2.5.3 Generalization . . . 52
2.5.4 State-space models used in this thesis . . . 53

Chapter 3 The effects of cerebellar tDCS on visuomotor adaptation 54

3.1 Introduction . . . 55
3.2 Methods . . . 57
3.2.1 Participants . . . 57
3.2.2 Experimental Protocol . . . 58
3.2.3 tDCS . . . 60
3.2.4 Data Analysis . . . 60
3.2.4.1 Preprocessing . . . 60
3.2.4.2 Target Bias . . . 60
3.2.4.3 Modelling-free Analysis . . . 61
3.2.4.4 Modelling-based Analysis . . . 61
3.2.4.5 Statistical Analysis . . . 63
3.3 Results . . . 64
3.3.1 Baseline values are comparable across sessions . . . 64
3.3.2 Participants adapted to the rotation . . . 65
3.3.3 Effect of session: Improved adaptation in second session . . . 66
3.3.3.1 No difference in retention between first and second session . . . 67
3.3.4 Stimulation had no effect on adaptation . . . 68
3.3.4.1 Stimulation had no effect on retention . . . 69
3.3.4.2 Stimulation had no effect on adaptation in the first session . . . 69
3.3.5 Exploratory Analysis . . . 70
3.3.5.1 No effect of stimulation for perturbation-unaware participants when controlling for baseline. . . . 70
3.3.5.2 No effect of stimulation for specific targets when controlling for baseline. . . . 70
3.4 Discussion . . . 71
3.4.1 Savings may have obscured an effect of stimulation. . . . 72
3.4.2 Physiological effects of cerebellar tDCS . . . 73
3.4.3 Conclusions . . . 74

Chapter 4 M1 GABA predicts retention, but not adaptation: A 7T MRS study 76

4.1 Introduction . . . 77

4.2 Methods . . . 79
4.2.1 Participants . . . 79
4.2.2 Experimental Protocol . . . 80
4.2.3 Magnetic Resonance Acquisition . . . 81
4.2.4 Behavioural Data Analysis . . . 82
4.2.4.1 Modelling-free Analysis . . . 82
4.2.4.2 Modelling-based Analysis . . . 83
4.2.5 Magnetic Resonance Spectroscopy Analysis . . . 85
4.2.5.1 Metabolite Baseline index . . . 86
4.2.5.2 GABA Change index . . . 86
4.2.6 Statistical Analysis . . . 87
4.3 Results . . . 88
4.3.1 Behaviour . . . 89
4.3.1.1 Participants adapted for the majority of the task. . . . 90
4.3.1.2 Adaptation and retention do not correlate. . . . 90
4.3.1.3 Retention related to model parameter B in washout phase. . . . 90
4.3.2 Adaptation does not significantly affect GABA concentration in M1 . . . 91
4.3.3 M1 GABA relates to retention, but not adaptation . . . 92
4.3.3.1 GABA Baseline . . . 92
4.3.3.2 GABA change . . . 93
4.3.3.3 GABA at baseline predicts retention. . . . 93
4.3.4 M1 Glutamate does not relate to retention. . . . 94
4.4 Discussion . . . 94
4.4.1 No M1 GABA modulation in response to adaptation . . . 95
4.4.2 M1 GABA at baseline predicts retention . . . 95
4.4.3 M1 GABA change correlates with retention . . . 96
4.4.4 Limitations . . . 96
4.4.5 Conclusions . . . 97

Chapter 5 Adaptation modulates resting-state functional connectivity in the cerebellum 98

5.1 Introduction . . . 99
5.2 Methods . . . 101
5.2.1 Participants . . . 101
5.2.2 Magnetic Resonance Acquisition . . . 103
5.2.3 Magnetic Resonance Imaging Analysis . . . 103

5.2.3.1 Preprocessing . . . 103
5.2.3.2 Deriving Group Networks . . . 104
5.2.4 Statistical Analysis . . . 104
5.2.4.1 Behaviour . . . 104
5.2.4.2 Network Analysis (Dual Regression). . . . 106
5.2.4.3 Connectivity Analysis (Connectivity between ROIs). . . . 107
5.3 Results . . . 108
5.3.1 Adaptation affects resting-state network. . . . 108
5.3.1.1 Sensorimotor network . . . 109
5.3.1.2 Cerebellar network . . . 109
5.3.2 Adaptation performance correlates with change in network. . . . 110
5.3.2.1 Sensorimotor network . . . 110
5.3.2.2 Cerebellar network . . . 111
5.3.3 Adaptation does not affect connectivity between ROIs. . . . 112
5.3.4 Retention correlates with connectivity change. . . . 113
5.3.5 Connectivity change correlates with baseline GABA . . . 114
5.3.6 GABA does not correlate with connectivity in MRS voxel . . . 115
5.4 Discussion . . . 115
5.4.1 Adaptation affects network connectivity . . . 116
5.4.2 Retention relates to connectivity change . . . 117
5.4.3 Limitations . . . 118
5.4.4 Conclusions . . . 119

Chapter 6 Investigating cerebellar GABA during adaptation using 3T MRSI 120

6.1 Introduction . . . 122
6.2 Methods . . . 123
6.2.1 Participants . . . 123
6.2.2 Experimental Protocol . . . 123
6.2.3 Magnetic Resonance Imaging Acquisition . . . 125
6.2.3.1 Resting-state fMRI. . . . 125
6.2.3.2 MRSI. . . . 126
6.2.4 Behavioural Analysis . . . 126
6.2.4.1 Modelling-free Analysis . . . 126
6.2.4.2 Modelling-based Analysis . . . 127
6.2.5 Magnetic Resonance Imaging Analysis . . . 128

6.2.5.1 Preprocessing . . . 128
6.2.5.2 Deriving group networks . . . 128
6.2.5.3 Quantifying network strength . . . 129
6.2.6 Magnetic Resonance Spectroscopic Imaging Analysis . . . 129
6.2.6.1 Quality control . . . 129
6.2.6.2 MRSI alignment to standard space . . . 129
6.2.6.3 ROI Analysis . . . 129
6.2.6.4 Normalisation . . . 130
6.2.7 Relating adaptation performance to GABA measurements . . . 130
6.2.8 Statistical Analysis . . . 130
6.3 Results . . . 131
6.3.1 Control behaviour . . . 131
6.3.1.1 Error decreases during control condition . . . 131
6.3.1.2 Error decrease in the control condition was driven by a reduction in target bias . . . 132
6.3.1.3 Target bias is similar across sessions . . . 133
6.3.2 Adaptation behaviour. . . . 133
6.3.2.1 Participants adapted to the rotation. . . . 133
6.3.2.2 Participants retained the adapted movement. . . . 134
6.3.2.3 Participants retained the adapted movement outside the scanner . 134
6.3.2.4 Early adaptation correlates with retention, but late adaptation does not. . . . 135
6.3.3 MRSI . . . 136
6.3.3.1 GABA concentration at baseline in adapt and control session is not significantly different . . . 136
6.3.3.2 GABA does not scale with number of voxels included in ROI . . . 137
6.3.3.3 GABA during control task . . . 137
6.3.3.4 Normalised GABA reveals a significant GABA change during adaptation in right compared to left hemisphere . . . 138
6.3.3.5 GABA change does not correlate with adaptation. . . . 139
6.3.3.6 Changes in [GABA] are neurochemically specific. . . . 140
6.3.4 Resting-state Connectivity . . . 141
6.3.4.1 Relationship between cerebellar GABA and cerebellar connectivity 141
6.3.4.2 Relationship between adaptation and cerebellar connectivity . . . 143
6.3.5 Discussion . . . 144

6.3.6 [GABA] decreases ipsilaterally during adaptation. 145
6.3.7 [GABA] increases contralaterally during adaptation. 147
6.3.8 Adaptation does not modulate cerebellar network connectivity. 148
6.3.9 [GABA] relates to cerebellar network connectivity. 148
6.3.10 Limitations 149
6.3.11 Conclusions 150

Chapter 7 General Discussion **151**

7.1 Summary 151
7.2 General limitations 154
7.2.1 Observational nature of experiments 154
7.2.2 Generalisability of findings 154
7.3 Future research 155
7.3.1 Driving ipsilateral GABA decrease with tDCS to facilitate adaptation . . . 155
7.3.2 Assessing the effect of tDCS-induced GABA changes on cerebellar connectivity 155
7.3.3 Investigating the changes in cerebellar GABA during force-field and prism adaptation 156

References **157**

List of Figures

1.1 Visuomotor rotation task. 2
1.2 Savings and aftereffect 5
1.3 Purkinje cell 9

2.1 Schematic of a pulsed MR experiment. 22
2.2 Structure of a GABA molecule. 34
2.3 Example spectrum and LCModel fit from a single MRS voxel. 37
2.4 Trial Sequences. 44
2.5 Design of a single trial. 44
2.6 Experimental setup. 45
2.7 Single-state state-space model 49

3.1 Experimental Setup. 58
3.2 Task Protocol. 59
3.3 Trial Types. 59
3.4 Target Bias 61
3.5 Single-state state-space model. 62
3.6 Behavioural data 65
3.7 Modelling-based and modelling-free adaptation performance measures 66
3.8 Modelled adaptation in session 1 compared to session 2 66
3.9 Modelled adaptation for real compared to sham stimulation in first session. 68
3.10 Modelled adaptation in first session real compared to first session sham 69
3.11 Individual model fits for adaptation to the 90 degree target. 71

4.1 Experimental Protocol 80
4.2 Trial Types 81
4.3 M1 MRS Voxel Placement 81
4.4 Single-state state-space model fit to the washout data. 83
4.5 M1 Example Spectrum 85
4.6 Behaviour 89

4.7 Adaptation and retention do not correlate 90
4.8 Retention index and State-Space Model parameter B modelled on washout data . . 91
4.9 Group mean GABA concentrations normalised to baseline 91
4.10 GABA at baseline correlates with retention, but not adaptation 92

5.1 Experimental Protocol 102
5.2 Rotation Sequence 102
5.3 Trial Types 102
5.4 Networks of interest 106
5.5 Default Mode Network 107
5.6 Significant cluster of increased connectivity after adaptation 109
5.7 Connectivity change and Behaviour 111
5.8 Modelling-based results 112
5.9 Connectivity between left M1 and cerebellar ROIs over time 113
5.10 Connectivity change and Behaviour 114
5.11 Connectivity change and GABA at baseline 115

6.1 Experimental Protocol. 124
6.2 Task 125
6.3 MRSI Acquisition and Task Phases 126
6.4 Control Behaviour. 131
6.5 Adaptation Behaviour 133
6.6 Early adaptation correlates with retention while late adaptation does not 135
6.7 MRSI Volume Placement 136
6.8 Stability of baseline GABA across sessions 136
6.9 Hemispheric ROIs. 137
6.10 Cerebellar GABA concentration during task performance 138
6.11 Adaptation GABA normalised to control GABA. 139
6.12 Absolute GABA during late phase correlates with overall adaptation 140
6.13 Glutamate concentration during task performance 141
6.14 Adaptation Glutamate normalised to control Glutamate 141
6.15 Cerebellar network 142
6.16 Cerebellar network connectivity correlates with baseline GABA 142
6.17 Default Mode Network 143
6.18 Adaptation does not correlate with change in connectivity 144

List of Tables

3.1 Sample Characteristics 58
3.2 Summary of Adverse Sensations 64
3.3 Blinding Success 65
3.4 Task Performance in first and second session across the whole task 67
3.5 Adaptation Performance in sham and real session during the stimulation period . . 68

4.1 Sample Characteristics 88
4.2 Error at begin and end of each block of adaptation task 89

5.1 Sample Characteristics 108
5.2 Cluster Information 110
5.3 Cluster Location 110

6.1 Target Bias in control condition 132

Acronyms

AFNI Analysis of Functional NeuroImages

ANOVA Analysis of variance

AI Adaptation Index

ANOVA Analysis of Variance

ASD Autism spectrum disorder

ADHD Attention deficit hyperactivity disorder

BBR Boundary-Based Registration

BOLD Blood Oxygen Dependent Level

CBI cerebellar brain inhibition

CHESS CHEmical Shift-Selective

Cho Choline

Cr Creatine

CI Confidence Interval

CRLB Cramér-Rao Lower Bound

CRT Concentric ring trajectory

CSF Cerebrospinal Fluid

CT Computer Tomography

DMN Default Mode Network

DW Density weighted

EEG Electroencephalogram

EMG Electromyogram

EPI Echo Planar Imaging

FID Free induction decay

fMRI functional Magnetic Resonance Imaging

FMRIB Oxford Centre for Functional MRI of the Brain

FOV Field of View

FSL FMRIB Software Library

FWHM Full Width at Half Maximum

GABA γ-aminobutyric acid

[GABA]γ-aminobutyric acid concentration

Gln Glutamine

Glu Glutamate

Glx Composite measure of glutamate and glutamine

GM Grey Matter

GRAPPA Generalized Autocalibrating Partial Parallel Acquisition

H Hydrogen

HLSVD Hankel-Lanczos singular value decomposition

HRF Haemodynamic response function

ICA Independent Components Analysis

ICC intraclass-correlation coefficient

IPS Intraparietal sulcus

LASER Localised by Adiabatic Selective Refocusing

LME Linear mixed effects model

LTD Long-term depression

LTP Long-term potentiation

M1 primary motor cortex

MEGA Mescher-Garwood

MEP Motor Evoked Potential

MPRAGE Magnetization-Prepared Rapid Gradient-Echo

MR Magnetic Resonance

MRI Magnetic Resonance Imaging

MRS Magnetic Resonance Spectroscopy

MRSI Magnetic Resonance Spectroscopy Imaging

ms milliseconds

NAA N-acetyl aspartate

NIBS Non-Invasive Brain Stimulation

P Phosphorous

PCA Principle components analysis

PCr Phosphocreatine

PET Positron Emission Tomography

PMC Premotor cortex

PPC Posterior Parietal Cortex

ppm parts per million

PRESS Point Resolved Spectroscopy

RF Radio Frequency

RI Retention Index

ROI Region of Interest

RT Reaction Time

rTMS repetitive Transcranial Magnetic Stimulation

SEM Standard Error of the Mean

semi LASER Semi-localisation by adiabatic selective refocusing

SMA Supplementary motor area

SNR Signal-to-Noise Ratio

SSM State-Space Model

SPECIAL Spin echo full-intensity acquired localised

SRTT Serial reaction time task

STEAM Stimulated echo acquisition mode

SVS Single Voxel Spectroscopy

T Tesla

T1 Magnetisation signal parallel to B0

T2 Magnetisation signal in the transverse plane

tCr Total Creatine (including phosphocreatine)

tDCS Transcranial Direct Current Stimulation

TE Echo Time

TMS Transcranial Magnetic Stimulation

TR Repetition Time

VAPOR Variable Power Radiofrequency Pulses with Optimized Relaxation Delays

VOI Volume of Interest

WI Washout Index

WM White Matter

CHAPTER 1.0

Introduction

1.1 Adaptation

When we perform a movement, we need to make assumptions about the properties of our environment. For example, when we pick up a milk carton, we exert more force if we expect the carton to be full than if we expect it to be empty. If we expect a full carton and pick it up with the according force but, contrary to our expectation, the carton is empty, then our hand will jerk upwards resulting in a movement error. In response to this movement error, we immediately adjust the applied force, according to the actual weight of the milk carton. Adjusting our movement reduces the error. This process of reducing movement errors that arise due to unexpected conditions and returning errors to a former level, is called motor adaptation.

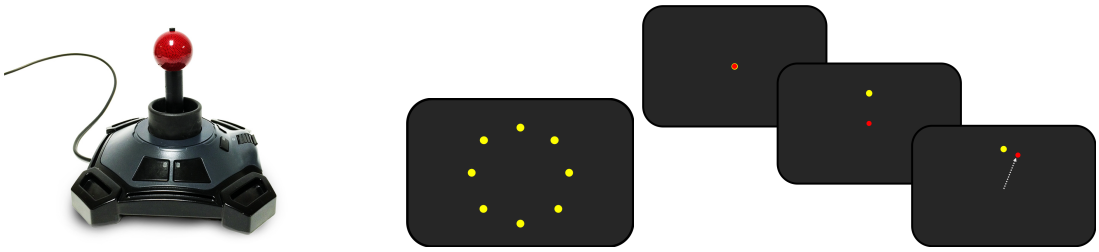
Adaptation can occur in response to a variety of external and internal conditions. An external condition is a property of the environment, an internal condition a property of the body. The unexpected lightness of the empty milk carton in our example is an external condition. Picking up a milk carton with fatigued muscles because we already stacked several supermarket shelves with milk cartons, requires compensating an internal condition: muscle fatigue. Internal conditions can change due to exercise, injury, growth, or disease. External conditions can change because we are navigating different environments. In our daily lives, we are therefore constantly required to adapt to changes in both external and internal conditions and adaptation is a fundamental property of the nervous system [383] [319].

Adaptation usually falls under the umbrella term of motor learning. Motor learning can be defined as change in movement parameters - speed, accuracy, smoothness - due to experience or practice [117]. Although adaptation falls under this definition, it is distinct from another aspect of motor learning: *de novo* skill acquisition. This distinction becomes clear if we consider a motor controller. The term motor controller (borrowed from control engineering) refers to some network or process that generates a motor output given the state of the body and the goal [189]. During adaptation, we derive our new controller from an existing one. We adapt by either modifying how our current movement is executed or select an alternative familiar movement. We do not need to learn from scratch how to hold a milk carton, but can simply correct our movement. In contrast, *de*

novo learning requires the formation of a new motor controller. Learning to control a prosthesis that picks up the milk carton by changing muscle activity measured with via Electromyogram (EMG) would be *de novo* learning: the mapping between the EMG-measured activity and the prosthetis is new to us and needs to be learned. The term motor learning as used in this thesis will refer to the umbrella term of motor learning, which includes *de novo* learning as well as adaptation, i.e. learning to compensate for changes in conditions.

1.1.1 Adaptation paradigms

In the laboratory, conditions are changed experimentally to measure how participants adapt. Early studies of this adaptation involved the use of prism glasses [368]. Prism glasses refract the light entering the eye and thus shifting the visual field - for example 10° to the right. When participants start to make pointing movements while wearing prisms, they initially make unexpected errors as the target appears shifted - in this case around 10° to the right. Gradually, over time, with repetition participants learn to adapt their movements to accommodate for the visual displacement. Since the relationship that is manipulated is between the movement of the arm and the visual feedback, this is an example of visuomotor adaptation.



(A) Joystick. (B) Possible targets. (C) Example trial.

Figure 1.1: Visuomotor rotation task.

Another visuomotor adaptation paradigm is the visuomotor rotation task, made possible through the development of computer-based setups [189]. Here, participants control an on-screen cursor by moving a hand-held joystick or tablet pen (figure 1.1A). Typically, they make movements to a target that is presented at one of eight possible locations radially aligned around a central starting position of the cursor (figure 1.1B). Participants cannot see their hand holding the joystick as it is shielded from their view. To induce adaptation, the cursor feedback is rotated (figure 1.1C), unbeknownst to the participants, and participants adapt to this rotation. The visuomotor rotation paradigm allows the extent and character of the rotation to be changed throughout the experiment. Typically, visuomotor rotation studies impose a constant rotation between 30° - 60°, although changing rotations that increase with every trial or with every fixed number of trials have been used [169]. The flexibility that the visuomotor rotation paradigm affords to the experimental protocol is utilised in this thesis to develop a novel adaptation task. Details of this task are

discussed in chapter 2.1.

1.1.2 Internal models

The process of error reduction during adaptation is intimately linked with the idea that the nervous system uses internal models for motor control, specifically forward models [385] [165]. Forward models predict the end-state of an effector given its current state and a given motor command. For example, given the current position of the arm (effector) and a movement (motor command), the forward model predicts the next position of the arm [385]. Why should the nervous system use an internal forward model? Forward models counter an important problem in motor control: delay. Delays in the sensorimotor loop are large enough that waiting for the arrival of sensory feedback to correct our movements would lead to behavioural instability. In other words, movement corrections would constantly overcompensate because they are based on out-of-date sensory feedback, making our behaviour unstable. The delays to sensorimotor feedback are therefore too large to be used to control rapid movements [149]. Using a forward model for internal feedback, the system can estimate the consequences of a movement before sensory feedback is available and effectively eliminate instability [231] [386] [229] [319].

How does this forward model relate to adaptation? Updating of a forward model is thought to be the main mechanism behind adaptation. In a visuomotor rotation task, the forward model predicts the position of the cursor given its start position and the movement performed with the joystick. This prediction is then compared with the end position of the cursor, resulting in a prediction error because the experimenter rotated the cursor feedback. Using this prediction error, the forward model gets updated. The next movement that the participant makes with the joystick is going to be based on the updated forward model and therefore begins to compensate for the rotation. However, as the internal forward model can only be updated iteratively and incrementally, adaptation takes place gradually over many repetitions of the movement.

Discussion of internal models in this thesis focusses on forward models, because cerebellar function in adaptation is frequently linked to the updating of a forward model. However, another type of internal model has also been proposed to rely on the cerebellum, the inverse model [172]. Inverse models derive a motor command to be applied to an effector given its current state and a desired state. For example, given the current position of the arm and the desired position of the arm, the inverse model provides the command necessary to achieve the desired position [385]. While the forward model is a predictor (predicting the next state), the inverse model is a controller (deriving the necessary motor command).

It should be noted that in addition to the implementation of internal forward and inverse models, several other accounts of cerebellar function have also been brought forward. For example,

the cerebellum has been proposed to serve as an internal clock or timing organ [38]. This theory was inspired by the lattice structure found in the cerebellar cortex which is formed by parallel fibres that are arranged perpendicularly to the dendritic trees of Purkinje cells. The parallel fibres were theorised to implement a system of delay lines which generate regular timing intervals in the millisecond range.

Notable theories of the cerebellum also include the adaptive filter model of the cerebellum [97] which reformulated the Marr-Albus model based on the theory of adaptive filters [378], the Smith predictor model of the cerebellum [230] which next to the rapid prediction of the outcome of a motor command postulates a delayed copy of this prediction matched in time with the arrival of sensory feedback to allow comparison between the two, as well as adaptive control models of the saccadic system [313]. The cerebellum has inspired a plethora of other models describing its organization and function originating in various fields of study. However, these models are less frequently discussed in the context of adaptation and are therefore outside of the focus of this thesis (for a review see [20]).

1.1.3 Features and terminology of adaptation

If adaptation is the result of an updated forward model, then taking away the rotation should reveal this updated mapping between joystick movements and cursor movements. Indeed, when performing movements that are unperturbed after having adapted to a rotation, participants show an aftereffect [293] [34] [127]. That means, if we imposed a clockwise rotation, which the participant learn to compensate for with a counter-clockwise rotation, then abruptly removing the clockwise rotation will result in counter-clockwise errors. These aftereffects are present even when the participant is aware that the rotation has been removed, showing that aftereffects can be involuntary [180] [293] [345]. Such aftereffects are a hallmark of adaptation and are seen in all adaptation paradigms [274] [233]. Because this aftereffect can occur against the participants intentions, adaptation has been deemed implicit. However, increasing evidence suggests explicit as well as implicit processes contribute to adaptation [346] [221] [175]. We will discuss explicit and implicit contributions to adaptation in section 1.1.4.

Aftereffects disappear when participants continue to perform movements in the absence of a rotation, washing out the compensatory movement [189]. This phenomenon is called *washout* or *de-adaptation* and is essentially the removal of the aftereffect. During washout, the counter-clockwise error serves as a teaching signal that updates the forward model.

We can see this spontaneous decay when we remove visual feedback of the cursor. In the absence of a visual prediction error, error levels revert to baseline [233] [187]. But, one could argue, even though there is no visual feedback and hence no visual error, the return of errors to baseline

could be explained by the presence of proprioceptive feedback. However, even if participants perform no movements after adaptation, but simply sit idle for a few minutes, then the adaptive memory will decay by approximately 50% [178]. This means if participants adapt fully to a 30° counter-clockwise rotation and demonstrate a 30° aftereffect if probed immediately, then after a brief (approximately 12 min) waiting period, they show only an aftereffect of 15° [178]. Because participants did not perform any movements between the adaptation period and the aftereffect assessment phase, they were not exposed to any sensory prediction error during that time - neither visual, nor proprioceptive - that could have led to an update of the forward model. Hence, the behaviour must have decayed by itself. This phenomenon is called *retention*, reflecting the tendency of the motor system to retain only a fraction of the adapted behaviour. Accordingly, in this thesis, more retention means less decay of the adapted behaviour.

Although the decay of the adaptive behaviour shows that this behaviour is short-lived, adaptation can have long-lasting effects.

Firstly, aftereffects can last more than 24 hours when the rotation has not been washed out after adaptation [380] [187]. Secondly, even after the rotation has been fully washed out and no aftereffect can be detected (i.e. errors have returned to baseline levels), participants show another signature of a long-term memory: *Savings*. Savings mean that participants adapt faster when they are exposed to the same perturbation after a time interval - having saved some memory of the initial adaptation. Savings can be evident weeks after the initial adaptation [187] and can even transfer to the untrained limb [371]. Although savings are a long-term effect of adaptation, they are not to be confused with aftereffects: While aftereffects pertain to the initial error on second exposure, savings refer to the faster re-adaptation or lower initial errors on second exposure.

We can illustrate this graphically (figure 1.2). Error reduction during adaptation and re-adaptation is well described by an exponential curve [62] [185]. When fitting an exponential curve to the re-adaptation errors, the y-intercept of the curve shows the aftereffect and the rate shows the savings: it is larger in re-adaptation than adaptation because errors decay faster (figure 1.2).

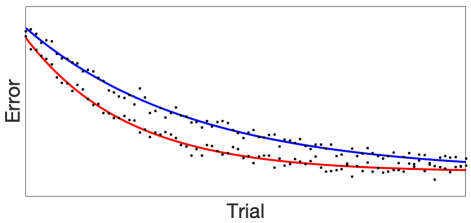


Figure 1.2: Savings and aftereffect. Adaptation (blue) and re-adaptation curves (red) are overlaid to make visual comparison easier. Black dots are simulated error data.

Savings can make repeated comparison of adaptation between sessions difficult. When

evaluating the effect of an intervention on adaptation using a within-subject design, savings will bias the effect of the intervention, potentially obscuring an effect. It is therefore important to minimize savings when comparing adaptation at different sessions.

Washing out the rotation without visual feedback can eliminate savings [178], but no-feedback washout needs to be performed for considerably longer than the initial adaptation phase [178]. When the no-feedback washout phase is only as long as the adaptation phase, savings are reduced, but not eliminated [398] [138]. Washing out the rotation with visual feedback can also reduce savings, but does not eliminate them, even when the with-feedback washout is performed for more than twice the length of the adaptation phase [178].

Gradually introducing the rotation during initial adaptation has been shown to reduce savings [195] [130] [267] [359], showing that savings rely on the presence of a sizeable error that is being reduced.

It has been argued that the reduction of this sizeable error acts as a reward that reinforces the successful movement and that savings reflect the recall of the reinforced movement rather than a recall of the forward model [138]. This idea is corroborated by studies showing that participants can adapt using reward prediction errors which informs only about the success or failure of the movement, and that this adaptation results in reduced update of a forward model [152]. These two distinct mechanisms, updating of a forward model and reward-based reinforcement of successful actions, are two possible solutions of reinforcement learning problems: model-based and model-free learning [342]. Model-based learning means that the system builds a model of the environment from experience. Model-free learning means that the value of executing an action is learned directly from the experienced success or failure of this action, without building a model of the environment. While model-based learning has traditionally been thought of as the primary mechanism behind adaptation, model-free mechanisms still seem to play a role in adaptation [138] [152].

1.1.4 Explicit and implicit contributions to adaptation

Similarly, adaptation has traditionally been thought of as relying on purely implicit processes, but recent studies have highlighted explicit strategies contributing to adaptation [348] [118] [85]. A process is commonly considered implicit if it shows at least one of two characteristics: First, it is non-intentional or automatic, and second, it takes place unconsciously or without awareness. Both of these characteristics were shown in studies where adapting to a sensory prediction error was in conflict with an explicit strategy [218] [345].

Participants adapted to the sensory prediction error although they did not intend to and they were unable to describe why they were failing at the task, showing both characteristics of an implicit process. A second argument for implicitness of adaptation comes from considering washout

of a rotation with visual feedback. Errors during this washout show exponential decay of errors, similar to errors during initial adaptation, although steeper in rate. Had participants employed a strategy during adaptation, they could choose to not apply this strategy after experiencing the first unexpected error during washout and immediately return errors to baseline. Since there is no such rapid drop in errors during washout after the first few trials, strategy-based learning is unlikely to be the main contributor to adaptation. Nevertheless, it is plausible that typical adaptation paradigms can evoke use of explicit strategies to counter the perturbed environment, particularly when first confronted with a noticeable - because large and abruptly introduced - perturbation. Indeed, when probing explicit strategies, by having participants report aiming directions throughout adaptation, the use of explicit strategies particularly during early adaptation is revealed [348]. These were driven by target error and associated with exploration of the target space [348]. Strategies also seem to be associated with higher reaction times, potentially reflecting movement preparation [118]. An example of explicit strategies that might be used in early adaptation is mental rotation, the ability of which correlates with early adaptation [13].

Although the precise interplay between explicit and implicit mechanisms or model-based and model-free processes has not fully been characterised [175], the aforementioned studies highlight a multitude of qualitatively different processes. They also highlight how contributions of these processes can be up- or down-regulated depending on the task design [85] [175] [348] [218].

As I will describe in later section 1.2, there is evidence that different motor learning processes are (at least partially) mapped onto different brain areas. When aiming to probe a particular part of the motor system, it is therefore helpful to consider how properties of the adaptation task evoke contribution of some processes more than others. We will revisit this issue in section 2.4, where we discuss the design of the adaptation task used in this thesis.

1.1.5 State-space models of adaptation

A common way to study the principles underlying behaviour is to describe them with a mathematical model. In adaptation, many features are well captured by a class of models called *state-space models* [59] [71] [193]. Modelling adaptation with state-space models allows examination of hidden variables. One such hidden variable is generalization, which refers to how much the error experienced in one direction generalizes to other directions. For example, a single-state state-space model that captures generalization describes adapting on an 8-target adaptation task remarkably well [344]. Examining this latent variable with state-space modelling suggests generalization falls off beyond 45° target separation [343] [71]. That means, for example adapting to a rotation at target 0° generalizes very little to target 90°.

By including multiple systems that adapt in parallel but at different timescales, phenomena

such as savings or spontaneous recovery of the adaptive response after washout can be captured [325] [183]. This type of state-space model is also referred to as *multi-rate* or *multi-state* state-space model, e.g. dual-state state-space model which comprises two systems adapting at the same time at different rates: one fast system, which adapts quickly and forgets quickly and one slow system, which adapts slowly and forgets slowly.

In light of how well the dual-state model captures adaptation behaviour, researchers have attempted to link the two systems to distinct learning mechanisms [220], models in motor control [394] and even brain areas [325]. The two systems of this model have been proposed to relate to the explicit (fast system) and implicit (slow system) contributions to adaptation [220]. Specifically, they have been suggested to map onto updating of forward models (fast system) and inverse models (slow system) [394]. Lastly, based on the observation that the response of cells in the deep cerebellar nuclei during eye blink conditioning, changes gradually and slowly (and is correlated with the amount of savings), while performance improves rapidly [225], the cerebellar nuclei have been proposed to act as the slow system, and the cerebellar cortex as the fast system [325]. However, as of yet there is little consensus around which physiological mechanisms or which theoretical concepts map onto the fast and slow system [220].

In this thesis, state-space models of adaptation are used as a method to quantify adaptation. Since the task paradigm used in this thesis is different from traditional paradigms, we wanted to test whether results relating to adaptation behaviour in our task still hold when adaptation is modelled using a state-space model. As such, the state-space models used in this thesis complement model-free analysis approaches to corroborate findings. The state-space models used in this thesis are described in section 2.5. We will refer to the analysis approach based on state-space modelling as modelling-based analysis. We will refer to the analysis approach that does not entail state-space modelling as modelling-free analysis. This is not to be confused with the use of model-based and model-free learning that describe different solutions to reinforcement learning problems, in accordance with the definition in [342].

1.2 Adaptation and the brain

Generating movements involves a distributed network of brain areas. Among these are the cerebellum, the primary motor cortex (M1), the premotor motor cortex and supplementary motor area as well as the basal ganglia. In the following text, we will discuss these and review how they are involved in motor control with particular focus on adaptation.

1.2.1 Cerebellum

Cerebellum, diminutive of the latin *cerebrum*, translates to "little brain" and refers to the complex structure situated inferiorly to the cerebral cortex of the brain. Despite its small volume, the thinly folded cerebellar cortex holds approximately 69 billion cells, which make up approximately 80% of all the neurons in the entire human brain at roughly 86 billion cells [16].

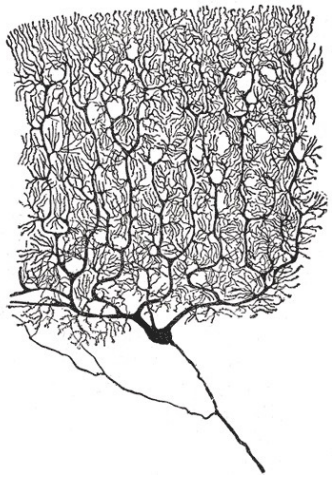


Figure 1.3: Sketch of a Purkinje cell from the human cerebellum by Ramón y Cajal.

The cerebellar cortex is highly uniform in its circuitry. The single output cell of the cerebellar cortex is the Purkinje cell. Each Purkinje cell receives inputs via two streams. First, they receive multiple inputs from multiple parallel fibres. Parallel fibers arise from the densely packed granule cells. Granule cells receive information via mossy fibres that originate in the spinal cord, medulla oblongata, and most massively from the pontine nuclei. The majority of axons exiting the neocortex for the brainstem, either project directly to the pons, or send a collateral there which projects onto the granule cells [356]. Granule cells then innervate Purkinje cells via parallel fibres. Second, each Purkinje cell receives input from a single climbing fibre, originating in the inferior olivary nucleus, though a single climbing fibre branches to innervate one to seven Purkinje cells. The output of each Purkinje cell is sent via one of three deep-cerebellar nuclei. The dentate cerebellar nucleus and vestibular nuclei are the only output of the cerebellum and target many areas of the brain that are mainly motoric in function and include direct connections to the spinal cord, red nucleus and frontal and parietal areas of the cortex.

Detailed description of the cerebellar circuit [79] has led to the development of the Marr-Albus-Ito model of cerebellar function [213] [4] [150]. This model is based on the convergence of the two input types at the Purkinje cell. First, the many inputs from parallel fibres is proposed to represent a detailed context. Second, the single climbing fiber input is proposed to represent an error, or 'teaching' signal. When a Purkinje cell receives climbing fibre activation (error signal) shortly after activation of a set of parallel fibres (context), then the synaptic weights of this

particular set of parallel fibres change through long-term depression [150]. When this set of parallel fibres is activated again at this Purkinje cell, the Purkinje cell firing is reduced compared to before. The change in Purkinje cell firing leads to change in behaviour, change in output to the deep cerebellar nuclei and suppression of the climbing fibre input [224].

One proposed function of the cerebellum is the updating of internal forward models, the primary mechanism probed in adaptation [147] [385]. Several lines of argumentation support this:

First, animal studies have shown that neuronal firing patterns in the cerebellum match what would be expected from forward model updating. When monkeys are confronted with a perturbation, increased complex spike activity can be measured, which is a signature of climbing fibre activation [329]. Complex spike activity ceases when they successfully compensate for the perturbation [84].

Second, patient studies suggest that an intact cerebellum is crucial for processing of sensory prediction errors. Patients with damage to the cerebellum show difficulties adapting [358] [347] [275]. The more severe the patients' cerebellar impairment, the worse they adapt [358]. They also show reduced aftereffects when the perturbation is removed [307].

Third, neuroimaging studies in healthy participants show engagement of the cerebellum in adaptation. Increased cerebellar activity has been shown during early adaptation [315] [145] and in response to sensory prediction errors [308]. Although in a recent meta-analysis of fMRI-studies reporting activity in response to altered sensory feedback, only half the studies reported cerebellar activity the studies that elicited an adaptive response were more likely to show cerebellar activity [164]. This finding may suggest that continually driving adaptive responses could be more effective in eliciting cerebellar activation [164].

Fourth, stimulation of the cerebellum with tDCS, which can increase cerebellar excitability [99], has been shown to increase the rate of adaptation [101] [373]. Cerebellar tDCS has since been found to facilitate adaptation to force-fields [129] and locomotor perturbations [159].

These studies provide a compelling argument for cerebellar involvement in adaptation. However, how adaptation is implemented in the cerebellum has not been fully understood. This fact is highlighted by the fact that tDCS interventions that target the cerebellum to facilitate adaptation fail to produce replicable effects [158] [209]. Understanding the physiological mechanisms behind adaptation in the cerebellum is important to make stimulation effects replicable.

A better understanding is especially relevant given that the cerebellum has been suggested as an intervention target not only for stroke recovery [377], but also for disorders beyond the motor domain [341]. Specifically, the cerebellum has been implicated in Autism spectrum disorder [372], schizophrenia [239] and Attention deficit hyperactivity disorder [32]. Accordingly, modulating cerebellar excitability with tDCS has been proposed as a potential therapeutic option for these

disorders [341] [300] [113].

1.2.1.1 Cerebellar connectivity

Another line of evidence supports the cerebellum as a control system for movements (and also cognition): its connectivity pattern. Tracer studies have shown that motor areas of the motor cortex are connected in a closed loop with the cerebellar cortex [174]. Specifically, Purkinje cells in the cerebellar cortex of lobules IV-VI project to the arm area of M1 [174]. In turn, neurons in the M1 arm area project back to granule cells in the cerebellar cortex of lobules IV-VI via the pontine nuclei [174].

These tracer studies in non-human primates suggest closed cerebro-cerebellar loops for motor functions. Assessing cerebro-cerebellar structural connectivity directly in humans non-invasively is difficult. Diffusion imaging, a non-invasive technique to track white matter bundles, is limited in its ability to disentangle decussating fibres in regions of dense fibres, to track connections across synapses, and to spatially distinguish subregions of dense and narrow regions, all of which occur in cerebro-cerebellar connections [256].

An alternative approach is assessing *functional connectivity*. Here, one correlates fMRI-activity of the cerebellar cortex with fMRI-activity of cerebral cortex regions to obtain a map of cerebellar areas that likely work in concert with specific cerebral areas [151]. Although there may not be a direct anatomical connection between these regions, we can conclude from this map that they are functionally connected. Because these measurements are commonly taken at rest, this is also referred to as *resting-state functional connectivity*.

Several studies have probed cerebellar-cerebral functional connectivity at rest [256] [45]. Resting-state fMRI data from 1000 participants demonstrated a somatomotor map of the body including foot, hand and tongue representations in the anterior cerebellum [45]. Interestingly, resting-state as well as task-based mapping of somatomotor representations in this study revealed that lateralization of somatomotor representations in the cerebellum varies with body part. Lateralization refers to fMRI-activity confined to one hemisphere. While tongue representation is bilateral, foot and hand are lateralized, with hand representation showing the strongest lateralization. That is, the right cerebellar cortex holds representations of the right hand and is functionally connected with the left M1 hand area [45] (because white matter fibres cross the midline at the superior cerebellar peduncles and the pons [364] [272]).

Because the cerebellum has a highly uniform cortical microcircuit, but a diverse connectivity pattern - connecting to motor and association areas -, it has been proposed that the cerebellum performs a "universal transform" in a wide variety of tasks [310]. However, testing theories of a universal cerebellar transform in non-motor domains is more difficult, because the representations which the cerebellum uses are less directly observable [70]. Investigating the substrates of cerebellar

function in a cerebellum-typical task such as adaptation may therefore help constrain the search space.

1.2.1.2 Plasticity in the cerebellum

The Marr-Albus-Ito model rests on the assumption that synaptic plasticity occurs at Purkinje cells which depends on climbing fibre input, i.e. at synapses between Purkinje cells and parallel fibres. Indeed, when a climbing fibre input arrives at Purkinje cells in conjunction with a set of parallel fibre inputs, then synapses from parallel fibres to Purkinje cells undergo Long-term depression (LTD) [148]. This form of LTD in the cerebellum differs in its properties from the more widely known form of LTD in the hippocampus [286]. Both forms of LTD decrease the efficacy of synaptic transmission. However, LTD in the hippocampus occurs after low rate stimulation for long periods and prevents from reaching a level of maximum efficacy where no new information can be encoded [245]. In contrast, LTD arises when climbing fiber input and parallel fiber input converge at a Purkinje cell and LTD in the cerebellum is therefore associative [286].

LTD-based plasticity has been linked to motor learning in animals [397]. Impaired LTD induction together with impaired motor learning has been observed in knockout mice [143], and blocking LTD in mice has been linked to impaired adaptation [194]. More recently, an interplay between LTD and LTP, has been suggested as a basis for motor learning, in line with the Marr-Albus-Ito model [392]. The prevailing view currently is that climbing fibre signals convey error signals and therefore suppress parallel fibre synapses that signal in erroneous performance via LTD [146].

Another site of synaptic plasticity in the microcircuit of the cerebellar cortex has been shown at synapses of parallel fibres with inhibitory interneurons, specifically basket or stellate cells. Conjunctive stimulation of parallel fibre and climbing fibre induces LTP at the parallel fibre - interneuron synapses [166]. Conversely, LTD is induced in these when parallel fibres alone are activated [146]. As basket cells and stellate cells synapse back to Purkinje cells in an inhibitory fashion, the parallel fibre - interneuron synaptic plasticity has synergistic effects on the parallel fibre - Purkinje cell synaptic plasticity. Synaptic plasticity has also been shown at synapses between mossy fibres and granule cells, between climbing fibres and Purkinje cells, as well as subcortically at mossy fibre synapses with neurons of cerebellar or vestibular nuclei [146].

1.2.2 Primary motor cortex

The M1 is located in the frontal lobe of the human cerebrum, specifically in the precentral gyrus. Histologically, it can be defined as the region containing Betz cells. Betz cells are large pyramidal neurons in layer V with distinctively long axons that project to the alpha motor neurons of the spinal cord which in turn connects to the muscles. Muscle twitches and movements can be evoked

by electrically stimulating M1 [96] [86]. Because of this direct muscle response, M1 is thought to be an area of the cerebral cortex that directly controls non-reflexive movement [263].

M1 broadly contains a motor *homunculus*, i.e. a representation of different body parts that is similarly arranged to how the human body is [279] (which is also referred to as somatotopic arrangement). The motor homunculus was revealed in humans by stimulating areas of M1 of epilepsy patients undergoing open brain surgery [279]. While the arrangement of the body representations broadly matches the arrangement of the body parts (medial-to-lateral leg, arm and face representation of the contra-lateral side), the extent of their dedicated area of the motor cortex does not match the size of the body part. That is, more finely controlled body parts, such as hands and tongue, are overrepresented compared to body parts that are more coarsely controlled, such as the trunk – this enlargement is related to the number of motor units controlling a given body part.

Since the first schematic illustration of the homunculus [279], the segregation of dedicated areas for legs, arms and head has been largely upheld [303]. However, within these areas, the representation for a particular body part appears at multiple and distributed locations that can overlap with others [303]. That means, principal body parts like leg, arm and head, are represented in separate cortical locations, but there is no orderly topography of digits, elbow and wrist within the arm area [72].

In light of the direct influence that M1 exerts over movements, several attempts have been made to characterize what M1 activity represents and thereby describe the function of M1 [263]. One largely agreed upon function of M1 is to control low-level parameters of movements, such as force [83] [323] [208]. However, M1 is a highly diverse structure whose inputs and outputs likely vary across its layers and across the extent of the cortical sheet [291] [292], some of which are better understood than others (e.g. there is more information about properties of M1 output neurons that are connected monosynaptically with motoneurons). It has been proposed that in addition to representing lower-level parameters, M1 functions as a 'tutor' when acquiring new motor skills or sequences [171] or that it supports mental simulation of action [355]. But to date, little consensus exists on the role of M1 in this higher-level control of movements [263].

As mentioned in section 1.2.1, the cerebellar cortex forms a closed loop with M1 [174]. The cerebellum has been shown to exert an inhibitory tone over M1, a phenomenon that is known as cerebellar brain inhibition (CBI) [360]. Purkinje cells in the cerebellar cortex inhibit cells in the dentate nucleus, which in turn have disynaptic excitatory connections to M1 via the thalamus [234] [174]. Therefore, activity of the Purkinje cells inhibits M1, whereas a reduced Purkinje cell activity disinhibits M1.

1.2.2.1 Plasticity in the primary motor cortex

M1 is not a static structure, but rather is changeable. It possesses both the substrate and the mechanism for reorganization.

The substrate in M1 that is a candidate site for M1 reorganization is the horizontal connections that span M1. These synapses, which are likely normally blocked by feed-forward inhibition, can be unmasked by disinhibiting M1 locally, as shown in adult rats [155].

Long-lasting reorganization of M1, however, should require long-term synaptic modification. Two mechanisms for long-lasting synaptic modification, Long-term potentiation (LTP) and LTD, have been shown in M1 of rats [133] [131]. LTP of the horizontal pathways in the adult M1 seems to occur only when it coincides with local disinhibition, suggesting a 'window of opportunity' may open up when levels of inhibition are altered [133].

Though these studies were conducted in animals, LTP-like plasticity has been shown in M1 in humans. We will discuss potential mechanisms underlying M1 plasticity in humans in section 1.3.

1.2.2.2 Primary motor cortex and adaptation

In adaptation, M1 seems to be involved in retention of the adapted movement, rather than adaptation itself. Several lines of evidence support this. First, disrupting M1 activity with repetitive Transcranial Magnetic Stimulation (rTMS) before adaptation does not change adaptation to a force field, but impairs retention of the adapted movement when probed 24 hours after the initial adaptation [295]. This lowered retention was also shown in visuomotor adaptation, when M1 activity was disrupted immediately at the end of each adaptation trial [116]. Immediate disruption of M1 resulted in faster de-adaptation rates, while leaving adaptation rates unaffected. Because faster de-adaptation is likely due to a more fragile motor memory, the authors concluded that M1 disruption impaired retention.

Second, electrophysiological recordings in monkeys show learning and retention-related changes in M1 neuronal activity [199] [277]. In monkeys performing a visuomotor adaptation task, activity and spatial tuning functions of M1 neurons changed as a result of the adaptation [277]. This change was evident in the advanced phases of learning and lasted when a steady state of adapted behaviour was reached. It persisted during washout of the adapted movement and was sustained until the monkeys were exposed to the same rotation (re-learning). Because this activity change was specific to learning and lasted from initial learning throughout all phases after learning and until re-learning, these neural changes are likely related to retention [277].

Third, increasing M1 excitability using anodal tDCS during adaptation improves retention, but not adaptation. This was shown in human participants adapting to a visuomotor rotation [101], and later replicated in studies of force-field adaptation [140] [129].

Although these studies suggest that M1 is involved in retaining an adapted movement, the underlying physiological changes in M1 that underpin retention remain to be elucidated.

1.2.3 Premotor cortex and supplementary motor areas

The premotor cortex is located in the frontal lobe, directly anterior to M1. Similarly to M1, the premotor cortex directly projects to the spinal cord and other subcortical structures [74]. However, the premotor cortex can be distinguished from M1 by its cytoarchitecture, specifically by its lack of Betz cells [47] [46]. It also connects to the cerebellum [75] and to M1 [77] [76].

The Supplementary motor area (SMA) are located on the medial wall, immediately anterior to the M1 leg area. The most anterior subregion of SMA, termed pre-SMA connects primarily with prefrontal areas and has sparse or no connections to spinal cord or M1 [125] [24] [74] [203] [205]. Other subregions of SMA project directly to the spinal cord [126] [125].

Both PMC and SMA play a role in preparing movements [119]. SMA activity is closely related to preparation and execution of movement [6] [61] [271]. PMC activity increases during movement preparation and decreases after movement execution [374].

In studies of adaptation SMA neurons have been shown to undergo changes when monkeys adapt to a force-field [271]. Studies of monkeys adapting to a visuomotor supports the notion that SMA undergoes reorganization during adaptation. Early in adaptation a higher number of neuron clusters are recruited than late in adaptation [278].

A recent study suggests that PMC activity changes underlie force-field adaptation, but not visuomotor adaptation [280]. In this study, neural activity was recorded from PMC and M1 of monkeys adapting to a force-field or to a visuomotor rotation. Four computational models of functional connectivity within and between M1 and PMC neuron populations were developed to test four hypothesised mechanisms of connectivity changes that could underlie adaptation behaviour. The authors found that neural spiking during adaptation to a force-field was best predicted by a model where PMC activity changes that does not directly affect M1 activity. The authors interpret this finding as suggesting that PMC alters preparatory activity during force-field adaptation in a way that does not directly influence M1. A different picture emerged for visuomotor adaptation: The four models did not differ significantly in how well they explained the neural data recorded during adaptation to a rotation. The authors interpreted this result as evidence for neural changes occurring upstream of the inputs to PMC, because those changes would not be captured by the models or the neural recordings. Indeed, visuomotor adaptation has previously been suggested to involve changes in functional connectivity between parietal cortex and motor and premotor cortex [344]. Moreover, there is evidence that neural processes underlying adaptation to a visuomotor rotation differ from those underlying force-field adaptation [216] [188].

1.2.4 Posterior parietal cortex

The Posterior Parietal Cortex (PPC) is the area of the parietal cortex that is directly posterior to the primary somatosensory cortex. It is known as an 'associative' region, because although it receives inputs from somatosensory and motor regions, it also combines inputs from visual, auditory and prefrontal areas. The PPC is thought to be involved in representation of space and sensorimotor transformations that are necessary to plan and control movements [153]. It has been implicated in prism adaptation [154], force-field adaptation [64] and visuomotor adaptation. In visuomotor adaptation, increased PPC activity has been shown during late adaptation compared to early adaptation. Evidence from patients with lateralized parietal damage has suggested that visuomotor adaptation could rely more heavily on left compared to right parietal areas. Patients with left parietal damage showed impaired visuomotor adaptation, whereas patients with right parietal damage adapted normally and showed aftereffects comparable to healthy controls[248]. However, the precise contribution of the PPC to adaptation and its interplay with the cerebellum and motor areas has not been characterised yet.

1.2.5 Basal ganglia

The basal ganglia are a group of subcortical nuclei located deep within the cerebrum and brainstem. Among them are the caudate, putamen, globus pallidus, as well as the substantia nigra and the subthalamic nucleus. The basal ganglia are connected with motor cortical areas in a closed loop via the thalamus [5]. Other regions of the cerebral cortex are also connected with the basal ganglia in several parallel closed loops [5]. The basal ganglia circuitry is particularly suited to processing signals from multiple cortical regions to influence behaviour [217]. Because of its circuitry and diverse connections, the basal ganglia have been proposed to carry out this computation in multiple functional domains, similar to the universal transform hypothesis of the cerebellum [5].

In the motor domain, the basal ganglia have been proposed to 'filter' motor plans by suppressing neural signals for undesired movements and enhancing neural signals for desired movements [237].

Part of the basal ganglia - dopaminergic neurons in the substantia nigra - has been found to represent reward prediction error [241] [297] [312], consistent with the idea that the basal ganglia are involved in reinforcement learning.

Imaging studies show higher basal ganglia activation in early compared to late adaptation to a force-field [317] and to a visuomotor rotation [315], suggesting that the basal ganglia are involved in early rather than late adaptation. Patients with damage to the basal ganglia have been shown to adapt at a rate comparable to healthy controls, but to exhibit a lack of savings [211] [196].

1.3 GABA and motor learning

γ-aminobutyric acid (GABA) is the primary inhibitory neurotransmitter in the central nervous system of adult mammals and plays an important role in plasticity and modulating behaviour. Within GABAergic neurons, GABA occurs in two pools: one vesicular, within the presynaptic boutons, and one distributed throughout the cytoplasm of the neuron [214]. However, GABA is also found in a third major pool, in extracellular fluid.

GABA acts on two types of GABA receptors, $GABA_A$ and $GABA_B$ receptors. $GABA_A$ receptors can be found at the $GABA_A$ synapse as well as extrasynaptically. When GABA binds to a $GABA_A$ receptor, an associated ion channel opens, causing influx of negatively charged chloride ions. This addition of negative charge hyperpolarizes the neuron, which makes it less likely to fire. Synaptic $GABA_A$ receptors thereby mediate fast inhibitory neurotransmission.

In contrast to synaptic $GABA_A$, $GABA_A$ that are located outside the synaptic cleft are thought to mediate slow, *tonic* inhibition. This is because some extrasynaptic $GABA_A$ receptors contain subunits that are generally associated with slower and less complete desensitization [114]. Extrasynaptic $GABA_A$ receptors, which are activated by GABA "spilling over" from the synaptic cleft, are therefore thought to underpin the GABAergic *tone* [370].

$GABA_B$ receptors are located pre- and postsynaptically throughout the central nervous system. $GABA_B$ receptors are metabotropic, since they are coupled with a G-protein. When activated, they cause outflux of positively charged potassium ions, thereby hyperpolarising the neuron membrane and reducing its excitability. Because this hyperpolarization is characteristically slow, the $GABA_B$ receptors are considered slow-acting, contrary to the fast-acting synaptic $GABA_A$ receptors.

In animals, GABA reduction in M1 is crucial for inducing LTP plasticity [155]. Moreover, reorganization of motor representations in M1 is thought to rely on M1 GABA reduction [132]. In line with this, GABA reduction facilitates LTP-like plasticity [357], whereas preventing M1 GABA reduction impairs LTP-like plasticity [52].

In humans, the link between local GABA reduction and LTP-like plasticity has been supported by pharmacological intervention studies. Participants who received a GABA agonist, show reduced M1 plasticity [219] [402]. Moreover, measuring M1 GABA in vivo in humans through Magnetic Resonance Spectroscopy (MRS) has allowed investigation of GABA fluctuations during learning. These studies have shown M1 GABA reduction during learning of a motor sequence. When participants were simply performing random button presses, without a learning component, GABA levels did not change [91] [181]. M1 GABA levels at baseline, when participants were performing no task, have been shown to correlate with motor performance (faster reaction times) [332]. Moreover, a reduction in M1 GABA was found to relate to subsequent motor learning (peak reduction in reaction times) [181].

Studies have also probed the human GABAergic system using non-invasive brain stimulation interventions to relate the system's responsiveness to motor learning. Stimulation-induced changes in M1 GABA concentration have been linked to learning on a motor sequence task [332], as well as adaptation to a force-field and washout of the adapted movement [176].

GABA has been suggested to play a fundamental role in cerebellar plasticity, at parallel fiber - interneuron synapses [268], as well as interneuron-Purkinje cell synapses [124] and GABA is the sole transmitter from the cerebellar cortex to the deep cerebellar nuclei. Despite the apparent importance of GABA for plasticity and motor learning, how cerebellar GABA underpins motor adaptation has not been fully understood. This is likely because, although there is an abundance of GABA in the human cerebellum [369], measuring GABA non-invasively and in vivo with confidence is technically challenging. However, these technical challenges have recently been overcome (see section 2.2 for a detailed discussion of the methods).

1.4 Aims of this thesis

The research presented above has shown that adaptation is a fundamental property of the nervous system which engages a variety of structures, but primarily relies on the cerebellum. The cerebellum plays an important role not only in motor adaptation, but also in higher-level functions. Understanding changes in the human cerebellum is crucial for the development and refinement of cerebellar interventions for motor and non-motor functions. These cerebellar changes likely involve GABAergic changes. My primary aim in this thesis is therefore to investigate the role of cerebellar GABA in adaptation. I address this aim in the subsequent chapters in the following way:

In chapter 2, I describe the novel adaptation paradigm used in this thesis to maximize cerebellar engagement. I describe the methods used to measure GABA non-invasively and in vivo and I outline the methods to quantify functional connectivity. I also discuss the non-invasive brain stimulation technique, Transcranial Direct Current Stimulation (tDCS), used to stimulate the cerebellum. Lastly, I describe the computational models used in this thesis to quantify adaptation as a modelling-based measure of adaptation that complements the traditional, modelling-free measures of adaptation.

In chapter 3, I investigate the effects of cerebellar tDCS on adaptation and retention, where behaviour is quantified with modelling-free and modelling-based methods.

In chapter 4, I study M1 GABA changes over the course of adaptation and whether M1 GABA relates to retention of the adapted movement. Following that, in chapter 5, I test for potential functional connectivity changes evoked by the novel adaptation paradigm. I also test whether these network-level connectivity changes relate to adaptation performance.

In the final experiment, presented in chapter 6, I probe changes in cerebellar GABA during

adaptation. I examine whether these changes relate to adaptation performance quantified with modelling-free or modelling-based methods. I also explore a potential relationship between cerebellar GABA and local network-level functional connectivity.

Lastly, in chapter 7, I discuss the findings presented in the experimental chapters 3 to 6 as well as directions for future research.

CHAPTER 2.0

Methods

2.1 Measuring brain function

Magnetic Resonance Imaging (MRI) allows researchers and clinicians to non-invasively image the human body *in vivo*. After its development as a feasible technique to be used in humans in the 1970s, MRI has been widely used to investigate brain structure and function in humans.

In the following sections, I will review the principles of MRI with particular focus on resting-state fMRI and imaging of the cerebellum. In reviewing these principles, I will discuss the specific acquisition and analysis choices made in this thesis.

2.1.1 Principles of magnetic resonance imaging

Magnetic resonance imaging allows for the non-invasive measurement of a signal from a sample - here, the brain - without delivering sample-damaging ionising radiation (like plain film radiographs or Computer Tomography (CT)) and without injection of a tracer (like Positron Emission Tomography (PET)). It therefore offers substantial advantages over these technologies and is frequently used for research. Instead of relying on ionising radiation, magnetic resonance imaging relies on the nuclear magnetic resonance phenomenon.

In routine magnetic resonance imaging, we record the signal from hydrogen (^{1}H) nuclei, particularly those in water molecules. Other molecules contain nuclei that can be used for MRI, for example phosphorus (which has a naturally occurring stable isotope ^{31}P). However, ^{1}H is most commonly used in MRI because of its abundance in biological tissue and the MRI techniques used in this thesis rely on ^{1}H proton imaging only. For simplicity, in this section we will consider only the ^{1}H nucleus and describe the interactions of its proton with magnetic fields.

Some particles, among them the ^{1}H proton, exhibit a quantum mechanical property called *spin*. This spin can be likened to angular momentum of rotating objects known in classical physics.

Although this is only an analogy and there are fundamental differences between spin and angular momentum, it is helpful to imagine a particle with spin as a tiny spinning ball, rotating about an axis, in order to describe its behaviour. Because the ^{1}H proton is charged, it interacts with an external magnetic field. The proton's magnetic properties are often visualised as those of a tiny

bar magnet or a compass needle, with a north and a south pole. Since the proton also appears to rotate about its axis, it has a *magnetic moment*.

When we place a person into a large magnetic field (commonly denoted B_0), the magnetic moments of the protons in the biological tissue will tend to align themselves parallel to the magnetic field, like a compass needle. However, rather than settling down in the direction of the magnetic field B_0, each proton's magnetic moment will precess around the direction of B_0. One can imagine this circular motion like that of a gyroscope after it has spun for a while and its angular momentum is being pulled towards the ground. The frequency f_0 at which the individual proton's magnetic moment will precess is proportional to the strength of the magnetic field B_0 with a particle-specific proportionality factor called the gyromagnetic ratio γ:

$$f_0 = \gamma * B_0 \tag{2.1}$$

For protons, this characteristic resonance frequency is in the radio-frequency range.

The averaged sum of the magnetic moments of the ^{1}H atoms create a *net magnetization (M)*. We can treat this net magnetization M as a vector. It is helpful to describe a three-dimensional coordinate system in which the vector M exists, oriented at the direction of the main magnetic field B_0 (figure 2.1A). Parallel to B_0 is the z-axis, also called longitudinal axis. Perpendicular to B_0 is a plane along the x and y axis, also called the transverse plane.

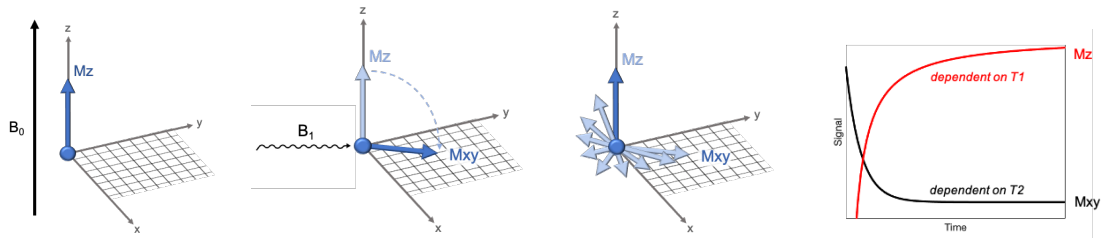
During scanning, M is purposely tipped out of alignment with B_0 (figure 2.1B). That is, M is tipped out of the longitudinal axis towards the transverse plane. This is called excitation and is achieved by applying a second, rotating magnetic field (denoted B_1). The rotating magnetic field is created by passing alternating current through a nearby Radio Frequency (RF) coil, the transmit coil. The frequency of the rotating magnetic field is at or near resonance frequency of the ^{1}H protons.

As soon as M has been moved out of the longitudinal axis, we can detect M in the transverse plane with a receiver coil: This is because the changing magnetic field M in the transverse plane induces a current in the receiver coil, which is a coiled wire. When we remove B_1, M slowly returns to alignment with the main magnetic field B_0 in a process called *relaxation* (figure 2.1C). The speed of this relaxation depends on the content of the sample. Because it gives information about the content of the sample, the detectable signal in the transverse plane and along the longitudinal axis and the speed of relaxation provide the basis for the MR image.

2.1.1.1 T1 and T2

We can separate M into its component in the transverse plane, M_{xy}, and its component along the longitudinal axis, M_z. When we tip M into the transverse plane, we maximize M_{xy} and minimize

M_z. As M undergoes relaxation, M_{xy} decays exponentially and M_z increases exponentially. This signal in the transverse plane is also called a free induction decay or FID. The measured signal is also called a spin echo when a refocusing pulse has been applied.



(A) Equilibrium. (B) Excitation. (C) Relaxation. (D) Signal Development.

Figure 2.1: Schematic of a pulsed MR experiment.

The relaxation process is governed by two time constants, T1 and T2 (figure 2.1D). T1 is the time constant for the growth of M_z after excitation. T2 is the time constant for decay of M_{xy} after excitation. Different tissues have different T1 and T2 values. By measuring the T1 and T2 relaxation signal, we obtain information about the type of tissue contained in the sample.

2.1.1.2 Localization

So far we have treated the MR signal as if it were a single FID. In MR imaging, however, FID signals come from multiple locations in the sample. The resulting total MR signal is therefore the sum of thousands of FIDs. In order to create an image, we need to spatially resolve the signal. We do this by changing the main magnetic field B_0 slightly along the three dimensions x, y and z. That is, we impose spatially varying gradients along the x, y and z direction. Because the precession frequency depends on B_0, the frequencies of the protons now differ slightly, depending on where they are located.

If we impose a gradient along the z-direction only, we can now selectively excite only one slice in that direction. We achieve this by matching the RF pulse to the frequency at a particular location of the field in the z-direction, a process called slice selection. Now we are dealing only with the signals from this particular slice, made detectable in the transverse plane through slice-selective excitation.

To resolve the last two dimensions, x and y, we impose the other two gradients along the x and y direction. By imposing those two gradients, we can alter the phase and frequency of the signal, thereby encoding spatial information into the signal. After we have measured this signal, we use our knowledge about the imposed gradients and apply a series of inverse Fourier transforms to reconstruct the image from the sum of the FIDs. We can also use information about the distance from receiver coils and differences in timing of a signal to recover spatial information.

2.1.1.3 Pulse sequence parameters

We acquire an MR image by applying a set of pre-selected RF pulses in concert with spatial gradients and read out the generated signal via the receiver coils. The sequence in which these steps occur is dictated by the *pulse sequence*. The pulse sequence can be tailored to our experiment, such that we maximize our ability to resolve a particular tissue type, image a specific brain area or minimize certain artefacts.

Among the most important parameters of the pulse sequence are the Echo Time (TE) and the repetition time Repetition Time (TR). Both are typically measured in milliseconds (ms). The TE is the length of time between the RF-pulse and the readout of the signal. The TR is the length of time between corresponding consecutive points on a repeating series of pulses [80]. The TR therefore represents the time to acquire one whole 3D image [80].

2.1.1.4 Image Contrast

Although T1 and T2 relaxation happens simultaneously, T1 and T2 relaxation times are independent of each other. By altering TE and TR we can weigh the contrast of our image towards capturing differences in the T1 values or differences in the T2 values of tissues. This is helpful because certain types of tissues may differ in their T1 times more than they differ in their T2 times and vice versa. By adjusting TE and TR to maximize one relaxation time difference, we are weighing the contrast of the image towards that relaxation time.

2.1.1.5 T1-weighted images

Grey Matter (GM), White Matter (WM) and Cerebrospinal Fluid (CSF) have slightly different T1 relaxation times. This difference can be maximized by shortening the TR and the TE. T1-weighted images therefore have short TRs and TEs. Because the structure of the brain, consisting mainly of GM, WM and CSF is highly visible on these images, T1-weighted images are also referred to as structural images.

2.1.1.6 T2 and T2*-weighted images

Apart from the magnetization M returning into alignment with B_0, there is another process that leads to T2 decay. We know this because in any real MRI scan, the magnetization in the transverse plane decays much faster than would be predicted when just considering the natural atomic and molecular mechanisms described above. This rate is denoted T2* [80].

The second process contributing to the decay is *dephasing*. Because of inhomogeneities in the main magnetic field, the individual magnetic moments of the protons dephase, meaning they get slightly offset in their phase. Because of this slight offset, they start to cancel each other out, resulting in slight signal loss that gets larger as time proceeds. Why are there inhomogeneities

in the main magnetic field? Several sources of inhomogeneities are possible. One may be intrinsic defects in the magnet itself. More interestingly though, inhomogeneities also result from susceptibility-induced field distortions that are produced by the tissue itself. For example, inhomogeneities can reflect increased metabolic demand in a specific area of the brain because of increased brain activity. Therefore pulse sequences that are sensitive to T2* contrast can be used to measure brain function, also referred to as BOLD-contrast imaging or functional Magnetic Resonance Imaging (fMRI). We will review the details of the BOLD contrast and specifically resting-state fMRI in the following sections.

2.1.2 Functional MRI

MRI can not only tell us about the structure of the brain, but also how it changes its function over the course of a scanning session. To assess changes in brain function, either in response to an external stimulus or at rest, we acquire T2*-weighted images in rapid succession that are sensitive to the BOLD signal and therefore indirectly sensitive to changes in neural firing.

2.1.2.1 BOLD Contrast

De-oxygenated haemoglobin, is more paramagnetic, than oxygenated haemoglobin. The precessing spins in a voxel containing a blood vessel with deoxygenated blood will therefore dephase and cancel each other out, resulting in signal loss and a quicker T2* decay. The signal difference due to oxygenation levels gives rise to the Blood Oxygen Dependent Level (BOLD) contrast.

The BOLD contrast is thought to be an indirect measure of neural firing because active neural tissue consumes more oxygen than less active neural tissue. The relationship between BOLD signal and neural activity, however, is slightly counter-intuitive. Increased neural firing creates an initial increase in deoxygenated blood relative to the oxygenated blood. But, in response to this increase, the vasculature supplies more oxygenated blood, increasing blood flow and blood volume. In fact, the vasculature provides more oxygenated blood than is being consumed in that active area. This oversupply results in an increase in T2*. A higher MR signal in this instance then reflects higher neural activity. This dynamic relationship between neural activity and BOLD signal is characterised by the Haemodynamic response function (HRF). After increase in firing we can see an initial dip, due to initial decrease in amount of oxygenated blood, after which the MR signal quickly recovers and 'overshoots' the baseline signal level.

After the initial discovery of the BOLD-contrast MRI [259], the relationship between external stimuli and BOLD signal was demonstrated in visual cortex and in motor cortex, showing the suitability of BOLD fMRI for measuring brain activity [259]. This was achieved by employing rapid k-space sampling techniques, e.g. single-shot Echo Planar Imaging (EPI), ensuring that a whole-brain image can be collected rapidly enough so that rapid changes in brain function are

captured [339].

The process by which an increase in regional neural firing leads to a change in local blood flow is called *neurovascular coupling*. Since the discovery of the BOLD contrast, there has been debate about the mechanisms that underpin neurovascular coupling at the molecular and cellular level. For example, it is widely believed that, in response to increased neural firing, the neurons themselves or surrounding astrocytes release signals that act directly on smooth muscle cells and cause them to dilate local capillary beds [142]. Recent evidence, however, indicates that increased neural firing can also be sensed by the blood vessels themselves [57] [201] and that neurovascular coupling is mediated by cells located at the interior surface of the blood vessels [60].

2.1.2.2 Imaging the cerebellum

When using the BOLD signal as a proxy for brain function and interpreting BOLD signal changes, it is important to understand how local blood flow and metabolism reflect the activity of specific neurons. This can vary between the cerebrum and the cerebellum [361].

An implicit assumption of most functional imaging studies is that the activity of principal output neurons of a particular brain area are primarily responsible for the energy use, and therefore BOLD changes and functional imaging signals. However, comparing electro-physiological recordings to simultaneously recorded fMRI measurements suggests that the BOLD contrast actually reflects the input into a specific area and intracortical processing that occurs within that area rather than the activity of its principal output neurons [200].

In line with this, modelling the energy used in the cerebellar rat cortex suggests that the principal output neurons of the cerebellar cortex, the Purkinje cells, use only a small fraction of the total energy consumed by the cerebellar cortex (18% of energy [136]). Instead, the much larger number of granule cells consume the majority of energy used in the cerebellar cortex (67% of energy [136]).

Moreover, there is evidence that measurable changes in cerebellar blood flow are due to mossy fiber input and granular cell activity [49] [215], rather than change in Purkinje cell firing rates [351] [352] [14].

These studies suggest that the BOLD response may be more sensitive to mossy fiber and granule cell activity and less sensitive to activity of the Purkinje cells.

In light of the difficulties to detect changes in Purkinje cell firing with BOLD contrast, it has been suggested that in human fMRI experiments driving mossy fiber inputs instead of climbing fiber inputs could help make cerebellar activity changes during a task detectable [164]. However, how a task needs to be designed in order to maximize mossy fiber activity is unclear.

As mentioned in section 2.1.2.1, the relationship between neural activity and BOLD response is characterised by the HRF. Since the relationship between BOLD response and neural activity takes

on a similar form across various conditions [95], in most fMRI studies, a canonical HRF is used. While a canonical HRF simplifies fMRI analysis, it also assumes minimal variability across subjects and brain regions. This assumption is called into question by evidence showing the HRF differs across subjects, brain regions and even tasks [2] [235]. Specifically, brain stem and its surrounding areas, among them the cerebellum, have been shown to have a different HRF [390]. This HRF variability has been shown to significantly affect fMRI statistical analyses [121].

In functional connectivity studies, HRF variability can pose a particular problem when trying to assign the flow of information between regions to a direction in time, e.g. using Granger causality [120]. Some of these methods try to infer a direction of information flow from time series within the regions that are shifted in phase with respect to each other. These rely on a lag between timecourses being informative about a lag in neural activity. However, differences in shape or magnitude of the HRF between brain regions can be caused by various factors such as vasculature differences, respiration differences, and baseline cerebral blood flow [121]. Though efforts have been made to incorporate variations in the delay of the HRF response into these models, even with these adjustments for HRF variability, lag-based methods perform poorly [328].

Even in standard functional connectivity methods that do not aim to model directional information flow in the brain, HRF variability may confound results, potentially leading to false connectivities [290]. Although some methods have been developed to estimate a voxel-specific HRF from resting-state fMRI data [389], these approaches need to be validated using electrophysiological data and cardiovascular data before wide-spread implementation [389] [120]. Until then, studies investigating functional connectivity are recommended to dissociate between responses to different conditions [120]. For these reasons, caution should be taken when interpreting functional connectivity modulation in response to only a single condition. Instead, in addition to showing connectivity changes to a manipulated condition, studies should test connectivity modulation in response to a control condition or additional experimental conditions with different doses of the manipulation. These results can corroborate the manipulation-specific or dose-specific effect on connectivity.

Since HRF variability and its estimation from resting-state fMRI data is an area of ongoing research, in this thesis we have used a canonical HRF shape. Any modulation of connectivity in this thesis is tested with respect to baseline connectivity and any potential results are re-tested in a control condition consisting of the same subjects.

2.1.3 Resting-state fMRI

fMRI can be used to quantify the BOLD response to an external stimulus or performance of a task, such as a finger tapping task. However, we can also study spontaneous fluctuations of the

BOLD signal to gain an understanding of brain function. Because in that case we are studying the brain at rest, the approach is also called *resting-state fMRI.*

In a seminal study of resting-state fMRI, Biswal and colleagues observed a high degree of temporal correlation between the timecourses of motor regions [151]. The motor regions that co-activated at rest closely resembled the motor regions co-activating during performance of a motor task, e.g. finger tapping. Because resting-state fMRI can allow us to identify signatures of functionally connected regions, these correlations show 'functional connectivity'. Functionally connected refers to similar patterns of activation, i.e. correlated timecourses of activation. The higher the correlation between timecourses of two separate regions, the stronger their functionally connectivity. This is in contrast to regions showing structural connectivity, which indicates an anatomical connection between them. Functional connectivity does not require a direct anatomical connection.

Although resting-state fMRI studies often show functional connectivity patterns that match connections found in anatomical studies [22] [93] [363] - such as cerebro-cerebellar circuits [210] - monosynaptic or polysynaptic anatomic connections are not the only driver of functional connectivity [44]. Two regions can appear functionally connected due to other reasons, such as both being connected to a third region [44].

Despite the variety of possible sources for functional connectivity, an underlying assumption of resting-state functional connectivity studies is that it has neural origins. This assumption appears to be valid when considering recordings in animal studies. Simultaneous measurement of blood oxygenation ratio and neural activity in mice at rest revealed that the timecourses of both signals are closely matched [206]. Similarly, electrophysiological measurements were coupled to the hemodynamic response in monkeys undergoing anesthesia, although shifted by approximately five seconds [246]. Although these studies do not preclude other cellular activity in the brain contributing to spontaneous fluctuations in the BOLD signal, they suggest that studying resting-state functional connectivity can give insight into brain function.

Functional connectivity networks have been shown to closely resemble task-based activation maps [327] [36]. Particularly close correspondence has been shown for the motor network [151].

Functional connectivity networks can change in strength due to recent experience and learning. Connectivity within a cerebellar resting-state network has been shown to increase in response to adaptation [3]. This effect was evident after task performance although participants adapted to a rotation for only ten minutes.

Because resting-state fMRI is sensitive to learning-related changes and because these changing networks closely resemble task-based activation maps, resting-state fMRI can be used to localise learning-related responses. Moreover, the fact that resting-state fMRI is not acquired during -

but before and after - task performance, enables measuring other learning-related changes, such as neurochemistry, as learning progresses. These advantages of resting-state fMRI are utilised in this thesis. In order to test whether the novel adaptation paradigm used in this thesis elicits changes in cerebellar function, we measure resting-state functional connectivity in chapter 5. We measure connectivity before and after adaptation task performance and compare it to connectivity before and after performance of a control task. This affords us the advantage that during task performance, we can measure neurochemistry. We will describe the technique to measure neurochemistry in a later section of this chapter.

Although resting-state fMRI can capture similar changes in brain function to task-based fMRI and affords the experimenter flexibility in taking additional, non-fMRI measurements during task-performance, it requires more elaborate preprocessing than task-based fMRI. This is because fMRI measurements are inherently noisy and susceptible to physiological processes unrelated to neural firing, participant movement and hardware artefacts. As we are measuring spontaneous fluctuations of MR signal and not fluctuations that are time-locked to an external stimulus, identifying relevant signal among the inherently noisy fMRI measurements is challenging in resting-state fMRI. Before statistical analysis, resting-state data is therefore typically cleaned by separating noise from signal components and removing the noise from the data in a process also referred to as *denoising*. In the following sections, I will outline the preprocessing pipeline and analysis steps I have performed on the resting-state data.

2.1.3.1 Preprocessing

Participants moving during the fMRI acquisition can introduce artefacts into the data that vary in how receptive they are to noise reduction steps taken after data acquisition. One type of artefacts, called spin-history artefacts, are due to the localization principle of MR imaging. As outlined before, during acquisition a slice is selectively excited by imposing gradients along the B_0 field, the z-direction. Then, to encode spatial information into the acquired signal, gradients are imposed along the x and y-direction of the transverse plane. These spatial encoding steps rest on the assumption that the location of the spins remains the same. Violating this assumption can cause various artefacts, depending on the pulse sequence as well as extent and timing of the movement. Among them are striping throughout the image or signal loss due to dephasing. Some of these artefacts can be countered through censoring of single volumes (scrubbing) or correcting outlier timepoints (despiking).

Another consequence of movement is the shifting MR images relative to each other. This motion artefact can be corrected by registering the images to each other. In this thesis, I used MCFLIRT from the FSL toolbox to correct for motion artefacts through registration [161]. We also estimated spatial distortions in the B_0 field on the basis of a field map acquired during the same session and

corrected the fMRI data for them using FUGUE implemented in FSL [326]. We then registered the fMRI data to the high-resolution structural image using Boundary-Based Registration (BBR) as implemented in FSL [326].

In addition to these preprocessing steps that are commonly applied to functional MRI data, resting-state fMRI pipelines often use spatial Independent Components Analysis (ICA) at the single-subject level to clean the data from noise arising from motion, scanner artefacts and various other sources. In brief, ICA is a model-free technique that linearly decomposes the fMRI data into underlying features. Model-free in this case means that there is no explicit time-series model of assumed activity specified from a time-varying feature, such as a task, which is fit to the data. Instead, ICA decomposes the data into several components, by trying to find maximally independent components which, taken together, explain the data. The fMRI data is made up of signal as well as structured and stochastic noise. Both signal and structured noise are non-Gaussian. ICA decomposition aims to un-mix the data into non-Gaussian components plus the residual, Gaussian noise. Depending on data quality and preprocessing steps applied, the number of extracted components can range from 70 to over 500.

Each component consists of a time series and an associated spatial map. Using the information from the time series and the spatial map, each component is classified as either signal or structured noise. In describing the denoising process, we will from now on refer to the structured noise simply as noise. Note that any denoising steps that are applied only pertain to the structured noise components that can be identified from the ICA.

Once the noise components have been identified, we can regress out their time courses from the original data [110]. Instead of regressing out the time courses of the noise components, one could reconstruct the fMRI data from the identified signal components. However, when regressing out the noise, no assumptions are made about the signal of interest, unlike in the reconstruction approach [108]. The regression approach can therefore be combined with later null hypothesis testing, such as in a GLM analysis [25]. Additionally, noise may appear stochastic when cleaning the data at the single subject level, but can be identified by the ICA when decomposing the data concatenated over all subjects. We will review the decomposition at the group level, termed group-level ICA, in a later section.

How do we separate noise from signal components? Automatic classification toolboxes, such as FIX can extract features from each component and classify it as signal or noise using machine learning algorithms [301] [109]. However, this approach relies on training the algorithm on already labelled training data. Although there are sets of labelled training data available, this data has to be well matched to our unlabelled fMRI data in their acquisition parameters, studied cohort and other factors of the experiment. Otherwise, it is strongly recommended to train FIX on

one's own study data, after hand-labelling the study data. In this thesis, FIX was trained on readily available training data (UK biobank data [31]) and then applied to the data in chapter 6. Acquisition parameters for the data in chapter 6 were the same as the ones used for the biobank data and the participants studied were healthy controls, same as in the training data. However, to ensure perfect correspondence, I manually classified four fMRI datasets from four different subjects, sessions and timepoints by hand and compared it with the FIX classification. Because the FIX classifier achieved perfect correspondence with my hand classification, the FIX classification was then applied to the rest of the data.

For the data presented in chapter 5, all components were classified manually. This was because during the acquisition of this data, a dielectric pad was present over the left hemisphere. It was placed there to enhance the signal coming from the left M1 hand area and was not taken away for the resting-state acquisition. The unusual characteristics of this dataset therefore required manual classification for effective artefact removal.

The gold standard for component classification is manual classification [173] [223] [243], but this is time consuming and requires expertise. In this thesis, I manually identified noise and signal components on the basis of several characteristics (in line with guidelines on manual component classification [108]). These relate to the time-series of the component, its power spectrum and its associated spatial map.

BOLD signal driven by neural sources typically fluctuates at low frequencies (0.01 - 0.1 Hz), although higher frequencies are possible [58]. One indicator of signal components therefore is low-frequency power and regular oscillations. However, physiological noise arising from cardiac and respiratory cycle introduces fluctuations at approximately 1 Hz (cardiac) and approximately 0.3 Hz (respiratory). With a long TR of approximately 2 to 3 seconds - commonly used in standard BOLD acquisitions and also used in chapter 5 - these fluctuations can become aliased into a low-frequency range [202] [247] and are therefore easily confused with neurally driven MR signal. Therefore, inspecting the associated spatial map for low-frequency components can help identify these aliased physiological noise components, especially when overlaid on top of a structural image. This is because components that are driven by voxels located not in GM, but in WM-CSF boundaries are likely noise. Moreover, spatial maps restricted to vasculature, ventricles and white-matter indicate noise components.

The distinction between signal and noise components is particularly difficult for cerebellar components. The cerebellum is a relatively small structure, close to the cranial sinuses and surrounded by dense vasculature. Although cerebellar signal components are characterized by peak activity coming from GM voxels and noise components by peaks in the veins, this separation can become blurred with lower spatial resolution. Moreover, cerebellar component maps can include

both grey matter as well as nearby veins and the component may therefore be a mixture of signal and noise. As the general verdict in component classification should be 'innocent until proven guilty', if inspection of the timeseries, power spectrum and spatial map does not result in a clear rejection, the component is then kept.

Noise components that are not physiological are normally more easily identifiable than those discussed above. Scanner and sequence related artefacts are commonly characterised by high frequency fluctuations and a biologically implausible spatial map, e.g. a 'striped' activation pattern where every other slice shows high activation. Motion artefacts can be spotted by comparing the time series with motion parameters estimated from the applied motion correction. Motion parameters indicate how much the images are misaligned with respect to the reference image. Plotted as a function of time, they can be compared to the time series of a component, where a close match indicates the component is driven by subject movement.

Using these characteristic features of the single-subject ICA components, resting-state fMRI data can be cleaned from structured noise before analysed further at the group level.

2.1.3.2 Group-level analysis

Two approaches were employed in this thesis for analysing resting-state data at the group-level.

The first approach is based on correlating the timeseries of two regions of interest, also referred to in this thesis as a ROI-based approach. In this, the timeseries of two ROIs is extracted from the cleaned fMRI data and then correlated to get an estimate of connectivity between the two ROIs (given as the Pearson's linear correlation coefficient r). This is done for each subject and each session separately, resulting in one connectivity value per subject per session. To ensure that results are not driven by a global signal change, we also calculated partial correlation values controlling for a timecourse extracted from a CSF region. We then re-tested for connectivity changes using the partial correlation strength.

The second approach again utilizes ICA. In this approach, we concatenate all subjects' and all sessions' data and let ICA decompose the dataset. The number of components that are calculated from the data here is predefined. This is in contrast to single-subject ICA, in which the number of components is set through automatic dimensionality reduction and can therefore differ slightly between subjects and sessions. From the spatial maps of the group-level components, we identify a network of interest and obtain subject-specific network maps for this network using dual regression. Details of network identification and the dual regression process are described in the methods sections of the relevant chapters (chapter 4 and 5). Finally, subject-specific maps are then compared to each other to test for differences in connectivity.

The first approach allows to investigate connectivity between two anatomical regions. One can test hypotheses that relate to the correlation of activity between two regions whose boundaries can

be defined a priori instead of relying on a data-driven decomposition of the data. We therefore used this approach in order to test hypotheses that related to the connectivity of two specific regions in response to adaptation: M1 and the cerebellum.

The second approach, however, does not require the precise definition of regions of interest. Although it requires selection of networks of interest, in this approach the precise shape of the network whose connectivity will be investigated is not specified. Instead, the group networks are estimated in a data-driven approach, namely from the group-level ICA. This allows for some variability at the subject level in the shape of the network that is investigated. Because there is likely some variability between subjects in task activation evoked by adaptation, this approach is advantageous when testing hypotheses that concern the modulation of resting-state connectivity by a task. We therefore chose the latter approach in order to test for a modulation of a resting-state network by task performance.

2.2 Measuring neurochemistry

While fMRI enables us to investigate how the brain is organised and how its different regions are functionally connected, the BOLD contrast itself only provides a proxy signal for neural activity. This precludes us from understanding mechanisms of functional changes in the brain at the neuron level. Measuring neurochemistry can provide insight into the electrochemical processes that take place in the brain. We can measure neurochemistry in the human body non-invasively and *in vivo* using MRS.

In the following sections, I will review the principles of detecting and quantifying chemical compounds using MRS. I will focus specifically on detection of GABA and on measuring neurochemistry in the cerebellum. In reviewing the challenges associated with this, I will discuss the measurement and quantification choices made in this thesis.

2.2.1 Principles of magnetic resonance spectroscopy

As described in section 2.1.1, the resonance frequency of a proton with spin in a magnetic field is described by the Larmor equation:

$$f_0 = \gamma * B_0 \tag{2.2}$$

Equation 2.2 describes the precession frequency f_0 as being proportional to the strength of the magnetic field B_0 with the particle-specific proportionality factor γ, called the gyromagnetic ratio.

However, the proton is not free, but is part of the hydrogen atom. The electrons surrounding the proton in the atom shield the proton from the external field B_0. The proton therefore does not experience precisely the field B_0, but the slightly attenuated field B_{local}. It therefore resonates

at a slightly different frequency, which depends on the chemical environment of the proton. For ^{1}H these shifts are relatively small, but still detectable at field strengths from 1.5T onwards. The shift in resonance frequency is referred to as *frequency shift*. Detecting molecules based on their frequency shift forms the basis of MRS. As with MRI, in describing MRS we will consider only the ^{1}H nucleus, consisting of a single proton. Although other nuclei can be used for MRS, such as Phosphorus (^{31}P), most MRS studies rely on ^{1}H. This is because ^{1}H is most sensitive to MR experiments and present in most metabolites of the human brain, which means ^{1}H MRS can detect a series of brain metabolites.

When transforming the FID obtained from MRS into the frequency domain (using a Fourier transform), we obtain a spectrum. Different metabolites resonate at different frequencies and therefore appear at different points in the spectrum. Because the resonance frequency depends on B_0, the frequency shift does, too. In order to compare spectra between scanners with different field strengths B_0, the frequency shift is divided by the scanner frequency resulting in the *chemical shift*. The chemical shift is expressed in parts per million (ppm), a suffix that is interchangeable with 10^{-6}. MRS typically covers the 0-6 ppm range. The peaks at those points are proportional to the concentration of resonating protons that exist as part of a particular molecule. The height of the peaks therefore tells us about the quantity of the molecule present in the sample (other factors that determine the height of the spectral peaks will be discussed in section 2.2.2.1). We quantify the metabolite concentration from the spectrum by measuring the height of a spectral peak. The specific method used in this thesis to quantify metabolite concentration will be discussed in section 2.2.2.

2.2.1.1 Localization

In contrast to fMRI, in MRS the frequency dimension cannot be used for encoding spatial information, as it already encodes metabolite information. In other words, we rely on the frequency information to tell us about which metabolite we are looking at, instead of informing about the location that the FID has been recorded from. However, in MRS we typically need to obtain spatially specific information about metabolites, rather than quantifying metabolite concentration in the brain as a whole. In order to do this, in traditional Single Voxel Spectroscopy (SVS), we localise a voxel from which we obtain a spectrum. Similarly to slice selection explained in section 2.1.1.2, we do so by imposing magnetic field gradients along a chosen dimension and apply a frequency-specific RF excitation pulse. We apply this slice selection three times, along three dimensions, thereby exciting only protons from a pre-selected volume. This ensures that the acquired spectral signals stem only from the selected volume. The volume, also referred to as MRS voxel, is typically cube-shaped and 2 x 2 x 2 cm^3 in size.

2.2.1.2 J-coupling and Spectral editing

. The shielding of the proton not only depends on its surrounding electrons, but also on its interaction with neighbouring protons. Two protons residing in the same molecule interact via their binding electrons, a phenomenon termed *J-coupling*. One proton's spin polarizes its binding electrons. The binding electron, in turn, transfers this polarization via chemical bonds to the spin of another proton from a distant nucleus. As a result of J-coupling, some metabolite peaks are 'split' into doublets, triplets or other multiplets. J-coupling can be used to make specific metabolites more detectable in a process called spectral editing.

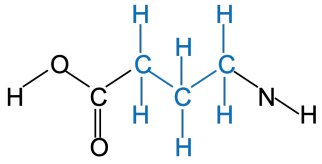


Figure 2.2: Structure of a GABA molecule. The three CH_2 groups that are detectable with MRS are shown in blue.

Consider the neurotransmitter GABA. GABA has three CH_2 groups that are detectable with MRS, shown in blue in figure 2.2. Because they have different chemical environments, they experience a different chemical shift. They resonate at 1.9, 2.3 and 3.0 ppm. The resonances at 1.9 and 3.0 ppm couple to each other due to J-coupling. If we apply a RF pulse selectively at the frequency of the 1.9 ppm resonance, we manipulate the coupled peak at 3.0 ppm, inverting it. After acquiring this edited spectrum, we acquire an non-edited spectrum. By subtracting the edited from the non-edited spectrum, we obtain a difference spectrum that contains only the edited GABA signal at 3.0 ppm. All overlapping singlet resonances at 3.0 ppm have been eliminated by the subtraction. A commonly used spectral editing sequence is the MEscher-GArwood Point RESolved Spectroscopy (MEGA-PRESS) [226]. Spectral editing is effective for making GABA detectable [299] and GABA has been reliably quantified in vivo using this technique [270] [242].

2.2.1.3 Water Suppression

The most abundant molecule in the human body is water. When it comes to the brain, 83% of grey matter and 70% of white matter consists of water in healthy humans [222]. Detectable metabolites of interest, on the other hand, are concentrated in quantities that are in the order of 10 000 times smaller than water concentration. Put differently, relevant metabolites exist in the millimolar range in the brain, whereas water is concentrated in the tens of moles [400]. Water therefore contributes by far the largest peak to the MRS spectrum, which renders metabolites almost undetectable against the background noise. Most MRS experiments therefore aim at minimizing the water signal [167].

One commonly used technique applies a selective excitation pulse at the resonance frequency of water. After excitation of the water signal, it is then minimized by applying spoiler gradients that disperse the spins of the water protons. The metabolite signals remain unaffected by this process. Repeating the process of water suppression several times usually improves the suppression. Variants of this CHEmical Shift-Selective (CHESS [115]) water suppression method include Variable Power Radiofrequency Pulses with Optimized Relaxation Delays (VAPOR) [354]. VAPOR includes 8 presaturation pulses whose parameters such as spacing between the pulses are optimized for water suppression. Although VAPOR thereby increases the minimum TR, it significantly improves water suppression compared to standard CHESS suppression. In this thesis, VAPOR water suppression was used for SVS acquisition described in chapter 4.

Instead of suppressing water directly, an alternative method is to invert the metabolite signal with a frequency-selective pulse in one of the MRS acquisitions [73]. The metabolite contribution to the spectrum is then calculated by subtracting the FID with and without inversion [338]. This method of minimizing water contribution was used for Magnetic Resonance Spectroscopy Imaging (MRSI) acquisition described in chapter 6.

Finally, for all acquired spectra (from SVS and MRSI experiments), the residual water peak was modelled and filtered out of the spectrum using Hankel-Lanczos singular value decomposition (HLSVD) following acquisition and during preprocessing [48] [282].

2.2.1.4 Magnetic Resonance Spectroscopic Imaging

While SVS allows us to study several metabolites from the same spectral acquisition and to make metabolite-specific inferences, it does not allow us to infer from this data that our effects are location-specific. Moreover, SVS requires us to carefully select the location in the brain from which we want to acquire spectra. Placement of the Volume of Interest (VOI) can be tricky depending on the structural properties of the area of interest (proximity to dura, brain stem and ventricles) and on the anatomy of the subject's brain (small cerebellum, atypically shaped M1 hand area). SVS cannot afford us the flexibility to divide the VOI into smaller ROIs. These limitations have been overcome by combining MRS and MRI acquisition techniques in a method called MRSI.

MRSI allows us to acquire spectra from several voxels at once. Resolving the spectral signal is possible in two and in three dimensions, referred to as 2D MRSI and 3D MRSI, respectively. In this thesis, 2D MRSI is used and I will therefore focus my description of the technique on 2D MRSI, referred to from here onwards simply as MRSI.

Similary to the localization technique of SVS, in MRSI a volume is selectively excited using slice-selective excitation pulses in three dimensions. I will refer to the VOI in MRSI as the MRSI slab, to help distinguish it from image slices acquired in MRI or VOIs in SVS. In contrast to the cube shape commonly used in SVS, the MRSI volume is typically a rectangular cuboid. However,

because the signal can be spatially resolved within the MRSI slab, it is usually much larger than VOIs used in SVS. We can resolve the signal spatially by using a technique stemming from MRI: phase encoding. That means, we encode location information in the phase of the frequencies using phase-encoding gradients along two spatial dimensions. After acquisition, we can then reconstruct the array of spectra in the MRSI slab. Because of this reconstruction process, the spectra are not immediately visible during the MRSI acquisition process. During SVS this is possible and visual inspection during acquisition can help immediately detect and address artefacts.

In this thesis, MRSI is used to acquire metabolite data from the cerebellum, which is presented in chapter 6. The MRSI sequence used has been described in detail in [338]. We will discuss the choice of this pulse sequence in a later section, after reviewing the challenges in measuring cerebellar neurochemistry and measuring GABA in section 2.2.4 and 2.2.3, respectively.

2.2.2 Quantifying metabolites

After we have obtained a spectrum, we need to estimate metabolite concentration from the metabolite peaks in the spectrum. One of the most commonly used techniques to quantify metabolite concentrations from a spectrum is *basis spectrum fitting* [250]. For this, we model the contribution of each metabolite to the spectrum by scaling and adding up each metabolite's *basis spectrum*. A basis spectrum is the spectral shape a metabolite will take on in a given experiment. This shape depends on experimental factors such as the strength of the main magnetic field B_0 and the pulse sequence used. The basis spectrum for a metabolite can be derived experimentally or, as is current standard, through simulations. Once we have a set of basis spectra of metabolites known to occur in the brain, the basis set, we can model the measured MRS spectrum as a linear combination of this set. An example spectrum along with the modelled contribution of each metabolite, the baseline and the residuals is shown in figure 2.3. In this thesis, the acquired MRS spectra are analysed with the basis spectrum fitting method, using a simulated basis set for the SVS data in chapter 4 and the MRSI data in chapter 6. This method is implemented with the LCModel software as well as in-house Matlab scripts [284].

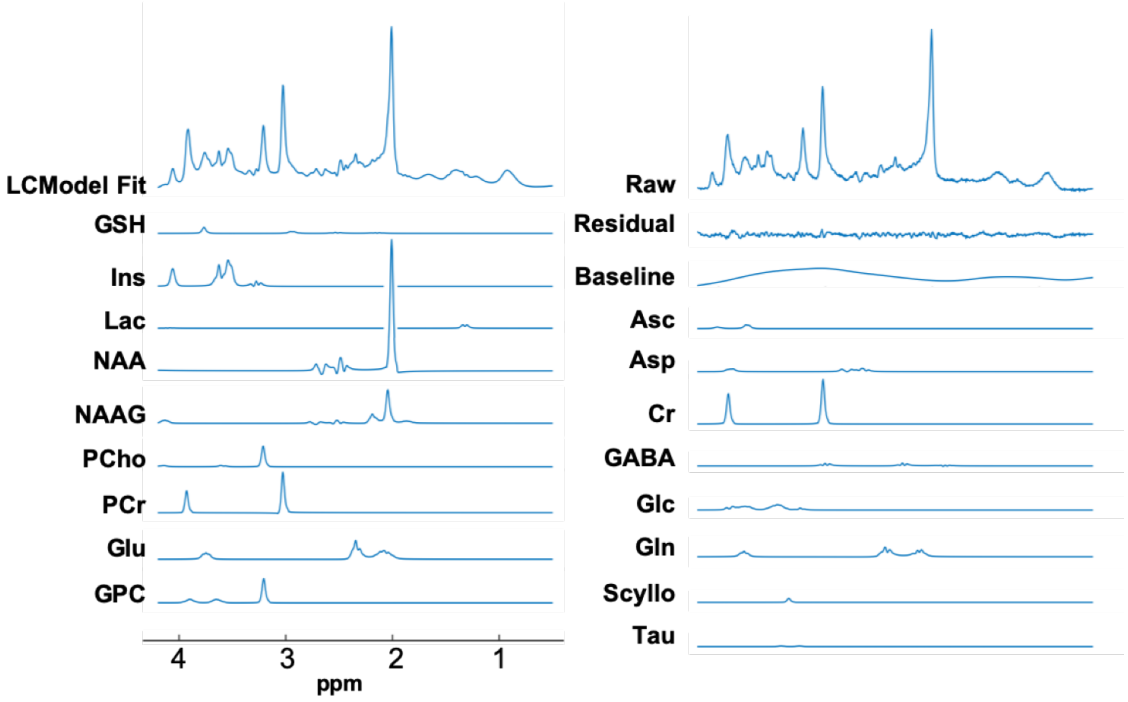


Figure 2.3: Example spectrum and LCModel fit from a single MRS voxel.

Once we have quantified the contribution of a metabolite to the MRS spectrum, we need to convert this quantity into a meaningful estimate of metabolite concentration. We can do this by referencing the metabolite quantity to another compound measured in our MRS spectrum whose quantity is known. Importantly, this reference compound has to be stable and appropriately chosen for our study, as some commonly used reference compounds, e.g. creatine are altered by pathologies and drug interventions [264] [250].

In the case of GABA, internal referencing is usually done to N-acetyl aspartate (NAA) or creatine [17]. As can be seen in figure 2.3, both these metabolites make a large contribution to the MRS spectrum, because they are highly concentrated in the brain. In this thesis, GABA concentrations are given as a fractions of total creatine, which is the sum of Creatine (Cr) and Phosphocreatine (PCr).

2.2.2.1 Quality Control

After metabolite estimation, it is important to evaluate the accuracy of these estimates. A commonly used measure for how certain we can be about the metabolite estimate is the Cramér-Rao Lower Bound (CRLB) of the variance [55]. The CRLB denotes the smallest possible variance on a fit parameter [250]. We obtain a CRLB value for every metabolite and threshold the data according to it. That is, we accept only metabolite estimates whose CRLB value is under a specific value. However, a low CRLB value does not guarantee accuracy and caution is advised when filtering by relative CRLB values (given in percentage values) for quality control [191]. Relative CRLB values

depend on the metabolite concentration, with lower concentrated metabolites often having higher relative CRLB values. That means, true value and error get conflated [191]. It is recommended to use CRLB along with other quality control metrics, particularly when quality filtering data of low concentration metabolites like GABA [190] [250].

Therefore, in this thesis, data quality is assessed on CRLB along with quality control metrics such as SNR of the data, line-width of the spectrum (Full width at half maximum; FWHM), as well as visual inspection of the fit residuals. The thresholding applied using these metrics is described in more detail in the respective chapters (chapter 4 and 6).

Spectral Separation An additional criterion for quality control that can be applied is the criterion of spectral separation. When two metabolite peaks overlap highly, then a good model fit to the measured spectrum can be produced by combining the basis spectra incorrectly, resulting in a wrong estimation of the metabolite concentrations. It is possible to quantify how much the scaled basis spectra that have been fit to the measured spectrum overlap with each other by correlating the data points in the spectral lines of two metabolites with each other. If two metabolite spectra are highly correlated (i.e. the absolute correlation coefficient exceeds 0.5 by convention [253]), then these two metabolites cannot be separated and need to be reported as a sum. An absolute correlation coefficient that is below this threshold indicates good spectral separation.

In this thesis, we achieved good spectral separation for GABA. The MRS data discussed in chapter 4 showed no strong correlation between GABA and other metabolite spectra, with the largest absolute correlation coefficient of GABA with another metabolite being r = 0.22.

2.2.3 Studying GABA with MRS

Quantifying GABA with MRS is challenging, because of two factors. Fist, despite being the major inhibitory neurotransmitter, GABA only exists in low concentrations in the brain compared to other neurotransmitters such as glutamate. Second, as can be seen in figure 2.3, GABA peaks overlap with peaks of other, more highly concentrated, neurotransmitters such as creatine, glutamate and glutamine [17].

However, recent technological advances have made it possible to accurately quantify GABA with MRS [299]. As described in section 2.2.1.2, spectral editing allows manipulating the GABA peaks such that a difference spectrum obtained from subtracting edited and non-edited spectra reveals the GABA contribution. Although spectral editing is widely used to assess GABA, the technique has some limitations. The ability to reveal GABA in the difference spectrum can be limited by subtraction artefacts due to participant motion or scanner imperfections and co-editing of macromolecules resonating near the GABA peak, particularly at lower field strengths such as 3T [18]. Therefore, GABA measurements obtained from editing sequences are often reported as

GABA+, reflecting the inseparability of GABA and macromolecules [250] [35] [252].

We can improve detection by increasing the field strength of the main magnetic field to 7T using ultra-high-field scanners [18]. This renders distinguishing GABA without spectral editing possible. In this thesis, we therefore use ultra-high-field (7T) MRS to measure GABA without spectral editing (SVS semi-LASER sequence [305], chapter 4).

Another strategy to circumvent spectral editing is to use short echo times. At 3T, short echo times for MRS measurements have been demonstrated to make GABA detection possible without spectral editing [253]. Short echo time MRSI has been recently demonstrated at 3T using a semi-LASER sequence [338]. Piloting the MRSI sequence as well as an edited SVS sequence at 3T revealed comparable quality of GABA measurements. Although the MRSI sequence leads to longer acquisition times for a single GABA measurement, it provides valuable spatial information that is crucial in answering our hemisphere-specific hypothesis described in chapter 6. We therefore use the MRSI sequence at 3T for the GABA measurements presented in chapter 6.

2.2.3.1 Interpreting MRS-measured GABA concentrations

MRS measures total GABA in the selected volume and can therefore not differentiate between the different GABA pools described in section 1.3. We are therefore agnostic to whether the MRS-assessed GABA concentration reflects synaptic GABA, vesicular GABA, or extracellular GABA. This complicates mapping MRS-assessed GABA to changes in synaptic activity.

However, studies assessing GABA with Transcranial Magnetic Stimulation (TMS) in addition to MRS have attempted to link MRS-assessed GABA concentration to specific GABA pools. Administering two TMS pulses in quick succession enables probing of intracortical inhibition. Varying the inter-pulse interval weighs the contribution of one GABA pool to this intracortical inhibition over another [333]. A study measuring inhibition within the same subjects with these techniques found no relationship between MRS-assessed GABA and TMS-assessed levels of synaptic $GABA_A$ or $GABA_B$ activity [330]. However, the same study demonstrated a relationship between TMS measures thought to reflect extracellular, extrasynaptic GABA tone and MRS-GABA [330]. Using a different MRS protocol and field strength, a recent study has been able to replicate the finding of no relationship between MRS-assessed GABA and TMS measures that reflect post-synaptic $GABA_A$ inhibition [78]. However, they were unable to replicate the previously shown relationship between TMS measures of extracellular, extrasynaptic GABA, leading the authors to conclude that the relationship between MRS-GABA and TMS measures thought to reflect extrasynaptic GABA is not reliable [78].

2.2.4 Studying cerebellar neurochemistry

Measuring neurochemistry in the cerebellum with MRS poses a technical challenge. The cerebellum is a relatively small structure and close to fatty tissue (on the posterior side) and the brain stem (on the anterior side).

Fat emits a signal over 100 times stronger than metabolites [298]. Because slice selection pulses are inherently imperfect, they always excite some spins outside the selected volume that are in close proximity [190]. If the signal stemming from these spins outside the volume is strong, like in the case of fat, the obtained spectrum will show lipid contamination (see figure 12 and figure 13 in [190]). This means, placing the MRS voxel over the area of interest in the cerebellum can be difficult. Not only do we aim to maximize grey matter content of the MRS voxel and avoid covering adjacent structures, as in standard MRS acquisitions. To avoid lipid signal 'bleeding' into the MRS voxel, the voxel is best placed at a great distance to the fat tissue surrounding the posterior cerebellum.

Similarly, its position next to the brain stem makes taking MRS measurements from the cerebellum difficult. The brain stem area is suffering from high levels of physiological noise due to cardiac and respiratory processes which can lead to inhomogeneities in the main magnetic field [41]. Field inhomogeneities, in turn, can lead to line broadening of the spectral peaks and result in lower quality of the MRS spectrum [167]. Although we are not measuring from the brain stem, these field inhomogeneities can affect the signal to noise ratio in the adjacent cerebellum. This is a particular problem when aiming to measure GABA. Minimizing magnetic field inhomogeneities during the experiment through a process called *shimming* is therefore integral [167]. However, standard 3T and 7T scanners lack features (e.g. equipment) necessary to achieve a shim that allows quantification of GABA from cerebellar areas [81]. At our facilities, these features have recently been implemented and piloted, allowing accurate GABA measurements from the cerebellum with MRSI.

In this thesis, MRSI is therefore used to investigate cerebellar GABA. We choose MRSI instead of SVS, because the added spatial dimension allows us to investigate changes that are specific to one cerebellar hemisphere.

2.3 Modulating brain function using NIBS

Brain stimulation techniques allow researchers to manipulate brain function in a minimally or non-invasive fashion through electrical stimulation. Applying electrical current to the brain dates back to ancient Roman times, with first reports of transcranial stimulation coming from a Roman physician who used the electric discharge of live torpedo fish to treat migraines by placing them on a person's scalp [304]. Modern tDCS, however, was not developed until 1998 [304] [43].

In this section, I will review the principles of tDCS, focussing on tDCS of the cerebellum. I will describe the effects tDCS has on the brain and the parameters that can change these effects. Lastly, I will discuss the parameter choices made for tDCS used in this thesis.

2.3.1 Principles of tDCS

tDCS induces a constant, low direct current between two electrodes with the goal of altering the underlying tissue's electrical properties to change brain function. At least one of the two electrodes are placed on the head, over the area that is to be stimulated. This electrode is often referred to as the active electrode, with the other electrode being the reference electrode. During anodal tDCS, the induced current flows from the active electrode to the reference electrode. The active electrode is therefore also referred to as the *anode*, because it is positively charged, whereas the reference electrode is the *cathode*, because it is the negatively charged electrode. Depending on electrode size and placement half of the current is shunted by the scalp. The fraction of current that travels through the brain to the reference electrode, does so along the path of lowest impedance [238].

Because tDCS uses a low current, usually ranging from 1 to 2 mA, it can only change the likelihood of neural firing, but not induce an action potential by itself. As such, tDCS is referred to as a *neuromodulation* technique, analogous to pharmacological neuromodulators [388]. This is in contrast to stimulation techniques such as TMS, which induces firing of action potentials that is detectable at the downstream muscles as Motor Evoked Potentials (MEPs), sometimes resulting in a visible muscle twitch. Because tDCS modulates spontaneous neuronal activity, its effect depends on the state the stimulated area is in [388].

The direction of the change in excitability of the stimulated area depends on the direction of the current flow, i.e. whether the area is receiving anodal or cathodal stimulation. Recordings from the cerebral cortex of cats [285] show anodal stimulation depolarizes neuronal cell bodies, whereas cathodal stimulation hyperpolarizes them. Recordings from the rat cerebral cortex demonstrate that after brief anodal stimulation of the sensory cortex, neural firing increases, with longer-lasting stimulation (5-10 min) producing persistent aftereffects that can last for minutes to hours [30] [255] [334]. Although the directionality of anodal and cathodal tDCS has been corroborated by studies in humans combining tDCS and TMS of M1 [367] [258], the individual responses show considerable variability [379].

In order to control for expectancy effects and ensure tDCS intervention effects are expressed only when substantial current is induced over the course of several minutes, tDCS studies commonly use sham stimulation as a control condition. During sham stimulation, the electrodes are placed exactly as they are for real stimulation. After ramping up the current for 5-15 seconds, as during real stimulation, the current is ramped down again after 30 seconds. The experiment then proceeds

as it would with real stimulation and finally, after the period of time that real stimulation would normally be applied, the current is ramped up, held for 30 seconds, and ramped down again in the sham condition [102]. This is because any side effects, such as tingling and itching of the skin under the electrodes, are most commonly reported during the ramp-up period and the first 30 seconds of stimulation [254]. Although the sensations elicited by the sham stimulation have been shown on average to be indistinguishable from real stimulation sensations [8], it is advisable to assess the participant's and the researcher's perceived stimulation condition in double-blind sham-controlled tDCS studies.

2.3.2 Cerebellar tDCS

For cerebellar tDCS, a common electrode montage consists of a rectangle active electrode placed 3 cm lateral to the inion and the reference electrode placed ipsilaterally over the buccinator muscle [111] [56]. Using computational modelling of the current flow in the human head, this electrode montage has been suggested to affect only one cerebellar hemisphere and result in little current spreading to non-cerebellar regions such as the brain stem and the visual cortex, as intended with this montage [289]. Corroborating evidence for the cerebellar specificity of this montage comes from a study using TMS to assess excitability of different potentially affected areas after cerebellar tDCS [99]. Following 25 minutes of cerebellar tDCS, cerebellar excitability was significantly affected, while brain stem and M1 excitability remained unchanged [99]. Specifically, anodal tDCS applied with this montage increased cerebellar excitability and cathodal tDCS decreased cerebellar excitability in participants, while sham tDCS did not affect it in either direction [99].

Cerebellar tDCS is thought to modulate the membrane potentials of neurons in the cerebellar cortex, such as Purkinje cells, but it could also act on fibres running through the cerebellar cortex (mossy fibres and climbing fibres) as well as on glial cells [88]. Recordings from the cerebellar cortex of the cat have shown that Purkinje cells and granular cells change firing in response to direct current stimulation in a manner that is consistent with the idea of directionality: While tonic neuronal activity is increased by anodal direct current stimulation, it is decreased by cathodal direct current stimulation [40].

Cerebellar tDCS has been shown to alter motor functions, learning and more cognitive functions such as working memory and emotional processing [90] [87]. As such, it provides a useful tool for studying cerebellar involvement in motor and non-motor behaviour [89]. Ultimately, targeting the cerebellum with tDCS could also lead to the development of novel therapeutic approaches: Cerebellar stimulation with tDCS has been proposed as a potential intervention for patients with cerebellar dysfunction [89] and people recovering from stroke [314], but also to treat disorders that are not directly related to motor function, such as schizophrenia [113], ADHD [300] and autism

spectrum disorder [341].

Anodal cerebellar tDCS can facilitate adaptation, as shown in various adaptation paradigms. Locomotor adaptation during a split-belt task was shown to increase with application of cerebellar tDCS, without the stimulation influencing de-adaptation [159]. In force-field adaptation, participants adapted better with anodal cerebellar tDCS, while retention was unaffected [129]. In visuomotor adaptation, anodal cerebellar tDCS resulted in faster adaptation to a rotation compared to M1 tDCS and sham tDCS [101]. It did not affect retention of the previously learned adaptive movement, in line with an adaptation-specific role for the cerebellum [101].

After the initial finding that cerebellar tDCS can facilitate adaptation [101], several studies have reported facilitatory effects of cerebellar tDCS on adaptation tasks [33] [50] [122]. However, others have found no facilitatory effects on adaptation [209] [139] or shown inconsistent results [158].

A possible explanation for failed replication efforts of the effect lies in the inter-individual variability in responsiveness to tDCS: Different people respond differently to the same stimulation. This finding has been shown in the response to tDCS over M1. The degree to which corticospinal excitability changes in response to the stimulation was found to be highly variable between participants. While half of the participants showed an increase in excitability following anodal tDCS, the other half showed no or little response [379]. The variability in responses might be a result of anatomical differences. Modelling of the spatial distribution of the current that is induced during tDCS reveals that the spread depends on several anatomical factors: skull thickness and composition, thickness of the CSF layer and depth of the sulci [265]. Given the hypergyrification of the cerebellum, this could pose an even greater determining factor for the effects of cerebellar tDCS. Comparing commonly used cerebral and cerebellar tDCS montages reveals that the cerebellar cortex experiences a much lower electric field than cerebral stimulation sites, likely because of the shunting of the current by the occipital bone [289].

In light of this inter-individual variability, it has been suggested that the effects of cerebellar tDCS should be investigated using a within-subject, crossover design [158] [209]. In this thesis, we therefore studied the effects of anodal cerebellar tDCS on adaptation in a sham-controlled, within-subject crossover study, as reported in chapter 3.

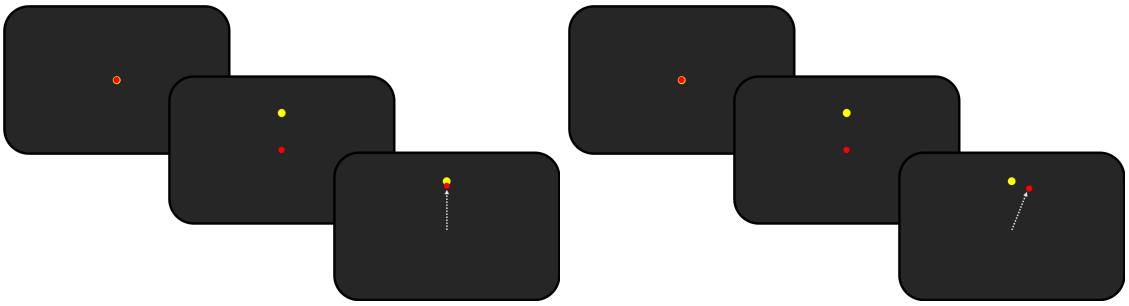
2.4 Visuomotor adaptation task

To investigate the primary aim of this thesis, studying the role of cerebellar GABA in adaptation, I use a novel visuomotor adaptation task designed to drive adaptation processes that engage the cerebellum. As described in section 1.1, visuomotor adaptation tasks are well known and widely used, but different features of a visuomotor adaptation task can be changed to enhance the

contribution of some processes over others. In the following section, I will describe the features of the visuomotor adaptation task used in this thesis and discuss the rationale behind the design of the adaptation task. The features described in this section are shared across all versions of the adaptation task used in this thesis. Those features of the adaptation task, that are specific for the task used in each chapter, are discussed in those respective chapters.

2.4.1 Features of the adaptation task

Participants were positioned in front of a computer screen holding a joystick in their right hand (figure 2.6A). Using the joystick, participants controlled a red cursor (8 mm diameter) on the computer screen (figure 2.4). They were instructed to make discrete movements to a yellow target (8 mm diameter). Specifically, participants were instructed to make fast, accurate and ballistic movements to 'shoot' through the target.



(A) No Rotation trial. (B) Rotation trial.

Figure 2.4: Trial Sequences.

A single trial of the task started with the yellow dot presented at the centre starting position with the red cursor overlaid (upper panels in 2.4). After this fixation period, the yellow dot switched positions to one of eight possible locations around the starting position (middle panels of 2.4). From this point of target onset, participants could perform the centre-out movement with the red cursor to the target. As soon as participants moved the red cursor out of the centre starting position, a timer started and the red cursor disappeared after 250 ms to encourage rapid movements (shooting period, shown in dark red in figure 2.5). The cursor disappeared once it had passed through an invisible boundary circle larger than the target circle.

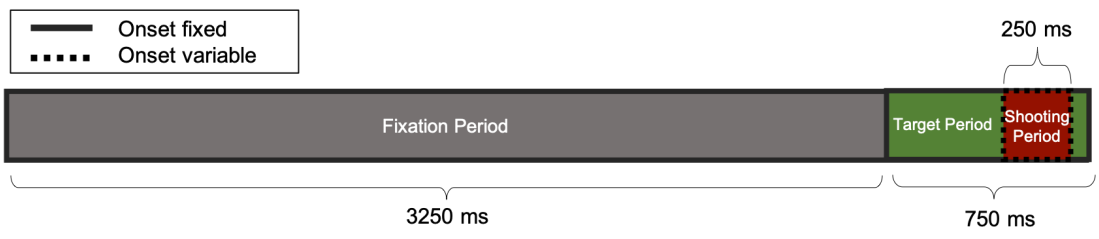


Figure 2.5: Design of a single trial.

The fixation period, i.e. the time between the start of the trial and the target onset, lasted 3250 ms (grey in figure 2.5). The target period, i.e. the time between target onset and target offset, lasted 750 ms (green in figure 2.5). Each trial therefore in total lasted 4 seconds.

The target appeared in one of eight possible locations radially aligned around the centre starting position, separated by 45°. All possible target locations are shown in 2.6B. In this thesis, we will refer to the target at the highest position of the target circle as 0°. The next target clockwise on the target circle is 45°, followed by 90°, 135°, 180°, 225°, 270° and 315°. The order in which the targets appeared was pseudorandomised, so that the order was random but within eight trials all eight possible target locations had to appear.

A stereotypical baseline trial where the participant moves the joystick perfectly to hit the target is shown in 2.4A. In the adaptation version of the task, after a number of baseline trials, the visual feedback of the cursor was rotated by 10°. This resulted in a 10° offset between joystick movement and cursor movement (lower panel in figure 2.4B). Over time, participants learned to adapt to this offset. In the control version of the task, the visual feedback was never rotated.

Vision of the hand holding the joystick was either shielded by a wooden box or prevented naturally by the position of the participant, when participants were lying down inside the MR scanner with the joystick on their lap and the head coil obscuring the view.



(A) MR-safe Joystick.

(B) Possible target positions.

Figure 2.6: Experimental setup.

2.4.2 Tailoring the task to maximize adaptation

With the design of this task, we aimed to maximize engagement of the cerebellum. As outlined in chapter 1, the cerebellum is thought to contribute primarily to learning that is based on sensory prediction errors and that is implicit. Therefore, the features of this task were chosen to minimize strategic components, eliminate online corrections and drive improvements in directional accuracy rather than speed.

First, we provided no endpoint, or any other kind of accuracy feedback, nor feedback about speed to avoid providing any form of explicit reward. Our goal with the task design was to induce a mismatch between the performed movement and the visual feedback, i.e. a sensory prediction error. Although any task will have an inherent reward structure, providing feedback after the end

of each trial about success or failure of any kind could shift the focus away from this prediction error and instead emphasise the task feedback. As outlined in chapter 1, the literature indicates that implicit adaptation can occur at the expense of task success [218]. Therefore, we chose to provide no explicit feedback about task success of any form.

Second, we instructed participants to make short, quick movements that shoot through the target, instead of land on it. This instruction was to ensure the short, ballistic nature of the movement and to prevent online corrections. It also ensures that the emphasis is on the direction (shooting through the target), instead of the extent of the movement (landing on the target). Participants therefore did not have to allocate resources to planning the extent of the movement, but could concentrate on the direction. We also instructed participants to focus on being accurate and prioritise accuracy over speed. At the same time, the trial design required participants to move quickly and left little time for explicit re-aiming or mental rotation of the target. This instruction in combination with the trial design aimed at allowing participants to focus on the relevant learning component (direction), while impairing the ability to form explicit strategies to aid adaptation.

Third, we introduced a relatively small rotation of 10°, incrementing in steps of further 10° every 40 trials. This design was similar to the one used in [169], which showed that adaptation to a stepwise incrementing rotation resulted in more adaptation than to an abruptly introduced rotation of the same ultimate extent. We chose this stepwise rotation sequence for several reasons. The aforementioned study [169] indicates that we are able to maximize adaptation with this design. Importantly, with this we aim to drive adaptation over an extended period of time, keeping the adapting system engaged. Despite maximising adaptation, this task design keeps participants largely unaware of the imposed rotation. According to a recent study [98], trial-to-trial endpoint variability in reaching movements without perturbations determine the size of the perturbation that can be detected in later trials with an applied perturbation. Specifically, only perturbations that exceed 1.5 times the standard deviation of trial-to-trial endpoint variability are verbally reported. This finding could indicate that in visuomotor adaptation a perturbation that is smaller than 1.5 times the angular error stays below the threshold of awareness. In our task, baseline variability of a single subject's angular error exceeds 1.5 times of our imposed rotation (15°) by far. Therefore, our task design minimized explicit awareness of the imposed rotation. Nevertheless, in order to be able to control for potential awareness of the rotation, we assessed participant awareness after the last testing session of the experiments reported in chapter 3 and 5.

Fourth, in our task, participants adapted to eight targets, instead of fewer target directions. Having more target directions increases task difficulty and decreases the rate at which participants adapt. It also imposes difficulties when modelling adaptation performance computationally, as discussed in the later section 2.5.3. However, adapting to eight targets reduces the likelihood of

the participant becoming aware of the imposed rotation. Moreover, it makes it harder for the participant to observe the stepwise change in rotation, reducing the likelihood of the participant understanding the underlying task structure of a stepwise increasing rotation. Keeping the participant unaware of the underlying task structure likely reduces the use of strategies, because the participant cannot predict how and when the rotation is going to change and is therefore unable to form an explicit strategy from that knowledge. We thereby reduce explicit contributions to adaptation.

It should be noted that there are other task designs that help control for explicit contributions to adaptation. Most notably, verbal reporting of aiming direction after each trial [220] and constraining reaction times on each trial below 100 ms by providing feedback about speed ('Too slow') [221]. Although modifications of the adaptation task have been shown suitable for dissociating implicit and explicit contributions to adaptation, we did not choose to incorporate them into our task design. Verbal reporting during the adaptation task bears the risk of increasing awareness of the imposed rotation, as participants will consciously evaluate where they aimed in order to report aiming direction, which might lead them to reflect on a potential manipulation by the task. While posing a good measurement of explicit contributions, this method can therefore increase use of explicit strategies. We also did not constrain preparation time in our task below the 250 ms time window, described above, for two reasons. First, as described before, providing feedback about speed could unintentionally shift the participant's attention to the wrong task dimension, i.e. speed. Second, the adaptation task used in this thesis was designed for the purpose of performing it inside the scanner. Considerably constraining reaction time could increase participant arousal to the point that participants will make 'jerking' movements at every trial. This could result in severe movement artefacts, which would reduce our ability to track MRS-assessed neurotransmitter changes. We therefore chose to not constrain reaction times below the outlined 250 ms, a time window that was perceived as manageable during piloting.

Lastly, some of the results presented in this thesis are based on adaptation data that was acquired in different postures, specifically the data presented in chapters 4,5 and 6. In the experiments presented in these chapters, the adaptation task was performed inside the scanner, where the participant was lying down. The compensatory movement was then washed out during a washout phase performed outside of the scanner after the scan had finished. During this washout phase, participants were seated in front of a computer screen, rather than lying down. Our working assumption for these experiments is that changing the posture does not change the underlying learning that is being expressed. That is, the same cursor movements (extrinsic coordinate frame) are now governed by slightly different intrinsic movements (intrinsic coordinate frame). Our assessment of washout assumes that the previously learned compensatory movement generalizes to

the new posture. Therefore, we assume that adaptation is taking place in an extrinsic coordinate frame, rather than in an intrinsic coordinate frame [189]. In visuomotor adaptation, there is evidence suggesting that adaptation occurs in an extrinsic coordinate frame [185], while force field adaptation is more intrinsic [316] [318]. However, recent studies suggest that there are multiple reference frames in both visuomotor and force-field adaptation [29] [39] and the reference frames in which adaptation occurs is an area of ongoing research.

2.5 Quantifying adaptation

The task paradigm used in this thesis is different from traditional paradigms and I therefore wanted to test whether results relating to modelling-free indices of adaptation behaviour in our task hold when using modelling-based indices of adaptation. Adaptation in this thesis is therefore quantified using modelling-free as well as modelling-based methods.

In the following section, I will describe the modelling-based approach to quantify adaptation. The modelling-free approach to quantify adaptation is described in the respective chapters.

2.5.1 Single-state state-space model

As described in subsection 1.1.5, we can use *state-space models* to model adaptation.

The State-Space Model (SSM) we are considering here in its simplest form uses two equations to describe the learning process.

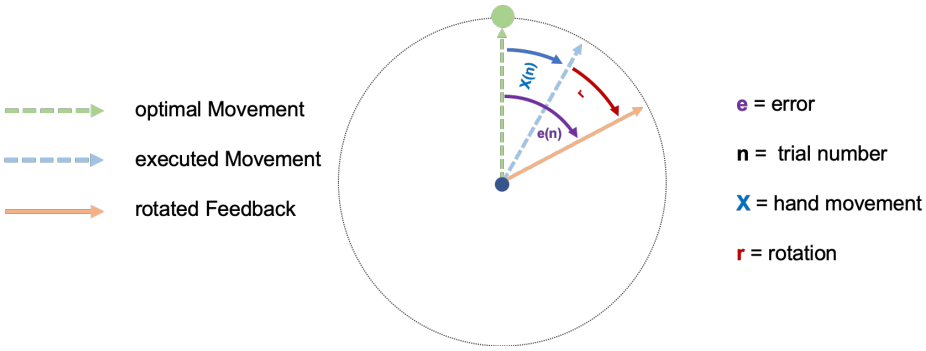


Figure 2.7: Single-state state-space model describes the error.

The first equation

$$e(n) = X(n) + r \tag{2.3}$$

describes that the error at trial n is given by the movement X at trial n plus the rotation.

The second equation

$$X(n) = A * X(n-1) - B * e(n-1) \tag{2.4}$$

where:

$$A = Retention\ Parameter$$

$$B = Adaptation\ Parameter$$

$$and\ X,\ e\ and\ r\ as\ in\ figure\ 2.7$$

describes how the movement X at trial n results from the previous movement *X(n-1)* and the previous error *e(n-1)*. Both terms on the right side of equation (2.4), *X(n-1)* and *e(n-1)* are weighted by a factor A and B, respectively. The previous movement *X(n-1)* is weighted by a so-called retention factor A. This retention factor reflects that only a fraction of the previous movement is retained. The previous error *e(n-1)* is weighted by an adaptation factor B. This adaptation factor reflects that the next movement corrects only for a fraction of the error. Retention factor A and adaptation factor B are real numbers between 0 and 1.

$A = 1$ would mean that, in the absence of error (e.g. through removed or clamped feedback), movements are retained perfectly. $A < 1$, in the absence of error, corresponds to a decay of the adapted movement, with the decay becoming quicker, the smaller the value of A. For this case ($A < 1$), one can also show that during adaptation, the adapted movements never compensate for the full perturbation. This means that errors do not fully return to baseline during adaptation, which has been experimentally established in visuomotor adaptation [362] [366].

The higher the adaptation factor B, the more a movement is corrected for the error on the previous trial. It can therefore also be understood as sensitivity to error. The adaptation factor commonly takes values between 0.1 and 0.3, but can be lower depending on the task [106] [325] [100].

From equations (2.3) and (2.4) one can derive a recursion formula for the error e:

$$\begin{aligned} e(n) &= A * X(n-1) - B * e(n-1) + r \\ &= (A - B) * e(n-1) + (1 - A) * r \end{aligned} \tag{2.5}$$

Using equation 2.5, we can now model the adaptation process. That is, for a given retention factor A and adaptation factor B, we can calculate the errors at each trial from equation 2.5. We can then compare those errors to the measured errors from participant data and quantify the difference, for example as sum of the squared differences between the errors. Using gradient descent algorithms to minimize the sum of squares, we can find values for the parameters A and B such that the resulting error function e forms an optimal fit for the data. As mentioned before, adaptation is well described by an exponential curve [62]. Accordingly, the error function e gives an optimally fitting exponential curve.

2.5.2 Dual-state state-space model

The dual-state state-space model extends the single-state state-space model by including two systems that adapt in parallel but at different timescales [325]. It consists of the fast system, which adapts quickly and forgets quickly, and the slow system, which adapts slowly and forgets

slowly. Accordingly, for the dual-state state-space model, equations 2.3 and 2.4 take the form

$$e(n) = X_{fast}(n) + X_{slow}(n) + r \tag{2.6}$$

and

$$\begin{aligned} X_{fast}(n) &= A_{fast} * X_{fast}(n-1) - B_{fast} * e(n-1) \\ X_{slow}(n) &= A_{slow} * X_{slow}(n-1) - B_{slow} * e(n-1) \end{aligned} \tag{2.7}$$

where:

$$\begin{aligned} e &= error \\ n &= trial\ number \\ r &= rotation \\ X_{fast} &= Movement\ fast\ system \\ A_{fast} &= Retention\ Parameter\ fast\ system \\ B_{fast} &= Adaptation\ Parameter\ fast\ system \\ X_{slow} &= Movement\ slow\ system \\ A_{slow} &= Retention\ Parameter\ slow\ system \\ B_{slow} &= Adaptation\ Parameter\ slow\ system \end{aligned}$$

Analogously to 2.5, the equation governing error reduction reads:

$$\begin{aligned} e(n) = {} & A_{fast} * X_{fast}(n-1) - B_{fast} * e(n-1) \\ & + A_{slow} * X_{slow}(n-1) - B_{slow} * e(n-1) + r \end{aligned} \tag{2.8}$$

To ensure that one system adapts and forgets fast and the other one slow, the parameters of

the two systems are constrained such that:

$$0 < A_{fast} < A_{slow} < 1$$

$$0 < B_{slow} < B_{fast} < 1$$

Analogously to the single-state case before, one can find values for the dual-state case now for A_{fast}, A_{slow}, B_{fast} and B_{slow} such that the error function e forms an optimal fit for the data. One can show, that in this case the error function e is an optimally fitting sum of two exponential curves.

2.5.3 Generalization

When modelling adaptation in more than one direction, for example in an eight-target visuomotor adaptation task like the one used in this thesis, it is important to consider how much the error experienced on one target in one trial generalizes to other directions in the next trial. That means a further extension over and above both the single-state and the dual-state state-space models mentioned before. These imply that errors experienced in the direction of the 0° target generalize perfectly to all other targets, be it 45°, 90°, 135°, 180°, 225°, 270°, 315°. In the terminology of state-space models, this would mean that the adaptation parameter B, which determines the fraction of the error experienced on the current trial, that the next movement will be corrected for, is the same regardless of how far the next target is separated from the current target. In other words, there is complete generalization of error experienced on the current target to all other targets. In contrast, if generalization depended on how far the current and the next target were separated, then the adaptation parameter B would be multiplied by a generalization parameter that varied depending on the target separation between zero and one. Were there no generalization from the current to the next target, then the generalization parameter would be zero. Conversely, for full generalization, the generalization parameter would take a value of one. For example, full generalization occurs when two consecutive trials are performed to the same target. For an eight-target adaptation task, there are eight possible generalization parameters, each of them determining the amount of generalization for a particular target difference.

The generalization function takes as input the target difference and returns the generalization term. When modelling adaptation on a task that includes more than one target direction using a state-space model which does not allow for the generalization parameter to vary depending on target separation, the model implicitly assumes that the error experienced at one target generalizes to all other targets. Hence, the generalization function for such a model takes a value of one regardless of separation between consecutive targets.

It has been shown in visuomotor adaptation that the further away two consecutive targets are,

the less adaptation generalizes [344]. Target separation of more than 45° angular distance lets generalization drop to values close to zero [344] [39] [53] [185]. Hence, when modelling adaptation on a task that includes more than one target direction, generalization should be considered.

There are two approaches commonly taken to deal with incorporating generalization into a single-state state-space model. One is to use a fixed generalization function that has been estimated on the basis of separate experiments, for example taking the values from previous literature as done in [100]. This approach can be applied when the experimental design makes comparison of a generalization function between participants difficult, because the sequence of targets is different for every participant [100].

Another approach is to model the generalization function for each individual from the data directly [344]. In the case of an eight-target adaptation task we would then get eight adaptation parameters for the single-state state-space model instead of the one parameter B before. So together with the retention parameter A this gives a total of nine parameters to estimate.

Accordingly, extending the dual-state state-space model to capture generalization would lead to a total of 18 parameters.

2.5.4 State-space models used in this thesis

In this thesis, we use state-space models to corroborate any results that we have found with modelling-free quantification of adaptation.

In chapter 3, we tested for an effect of cerebellar tDCS on overall adaptation. We chose the single-state model, as our hypothesis did not relate to a particular system in the dual-state model and we set generalization to 1, since the target sequence differed between sessions in this study and therefore comparison of generalization functions would be difficult across sessions and participants.

In chapter 4 and 5, we applied the single-state state-space model with and without generalization, respectively. Although the target sequence for the data used in these chapters differed between participants, we wanted to ensure that the results shown with the modelling-free method in chapter 5 hold when generalization is captured by the model.

Lastly, we used a target sequence fixed across participants for the experiment in chapter 6. We applied both, the single-state state-space model as well as the dual-state state-space model to the data in this study. The single-state state-space model included a generalization function estimated from the data. The dual-state state-space model did not include a generalization function estimated from the data, because of the aforementioned difficulties to estimate 18 free parameters from the data (problem of overfitting). The dual-state state-space model was applied in this study, as we hypothesized that one of the systems, the slow system, would relate to the measured MRS data.

CHAPTER 3.0

The effects of cerebellar tDCS on visuomotor adaptation

Abstract

The cerebellum is a part of the motor network which is involved in motor adaptation. Anodal transcranial direct current stimulation (tDCS) applied to the cerebellum has been found to cause faster adaptation as shown by a more rapid reduction of movement errors. However, replicating this result has been difficult. To investigate the effect of cerebellar stimulation on adaptation, we conducted a within-subject, double-blind cerebellar tDCS study using a novel task design.

Methods. 29 healthy, right-handed participants (17 female) attended two experimental sessions (counterbalanced, at least 7 days apart) during which they received either anodal or sham tDCS to the cerebellum (20 min, 1.5 mA). During stimulation, participants performed a visuomotor adaptation task in which participants were required to adapt their joystick movements to an rotation between an on-screen cursor and the joystick. The rotation increased every 40 trials by 10 degrees. This 37-minute adaptation period was followed by a washout period where participants completed 10 minutes of baseline trials which involved no angle offset. Adaptation performance was quantified with a modelling-free analysis as well as a modelling-based analysis by computationally modelling the adaptation behaviour using a single-rate state-space model.

Results. We found no significant effects of anodal tDCS compared to sham tDCS on visuomotor adaptation. However, there was significantly improved adaptation in the second session, suggesting the presence of savings from the first session.

We were unable to replicate a facilitatory effect of cerebellar tDCS on visuomotor adaptation. Although we cannot rule out the possibility that stimulation did not affect adaptation behaviour, a true effect of stimulation was potentially obscured by savings in the adaptation performance of the second session. Although the within-subject design of this study had the advantage of controlling for inter-individual variability in the response to tDCS, effective washout techniques are needed to remove the influence of task experience on performance.

3.1 Introduction

Motor adaptation is commonly defined as the reduction of systematic errors in response to an imposed perturbation in order to return performance to baseline levels. Humans are constantly required to adapt motor commands to changing properties of the environment, be it to internal perturbations such as disease, injury, fatigue, exercise or growth, or to external perturbations such as to the weight or size of different objects, or to external forces acting on the object (e.g. wind). In a clinical context, motor adaptation has been studied as a potential therapeutic intervention [257] and impairments in motor adaptation have been proposed as a behavioural biomarker of future motor deficits in spinocerebellar ataxia [275]. Adaptation is therefore a fundamental property of the central nervous system and understanding the neural basis of adaptation could have important clinical implications.

In an experiment, perturbations to which participants need to adapt to can be imposed through prism glasses, a force-field or through rotated visual feedback. Motor adaptation is considered distinct from motor skill learning, as it does not require the acquisition of a novel skill, but rather the return to a former, baseline level of performance by remapping movements that are already well learned with a target in space. Motor adaptation is thought to rely on the formation of an internal model of the environment updated on the basis of sensorimotor prediction errors [231] [184]. These prediction errors are computed by comparing the predicted consequences of the motor command with sensory feedback. The cerebellum has been proposed as a likely site for the formation of this forward model [144], and studies in which cerebellar function was disrupted through transcranial magnetic stimulation (TMS) [232] or lesioned in patients [358] support this notion. Specifically the lateral and anterior cerebellum [144] are candidate regions for this process and a recent quantitative meta-analysis of functional activation in response to motor tasks [123] has confirmed the involvement of the bilateral and anterior medial cerebellum in sensorimotor tasks.

Anodal trancranial direct-current stimulation (tDCS), a non-invasive stimulation technique, applied while healthy subjects perform a visuomotor adaptation task, has been shown to facilitate error reduction compared to sham stimulation [101]. This effect on visuomotor adaptation has been replicated in young healthy subjects [395] [33] and older adults [122] [273] and extended to other adaptation paradigms such as force-field adaptation [129], locomotor adaptation [159] and saccade adaptation [274] [15]. However, some studies have reported no effect of cerebellar tDCS on adaptation [158] [209] and a recent replication effort has found the effect of the original study [101] to be difficult to replicate and revealed only small to medium effect sizes [158].

There has been growing interest in the use of cerebellar tDCS as an intervention to enhance stroke recovery. The cerebellum is a promising site for therapeutic stimulation because of its inherent plasticity and dense connections to cortical areas, and due to evidence suggesting

modulation of cerebellar function through tDCS is possible [377] [262] [365] [99]. However, for cerebellar tDCS to be implemented in a clinical context, the conditions under which a reliably facilitatory effect of cerebellar tDCS exists needs to be consolidated. To this end, the aim of the present study was to attempt to replicate the facilitatory effect of cerebellar anodal tDCS on visuomotor adaptation using a novel adaptation task paradigm and a within-subject design.

To increase the likelihood of observing an effect of cerebellar stimulation, we used a visuomotor adaptation task designed to bias learning towards processes thought to primarily recruit the cerebellum. In this task, a stepwise increasing rotation required participants to adapt movements to reduce errors, with the rotation increased by 10 degrees every 40 trials. Imaging studies of cerebellar involvement in motor coordination revealed high activation of the cerebellum during correction of and learning from significant movement errors [145] [227]. Since these studies show high cerebellar BOLD signal during early performance errors, we reasoned that having participants adapt to a consistently increasing rotation would keep adaptation learning from reaching a plateau (in other words, keep participants from reducing their performance errors to asymptotic levels) and facilitate engagement of the cerebellum. However, each step in rotation was only small in magnitude compared to commonly used visuomotor adaptation paradigms, as we added only 10 degrees to the rotation angle every 40 trials. Although adaptation is traditionally thought to be an implicit form of learning [169] [179], various researchers have proposed that participants can employ explicit strategies to overcome the rotation [218] [134] [127] [348] [345] [346]. Taylor and colleagues [348] have shown both explicit and implicit mechanisms contributing to adaptation and highlighted how different features of the adaptation task can lead to more engagement of one type of learning over the other. To note, abrupt, large visual rotations have been shown to reduce learning from sensory prediction error and enhance strategic learning, whereas smaller rotations amplify implicit, sensory prediction error dependent learning [220] [348] [37]. We therefore chose small step sizes in order to bias adaptation learning towards implicit forms of learning that rely on sensory prediction error. However, it should be noted that there is evidence that the cerebellum contributes to both explicit and implicit processes in sensorimotor adaptation [375] and that distinct regions of the cerebellum are involved in different phases of adaptation, thought to reflect explicit and implicit processes [192] [204] [306].

A common feature of studies investigating cerebellar tDCS is a between-subject design which can, however, limit the ability to observe consistent effects of stimulation. Generally, tDCS studies suffer from a source of great inter-subject variability, probably due to differing anatomy of the subjects' head and the responsiveness of an individual to tDCS. Modelling studies demonstrate distributions of the current density largely depend on the anatomical composition of the stimulated head [266]. Moreover, a study examining the effects of M1 tDCS on corticospinal excitability found

that 50 % of individuals showed only a small or no effect of tDCS on corticospinal excitability, suggesting large inter-subject variability in the response to tDCS [379]. These sources of variability can be minimized with a within-subject design. However, to employ a within-subject design to study adaptation to overcome this requires a design that ensures no learning carries over from one session to the next. When an individual is re-exposed to an adaptation protocol, faster adaptation rates (known as savings) can still be evident weeks after the initial exposure [186].. However, trials in which participant's the adapted state is 'washed out' by performing the task without perturbation have been shown to effectively interfere with the consolidation of the task memory and eliminate savings [135], when completed immediately after the adaptation task. In our study participants therefore performed a washout block immediately after completing the rotation task in an effort to remove any influence of prior task experience on the second exposure.

In addition to a replication of the facilitatory effect of cerebellar tDCS on motor adaptation, a secondary aim of this study was to establish a tDCS protocol for studying learning and tDCS-related changes in the cerebellum compatible with Magnetic Resonance Spectroscopy. We therefore chose to test a tDCS protocol using 1.5 mA as this is the limit for current applied inside the MRI scanner. Although most studies on cerebellar tDCS use a higher current (2 mA) [262], a current of 1.5 mA has been shown to lead to faster visuomotor adaptation [197] and saccade adaptation [15]. Moreover, evidence from a sham-controlled, within-subject study combining cerebellar tDCS with fMRI suggests that anodal stimulation targeting the right lateral cerebellum with a current of 1.5 mA is sufficient to increase cerebellar activation in this area [63].

In summary, we hypothesised that, during the stimulation, anodal cerebellar tDCS would facilitate visuomotor adaptation when compared with sham tDCS, corresponding to previous findings [101]. We expected this improved adaptation to be evident when quantifying adaptation using a modelling-free analysis approach as well as when computationally modelling adaptation behaviour in a modelling-based approach. We expected the stimulation to have no effect on retention, in line with previous studies [101].

3.2 Methods

3.2.1 Participants

We recruited twenty-nine healthy participants (17 female; 18-32 years; mean age 26 years) from the general public to participate in a within-subject, double-blind study. Each participated in two sessions in which they received either anodal or sham tDCS to the cerebellum while performing a visuomotor adaptation task. The order of sessions was counterbalanced, with 12 participants receiving real stimulation in the first session. Participants had no contraindications to tDCS, no history of neurological or psychiatric conditions and were not taking any medications that can

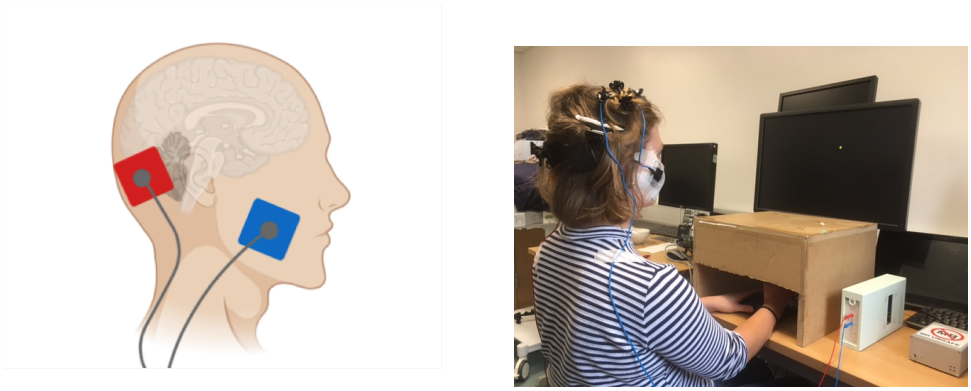
affect the central nervous system. All participants gave informed consent in line with central university research ethics committee regulations (University of Oxford; R53867/RE001) and were compensated for their time (see Table 3.1 for sample characteristics). All participants were right-handed as assessed by the Edinburgh Handedness Inventory [261].

Participants	
Recruited	29
Excluded	2
Final Sample	27
Gender	17 Female
Age	26 (±4.29)
1st Session Real	12
Days between sessions	8.4 ± 1.6

Table 3.1: Sample Characteristics.
Participants were excluded due to no or insufficient data in the second session.

3.2.2 Experimental Protocol

Participants were seated approximately 60 cm in front of a computer monitor (see figure 3.1B). Participants controlled a cursor on the computer screen using a joystick and made discrete movements to targets at eight possible locations around the central starting position. They were instructed to make fast, accurate and ballistic movements to 'shoot' through a target that appeared on the screen. The target appeared in a randomized fashion at one of the eight locations radially aligned around the starting position of the cursor. Participants had to perform the movement within a time window of 750 ms, after which the target disappeared. This was to ensure the short, ballistic nature of the movement and to prevent online corrections. The cursor was visible and no specific endpoint feedback was provided.



(A) Schematic Visualisation of tDCS Montage. (B) Task and tDCS Setup.

Figure 3.1: Experimental Setup.

At the beginning of each session, participants practised the task by performing 40 baseline trials (no rotation imposed, figure 3.3A.). Participants then performed the main task (figure 3.3B.), during which they learned to adapt to a stepwise increasing rotation of their movement (figure 3.2A.). During the main task, there was a brief pause of variable length (66 ± 36 seconds, range: 30-238) in the task between the first and the second baseline block to turn on the tDCS. To probe how much of the previously learned rotation participants retained, three blocks with removed visual feedback were interspersed (figure 3.3C. and figure 3.2A.). After each block with no visual feedback, there was a short break of 20 seconds. After the main task, participants performed 144 baseline trials to wash out the previously learned rotation.

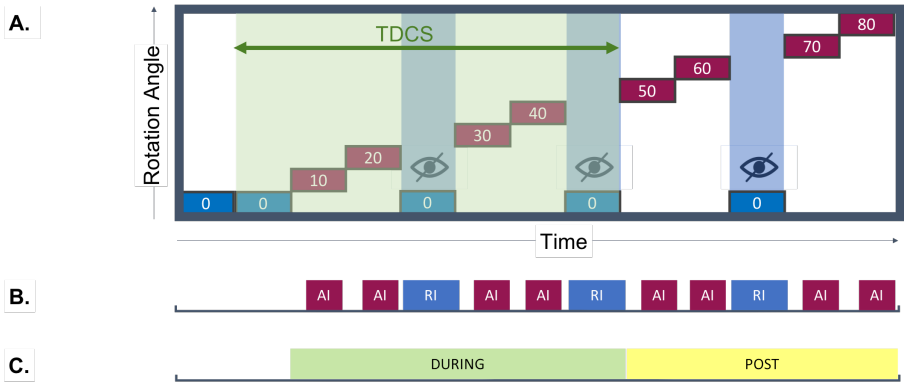


Figure 3.2: Task Protocol.
A. Stepwise increasing rotated feedback required participants to adapt movements to reduce errors (40 trials of 4 seconds duration each). Rotation was washed out after task (144 trials, no rotation). Light blue: visual feedback removed. Light green: tDCS applied.
B. Calculation of behavioural indices. Adaptation Index (AI) was calculated by averaging the error of all adaptation trials, excluding trials 1-8 of each adaptation block. Retention Index (RI) was calculated by averaging the error in all blocks where visual feedback was removed.
C. Stimulation Phases.

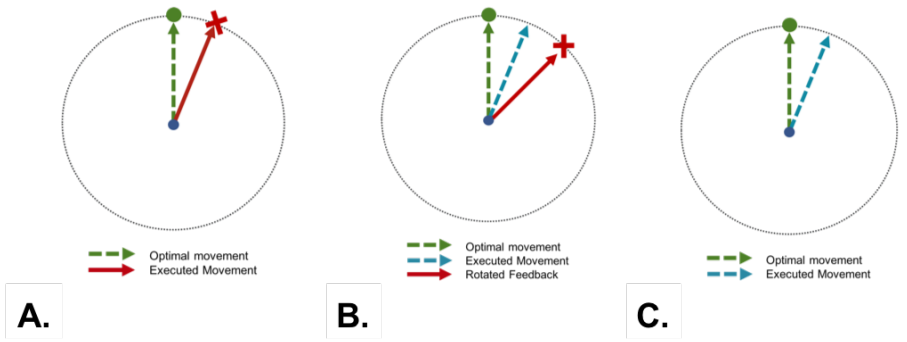


Figure 3.3: Trial Types.
A. Baseline Trials. Visual feedback is veridical.
B. Adaptation Trials. Visual feedback is rotated.
C. Retention Probe Trials. Visual feedback is removed.

3.2.3 tDCS

A DC-Stimulator (Magstim, Ltd; UK) delivered a 1.5 mA (0.06 mA/cm^2) current to the brain via two square electrodes measuring 5 x 5 cm (Easycap, GmbH; Germany) attached to the head using Ten20® conductive paste (Neurodiagnostic Electrode Paste, Weaver and Company, USA). The anodal electrode was centered on the right cerebellar cortex, placed 3 cm to the right of the inion in line with the pre-auricular point [101]. The reference electrode was placed over the right buccinator muscle (see figure 3.1). This montage was in accordance with previous studies [101] [99]. During anodal stimulation, the current was ramped up over 10 seconds and held at 1.5 mA for 20 minutes, then ramped down over 10 seconds. For sham stimulation the DC-stimulator was ramped up for 10 seconds and after 30 seconds ramped down for 10 seconds at the beginning of the stimulation interval and then again after 20 minutes, as previously described [332].

At the end of each session, participants were asked to report adverse sensations experienced during the stimulation and how strongly they believed these sensations to be caused by the stimulation (reported in table 3.2). Participants and experimenter also reported the perceived stimulation condition (Table 3.3).

3.2.4 Data Analysis

3.2.4.1 Preprocessing

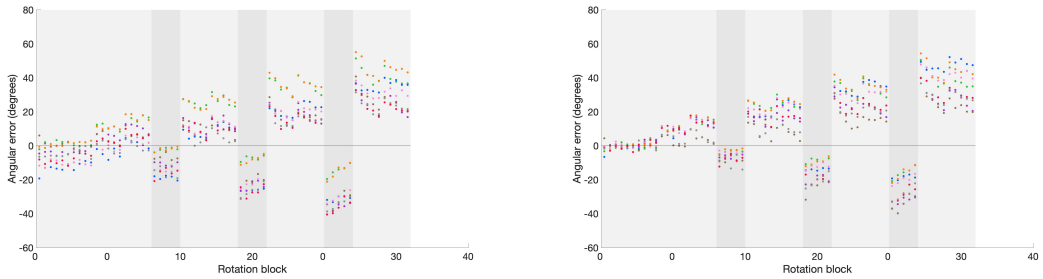
Cursor movements were analysed on a trial-by-trial basis using in-house software written in Matlab (Mathworks Inc, Natick, USA). The joystick position data (x- and y-coordinates) was collected at a sample rate of 60 Hz. The kinematic data was filtered with a zero-phase filter with a 25 Hz cut-off and numerically differentiated to determine velocity. For each trial, the angular error (°) was calculated as the angle between a line connecting the starting position with the position of peak velocity of the cursor and the line connecting the starting position with the target. Positive values indicate a clockwise error ('overshooting') and negative values indicate a counter-clockwise error ('undershooting').

We checked the calculation of angular error on the basis of peak velocity trial-by-trial. Trials with premeditated or otherwise poorly defined movements (i.e. movements that stopped before reaching half of the distance to the target circle) were rejected from further analysis (12.3 ± 12.2 trials excluded on average, range 0-55, which is approximately 0.02 ± 0.02 % of trials, range 0-10 %).

3.2.4.2 Target Bias

From visual inspection of the adaptation data it was evident that participants exhibited a different systematic bias towards each of the 8 targets (see figure 3.4A showing the adaptation data colour-coded by target). For most of the targets, this baseline bias was negative, meaning

participants 'undershoot' when shooting at the target. Because the imposed rotation at the beginning of the task is positive and relatively small, a large negative baseline bias could obscure successful adaptation. We therefore removed each subjects' bias for each session for each target. The target bias was calculated by averaging the error of trials shot towards the target during the two baseline blocks of the session. It was then subtracted from errors of the respective trials of the session (see figure 3.4B).



(A) Target Bias not removed.

(B) Target Bias removed.

Figure 3.4: Target Bias. Participants exhibit a different systematic bias towards each of the 8 targets as evident from the two baseline blocks. After the individual target bias has been subtracted from the data, adaptation performance still varies between targets. Data for the 8 targets is averaged across participants and colour coded.

3.2.4.3 Modelling-free Analysis

A modelling-free index for adaptation performance was calculated by averaging the error in all adaptation blocks, across all trials excluding the first 8. Excluding the first 8 trials of each adaptation block is standard [101] and has been established as a measure of adaptation as it captures the rapid error reduction of the adaptation performance rather than performance during the initial exposure to the rotation [187]. The blocks that went into calculating the adaptation index are marked with dark red blocks in figure 3.2B. This index for adaptation performance is referred to as the Adaptation Index (AI). This adaptation index is different from the adaptation index commonly used in force-field adaptation [322]. A separate adaptation index was calculated for adaptation during the stimulation period (Green rectangle in 3.2C.) and for adaptation during the full task period (During and Post, green and yellow rectangle in figure 3.2C.).

A Retention Index (RI) was calculated by averaging the error in all blocks with no visual feedback, also in line with previous literature [101]. See blue blocks in figure 3.2B.

3.2.4.4 Modelling-based Analysis

We used a single-state state-space model (SSM) [71] to model trial-by-trial adaptation for each subject for each session. By computationally modelling the individual subjects' behaviour during the adaptation task, we can extract an adaptation parameter (Parameter B) and a retention parameter (Parameter A) for every subject for every session.

As discussed in section 2.5, the adaptation parameter B reflects the rate of adaptation or the *adaptation rate*. This is the fraction of the error that the participant corrects for at each trial. A larger adaptation parameter B therefore means the participant adapts quicker and reflects better adaptation performance.

The retention parameter A reflects how much the participant retains the previous movement. The retention parameter therefore governs the rate of forgetting when visual feedback is removed (light blue blocks with crossed out eyes in figure 3.2).

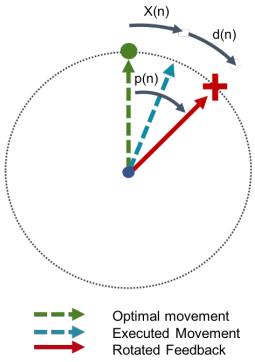


Figure 3.5: Single-state state-space model.

A detailed description of the SSM can be found in section 2.5. In brief, the SSM used in this chapter takes the following form:

$$X(n) = A * X(n-1) - B * p(n-1) \tag{3.1}$$

$$p(n) = X(n) + d(n) \tag{3.2}$$

where:

$$X = Movement$$

$$n = trial\ number$$

$$A = Retention\ Parameter$$

$$B = Adaptation\ Parameter$$

$$p = error\ point$$

$$d = imposed\ rotation$$

Adaptation across targets. As a first approximation of the adaptation process, we modelled adaptation across all targets, using all of the available data from the experiment. It should be

noted that previous modelling studies of visuomotor adaptation revealed that adaptation learning does not generalize beyond adjacent targets separated by more than 45 degrees [344]. Past studies have therefore estimated a generalization function from the experimental data, which quantifies how much participants generalised from one target to the next [343]. However, in order to estimate a generalisation function from the data with some accuracy, it is crucial to have a fixed sequence of presented targets for all participants. Since this experiment was not designed to estimate a generalisation function from the data it operated with a target sequence that was randomised across participants and we therefore set the generalisation across targets to 1, assuming complete generalisation from one target to the next.

Adaptation to different targets. As evident in figure 3.4B, even with the baseline bias removed adaptation performance for each individual target still differs. To investigate target specific adaptation, we therefore also modelled adaptation behaviour separately for each target.

When modelling adaptation for a specific target, we modelled adaptation only on trials performed to specific targets and treated all other trials as missing data, but did not remove them from the data. For example, when modelling adaptation to only the 90 degree target, trials that occur to any other target than the 90 degree target are not taken into the calculation of the model fit. However, these trials are not removed from the data in order to preserve the duration over which adaptation took place in the experiment. One could imagine that if the sparse trials that are performed to the 90 degree target shown in figure 3.11A as black dots were to be concatenated, then the duration over which adaptation takes place is shortened considerably. If the model were to estimate adaptation parameters on the basis of this shortened data with no gaps between the trials, we would artificially inflate adaptation parameters due to the rapid decrease in error over trials that are in fact spaced further apart in the experiment. To avoid this, we instead set all errors during trials that should be ignored by the model to 'not a number' and calculated the model fit on the basis of only the error data from valid trials.

3.2.4.5 Statistical Analysis

All statistical tests were performed using R [287].

Between-subjects analysis. To test the effect of stimulation on adaptation within the first and the second session separately, we constructed a general linear model of adaptation performance. We entered session and stimulation (without interaction term) into the model. P-values were obtained by comparing the computed F-value for the explanatory variable in question with the critical F-value given the degrees of freedom.

Within-subjects analysis. To test the effect of stimulation on adaptation, we used the R package lme4 [23] to construct a linear mixed effects model of adaptation performance. As fixed effects, we entered session and stimulation (without interaction term) into the model. We allowed intercepts

for different subjects to vary in order to account for covarying residuals within subjects, creating a random intercept model. Visual inspection of residual plots did not reveal any obvious deviations from homoscedasticity or normality. P-values were obtained by likelihood ratio tests of the full model with the effect in question against the model without the effect in question.

3.3 Results

3.3.1 Baseline values are comparable across sessions

To test for differences in baseline error between real and sham stimulation sessions, a linear mixed effects model of mean error at baseline was constructed before and after target bias correction, with stimulation as fixed effect and varying intercepts for subjects. There was no significant difference in baseline performance before or after correcting for individual target bias (before bias correction: $\chi^2(1)=1.64$, $p>.1$; after bias correction ($\chi^2(1)=1.48$, $p>.1$)).

There was no difference in ratings of adverse sensations between the stimulation conditions (see table 3.2) and blinding of experimenter and participant was successful, as correct guesses of condition were at or below chance level (see table 3.3). In the first session, participants' correct guesses were well below chance level. This was because 24 out of 29 participants guessed that they had experienced real stimulation after the first session. It it is unclear why participants were biased towards guessing they had received real stimulation in the first session.

	Real	Sham
Pain	0,36 (±0,61)	0,36 (±0,67)
Fatigue	0,52 (±0,71)	0,52 (±0,75)
Mood	0,08 (±0,27)	0,00 (±0,00)

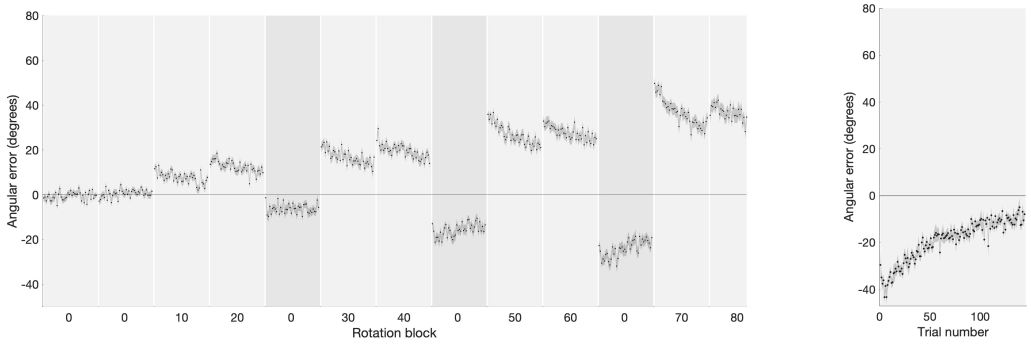
Table 3.2: Summary of Adverse Sensations.
Adverse sensations were assessed using a questionnaire based on the adverse effect questionnaire proposed by [42]. Questionnaire consisted of 12 items. Each item asked about the presence of a potential adverse effect ("Did you experience any of the following during the session?"), and about the participants' belief that this effect was related to the stimulation ("If yes, how strongly do you think it was related to tDCS?"). For example, items asked about experience of headache, scalp pain, fatigue, sleepiness and mood change. Presence of the effect was indicated on a four-point rating scale (0: Absent; 1: Mild; 2: Moderate; 3: Severe). Belief about the effect being related to the stimulation was indicated on a five-point rating scale (0: Not at all; 1: Remotely; 2: Possibly; 3: Probably; 4: Definitely). To summarise the responses, items were grouped into three categories (Pain, Fatigue and Mood). Shown here for each category is the response to the question about presence of adverse effects averaged across participants for each session separately. There was no difference in the extent to which participants reported the presence of potential adverse effects between the real and sham sessions.

Blinding	Participant	Experimenter
Correct guesses		
Session 1	26 %	46 %
Session 2	48 %	51 %
Certainty		
Session 1	75,17 (± 17,45)	
Session 2	73,52 (± 15,70)	

Table 3.3: Blinding Success.
Participants and Experimenter indicated whether they believed the session involved real or sham stimulation at the end of every session. Participants also rated their certainty in percent. In both the first and the second session the participants and the experimenter guessed the stimulation condition at or below chance level.

A linear mixed effects model of mean error at baseline was constructed before and after target bias correction, with session as fixed effect and varying intercepts for subjects revealed no significant difference in baseline performance before or after correcting for individual target bias (before bias correction: $\chi^2(1)$=0.41, p>.1; after bias correction ($\chi^2(1)$=1.59, p>.1)).

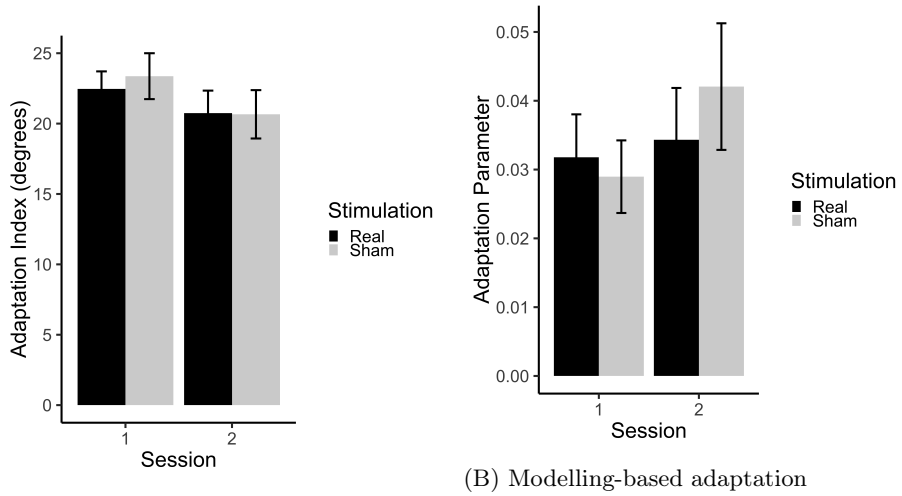
3.3.2 Participants adapted to the rotation



(A) Adaptation. (B) Washout.

Figure 3.6: Behavioural data. Individual data points are averaged across participants and sessions. Shaded area shows the standard error of the mean.

Participants learned to compensate for the imposed rotation until the end of the experiment, shown by a significant reduction in error in the last block of the main task (80° rotation block in figure 3.6A; Paired t-test between initial eight and last eight trials $t(53) = 5.5$, $p < 0.001$, mean difference of 6.65 ± 8.88).



(A) Modelling-free adaptation index.

(B) Modelling-based adaptation parameter.

Figure 3.7: Modelling-based and modelling-free adaptation performance measures by session and stimulation across the whole experiment. Error bars correspond to standard error of the mean.

3.3.3 Effect of session: Improved adaptation in second session

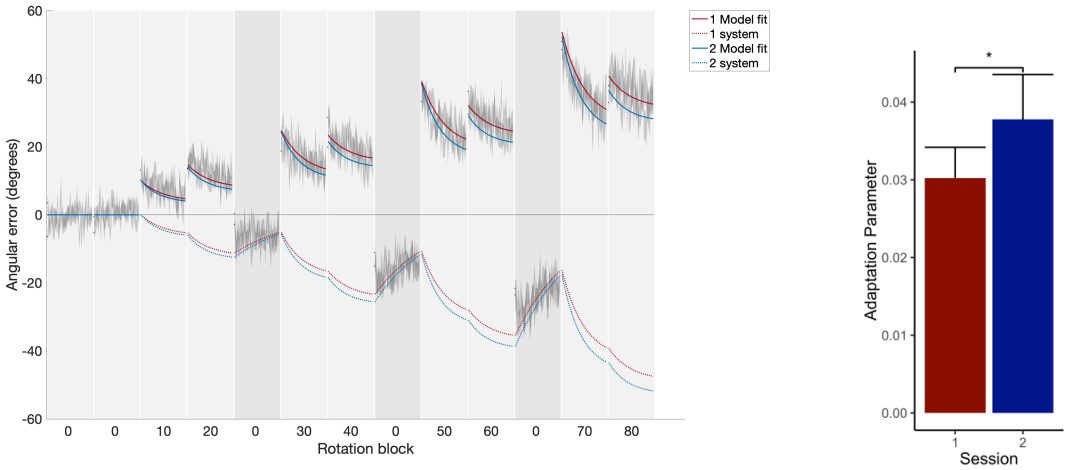


Figure 3.8: Modelled adaptation in session 1 compared to session 2.
Savings are evident in the modelled adaptation performance. The greater adaptation parameter in session 2 causes the modelled error curves to fan out. Improved adaptation is therefore visible particularly in the later task blocks. Note that the target bias has been removed to improve the modelling of the adaptation behaviour across targets.

Participants performed better on the task during the second session than during the first session, showing evidence of savings. Session affected adaptation index across the whole experiment ($\chi^2(1)$=4.81, p = 0.028), with savings in the second session lowering the error in the second by about 1.7 degrees ± 0.7 (standard errors). When only calculating an adaptation index for the duration of the stimulation, this effect was reduced to a trend ($\chi^2(1)$=3, p = 0.08), with a trend wise reduction in error from the first session to the second session by about 1.2 degrees ± 0.7

(standard errors).

This was despite initially starting out at the same level in the second session (6.16 ± 5.60) as during the first session (4.37 ± 5.14), when first confronted with the imposed rotation (Session did not affect initial error ($\chi^2(1)$=1.88, p>.1)). This shows that although the adapted system had been brought back to its baseline state through the washout period after the first experimental session (see 3.6B), savings had not been washed out successfully, demonstrated by the ability to more rapidly reduce the error in the second session. The performance during baseline trials also did not differ between sessions (first session -4.38 ± 3.48, second session -3.51 ± 3.47, no effect of session on baseline error ($\chi^2(1)$=1.65, p>.1)).

Savings evident in model parameters for full task session. The state-space model revealed improved adaptation performance in the second, compared to the first session (Trend towards larger adaptation parameter (SSM Parameter B) ($\chi^2(1)$=2.75, p = 0.09)), with an increased adaptation parameter in the second session by 0.0077 ± 0.0064 (standard errors). However, this effect was not significant at the 5% significance threshold. When modelling the adaptation during the stimulation phase only, there was no difference in adaptation parameters between sessions ($\chi^2(1)$=1.41, p>.1)).

3.3.3.1 No difference in retention between first and second session

There was no effect of session on retention index during the stimulation phase ($\chi^2(1)$=0.66, p>.1) or across the whole experiment ($\chi^2(1)$=1.11, p>.1). The computational model of the adaptation behaviour also showed no session difference in the retention parameter when the parameter was estimated for the stimulation period ($\chi^2(1)$=0.05, p>.1) or for the whole experiment ($\chi^2(1)$=0, p>.1).

Performance Measure	Session 1	Session 2
Modelling-free		
Adaptation Index	18.13 ± 4.15	16.41 ± 5.17
Retention Index	19.68 ± 4.22	20.25 ± 4.08
Modelling-based		
Adaptation Parameter	0.04 ± 0.02	0.05 ± 0.03
Retention Parameter	0.98 ± 0.01	0.98 ± 0.01

Table 3.4: Task Performance in first and second session across the whole task.

3.3.4 Stimulation had no effect on adaptation

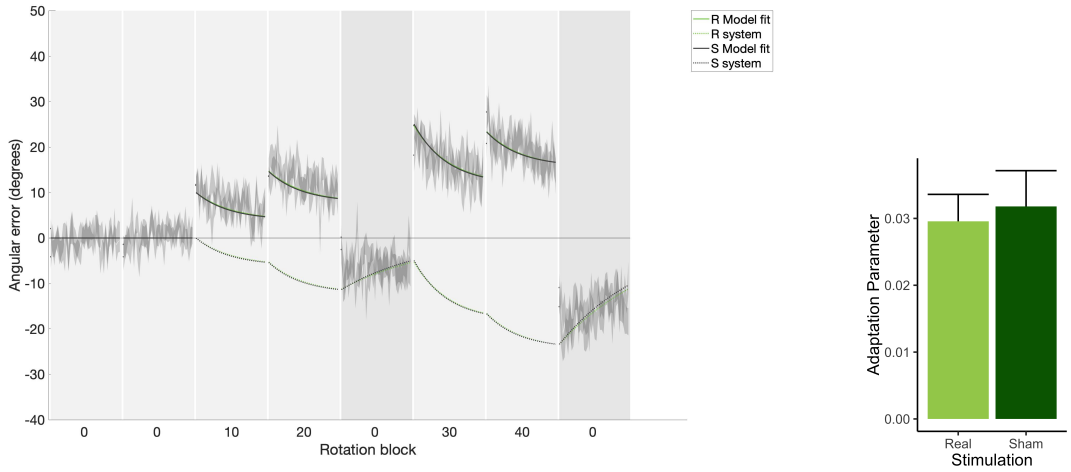


Figure 3.9: Modelled adaptation for real vs. sham stimulation in first session.
Note that the target bias has been removed to improve the modelling of the adaptation behaviour across targets. Shaded area in left figure and error bars in right figure correspond to standard error of the mean.

Performance Measure	Sham	Real
Modelling-free		
Adaptation Index	13.99 ± 4.46	12.88 ± 3.35
Retention Index	10.71 ± 4.41	11.43 ± 4.50
Modelling-based		
Adaptation Parameter	0.03 ± 0.03	0.03 ± 0.02
Retention Parameter	0.98 ± 0.01	0.98 ± 0.01

Table 3.5: Adaptation Performance in sham and real session during the stimulation period.

For the analysis of the effect of stimulation on the adaptation performance we considered the performance during only the stimulation period for two reasons. First, in accordance with previous literature, our hypothesis of a facilitative effect of stimulation primarily concerned effects during the stimulation period. Second, as savings were particularly evident in the later phases of the experiment, we assumed a greater chance of finding an effect of stimulation during the early phases of the task.

We tested the stimulation effect controlling for session. Here, adaptation performance did not differ significantly between real and sham sessions both when measured with the

modelling-free adaptation index ($\chi^2(1)$=0.01, p>.1)) or with the modelling-based adaptation parameter ($\chi^2(1)$=0.23, p>.1)).

The performance during baseline trials after the stimulation had been turned on (second baseline block) did not differ between real and sham sessions (real session -3.56 ± 3.31, sham session -4.33 ± 3.64, no effect of stimulation on error in second baseline block ($\chi^2(1)$=1.29, p>.1)).

3.3.4.1 Stimulation had no effect on retention

We expected no effect of stimulation on retention and this was confirmed for retention behaviour evaluated with both the modelling-free and the modelling-based analysis method. There was no effect of stimulation for retention index across the whole experiment ($\chi^2(1)$=0.16, p>.1) or during the stimulation phase ($\chi^2(1)$=0.35, p>.1). Equally, no effect of stimulation was evident in the modelling-based retention parameter when the parameter was estimated for the whole experiment ($\chi^2(1)$=0.76, p>.1) or for the stimulation period ($\chi^2(1)$=0.27, p>.1). Mean modelling-based retention parameter estimated for the whole experiment was 0.98 ± 0.01 (0.93 - 0.99) All analyses controlled for session.

3.3.4.2 Stimulation had no effect on adaptation in the first session

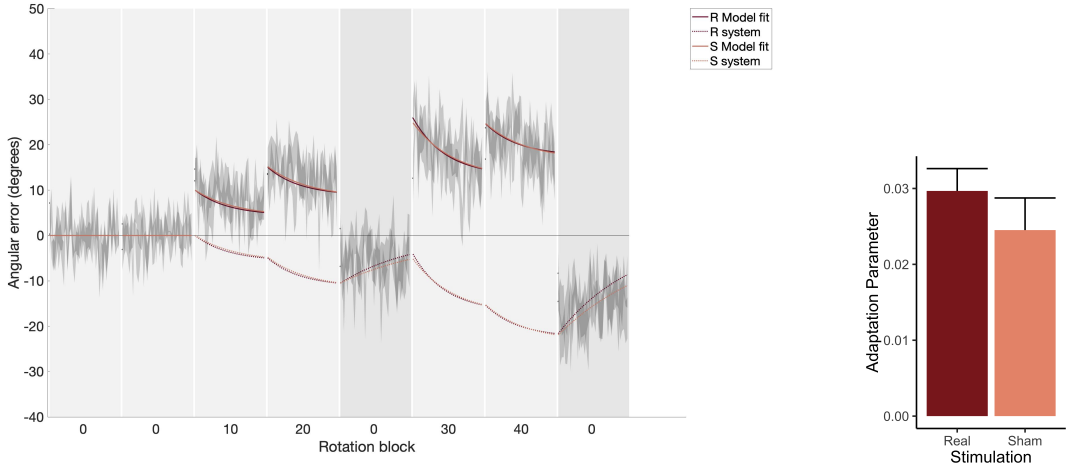


Figure 3.10: Modelled adaptation in first session real compared to first session sham. Note that the target bias has been removed to improve the modelling of the adaptation behaviour across targets. Shaded area in left figure and error bars in right figure correspond to standard error of the mean.

To avoid the potentially confounding effect of savings from the previous session, we tested for an effect of stimulation in the first session only. Even so, adaptation performance did not differ significantly between subjects receiving real and subjects receiving sham stimulation when measured with the modelling-free adaptation index (F(1, 25) = 0.18, p>.1) or when modelled

computationally ($F(1, 25) = 0.90$, $p>.1$). Adaptation performance in the first session for real and sham stimulation is plotted in figure 3.10 (left) along with the mean adaptation parameters for the two groups (right).

3.3.5 Exploratory Analysis

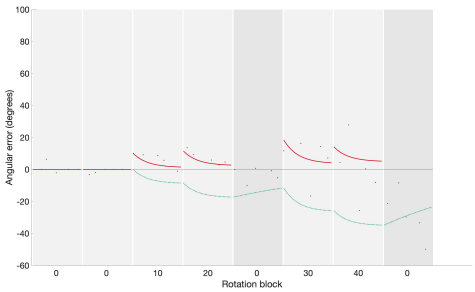
3.3.5.1 No effect of stimulation for perturbation-unaware participants when controlling for baseline.

Motor adaptation has traditionally been considered a highly implicit form of motor learning [169] [179], although more recently both implicit and explicit mechanisms have been shown to underlie learning of adaptation tasks [348]. Awareness of the perturbation could increase the use of explicit strategies which could potentially engage different neural substrates. In this study, we aimed to probe implicit mechanisms of adaptation and interviewed participants after the last experimental session on whether they noticed any form of perturbation. We tested for an effect of stimulation in participants that stayed unaware of the perturbation until they were debriefed about the task. Of the final sample of 27 participants, 13 participants reported that they did not notice any offset between their joystick movements and the movement of the cursor. When testing for an effect of adaptation in this subset of participants, we found a trend of stimulation improving adaptation ($\chi^2(1)=3.52$, $p = 0.06$) by 1.41 degrees ($\pm$ 0.7 standard errors) controlling for session. The improvement in adaptation index, however, was explained by differences in target bias at baseline ($\chi^2(1)=0.43$, $p>.1$ controlling for session and baseline).

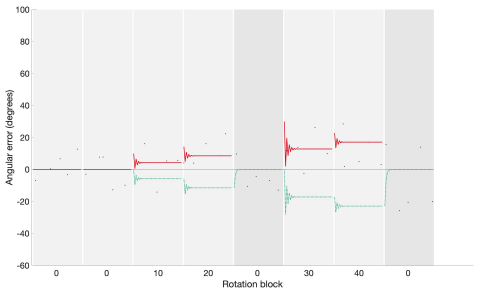
3.3.5.2 No effect of stimulation for specific targets when controlling for baseline.

Adaptation performance differed for targets, even after removing the systematic target bias (see figure 3.4B). We therefore tested for an effect of stimulation when adaptation is quantified for each of the eight targets separately.

Stimulation showed a trend towards lowering the adaptation index in the real session only for the 90 degree target angle ($\chi^2(1)=3.43$, $p = 0.06$) by 3.81 degrees ($\pm$ 2.02 standard errors)) controlling for session). However, adding baseline bias for the 90 degree target as a control variable removed the stimulation effect ($\chi^2(1)=0.92$, $p>.1$)). To probe whether the stimulation effect would be detectable when modelling adaptation to the 90 degree target, we estimated an adaptation parameter for this target only. Since the data per target and block is sparse, as every target occurs only five times in every block of the task, the model was only able to estimate parameters from 48 of the 54 datasets (after visual inspection of the estimated models, data from six participants was therefore excluded; for exemplary model fits see figure 3.11A (included participant) and figure 3.11B (excluded participant)).



(A) Included Model Fit.



(B) Excluded Model Fit.

Figure 3.11: Individual model fits for adaptation to the 90 degree target.

The model showed improved adaptation (trend) in response to stimulation in 21 remaining participants when controlling for session, with the adaptation parameter increased by 0.13 ($\pm$ 0.07 standard errors) in the real stimulation session ($\chi^2(1)$=4.34, p = 0.06). However, when controlling for baseline bias in addition to controlling for session the effect did not hold ($\chi^2(1)$=2.17, p>.1).

3.4 Discussion

This study aimed to characterise the effect of anodal cerebellar tDCS on visuomotor adaptation using a within-subject, sham-controlled crossover design and a novel adaptation task paradigm. The effects were evaluated using both modelling-free and modelling-based analysis strategies. We did not replicate a previously shown facilitatory effect of real compared to sham stimulation on error reduction during motor adaptation. When analysing adaptation across the whole task session, there were significant savings from the first session evident in the second session. When analysing the adaptation data acquired during the stimulation period only, savings were evident only trend-wise. We also did not find a significant effect of stimulation in a between-subjects analysis of the first session.

We explored the data for a stimulation effect in those participants who did not notice a perturbation in the experiment and found lower adaptation indices in the real stimulation sessions, but this effect was explained by differences in baseline error. Similarly, we found a significant effect of stimulation on adaptation to the 90 degree target, but there was no effect when controlling for baseline error. As expected, there were no differences in retention between first and second session or sham and real stimulation.

There are several reasons that could explain why no differences in adaptation behaviour between the stimulation conditions were evident in our data. The failure to detect a significant effect of stimulation on adaptation performance could be a fault of the method and design of this study or could reflect the absence of an effect of stimulation.

3.4.1 Savings may have obscured an effect of stimulation.

In motor adaptation, savings are defined as faster error reduction when exposed to a perturbation for the second time [189]. In this study we found that during the second session, participants reduced their error faster compared to performance in the first session, in line with the presence of savings. Savings should be differentiated from the presence of a residual adapted state due to incomplete washout. A residual adapted state due to incomplete washout should already be evident during the baseline trials of the second session. We found no difference between baseline levels of error in the first and in the second session, suggesting that the lower error in the second session was not driven by a residual adapted state. The lack of a significant difference in baseline error also suggests that the lower error in the second session was not due to practice-related improved control of the joystick that may result in a lower baseline error. Participants may still have improved their control of the joystick by reducing the variance of joystick movements and we cannot exclude the possibility that potential practice-related improvements in movement execution drive the savings. However, the faster error reduction during the second session that is evident in this study adheres to the definition of savings in motor adaptation, because it is not explained by a difference in mean baseline error levels between the sessions.

It is possible that the within-subject design used in this study has rendered the effects of the stimulation too small to detect when measured against the comparably large effects of savings. Although a within-subject design reduces variability relating to the underlying physiology of the participants [379], the considerable savings in the adaptation behaviour would represent an increase in performance larger than any increase in performance induced by stimulation - thereby masking it.

When we evaluated the effects in a between-subjects analysis of the first session only we were not able to detect a significant stimulation effect, although there was a numerical difference in adaptation index: subjects receiving real stimulation performed -2.1 ($\pm$ 1.61 standard errors) degrees better than subjects receiving sham stimulation (see table 3.5). A power analysis of the data of the first session revealed that the effect size for this difference of Cohen's $d = 0.49$ would be in the order of magnitude of effect sizes previously reported for tDCS studies [236]. In the case of cerebellar tDCS and motor adaptation, two recent studies estimated effect sizes that were much smaller than the strong effects initially shown by Galea and colleagues [101]: A replication effort by the same research team found an effect of stimulation when pooling the data from 192 participants acquired in several experiments, with an effect size of $d = 0.7$ [158]. Most recently, another group of researchers found no significant effect of cerebellar tDCS on adaptation (10 participants in real condition, 9 participants in sham condition) but estimated an effect size of $d = 0.8$ for the numerical difference evident in the adaptation data. Although effect sizes reported for the facilitatory effect

of cerebellar tDCS on adaptation (d = 0.49-0.7 in [197] and [158]) were larger than the difference evident in our data from the first session, detecting an effect of the size d = 0.6 with an alpha level of 0.05 and power of 0.80 would still require a minimum of 36 participants per group. It is therefore unsurprising that our analysis of the data of the first session has not yielded a significant effect of stimulation, considering this analysis is underpowered with our sample of 27 participants (12 participants receiving sham and 15 participants receiving real stimulation in the first session). Moreover, the authors acknowledge a difficulty in estimating a true effect size for the effect of cerebellar tDCS, as a publication bias towards over-reporting of significant results in the field of tDCS is likely [236] and authors finding null results in studies of cerebellar tDCS are slow to publish [158].

Therefore, although our sample size of 27 participants is comparable to other within-subject tDCS studies [262], the nature of the behaviour studied here, with its susceptibility to savings weeks after exposure to the task [186], could make an effect of stimulation challenging to detect using a repeated-measures design and this study therefore may have been underpowered.

In this study the learned rotation was washed out after the task with a washout block of 144 trials immediately after the initial exposure to the adaptation task. Although this washout block successfully brought participants back to baseline levels of behaviour (no difference in baseline error or in error at initial exposure to rotation), it did not fully interfere with consolidation of the memory of the task, as adaptation occurred at faster rates upon retest in the second session. There is evidence that extending the washout block to match the length of the adaptation task can fully remove savings in an isometric torque-production task [135]. For the case of visuomotor adaptation, washing out the rotation with visual feedback removed or performing a series of error-clamp trials has been demonstrated to eliminate savings [178]. However, it should be noted that this evidence comes from a study in which the task initially learned consisted of only 80 trials of adapting to a single target at 135 degrees with a single 30 degree rotation and the washout block with either removed or error-clamped feedback consisted of 200 trials. The effectiveness of an extended washout block paired with the removal or clamping of visual feedback for eliminating savings of the task used in this study therefore remains to be confirmed. Future studies using a within-subject paradigm to study visuomotor adaptation should therefore test the effectiveness of washout blocks for removing any savings at re-exposure to the task.

3.4.2 Physiological effects of cerebellar tDCS

Although a number of studies have shown cerebellar tDCS-induced changes in adaptation tasks with a recent quantitative review estimating an effect size of 0.71 (Hedges' d, unsigned cumulative) for motor tasks, the authors conclude that variability in outcome measures and stimulation

parameters prevent from unequivocally establishing that cerebellar tDCS is effective in all circumstances [262].

While there is a wealth of research into the physiological effects of cerebral stimulation protocols, with approximately 80% of published tDCS studies focussing on the primary motor cortex [331], physiological data on the effects of cerebellar tDCS is sparse. Generalisation of stimulation protocols from one site to the other is problematic, especially in montages that target structures at the back of the head like the cerebellum. Not only does the thick layer of corticospinal fluid and skull bone at the back of the head shunt local current strength [289] [266], leading some authors to recommend the use of larger input currents for cerebellar stimulation [289]. The brain itself is highly variable in gross anatomical structure (e.g. cortical folding) as well as cytoarchitecture. In the highly folded cortex of the cerebellum orientation of neuronal axons relative to the scalp varies to a large amount. Given that efficacy and directionality of an electrical field on a neuron depends not only on the strength of the current, but also on its orientation relative to the neuron [160], the heterogeneous orientation of neurons in the cortex of the folded cerebellum, could lead to heterogeneous acute effects of tDCS at this site. Whereas some consensus exists for the basic physiological effects of tDCS of the primary motor cortex, the underlying mechanisms of cerebellar tDCS are not fully understood [331] [112].

The montage used in this study has been shown to modulate the inhibitory tone the cerebellum exerts over the primary motor cortex (cerebellar inhibition or CBI, [99]) suggesting this montage effectively modulated cerebellar excitability. Moreover, modelling studies suggest that electric field distributions of this montage are more focused compared to montages targeting the cerebral cortex [289]. It should be noted that the input current in both of these studies was higher than the one used in the present study (2 mA vs. 1.5 mA used in this study). However, animal studies suggest that input impedance at Purkinje cells (the sole output of the cerebellar cortex), is about one third of that of pyramidal cells in the motor cortex, leading to larger current flow through the cell membrane of those cells [276], which could potentially compensate for the low maximum current strength in the cerebellum [401] [156]. Moreover, a current of 1.5 mA has previously been used to successfully modulate adaptation behaviour in humans [197].

Nevertheless, as no physiological data was acquired in the present study, the possibility that the current used in this study was insufficient to produce physiological changes in the cerebellum leading to null results in the adaptation task cannot be ruled out.

3.4.3 Conclusions

In conclusion, we found no significant effects of tDCS on visuomotor adaptation, but evidence of an effect of task experience on rate of adaptation. Although savings pose a difficulty for motor

adaptation studies, a within-subject design is important to control for the physiological variability in tDCS studies. There is a critical need for the development of effective washout techniques to remove the influence of savings and enable collecting repeated measures of adaptation performance independent of prior exposure to the task. Moreover, sparse physiological data on the effects of cerebellar tDCS make it difficult to reconcile the conflicting evidence on behavioural effects of cerebellar tDCS. An investigation into the precise physiological changes in the cerebellum in response to tDCS could help navigate the vast parameter space in which brain stimulation operates and further the development of cerebellar tDCS for clinical applications.

CHAPTER 4.0

M1 GABA predicts retention, but not adaptation: A 7T MRS study

Abstract

The primary motor cortex (M1) has been shown to undergo plastic changes during motor learning whereby cortical representations are functionally reorganized. Baseline levels of local neurotransmitter concentrations within M1 have been shown to predict task performance, and changes in neurotransmitter concentrations are thought to facilitate these plastic changes.

Specifically, reductions in M1 levels of GABA have been associated with the acquisition of new motor skills in a task probing model-free learning. However, how GABA concentration levels might specifically relate to changes in behavioural parameters of a model-based learning task has yet to be fully elucidated.

Methods. To investigate neurotransmitter changes underpinning model-based learning, we used a 7T Siemens scanner to acquire Magnetic Resonance Spectroscopy data from the hand area of the left M1 in 15 healthy right-handed participants performing a motor task in the scanner during two sessions. In both sessions (counterbalanced, scheduled at least 7 days apart), participants performed a task in which they controlled a cursor on a screen using a joystick. One of the sessions (Task session) probed a model-based form of motor learning by imposing a rotation of the visual feedback, which required the participants to adapt their joystick movements to the perturbed feedback (visuomotor adaptation task). The 40-minute learning period was followed by a washout period during which participants performed trials with no angle offset, hereby washing out the previously learned rotation. During the other session (Control session) participants performed the task with no rotation imposed for 40 minutes. Performance on the task was quantified using a modelling-free approach (average error), and for a more precise description of the task performance, computationally modelled, using a single-state SSM.

Results. Inter-individual differences in task performance correlated with Magnetic

Resonance Spectroscopy-assessed neurochemical concentration levels in M1. M1 GABA at baseline shows a positive relationship with error during the washout phase, with participants with high [GABA] at baseline retaining more of the compensatory movement and therefore showing larger negative errors. This relationship was specific for retention, as $GABA_{Baseline}$ did not correlate with adaptation, evidenced by error during the adaptation phase. The relationship was also specific for the session involving the learning component, as no relationship between behaviour and M1 neurochemistry was found in the control session. The relationship was neurochemically specific to GABA, as $Glu_{Baseline}$ showed no significant relationship with retention.

In conclusion, we find no evidence of M1 GABA changing significantly in response to adaptation and no significant relationship between M1 GABA and adaptation. Taken together, these results suggest a role for M1 GABA in retention, but not adaptation.

4.1 Introduction

Primary motor cortex (M1) γ-aminobutyric acid (GABA) plays an important role in LTP-like plasticity in animals [357] and local changes in M1 GABA have been linked to motor learning in humans [91] [181]. MRS-assessed baseline GABA concentration in M1 has been shown to relate to individual subjects' motor performance [332] and to predict their learning of a motor skill [181].

These studies have predominantly focused on *model-free*, habitual motor learning, commonly assessed with a serial reaction time task. GABAergic changes during *model-based* adaptation learning, during which goal-directed actions are evaluated with reference to an internal model, have not been studied before. One study has investigated GABAergic changes in M1 during an isometric motor sequence learning task, which involves habitual, model-free learning of a sequence as well as model-based modulation of grip strength on a force tracker [92]. However, these M1 [GABA] changes may differ from changes during a form of model-based learning that involves no sequence learning, such as adaptation.

While previous studies have probed the responsiveness of the GABAergic system using brain stimulation and linked those changes to features of adaptation [177] [157] [257], naturally occurring changes in M1 [GABA] during adaptation have yet to be studied. Investigating these changes in M1 [GABA] directly could help elucidate the role of M1 in formation of internal models during adaptation and the consolidation of these models. This information is not only important to understand physiological changes taking place during adaptation in the motor system. For example, contrasting the contribution of M1 to model-based learning against the contribution of M1 to model-free learning could also give insights into the unique role M1 plays in the different types of motor learning.

Model-based learning relies on the formation and updating of an internal model of the environment [384] and is commonly probed with adaptation paradigms. In brief, adaptation paradigms impose a systematic error such as visually rotated feedback or a force field, perturbing the participant's movement. In response, the participants attempt to reduce errors back to baseline levels by adapting their movements.

Model-based adaptation is integral to maintaining control over our movements, as not only does our environment change constantly, but also the properties of our muscles can change due to fatigue, disease or growth [21].

Although recent studies suggest that adaptation involves more than one learning process (for a review, see [189]), the primary mechanism appears to be the updating of an internal forward model on the basis of a sensory prediction error. The internal forward model generates an estimate of the next state of the body, given the current state and a motor command. This computation is widely believed to take place in the cerebellum because of its well-suited neural circuitry and its critical involvement in state estimation [385]. The Marr–Albus theory of the cerebellum proposes that climbing fibres originating from the inferior olive carry information about sensory prediction error, which serve as a 'teaching signal' for the internal forward model [213] [4]. The internal model itself is encoded in the connections of parallel fibres, that together with the climbing fibres synapse onto the major output neuron of the cerebellar cortex, the Purkinje cells [213]. The Purkinje cells should therefore represent the output of the internal model, a prediction about the sensory consequences of the movement, which is consistent with animal studies of adaptation [329]. Studies in humans found that enhancing cerebellar cortex excitability with Non-Invasive Brain Stimulation (NIBS) can increase adaptation [101] [130]. However, for adaptation to visuomotor rotations these results have been difficult to replicate [158].

While adaptation takes place in the cerebellum, retention of the compensatory movement appears to depend on M1. In visuomotor adaptation, increasing M1 excitability with NIBS has been demonstrated to increase retention, but not to affect adaptation [101] and disruption of M1 increases washout of the previously learned rotation [116]. However, despite its apparent contribution to retention, it remains unclear whether M1 undergoes plastic changes during adaptation. Moreover, it has yet to be investigated whether M1 [GABA] at baseline predict retention.

To answer these questions, we measured [GABA] in M1 using magnetic resonance spectroscopy (MRS) while participants performed a visuomotor adaptation task. Our primary aim in this study was to investigate M1 GABA changes during adaptation, not during retention. Retention and consolidation of an internal model has previously been linked to reaching a performance plateau [391]. In order to isolate changes in M1 GABA that are driven by adaptation from

changes driven by a process of consolidation and retention, we therefore designed a task that kept participants from reaching a plateau, driving adaptation over an extended period of time. This novel task paradigm required participants to adapt throughout the MRS-measurements by imposing an stepwise increasing rotation.

A previous study attempting to link motor adaptation to [GABA] changes suffered from lack of MRS-assessed GABA in a control condition [157]. In this study the authors probed the responsiveness of the GABAergic system by applying tDCS, but they did not assess GABA during a control condition that involved sham tDCS and therefore were unable to dissociate [GABA] changes driven by tDCS from [GABA] changes occuring naturally at rest. To ensure any effects on M1 GABA were not driven by motor performance or passage of time, but were specific to error-based adaptation, our protocol included another session where each participant performed a control task in the scanner without any rotation imposed (order of sessions was counterbalanced) to observe any movement-alone induced changes without adaptation. As adaptation is thought to primarily take place in the cerebellum, it is unclear whether adapting to an error would induce changes in M1 GABA.

Finally, after each session participants performed the task with no rotation imposed. This was done to wash out the previously learned rotation and serves as a measure of retention [116]. We expect M1 GABA at baseline to predict retention of the visuomotor rotation.

In this within-subject, sham-controlled study, we tested for a global change in M1 GABA over time depending on task condition (adaptation vs. control). Secondly, we tested for a relationship between GABA (change or baseline) and behaviour (adaptation vs. retention).

4.2 Methods

4.2.1 Participants

We recruited fifteen healthy, right-handed participants (8 female; 22-32 years; mean age 26 years) to participate in a within-subject study. Each participant took part in two sessions in which they underwent a MRS scan while performing a visuomotor task that either involved a learning component (adaptation task) or no learning component (control task). The order of sessions was counterbalanced, with eight participants completing the adaptation task in the first session. Participants had no contraindications to MRI, no history of neurological or psychiatric conditions and were not taking any medications that can affect the central nervous system. All participants gave informed consent in line with central university research ethics committee regulations (University of Oxford; C1-2014-090) and were compensated for their time (see table 4.1 for population characteristics).

4.2.2 Experimental Protocol

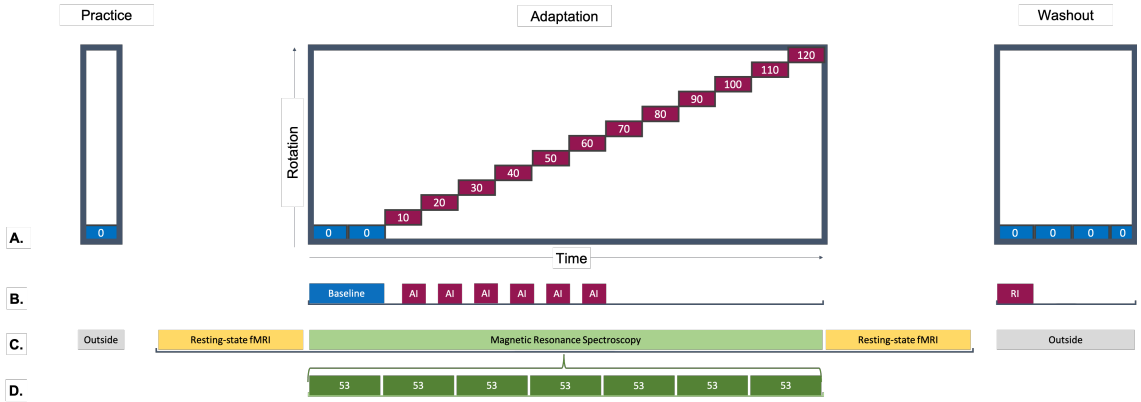
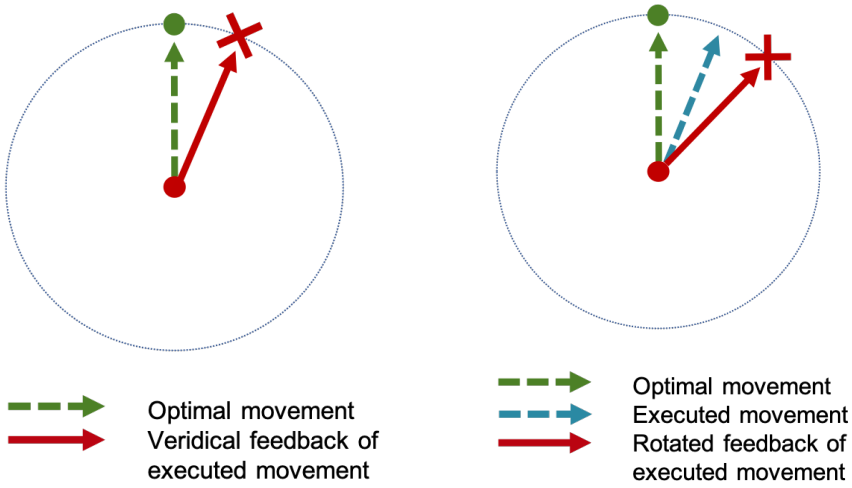


Figure 4.1: Experimental Protocol.
A. Task Blocks. Stepwise increasing rotated feedback required participants to adapt movements to reduce errors (one block at each angle, which consisted of 40 trials of 4 seconds duration each). The task was practised before the task (40 trials, no rotation) and rotation was washed out after task (144 trials, no rotation). Not depicted: In the control session, participants performed the task without any rotation imposed, but for the same length (560 trials in total for the main task).
B. Calculation of behavioural indices. Adaptation Index was calculated by averaging the errors of adaptation trials in adaptation blocks, excluding trial 1-8 of each adaptation block. Only blocks with a rotation less than 70° were included into the main analysis.
Retention Index was calculated by averaging the error of all washout trials in the first block of the washout task.
C. Scanning Protocol. MRS data was acquired during the task (adaptation or control). The task was practised outside the scanner and the rotation was washed out afterwards outside the scanner.
D. MRS Acquisitions. MRS data was acquired during the task and consisted of 53 individual spectra which were averaged. This resulted in seven MRS acquisitions.

All subjects participated in two testing sessions in which they performed a joystick task with a learning component (adaptation task) or without (control task) while undergoing a MRS scan. Participants controlled a cursor on a screen using a joystick and made discrete movements to targets at eight possible locations around a central starting position. They were instructed to make fast, accurate and ballistic movements to 'shoot' through the target that appeared on the screen. The target appeared in a randomized fashion at one of eight locations radially aligned around the starting position of the cursor and separated by 45°, with a different target sequence for each participant and session. Participants had to perform the movement within a time window of 750 ms, after which the target disappeared. The time cut-off was to ensure the short, ballistic nature of the movement and to prevent online corrections. No endpoint feedback was provided.

At the beginning of each session, participants practised the task by performing 40 baseline trials outside of the scanner (no rotation imposed, trials shown in figure 4.2A; protocol shown in figure 4.1). Participants then performed the main task inside the scanner, during which they learned to adapt to a stepwise increasing rotation of their movement in case of the adaptation task (schematic adaptation trial shown in 4.2B). After the scan, participants performed 144 trials of baseline trials

outside of the scanner to wash out the previously learned rotation.



(A) Baseline trials. (B) Adaptation trials.

Figure 4.2: Trial Types. Green, dashed arrows are the optimal movement, connecting starting position with target position. Blue, dashed arrows are the executed movement. Unbroken, red arrows represent the visual feedback of the cursor movement.
A. Baseline Trials. Visual feedback is veridical. Red arrow is superimposed over blue arrow, as the visual feedback corresponds to the executed movement.
B. Adaptation Trials. Visual feedback is rotated. Red arrow is deviating from blue arrow, as the visual feedback does not correspond to the executed movement.

4.2.3 Magnetic Resonance Acquisition

All Magnetic Resonance (MR) data were acquired on a 7T Siemens scanner with a 32-channel head coil. Structural MRI data were acquired using a magnetisation prepared rapid acquisition gradient echo (MPRAGE) sequence (Repetition Time 2200 ms, TE 2.82 ms, slice thickness 1.0 mm, in-plane resolution 1.0 x 1.0 mm^2, GRAPPA factor = 4, flip angle = 7, FOV 192 x 176).

Structural images were used to manually place a 20 x 20 x 20 mm^3 VOI over the left precentral knob, which is a landmark for the hand motor representation [396], avoiding contact with dura to minimize significant macromolecule contamination. Overlap maps of the MRS voxel for the adaptation and for the control session are shown in figure 4.3.

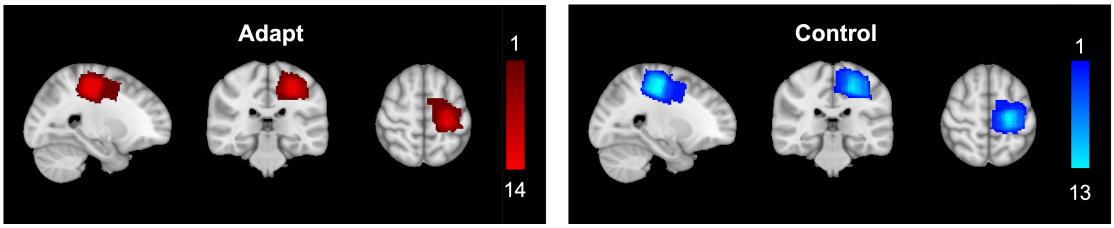


Figure 4.3: Voxel Placement. MRS voxel overlap maps for the two conditions, 20 x 20 x 20 mm^3 voxel centred over hand area of left M1. Colour bars represent number of participants.

MRS data were acquired using a semi-LASER sequence [305] (53 data points, TR 6000, TE 36 ms, voxel size 20 x 20 x 20 mm^3) using VAPOR (variable power RF pulses with optimized

relaxation delays) water suppression [354].

Spectra were acquired in acquisitions of 5 minutes and 30 seconds. With one MRS average acquired every 6 seconds and each trial of the joystick task lasting 4 seconds, each MRS acquisition corresponds to 80 trials, spanning two blocks of the task (MRS Acquisition: 53 x 6 seconds = 318 seconds. Two Task Blocks: 80 x 4 seconds = 320 seconds). Therefore, one MRS acquisition was acquired at baseline, and six MRS acquisitions were acquired during adaptation, one for every two rotation blocks. Participants performed the task for the entire MRS duration (see figure 4.1).

A multiband 2 mm isotropic EPI acquisition (TR/TE = 3500/28 ms, FOV = 256 x 138 mm^2, bandwidth = 1562 Hz/Px, multi-band acceleration factor 2, voxel dimension = 2 x 2 x 2.5 mm^3, whole brain, acquisition time = 8:05 min for a total of 132 volumes) was performed before and immediately after the task. Subjects fixated on a crosshair image presented centrally on the screen during resting fMRI acquisition and watched a nature video at all other times.

4.2.4 Behavioural Data Analysis

Cursor movements were analysed as described in section 3.2.4.1. Adaptation was quantified using modelling-free and modelling-based analysis methods.

4.2.4.1 Modelling-free Analysis

A modelling-free index of adaptation performance was calculated by averaging the errors in all adaptation blocks, across all trials excluding the first eight. This method of calculating an adaptation index by excluding the first eight trials has been established as standard [101], as it captures the rapid error reduction of the adaptation performance rather than performance during the initial exposure to the rotation [187]. The blocks from which the adaptation index was calculated are marked with dark red blocks in figure 4.1B.

A modelling-free index of retention of the previously learned rotation was calculated from the washout period acquired outside of the scanner (see figure 4.1). The retention index was calculated by averaging all forty trials from the first block of the washout period. Unlike in the calculation of the adaptation index, the initial eight trials of the washout block were included into the calculation of the retention index. These trials were excluded as a rapid decay of the previously learned motor memory could already take place during the first eight trials of the washout period, as visual feedback was provided throughout the washout block. Those initial trials could therefore reflect the amount of retention.

When discussing retention behaviour and adaptation behaviour in the context of this study, we are referring to the modelling-free retention index and the modelling-free adaptation index.

4.2.4.2 Modelling-based Analysis

A single-state State-Space Model [71] was used to model trial-by-trial adaptation for each subject during the adaptation task session, as well as trial-by-trial washout during the washout period.

Computationally modelling each subjects' data, yields an adaptation parameter (Parameter B) and a retention parameter (Parameter A) that best describe the adaptation and retention behaviour for the subject during the particular task period (adaptation period or washout period). The aim of this analysis was to explore whether neurochemical differences at baseline or during the adaptation task relate to these parameters of the SSM. Further, relating the indices calculated in the modelling-free analysis to the modelling-based SSM parameters can help explore whether the modelling-free indices and modelling-based parameters likely capture similar features of the data. For a detailed description of the SSM, see methods chapter 2.5.

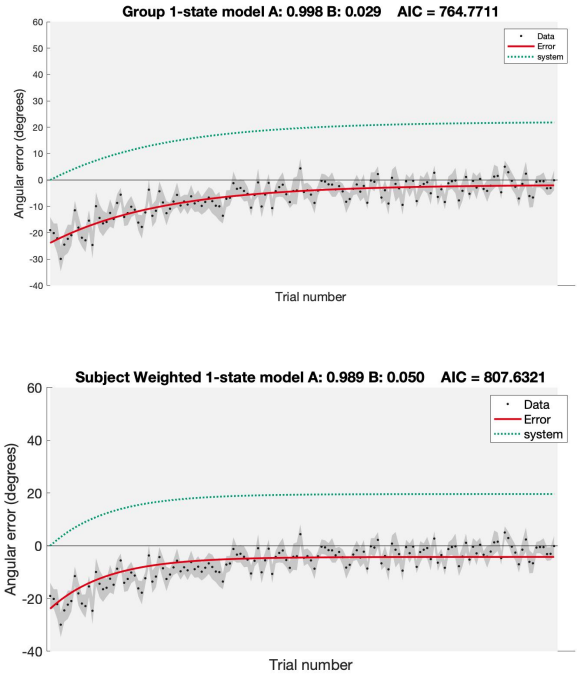


Figure 4.4: A single-state SSM was fit to the washout data. Group parameters were estimated on the basis of the averaged error data. Subject-specific parameters were then estimated for each participant by using the group parameters as starting parameters. Model resulting from group parameters is shown in upper panel over error data averaged across participants. Model resulting from averaged subject-specific parameters is shown in lower panel over error data averaged across participants Black dots show error data averaged across participants. Shaded area around data indicates standard error of the mean. Red line shows modelled error. Green, dotted line shows compensatory movement.

For the SSM to be able to fit a modelled error curve to the data, a start value for the error curve has to be fixed. This start value is typically given by the rotation, fixing the error in the first trial of an adaptation block of a 10° rotation to 10. However, for the washout period, it was evident from

the data that this initial start value varied significantly between participants , and therefore no error could be fixed for the first trial of all participants. For each participant the initial error was therefore calculated from the first eight trials. By fixing the initial error level, the model was able to estimate parameters describing the washout behaviour of each participant. In order to remove the influence of the initial error estimated for each individual participant separately, analysis of SSM parameters modelled on the washout data are conducted using partial correlations controlling for the initial error. The single-state SSM was estimated by first extracting group parameters from the error data averaged across participants.

Subject-specific parameters were then estimated for each participant using the group parameters as starting parameters. In order to ensure sensible model fits estimated for each participant the deviation of subject-specific parameters from group parameters was weighted by a penalty factor and added to the squared errors which were minimized to find an optimal model fit.

Group models are shown in figure 4.4. The upper panel shows group averaged data with modelled curves resulting from parameters that were estimated from the data averaged across participants. Lower panel shows group averaged data with modelled curves resulting from parameters that were averaged from the individual parameters of each participant.

4.2.5 Magnetic Resonance Spectroscopy Analysis

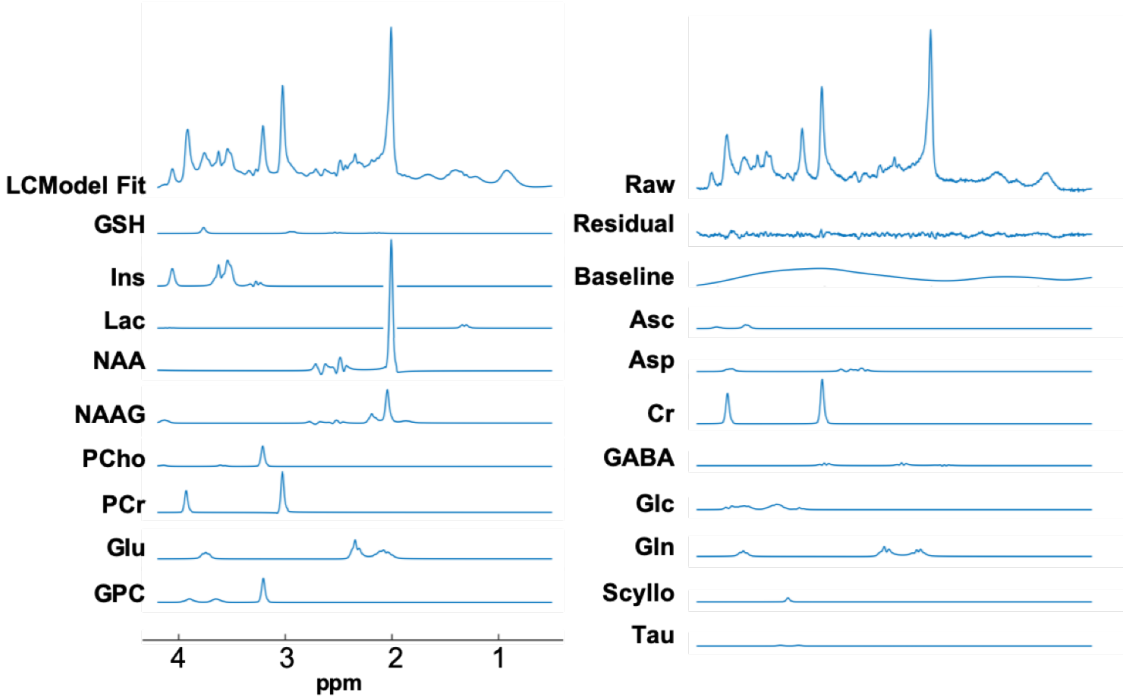


Figure 4.5: Spectrum. Image shows representative spectra of one subject including LCModel fit. Metabolite basis spectra have been scaled using LCModel such that a linear combination of the basis spectra, the residual and the baseline best fits the raw measured spectrum. Measured raw spectrum is shown in the right panel at the top and LCModel Fit is shown in the left panel at the top. GABA metabolite peaks can be seen in the right panel, with the GABA peaks appearing at 1.89 ppm, 2.29 ppm and 3.01 ppm.

MRS data was preprocessed using in-house scripts and the FID-A toolbox [321]. For each session, raw MRS data from all acquisitions were concatenated and corrected for frequency and phase shifts. Residual water signal was removed from the water suppressed MRS data using HLSVD [48], run on the individual data points. Outlier spectra were identified for each session by calculating a deviation metric for every data point. Data points whose deviation metric exceeded three standard deviations from the mean were removed. To ensure the same number of data points in each acquisition, these data points were replaced with an interpolated spectrum (mean percentage of data points removed 0.01 ± 0.01 % ; 0-6 data points per session). Data points were frequency- and phase-corrected and 53 data points were combined into each acquisition. LCModel [283] analysis was used to correct the averaged spectrum for each acquisition separately for eddy currents and for water using the unsuppressed water signal acquired from the same VOI. Concentration of neurochemicals was quantified within the chemical shift range of 0.5 to 4.2 ppm [283]. As discussed in section 2.2.2.1, it is recommended to assess MRS spectra on the basis of CRLB along with a combination of other quality assessment metrics, particularly when filtering data of low concentration metabolites, such as GABA. We therefore excluded spectra based on standard quality control measures [250] at

thresholds used previously on MRS-assessed GABA data [181]. Spectra were excluded on the basis of CRLB $> 50\%$, water linewidths at Full Width at Half Maximum (FWHM) > 15 Hz, or Signal-to-Noise Ratio (SNR) < 40.

In light of the link between cortical GABA and glutamate, both in terms of excitatory/inhibitory balance and their shared metabolic pathways, we calculated a correlation between GABA and Glutamate (Glu) at baseline. GABA and Glu at baseline showed a strong relationship ($r = .79$, $p < 0.01$). Because of this relationship and in order to determine whether any results were neurochemically specific for GABA, we computed all relevant analysis that were run on GABA also with Glu.

To correct for tissue composition, proportion of WM, GM and CSF in the VOI were quantified by applying FMRIB's Automated Segmentation Tool (FAST) [399] to the T1-weighted MPRAGE scan. GABA and glutamate concentration values were corrected for the proportion of GM in the VOI by including GM fraction into the model. That means, when testing for a relationship between GABA or glutamate and another variable, GM fraction was included as a covariate of no interest into the model.

Total creatine (including phosphocreatine:tCr) peaks were corrected for the proportion of total brain tissue in the VOI.

MRS data analysis therefore yielded independent quantification of neurochemical concentrations in seven acquisitions of 53 spectra each. All neurochemical concentrations are expressed as a ratio of tCr.

4.2.5.1 Metabolite Baseline index

The first MRS data acquisition was acquired during the baseline blocks (first 80 trials). We will refer to this acquisition as the $\text{Metabolite}_{\text{Baseline}}$.

4.2.5.2 GABA Change index

To quantify change in GABA concentration in response to adaptation, an index of GABA change was calculated. Since behavioural data analysis indicated that on average participants were only able to adapt to a rotation of up to 70° (see figure 4.6), we only included GABA data that was acquired during that period of time into the calculation of a GABA change index. That means GABA data from acquisitions 1 to 4 were included into the GABA change analysis. As described in the previous section, the first MRS data acquisition was acquired during the baseline blocks (first 80 trials), serving as the $\text{GABA}_{\text{Baseline}}$. MRS data acquisitions 2 to 4 were acquired at the same time as participants performed the first six adaptation blocks, i.e. concurrent to the block with imposed rotation 10°, 20°, 30°, 40°, 50° and 60°.

Previously used indices of GABA change have calculated GABA change as the percentage

change between two measures (e.g. pre and post an intervention in [332]). However, in this study, we acquired four measures of GABA concentration while participants were adaptation and therefore the calculation of our GABA change index took advantage of these four GABA measurements, by fitting a linear slope to the concentration values.

For this, we fitted a linear function of the form $y = a * x + b$ to the GABA measurements 1 to 4, where the intercept b is the GABA baseline concentration and the slope a is $\text{GABA}_{\text{Change}}$. We thereby captured the overall trend in GABA concentration.

4.2.6 Statistical Analysis

Statistical analyses on the data were conducted using R [287].

Because this study aimed at investigating GABA changes during adaptation, we needed to ensure that only changes that occur while participants are adapting were included. The first step of the analysis was therefore to constrain analysis of the MRS data and the adaptation data to periods of the adaptation task in which adaptation (evidenced by a reduction of error) was detectable. For this, we tested for a significant reduction of error in all of the adaptation blocks, in order to identify the blocks in which adaptation took place. To determine a significant reduction in error, paired-sample t-tests between average error in initial eight trials and average error in last eight trials for each block of the adaptation task were calculated.

Within the period of time where adaptation was detectable, we then tested for significant changes in GABA during adaptation compared to control. To test whether task condition affected GABA over the course of the experiment, we used the R package lme4 [23] to construct a linear mixed effects model of the connectivity variable of interest. As fixed effects, we entered acquisition (Acquisition 1, Acquisition 2, Acquisition 3, Acquisition 4, see figure 4.1), condition (adapt, control) and acquisition x condition interaction into the model. Intercepts were allowed to vary for different subjects to vary in order to account for covarying residuals within subjects, creating a random intercept model. P-values were obtained by likelihood ratio tests of the full model with the effect in question against the model without the effect in question.

A Spearman's rank-order correlation was calculated to determine the relationship between variables (two-tailed, unless otherwise stated). In order to test differences in associations between two behavioural variables (Adaptation, Retention) with a third variable (Metabolite of interest), a Fisher z-transformation was applied to the correlation coefficients. The difference between the z-transformed correlation coefficients was tested for statistical significance using a one-tailed t-test.

To ensure results were not driven by outliers, each of the participants were removed from the data once and correlations were calculated on the remaining data. Upper and lower limits of the resulting probability values are reported as Confidence Interval (CI) and given in brackets.

Control Analysis. To ensure that the relationship between retention and $GABA_{Baseline}$ was not driven by a covariate of no interest several control analyses were performed, controlling for a covariate of no interest in addition to GM fraction (covariates of no interest were SNR, FWHM, CRLB and voxel placement).

Moreover, to test the specificity of the relationship between retention and $GABA_{Baseline}$, we tested whether $GABA_{Baseline}$ correlated with adaptation (testing behaviour-specificity), whether $Glu_{Baseline}$ correlated with retention (testing neurotransmitter-specificity) and whether $GABA_{Baseline}$ correlated with retention in the control session (testing session-specificity). *Prediction Analysis.*

Finally, we constructed a linear model of retention to test whether the metabolite of interest at baseline predicted retention by calculating a linear regression. The model included GM fraction as a control variable.

4.3 Results

Participants	
Recruited	15
Gender	8 Female
Age	26.7 (±3.4)
1st Session Adaptation	8
Excluded (MRS data)	1
Excluded (Retention data)	1
Final Sample (MRS and Adaptation)	14
Final Sample (MRS and Retention)	13

Table 4.1: Sample Characteristics. One participant was excluded from analysis of adaptation and retention due to no MRS data in the adaptation session. One participant was excluded from analysis of retention due to no washout data.

4.3.1 Behaviour

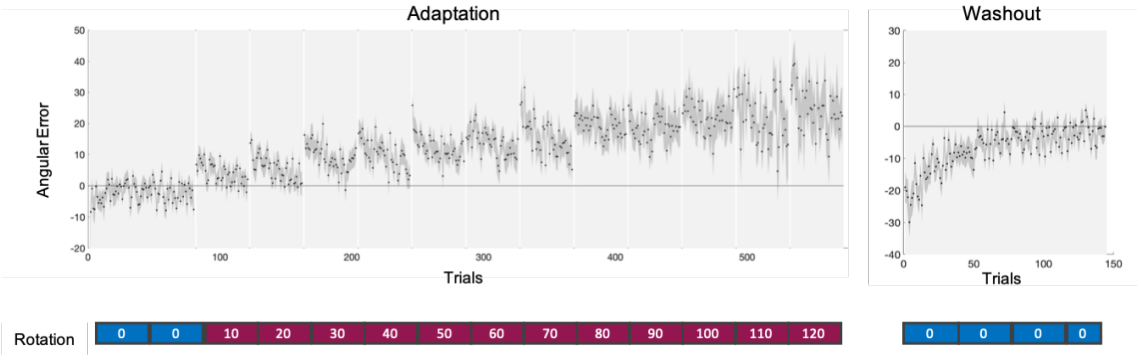


Figure 4.6: Behaviour. Shown is angular error at each trial averaged across participants. Shaded area represents standard error of the mean.

Block	Error			
	Begin	End	t-test	Mean Difference
Baseline	-5.44 ± 5.95	-2.54 ± 6.72	$t_{(13)}$ = 4.67, p = 0.24	2.90
10°	7.40 ± 4.94	1.27 ± 3.90	$t_{(13)}$ = -3.31, p = 0.01**	-6.13
20°	9.62 ± 6.07	2.64 ± 4.87	$t_{(13)}$ = -5.86, p = 0.01**	-6.97
30°	13.43 ± 4.90	8.14 ± 4.48	$t_{(13)}$ = -3.68, p = 0.00**	-5.28
40°	14.29 ± 6.41	6.89 ± 6.13	$t_{(13)}$ = -4.06, p = 0.01**	-7.39
50°	17.31 ± 6.06	9.83 ± 5.53	$t_{(13)}$ = -5.24, p = 0.01**	-7.49
60°	17.51 ± 8.58	11.24 ± 11.35	$t_{(13)}$ = -2.20, p = 0.046*	-6.26
70°	22.72 ± 10.97	11.01 ± 12.32	$t_{(13)}$ = -3.98, p = 0.01**	-11.69
80°	21.43 ± 14.89	18.55 ± 15.46	$t_{(13)}$ = -0.94, p = 0.36	-2.88
90°	19.93 ± 13.73	19.14 ± 15.58	$t_{(13)}$ = -0.35, p = 0.73	-0.79
100°	26.74 ± 16.71	22.46 ± 18.48	$t_{(13)}$ = -2.53, p = 0.02*	-4.28
110°	24.49 ± 18.49	18.04 ± 26.18	$t_{(13)}$ = -1.80, p = 0.09	-6.45
120°	28.91 ± 22.76	28.86 ± 26.62	$t_{(13)}$ = -0.01, p = 0.99	-0.05
Washout	-21.25 ±8.54	-9.01 ± 6.07	$t_{(13)}$ = -4.88, p = 0.01**	-12.22

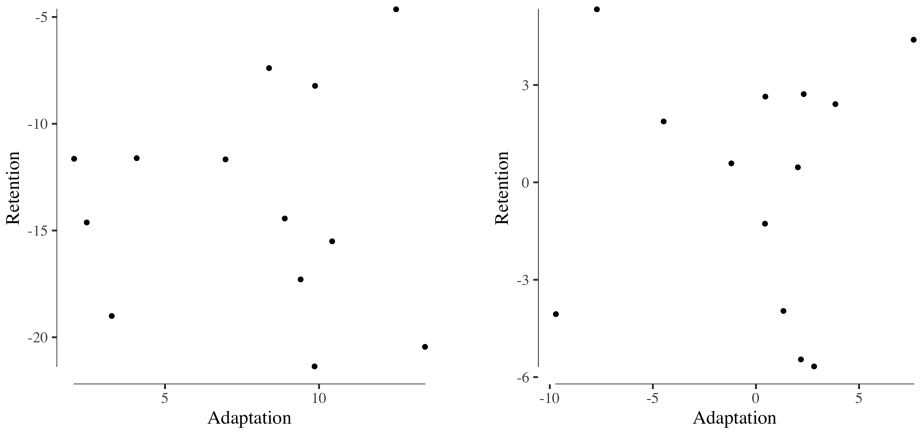
Table 4.2: Error at begin and end of each block of adaptation task, as well as first block of washout task. Paired sample t-tests between average error in initial eight trials and average error in last eight trials revealed that participants significantly reduced their error in every rotation block up to a rotation of 70°. Beyond 70°, there was significant reduction of error only in the 100° block. During the washout task, participants decreased their error significantly.
* p-value $<$ 0.05, ** p-value $<$ 0.01

4.3.1.1 Participants adapted for the majority of the task.

Participants decreased their error in response to the increasing rotation. However, as evident from figure 4.6 and table 4.2, participants had difficulty compensating for a rotation beyond 70° (block 9 of the task). Since the 70° block was acquired in the same MRS acquisition as the 80° block it was not possible to use only the 70° block without the inclusion of the 80° block. We therefore cut off all subsequent analyses at the 60° block (see figure 4.1).

4.3.1.2 Adaptation and retention do not correlate.

Adaptation behaviour showed no relationship with retention behaviour. This was the case when quantifying adaptation up to the 60° rotation (r = -0.01, p = 0.75 , uncorrected; figure 4.7A), as well as when taking into account performance up to the end of the adaptation task (up to 120°; r = -0.13, p = 0.67; figure 4.7B). Adaptation did not also correlate with retention behaviour when controlling for minutes elapsed between end of the adaptation task and begin of the washout task (Partial correlation controlling for time elapsed; r = .06, p = 0.83).



(A) Adaptation up to 60°.

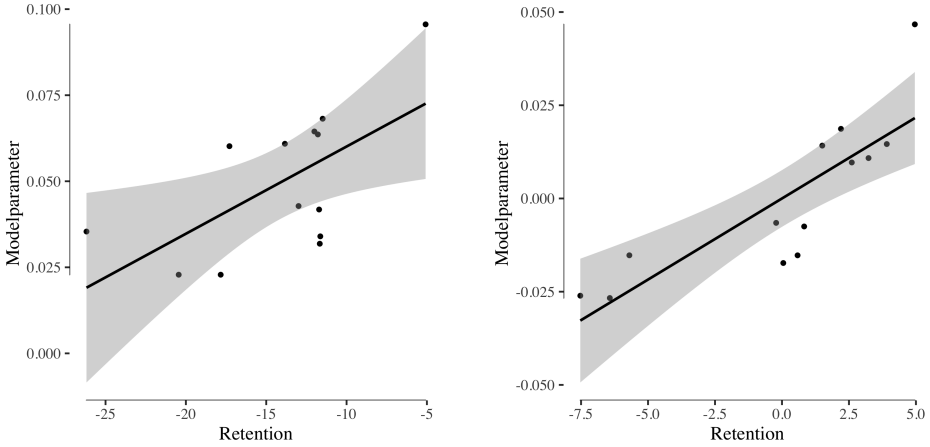
(B) Adaptation across full task.

Figure 4.7: Adaptation and retention do not correlate. No correlation of adaptation and retention when adaptation up to 60° or across the full task.

4.3.1.3 Retention related to model parameter B in washout phase.

Retention showed a trendwise correlation with a single-state SSM parameter B modelled on the washout task (r = .51, p = 0.07; figure 4.8A).

To remove the influence of the initial error which had to be fixed in order to estimate single-state SSM parameter B from the washout data, we calculated a partial correlation controlling for initial error (for a detailed description of the modelling method see 4.2.4.2). Retention correlates highly with single-state SSM parameter B modelled on the washout task (r = .87, p = 0.01; figure 4.8B; CI [0.00001, 0.001]), controlling for initial error.



(A) Retention and SSM parameter B (B) Controlling for initial error.

Figure 4.8: Retention index and State-Space Model parameter B modelled on washout task show a trendwise relationship (A), which becomes highly significant when controlling for initial error (B). Shaded area indicates 95% confidence interval.

4.3.2 Adaptation does not significantly affect GABA concentration in M1

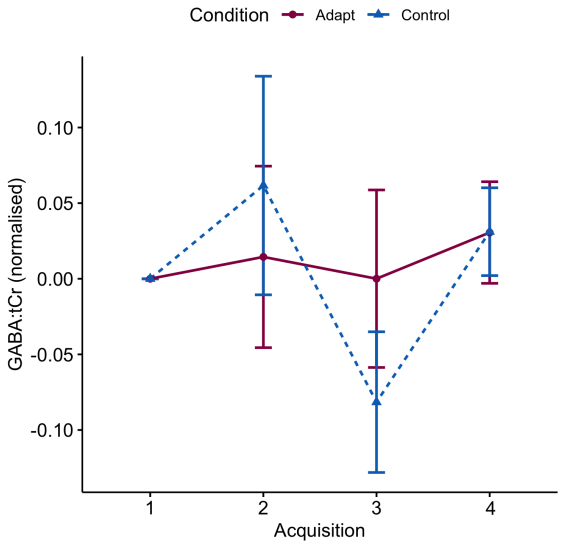


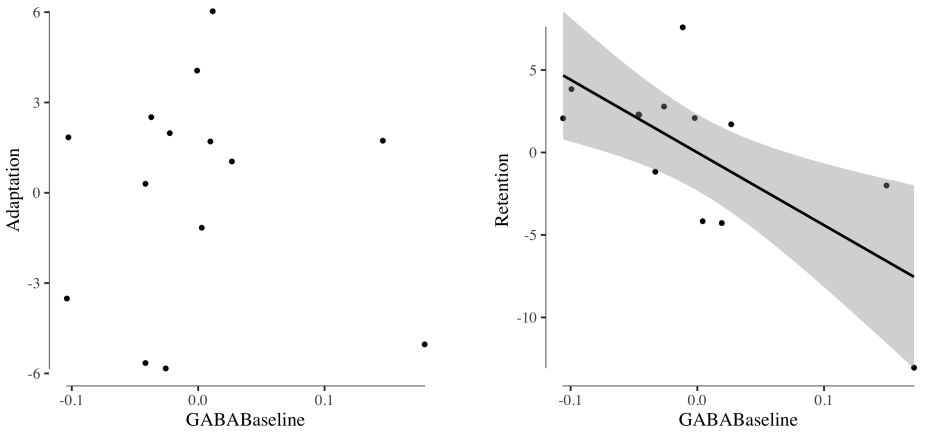
Figure 4.9: Group mean GABA:tCr concentrations (normalised to baseline). Error bars are standard error of the mean.

In line with the hypothesis that adaptation relies on brain regions distant from M1, we saw no change in GABA during performance of adaptation (Task condition did not result in a significant GABA change over time; No interaction of acquisition x condition: $F(2,64) = 0.42$, $p = 0.66$; figure 4.9) There was also no main effect of acquisition ($F(2,64) = 0.44$, $p = 0.65$) and no main effect of condition ($F(1,70) = 0.04$, $p = 0.84$).

4.3.3 M1 GABA relates to retention, but not adaptation

4.3.3.1 GABA Baseline

We then went on to investigate whether baseline neurochemical concentrations predicted behaviour. $GABA_{Baseline}$ correlates with retention, but not adaptation when controlling for GM in the model (figure 4.10; $GABA_{Baseline}$ and retention: r = -.61, p = 0.03, CI [0.02, 0.1]; $GABA_{Baseline}$ and adaptation: $_{14}$ = 0.26, p = 0.37, CI [0.12, 0.72]).



(A) $GABA_{Baseline}$ and adaptation. (B) $GABA_{Baseline}$ and retention.

Figure 4.10: $GABA_{Baseline}$ correlates with retention, but not adaptation. Units are arbitrary, since values have been regressed onto GM fraction before plotting to illustrate relationship controlling for GM fraction. For a plot of the raw values, see 4.10

To test for a difference between the relationship of $GABA_{Baseline}$ with adaptation and retention controlling for GM, both partial correlation coefficients were transformed into z-scores using Fisher's r-to-z transformation and their difference calculated. This analysis demonstrated that $GABA_{Baseline}$ and retention correlates significantly stronger than $GABA_{Baseline}$ and adaptation (z = -1.69, p = 0.045).

To ensure that the relationship between $GABA_{Baseline}$ and retention was not driven by differences in data quality indices, we performed partial correlations controlling for SNR and FWHM in addition to GM fraction, both of which remained significant (Partial correlation controlling for GM and SNR: =-0.67, p = 0.02; Partial correlation controlling for GM and FWHM: = -0.81, p < 0.01). Lastly, we wanted to ensure that results were not driven by differences in placement of the MRS voxel. We therefore calculated the overlap between a left M1 hand area mask and the MRS voxel. Controlling for overlap with the M1 mask in addition to GM, $GABA_{Baseline}$ correlates significantly with retention (Partial correlation controlling for GM and Overlap with M1: =-0.65, p = 0.03).

Relationship is specific for adaptation session. $GABA_{Baseline}$ in the control session does not correlate with task performance in the control session, neither with performance during the session

equivalent to adaptation performance (r = -0.27, p = 0.42), nor with performance after the session (r = .28, p = 0.41).

Modelling-based results. As reported in the previous section, using the modelling-free approach to quantify adaptation, we found no relationship between $GABA_{Baseline}$ and adaptation. To ensure that this null finding was not driven by the coarse measure of a modelling-free adaptation index, we tested for a correlation between $GABA_{Baseline}$ and adaptation quantified with a modelling-based approach, which results in a measure of more refined measure of adaptation. We found that $GABA_{Baseline}$ does not correlate with SSM parameter B estimated from the adaptation data (partial correlation controlling for GM: r = -0.39, p =0.19), corroborating our finding of no relationship between adaptation and M1 GABA at baseline.

Next, we tested whether $GABA_{Baseline}$ shows a relationship with the SSM parameter B estimated from the washout data, since the modelling-free retention index and the modelling-based washout parameter B are highly correlated. The washout parameter B reflects how quickly a participant de-adapts from the perturbation, as it describes the error curve that best fits the participant's washout data. There was no relationship of $GABA_{Baseline}$ with SSM parameter B estimated from the washout period (partial correlation controlling for GM: r = -0.45, p = 0.14). We also found no relationship of $GABA_{Baseline}$ with SSM parameter B when controlling for initial error in addition to GM (partial correlation controlling for GM and initial error: r = -0.49, p = 0.12).

4.3.3.2 GABA change

We tested for a relationship between $GABA_{Change}$ and adaptation performance, since previous research has linked performance improvements due to motor learning to a change in M1 GABA [332] [181]. $GABA_{Change}$ shows a trendwise relationship with retention (Partial correlation controlling for GM fraction: r = .55, p = 0.06) and no relationship with adaptation (Partial correlation controlling for GM fraction: r = -0.03, p = 0.93). However, $GABA_{Change}$ is also correlated with $GABA_{Baseline}$ (r = -0.67, p = 0.01). We therefore tested whether $GABA_{Change}$ correlates with retention controlling for $GABA_{Baseline}$ in addition to GM fraction. There was no significant correlation (Partial correlation controlling for GM fraction and $GABA_{Baseline}$: r = 0.21, p = 0.53).

4.3.3.3 GABA at baseline predicts retention.

Finally, to test whether retention could be predicted from $GABA_{Baseline}$, we constructed a linear model of retention with $GABA_{Baseline}$ and GM fraction as predictors. The advantage of calculating a linear regression over a correlation analysis is that the regression is a more detailed analysis. Linear regression provides an equation that can be used to make predictions, meaning that based on the values of the metabolite of interest (GABA), we can predict retention using the linear model.

Testing the model for significance using an F-test revealed that it predicts retention ($F_{2,10}$ = 4.56, p = 0.04), with the model explaining 48 % of the variance in retention (r^2 = 0.48). $GABA_{Baseline}$ was the only significant predictor in the model (t(10) = -3.01, p = 0.01)). $GABA_{Baseline}$ predicts retention with a parameter estimate of -43.45 ± 14.14 (standard errors), which means that with every point increase in $GABA_{Baseline}$ concentration, participants show a 43.45° larger negative angular error, and therefore more retention.

To ensure results were not driven by differences in placement of the MRS voxel, we tested whether $GABA_{Baseline}$ predicts retention when controlling for placement of the MRS voxel. For this we controlled for MRS voxel overlap with a left M1 hand area mask in the model in addition to GM. Controlling for both control variables, $GABA_{Baseline}$ remains the only significant predictor of retention (t(9) = -3.01, p = 0.01).

Lastly, we tested whether $GABA_{Baseline}$ predicts retention controlling for quality control indices. $GABA_{Baseline}$ significantly predicts retention when controlling for SNR in addition to GM ($F_{3,9}$ = 6.8, p = 0.01; $GABA_{Baseline}$ as predictor: (t(9) = -3.55, p < 0.01). $GABA_{Baseline}$ does not predict adaptation (controlling for GM; $F_{2,9}$ = 0.18, p = 0.84; $GABA_{Baseline}$ as predictor: (t(9) = -0.21, p = 0.84).

To test whether the predictive power of $GABA_{Baseline}$ was specific for the session that included the adaptation component, we tested whether $GABA_{Baseline}$ predicted retention in the control session. $GABA_{Baseline}$ in the control session does not predict retention in the control session (controlling for GM; $F_{2,11}$ = 0.86, p = 0.44; $GABA_{Baseline}$ as predictor: (t(11) = -0.21, p = 0.84).

4.3.4 M1 Glutamate does not relate to retention.

To investigate whether the relationship of M1 neurochemistry is specific for GABA, we tested for a relationship of retention with Glutamate at baseline.

$Glu_{Baseline}$ does not correlates with retention (Partial correlation controlling for GM in the model: r = -0.41, p = 0.18). However, in light of the strong correlation between GABA and Glu at baseline, we tested whether the relationship between $GABA_{Baseline}$ and retention holds controlling for $Glu_{Baseline}$ in addition to GM fraction. The correlation was reduced to a trend (r = -0.53;, p = 0.09).

4.4 Discussion

In this study, we aimed to characterise changes in M1 [GABA] in response to adaptation.

First, participants were able to perform the novel task paradigm used in this study and successfully adapted to the stepwise increasing rotation up to a rotation of 70°. Participants showed a significant aftereffect after the adaptation session, which was washed out during performance of

washout trials.

Second, we show that M1 [GABA] does not change significantly when error-based adaptation is introduced compared to when a control task is performed. There is also no correlation between the extent of adaptation and M1 [GABA] (at baseline or concentration changes).

Third, we demonstrate a significant relationship between M1 [GABA] at baseline and retention. Moreover, [GABA] at baseline can predict retention, where this relationship is behaviour-specific (no relationship with adaptation), metabolite-specific (no relationship with Glu) and specific to the adaptation session (no relationship in control session).

We also find a relationship of GABA change with retention, however, baseline [GABA] and change in [GABA] correlate strongly. Controlling for [GABA] baseline, we find no relationship between retention and [GABA] change, suggesting the relationship is driven by differences at baseline.

4.4.1 No M1 GABA modulation in response to adaptation

M1 [GABA] does not change significantly in response to adaptation. Although M1 [GABA] has been shown to significantly change when a motor learning component is introduced [181], this change occurred in response to a motor learning task known to involve M1 during acquisition. In the context of visuomotor adaptation the null finding presented in this study is not surprising, as past studies have implicated M1 in retention, but not the acquisition on an adaptation task [101] [116].

Despite this, a previous study has shown responsiveness of the MRS-assessed GABAergic system in M1, probed through tDCS, is linked to learning on a force-field adaptation task [177]. However, the design of that study limits generalisability of the findings to a naturally occurring visuomotor adaptation process as probed in this study. First, assessing GABAergic responsiveness with a brain stimulation intervention likely results in much stronger and directed changes than a natural learning process will elicit. Second, the reported link is unspecific to an adaptation component. The authors report significant correlations of GABAergic change and adaptation as well as deadaptation, but it is unclear whether baseline levels or a control task that lacks an adaptation component also correlate with GABAergic responsiveness. Hence, the relationship reported could be unspecific to error-based adaptation and therefore does not stand in contrast with the results reported here.

4.4.2 M1 GABA at baseline predicts retention

M1 GABA predicts retention in this visuomotor adaptation study.

The relationship between M1 [GABA] at baseline and retention was metabolite-specific, as [$\text{Glu}_{\text{Baseline}}$] and retention did not correlate. It was also specific to the experimental session involving the learning component and within that session, it was specific to one type of behaviour:

The relationship between [$GABA_{Baseline}$] and retention significantly exceeds the relationship of [$GABA_{Baseline}$] and adaptation.

The result of this study, that shows higher [$GABA_{Baseline}$] predicts more retention of the compensatory movement, seems puzzling at first glance considering that predictive relationship of $GABA_{Baseline}$ in model-free learning goes in the opposite direction. Here, higher [$GABA_{Baseline}$] predicts poorer subsequent learning. However, our measure of retention is not reflective of an initial learning process, as indicated by no significant correlation between retention and adaptation, but rather of a process of 'unlearning' or overwriting of a memory. Recent research has shown that an increase in [GABA] in the primary visual area can protect memories from interference on a visual learning task [320]. Conversely, a decrease in GABAergic inhibition in the lateral occipital complex has been shown to increase memory interference in proportion to the GABA reduction [182]. Taken together, these results suggest that increased baseline [GABA] do not affect error-based adaptation, but protect the formed compensatory movement from washing out.

4.4.3 M1 GABA change correlates with retention

We also observed a significant correlation between change in M1 [GABA] (as indicated by $GABA_{Change}$) and retention. Due to the trendwise correlation between M1 [GABA] change and baseline we tested for the relationship between [GABA] change and retention controlling for baseline, which did not reach significance. The relationship of [GABA] change with retention should therefore be interpreted with caution, as it seems to be driven by baseline differences. Further studies are warranted to determine whether change in [GABA] relates to retention when baseline [GABA] is held consistent.

4.4.4 Limitations

The relationship demonstrated in this study was metabolite-specific, behaviourally specific and specific to an adaptation task. However, in order to ensure a regionally specific result, MRS-data from a control region would need to show no relationship with retention. As MRS-data was only collected from M1, we cannot claim the relationship with retention is specific to this brain region. To achieve a double dissociation, we therefore set out to conduct a subsequent study, collecting MRSI data from the cerebellum during adaptation. Results from this study are discussed in the next chapter (section 6.1).

The novel task paradigm used in this study differs from more traditional visuomotor adaptation paradigms. It involves a stepwise increasing rotation, which scales up to 120° and eight targets to which movements are being adapted. This task design was chosen to make the task more difficult and keep participants from plateauing. Increasing task difficulty bears the risk of hindering learning and decreasing task engagement. However, in this study participants were able to adapt to a

rotation of up to 70° and showed a significant aftereffect, which suggests the task paradigm was successful in inducing adaptation. For subsequent studies, however, we took out rotation blocks past 80°.

Another limitation is the assessment of retention in this study. Strictly, retention refers only to the tendency for the adapted movement to 'decay' towards its original state, the baseline. This study's index of retention however, is derived from a period of washout where the decay of the adapted movement is aided by the same error-based process which is responsible for the initial adaptation, a process that is referred to as 'deadaptation'. In order to separate retention from deadaptation, visual feedback during the washout period is commonly removed. Our interpretation of the washout period reflecting retention is in line with previous adaptation studies which have derived an index of retention from a period of washout in which visual feedback was provided [116]. Nevertheless, we added a period of removed visual feedback after adaptation in our subsequent studies.

Lastly, it should be noted that MRS-measurements only reflect total concentration of a neurochemical within the voxel and cannot disentangle separate functional pools of GABA [333]. These measurements can therefore not differentiate between phasic and tonic inhibition. In order to achieve a better understanding of the precise inhibitory mechanisms underlying retention and the guarding of an adaptation memory, it is therefore necessary to employ techniques that are able to trace the origin of GABAergic changes, such as such as PET [11].

4.4.5 Conclusions

In conclusion, our study provides evidence for [$GABA_{Baseline}$] predicting retention in a visuomotor adaptation task. We found M1 GABA does not change significantly in response to adaptation and we found no significant relationship between M1 GABA and adaptation. Moreover, we have shown our novel task paradigm is able to drive adaptation for an extended amount of time and sufficient to introduce aftereffects. Taken together, these results suggest a role for M1 GABA in retention, but not adaptation. In the context of this thesis, the characterisation of the role of M1 GABA in motor adaptation provides a first step to describing plasticity in the adapting motor system.

CHAPTER 5.0

Adaptation modulates resting-state functional connectivity in the cerebellum

Abstract

Imaging studies of motor adaptation have shown both cerebellar activation and functional connectivity changes in a cerebellar network at rest. However, relating adaptation performance to these resting-state network change has proven to be difficult.

Methods. In this within-subject, sham-controlled study, we used a novel visuomotor adaptation paradigm to maximize adaptation while still allowing quantification of adaptation performance. We measured resting-state functional connectivity in 15 participants at 7T before and after participants performed either this adaptation task or a control task. During the adaptation session, a rotation of the visual feedback was imposed, requiring the participants to adapt their joystick movements to the perturbed feedback. The 40-minute learning period was followed by a washout period during which participants performed trials with no angle offset, thereby washing out the previously learned rotation. During the other session (control session) participants performed the task with no rotation imposed for 40 minutes. Performance on the task was quantified using a modelling-free approach (average error) and a computationally modelling approach, using a single-state SSM.

Results. We find that adaptation significantly modulated a cerebellar resting-state network, evidenced by significantly higher activation in the anterior cerebellum after participants performed the adaptation task, but not after the control task. No difference in connectivity in the cerebellar network was found between the two sessions at baseline (before task). Change in connectivity within this network correlated with adaptation performance, such that an increase in connectivity was linked to more adaptation, while a decrease in connectivity was linked to less adaptation. This effect was behaviour-specific (no correlation with retention), network-specific (no relation with default mode network) and session-specific (no correlation in control session data). The effect did not depend on the method used to quantify adaptation, but

remained highly significant with the SSM approach. Exploring connectivity between left M1 and right cerebellum revealed a significant relationship between connectivity change and retention, such that participants who showed a decrease in connectivity retained more of the previously learned movement. This effect was behaviour-specific (no correlation with adaptation), regionally specific (no correlation with control region), and session-specific (no correlation in control session data).

In conclusion, to our knowledge, this study provides the first evidence for a cerebellar resting-state network that is specifically modulated by adaptation and shows stronger connectivity when participants adapt better. In the context of this thesis, together with the results described in chapter 4, this study suggests feasibility and suitability of this novel adaptation task for studying plastic changes in the cerebellum in adaptation.

5.1 Introduction

Functional changes in the brain induced by learning are often studied by measuring BOLD-activity while the learning process takes place. A caveat of this approach is that when different brain regions are engaged at different stages of learning, then the functional changes shown may depend on the timepoint considered. If there is variability between subjects in the transitioning from one stage of learning to the other, this time-dependence may hinder attaining a clear picture of the functional changes induced by learning. This caveat is especially relevant when studying changes induced by adaptation, a process by which participants learn to adapt their movements to an imposed perturbation. The perturbation can be imposed by rotating visual feedback when participants are moving a cursor on a screen, as in the case of visuomotor rotation tasks. Adaptation seems to involve different processes to counter the perturbation, which come into play at different times during the task ([348]). Moreover, adaptation has been suggested to involve two systems adapting in parallel, with one system contributing more during early adaptation and less during late adaptation and vice versa (dual-process framework, for a recent review see [281]). In addition, the cerebellum, a structure known to be involved in error-based adaptation, has been shown to increase activity with performance errors, but also to sustain activity with improved performance [228]. These factors complicate the study of adaptation-induced activity changes while adaptation takes place.

An alternative approach to quantifying changes due to learning is to measure functional changes in the brain at rest before and after adaptation. This resting-state fMRI approach assumes that over the course of any given learning task, the connections between brain areas involved are strengthened e.g. by firing in synchrony, and that this strengthening of a task network is evident in the resting-state scan after the task. This assumption is supported in visual learning [198] and

motor learning [302]. A previous study demonstrated increased connectivity within a previously unreported cerebellar network after performance of a short adaptation task [3]. However, in this study the increase in connectivity strength could not be related to adaptation performance, which would be compelling evidence for the task-specificity of the proposed adaptation network. The authors argued that this relationship could not be demonstrated due to the design of the adaptation task. The adaptation task was intended to maximize adaptation by gradually increasing the imposed perturbation at every trial. However, while the task kept participants adapting, it did not allow a clear quantification of adaptation performance because the imposed rotation was different at every trial. A PET-study used a longitudinal design to demonstrate an increase in connectivity during late stages of prism adaptation within a motor network which included anterior cerebellar regions [65]. Although performance related to greater activity within the anterior cerebellum in this study, resting-state functional connectivity did not relate to performance.

More recently, changes in motor network strength at rest have been related to long-term retention of the previously learned adapted movement [66] and baseline motor network connectivity has been linked to early phases of adaptation [51]. However, the emergence of a cerebellar resting-state network after participants performed a single session of adaptation (but not after performing a control task [3]) has not yet been replicated. Moreover, to our knowledge, an increase in this session-specific network has yet to be linked to adaptation performance, corroborating the network's specificity to adaptation.

Therefore, in this study we set out to replicate the emergence of a cerebellar resting-state network after performance of an adaptation compared to a control task. Our second aim was to extend this finding by linking adaptation performance to an increase in connectivity of this network. To achieve this we conducted a within-subject, randomised, sham-controlled crossover study in which participants were scanned at rest directly before and after performing an adaptation task inside the scanner. We used a novel visuomotor adaptation paradigm in which participants adapted to a stepwise increasing rotation imposed on their cursor movements. While we attain constant adaptation with this task design and keep participants from reaching a performance plateau, similarly to the adaptation task used in [3], the stepwise rotation sequence allows us to quantify adaptation using traditional methods (adaptation index, see 5.2.4.1) and modelling techniques (state-space modelling, see 5.2.4.1). We also extend the rotation imposed to 120° and lengthen the task to 37 minutes of task performance, to increase difficulty and time spent engaged on the adaptation task, contrasting with the 90° maximum rotation and the 11 minutes spent on the task in the aforementioned study [3].

Above its merit in the context of studying adaptation-related plasticity, in the context of this thesis this study also served as an important step in confirming that this novel task design

was suitable for studying functional changes in the cerebellum. This chapter therefore aimed at establishing an adaptation task that was able to drive adaptation sufficiently to elicit detectable changes in cerebellar connectivity, but remained feasible to perform inside the scanner so that performance could be linked to potential activity changes.

In this study, we tested the following specific hypotheses:

1. Performing an adaptation task, compared to a control task, affects resting-state networks.

2. Changes in network connectivity relate to adaptation performance.

The data from this study was collected as part of the experiment described in chapter 4, which characterised the role of left M1 GABA in adaptation and retention. Finally, in addition to testing the specific hypotheses outlined above, we explored the relationship between left M1 activity and adaptation-related resting-state networks, as well as potential link between M1 GABA concentration and resting-state activity in left M1.

5.2 Methods

This chapter focusses on the resting-state data collected as part of the project presented in chapter 4. A detailed description of the behavioural data and the MRS data of that experiment can be found in section 4.3. In this section, we provide specific details of the resting-state fMRI methodology and analysis.

5.2.1 Participants

As described in chapter 4, we recruited fifteen healthy, right-handed participants (8 female; 22-32 years; mean age 26 years) to participate in a within-subject study. Each participant took part in two sessions in which they underwent an MRI scan in which resting-state fMRI data was collected before and after participants performed a visuomotor rotation task that either involved a learning component (adaptation task) or no learning component (control task; order of sessions counterbalanced across the group, with eight participants performing adaptation task in first session). Participants had no contraindications to MRI, no history of neurological or psychiatric conditions and were not taking any medications that affect the central nervous system. Further, in line with central university research ethics committee regulations (University of Oxford; C1-2014-090), all participants gave informed consent and were compensated for their time (see table 5.1 for sample characteristics).

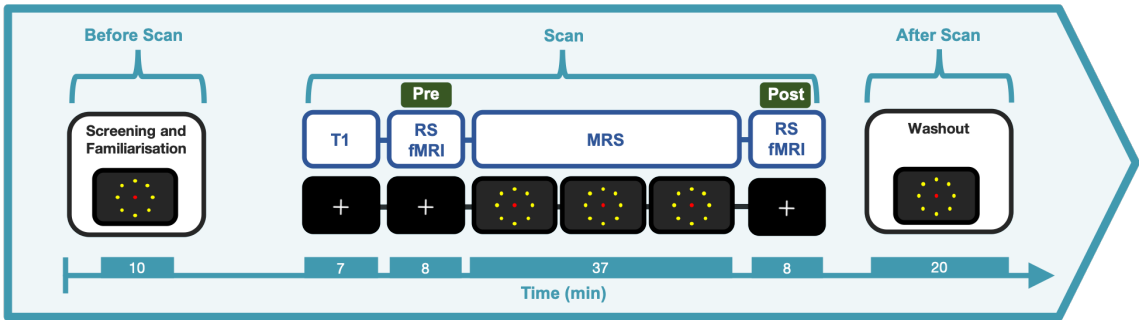


Figure 5.1: Experimental Protocol.
Experimental protocol as shown here was the same in each session. Participants underwent an MRI scan while performing a visuomotor adaptation task. Resting-state data was collected before and after the task (Green boxes marked with "Pre" and "Post"). Before each session participants practised the task outside the scanner (Familiarisation, 20 trials with no rotation). After each session, participants performed 144 trials without rotation (Washout).

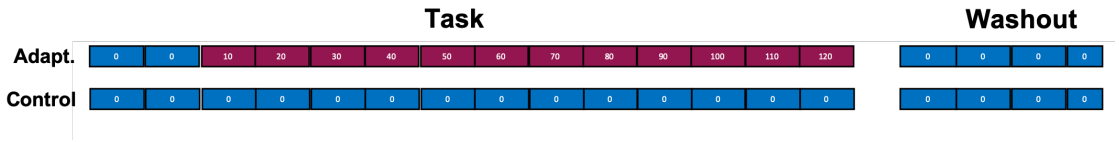


Figure 5.2: Rotation Sequence. Task: During the main task, participants performed a visuomotor adaptation task by shooting targets with a joystick, either adapting to a rotation or not.
Adapt. During the adaptation session, after 80 trials of no rotation (baseline), visual feedback was rotated by 10°. Rotation increased by 10° every 40 trials.
Control. During the control session, no rotation was imposed.
Washout: In both sessions, after the main task, participants performed 144 trials without rotation.

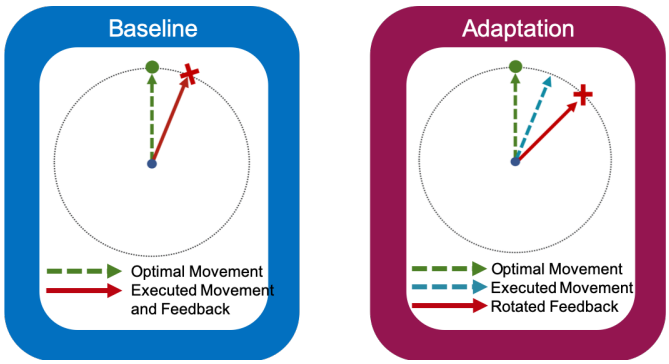


Figure 5.3: Trial Types. Green, dashed arrows are the optimal movement, connecting starting position with target position. Blue, dashed arrows are the executed movement. Unbroken, red arrows represent the visual feedback of the cursor movement.
Left. Baseline Trials. Visual feedback is veridical. Red arrow is superimposed over blue arrow, as the visual feedback corresponds to the executed movement.
Right. adaptation Trials. Visual feedback is rotated. Red arrow is deviating from blue arrow, as the visual feedback does not correspond to the executed movement.

As described in chapter 4.2.2, all subjects participated in two testing sessions in which they performed a joystick task that involved a learning component (adaptation task) or not (control task) while undergoing a MRS scan. The protocol for both sessions is shown in figure 5.1. Participants

made fast, ballistic movements to radially aligned targets on a computer screen. For a detailed description of the task, please see the task description in section 4.2.2.

At the beginning of each session, participants practised the task by performing 40 baseline trials outside of the scanner (no rotation imposed, trials shown in figure 5.3 left). Participants then performed the main task inside the scanner, during which they learned to adapt to a stepwise increasing rotation of their movement (schematic adaptation trial shown in figure 5.3 right, protocol shown in figure 5.2 in red). After the scan, participants performed 144 trials of baseline trials outside of the scanner to wash out the previously learned rotation (see figure 5.2).

5.2.2 Magnetic Resonance Acquisition

All MR data were acquired using a 7T Siemens scanner with a 32-channel head coil. Structural MRI data were acquired using a magnetisation prepared rapid acquisition gradient echo (MPRAGE) sequence (Repetition Time 2200 ms, TE 2.82 ms, slice thickness 1.0 mm, in-plane resolution 1.0 x 1.0 mm^2, GRAPPA factor = 4, flip angle = 7, FOV 192 x 176).

Structural images were used to manually place a 20 x 20 x 20 mm^3 VOI over the left pre-central knob, which is a landmark for the hand motor representation [396], avoiding contact with dura to minimize significant macromolecule contamination.

A multiband isotropic EPI acquisition (TR/TE = 3500/28 ms, FOV = 256 x 138 mm^2, bandwidth = 1562 Hz/Px, multi-band acceleration factor 2, voxel dimension = 2 x 2 x 2.5 mm^3, whole brain, acquisition time = 8:05 min for a total of 132 volumes) was performed before and immediately after the task. Subjects fixated on a cross-hair image presented centrally on the screen during resting fMRI acquisition and watched a nature video at all other times.

5.2.3 Magnetic Resonance Imaging Analysis

5.2.3.1 Preprocessing

Resting-state functional data processing was carried out using FSL (FMRIB's Software Library, Version 6.00, [162]).

Standard pre-processing steps were applied: The data was motion corrected using MCFLIRT [161], slice-timing corrected using Fourier-space time-series phase-shifting, distortion corrected using fieldmaps (B0 unwarping, stripped of non-brain voxels using BET [324], grand-mean intensity normalised and highpass temporally filtered (Gaussian-weighted least-squares straight line fitting, with sigma = 50.0s). To clean the functional data from noise, it was decomposed into independent components using probabilistic Independent Component Analysis (ICA) implemented in MELODIC. For each scan, these components were manually classified into signal or noise. The time-series from noise components were then regressed out of the data.

Functional data was registered to the high resolution structural image using boundary-based

registration (BBR; implemented in FLIRT) and registered to the MNI-152 template (standard space) using non-linear registration with 12 degrees of freedom. Lastly, functional data in standard space was spatially smoothed using a Gaussian kernel of 5 mm FWHM.

5.2.3.2 Deriving Group Networks

The preprocessed functional data was temporally concatenated across sessions and across subjects to create a single dataset. A group-ICA was then run, decomposing this concatenated dataset into 25 components. For the group-ICA a dimensionality of 25 was chosen after exploring dataset with automatic dimensionality estimation, which decomposed the data into 57 components. Visual inspection of the 57 showed that motor network and a cerebellar network of interest was split into several components, therefore a lower dimensionality of 25 was chosen to derive group networks. Further, previous literature had found 25 components to be sufficient to derive motor resting-state networks [335].

5.2.4 Statistical Analysis

All statistical tests were performed using R [287].

Within-subject analysis. To test whether task condition affected change in connectivity from pre to post, we used the R package lme4 [23] to construct a linear mixed effects model of the connectivity variable of interest. As fixed effects, we entered time (pre, post), condition (adapt, control) and time*condition interaction into the model. We allowed intercepts for different subjects to vary in order to account for covarying residuals within subjects, creating a random intercept model. Visual inspection of residual plots did not reveal any obvious deviations from homoscedasticity or normality. P-values were obtained by likelihood ratio tests of the full model with the effect in question against the model without the effect in question.

Between-subject analysis. To test for a relationship between connectivity and behaviour, we calculated Spearman's rank correlation coefficients. To determine whether two correlation coefficients are significantly different, Spearman's coefficients were converted into z-scores using Fisher's Z-transformation. we then performed z-tests on the z-scores given the standard error of each z-score. This method is standard for testing the equality between Pearson's correlation coefficients, but less commonly used for Spearman's coefficients. However, simulations show that this practice is justified for Spearman's coefficients and more robust than using Pearson's correlation coefficients on non-normal data to test for differences in correlations [249].

5.2.4.1 Behaviour

For a detailed analysis of the behavioural data, please see chapter 4. To test for a relationship between resting-state functional connectivity and behaviour, an Adaptation index as well as a

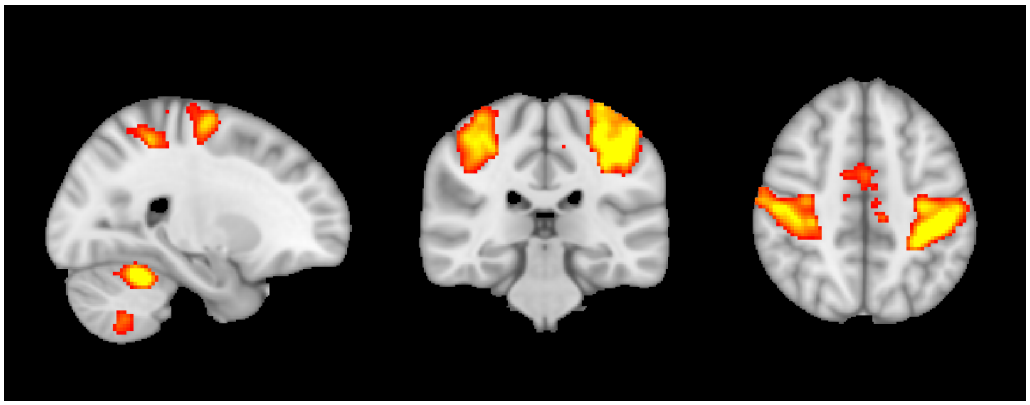
Retention index was calculated.

Adaptation index. Adaptation was quantified by averaging the error in all adaptation blocks up to 70° rotation. Larger rotation blocks were excluded from calculation of the adaptation index, since participants only showed a significant reduction of error in each block up to a rotation of 70°. In each block, the first 8 trials were also excluded from calculation of the adaptation index. This is standard [101] as it captures the rapid error reduction of the adaptation performance rather than performance during the initial exposure to the rotation [187].

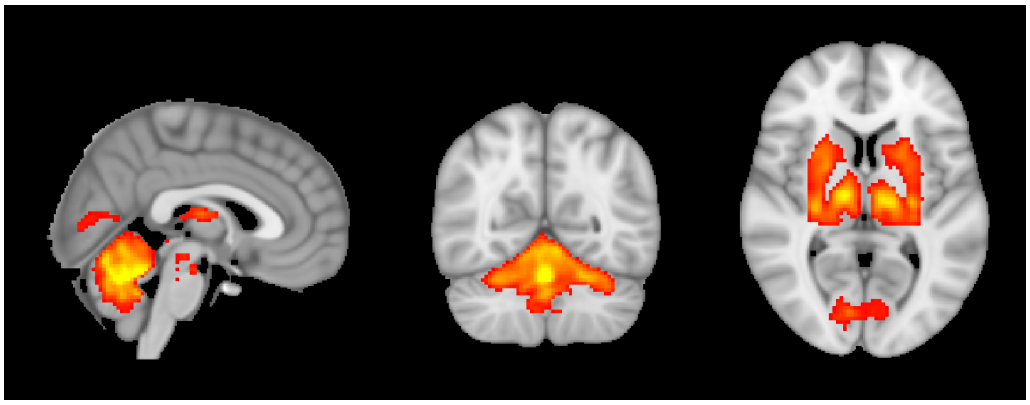
Retention index. Retention of the previously learned rotation was quantified using the error data acquired during the washout period after the scan (see figure 5.1). The Retention index was calculated by averaging all 40 trials from the first block of the washout period. This included the first 8 trials, because a rapid decay of the previously learned motor memory could already take place during the first 8 trials of the washout period, since visual feedback was provided throughout the washout block.

Modelling of trial-by-trial adaptation. To gain a refined measure of adaptation, trial-by-trial adaptation was modelled using a single-state State-Space Model that includes generalization parameters. This modelling technique differs from the technique used in chapter 4, as the previously used model assumes learning from error fully generalizes to all other targets. In other words, generalization parameters were set to equal 1. However, previous work has shown that in 8-target visuomotor adaptation tasks, adaptation does not generalize beyond targets that are more than 45° apart [343]. we therefore modelled each subject's adaptation data separately, resulting for each subject in one retention parameter (SSM parameter A) and 8 adaptation parameters (SSM parameter B_1, B_2, B_3, B_4, B_5, B_6, B_7, B_8). In order to test whether any relationships with adaptation quantified by the adaptation index would hold if adaptation was quantified by the model, we averaged the eight adaptation parameters obtaining SSM parameter B_{mean}. SSM parameter B_{mean} therefore reflects how much participants adapt to errors on an 8-target adaptation task.

5.2.4.2 Network Analysis (Dual Regression).



(A) sensorimotor network.



(B) Cerebellar network.

Figure 5.4: Networks of interest.
A. sensorimotor network.
B. Cerebellar network.

We first sought to identify networks of interest that include regions which would likely be engaged during adaptation to test whether connectivity in these networks changed in response to the task condition (adaptation or control). For this, we ran a group ICA on all resting-state scans to identify 25 independent components. We then spatially cross-correlated the 25 components with a mask that included regions likely engaged during the task. This mask was derived from previous literature [123]. Specifically, the mask represented converging activation during performance of a sensorimotor task obtained from a quantitative meta-analysis of 35 fMRI-studies and included activation in the bilateral anterior medial cerebellum and bilateral M1. Of the 25 components, we identified 2 networks as networks of interest. Both networks overlapped with the meta-analysis mask (sensorimotor network: $r = 0.24$; cerebellar network: $r = 0.15$).

The first network consisted primarily of primary motor cortex and included bilateral anterior cerebellar areas. We will refer to this network as the 'sensorimotor network', as this network is dominated by the motor cortex. The second network that we identified overlapped primarily with the cerebellum, specifically the superior anterior cerebellum and included activation in the bilateral

basal ganglia. We will refer to this network as the 'cerebellar network', as the network is dominated by the cerebellum. The identified networks of interest are shown in figure 5.4.

Lastly, we identified a control network, which we expect to be unaffected by task condition. We chose the Default Mode Network as the control network, shown in figure 5.5, which did not overlap with the ROIs.

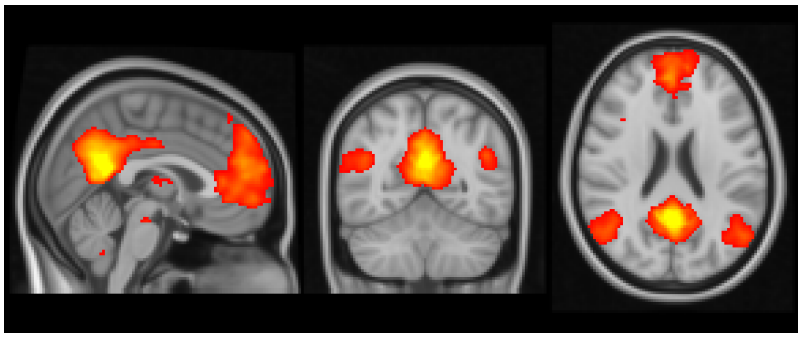


Figure 5.5: Control Network.
The Default Mode Network (DMN) was chosen as a control network. No significant effect of condition (Adapt vs. Control) was found on the DMN at timepoint pre or post or on the difference between pre and post (all $p > 0.24$).

In order to obtain subject-specific maps, we ran a dual regression on these three networks (sensorimotor network, Cerebellar network, Default Mode Network (DMN)). In short, this approach consists of two stages. First, the group networks of interest are spatially regressed against each FMRI dataset, resulting in a timecourse for each dataset for each network. Second, the timecourses are regressed temporally against the FMRI dataset, resulting in a spatial map specific to each dataset for each network.

We then tested for a significant effect of condition (Adapt vs. Control) on the network, by masking the subject-specific networks by the group mean network and comparing them using randomise [382]. Significant clusters were identified using cluster-wise thresholding, (z-threshold: 2.3, cluster p-threshold: 0.05, common thresholding levels [387]).

5.2.4.3 Connectivity Analysis (Connectivity between ROIs).

Next, we aimed to test whether the connectivity between M1 and the cerebellum changed due to adaptation. For this seed-based connectivity analysis, we drew a ROI for the M1 hand area on the standard MNI152 template image. The M1 ROI included the cortex in the anterior bank of the central sulcus as well as the posterior half of the precentral gyrus. It extended from the level of the dorsal surface of the lateral ventricles to the dorsal surface of the brain and from the lateral surface of the brain to the interhemispheric fissure.

ROIs for the cerebellum were defined from previous literature, namely a quantitative meta-analysis which identified three cerebellar regions involved in adaptation [123]. These were

located in the right cerebellar vermis in lobules I-IV, in the right cerebellum in lobules V-VI and in the left cerebellum in lobule VI (see table 2 in [123] and upper panel of figure 2 in [123]).

CSF activity was extracted from an ROI in the left lateral ventricle. This timecourse served as a measure of global signal change.

Connectivity between ROIs was calculated by correlating the activity extracted from two ROI. Change in connectivity was calculated by subtracting the correlation value in the pre-scan from the correlation value in the post-scan, with positive change values reflecting an increase in connectivity.

5.3 Results

Participants	
Recruited	15
Gender	8 Female
Age	26.7 (±3.4)
1st Session Adaptation	8
Excluded (RS data)	0
Excluded (Retention data)	1
Final Sample (RS and Adaptation)	14
Final Sample (RS and Retention)	13

Table 5.1: Sample Characteristics.
One participant was excluded from analysis of adaptation and retention due to failure to attend the adaptation session. Additionally, one participant was excluded from analysis of retention due to no washout data.

5.3.1 Adaptation affects resting-state network.

If task condition affected resting-state networks, these effects should only be evident after task performance, not before. Hence, we expected no differences in the networks at baseline. We tested this by testing the contrast Adapt > Control in the subject-specific networks at baseline (pre networks). If task condition affects resting-state connectivity, networks acquired after the task (post networks), should be modulated by condition. We therefore tested for an effect of condition on the post networks. Task condition could also affect the change in connectivity from pre to post. To test this, we constructed a "difference network", by subtracting the pre network from the post network of each subject in each condition.

All tests were performed for the two networks of interest, the sensorimotor network and the cerebellar network, expecting a significant effect of condition on these networks. Lastly, to test whether a potential effect was specific to these networks, we conducted the same analysis on a

control network (DMN, see figure 5.5). We expected no difference between Adapt and Control Condition in pre and post, nor in change from pre to post (difference between pre and post) for the DMN.

If task condition modulates resting-state networks, then one might expect task performance to relate to how much the network is modulated. We therefore tested whether better adaptation performance correlates with change in network strength from baseline (pre) to after the adaptation task was performed (post). For this, we quantified network strength by extracting the mean z-value from the subject-specific network maps masked by the group network mask. Change in network strength was calculated by subtracting the strength value from the subject's pre-scan from network strength in the post-scan, with positive change values reflecting an increase in network strength. We refer to this difference as connectivity change. To test for a relationship between connectivity change and adaptation performance, we calculated Spearman's rank correlation coefficients.

5.3.1.1 Sensorimotor network

Dual regression revealed no significant effect of condition on sensorimotor network in the resting-state network post task or pre task and no effect of condition on the difference networks (all $p > 0.1$).

5.3.1.2 Cerebellar network

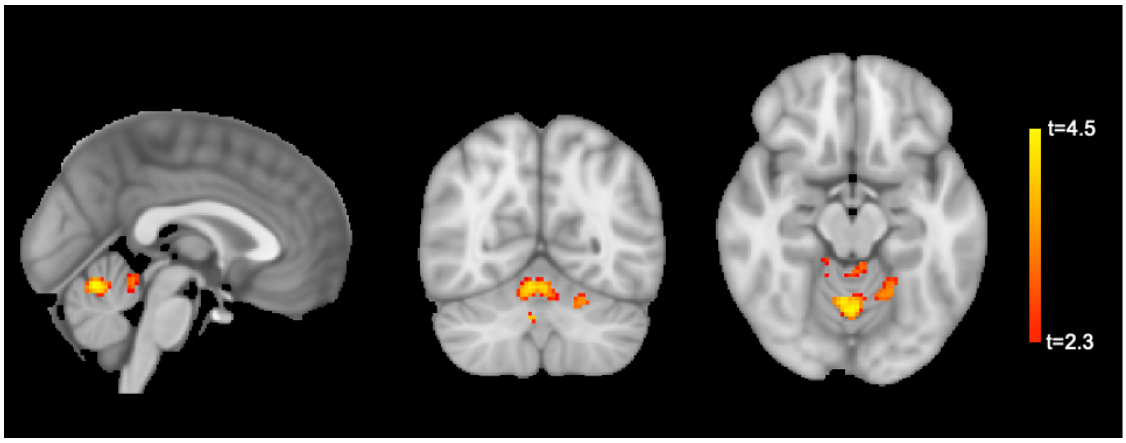


Figure 5.6: Significant cluster. Image shows t-values of voxels that are significant (family-wise error controlled)

Dual regression revealed three significant clusters for cerebellar network in the resting-state network post task (contrast adaptation > Control, see figure 5.6). Cluster information is displayed in table 5.2. No significant cluster for cerebellar network was shown in the pre resting-state scan, as expected ($p > 0.1$). Moreover, there was no significant cluster in the cerebellar network in the difference scan ($p > 0.1$).

Cluster Index	Voxels	Max	X	Y	Z	X_{COG}	Y_{COG}	Z_{COG}
1	596	5.08	8	-38	-22	0	-53	-17
2	14	4.28	-18	-34	-28	-19	-34	-27
3	10	6.54	4	-60	-32	4	-60	-32

Table 5.2: Cluster Information.
Voxels denotes number of voxels in cluster. *Max* denotes maximum intensity value (i.e. maximum z-score) within the cluster. *X / Y / Z* denotes coordinates of maximum intensity voxel, given in MNI standard space coordinates (mm). X_{COG} / Y_{COG} / Z_{COG} denotes coordinates of voxel at centre of gravity, given in standard space coordinates (mm).

Of the three clusters identified, the biggest cluster overlaps with a cerebellar ROI identified previously to be involved in sensorimotor tasks (ROI located in right cerebellar vermis Lobules we – IV; [123]; Overlap = 12 %).

Cluster Index	Location	Overlap
1	Right V	17 %
	Left V	17 %
	Right I-IV	15 %
	Left I-IV	9 %
2	Left I-IV	9 %
3	Vermis VIIIa	13 %

Table 5.3: Cluster Location.
Overlap between cluster and cerebellar regions was calculated by cross-correlating the cluster masks with cerebellar ROI masks. Cerebellar ROI masks were obtained from a cerebellar atlas in standard space after normalization with FNIRT[68]. Only regions with overlap of more than 9 % are reported. *Location* refers to cerebellar ROI label. *Overlap* refers to the percent of the region covered by the cluster.

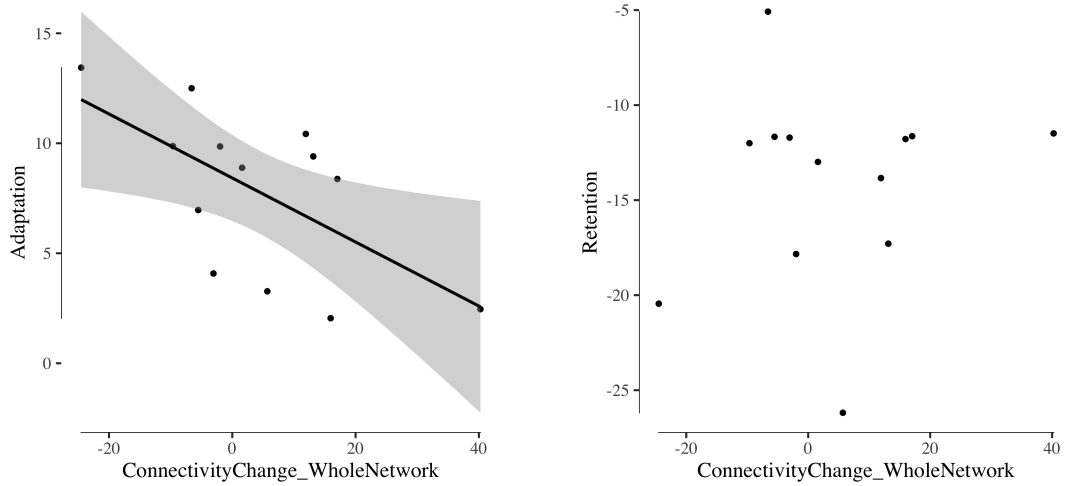
As shown in table 5.3, cluster 1 is located in the right and left hemispheres of the anterior cerebellum and spans several lobules. Cluster 2 is located in the left anterior cerebellar hemisphere, in lobule I-IV. Finally, cluster 3 is located medially in cerebellar vermis VIIIa.

5.3.2 Adaptation performance correlates with change in network.

5.3.2.1 Sensorimotor network

Change in connectivity strength of sensorimotor network did not correlate with adaptation or retention (all $p > 0.1$).

5.3.2.2 Cerebellar network



(A) Connectivity Change and adaptation.

(B) Connectivity Change and retention.

Figure 5.7: Connectivity change and Behaviour.
Change in cerebellar network connectivity from pre to post correlates with adaptation, but not retention.
A. Participants who adapted better to the rotation, show an increase in network strength from pre to post. Participants who adapted less, as shown by a larger adaptation index, show a decrease in network strength from pre to post, as shown by negative values.
B. No relationship between connectivity change and retention

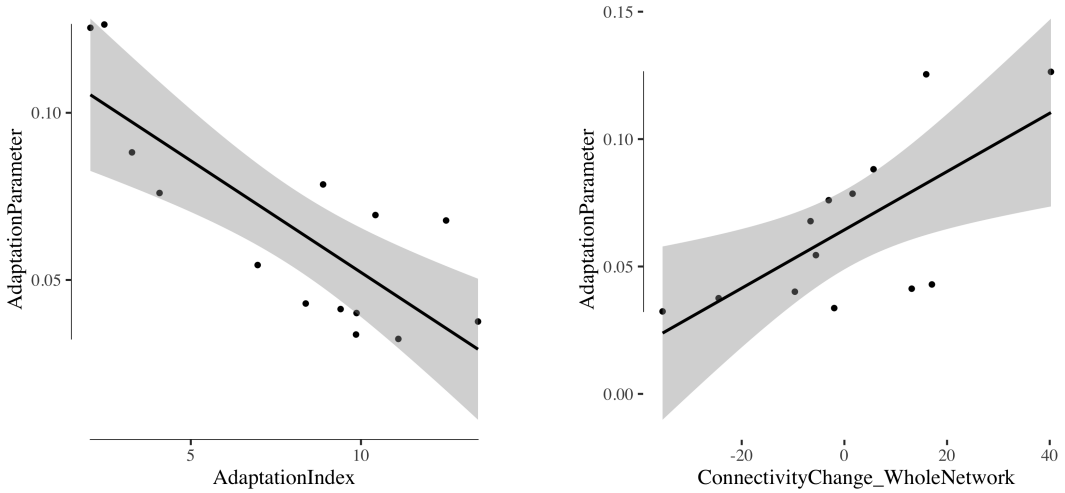
Change in connectivity strength of cerebellar network correlated significantly with adaptation (r = -0.77, p = .002; figure 5.7A), but not with retention (r = 0.11, p = .73; figure 5.7B). The two correlation coefficients were significantly different, as revealed by a significant difference between the coefficients transformed to z-scores (z-score difference = -1.83; $p < 0.03$).

Moreover, the correlation between connectivity change and adaptation was specific to the adaptation session, since no significant correlation between adaptation performance and connectivity change was observed in the control session (r = .19, p = 0.52).

As described in section 5.2.4.1, participants only learned to adapt to rotations up to 70° and the adaptation index was therefore calculated only from blocks up to 70°. Hence, we tested whether connectivity change also correlated with adaptation performance calculated over all rotation blocks. And indeed, connectivity change correlated significantly with adaptation performance quantified across the whole experiment (r = -.54, p = 0.047).

Modelling-based results. We expected the modelling-based measure of adaptation, B_{mean}, to be a refined measure of adaptation. Still, both measures should capture the adaptation process similarly and we therefore tested whether the modelling-free adaptation index and the modelling-based mean adaptation parameter correlate. Indeed, there is a strong relationship between the measures (r = -.74, $p < .01$; figure 5.8A).

Next, we tested whether the relationship shown between change in network strength and adaptation (significant correlation between adaptation index and connectivity change shown in 5.7A), held when adaptation was quantified using the modelling-based approach described in 5.2.4.1 instead of the modelling-free adaptation index. We found that change in network strength correlated with adaptation quantified with a modelling-based approach (significant correlation between B_{mean} and connectivity change; r = .60, p = .02; data shown in figure 5.8B)



(A) Modelling-free and modelling-based measures of adaptation.

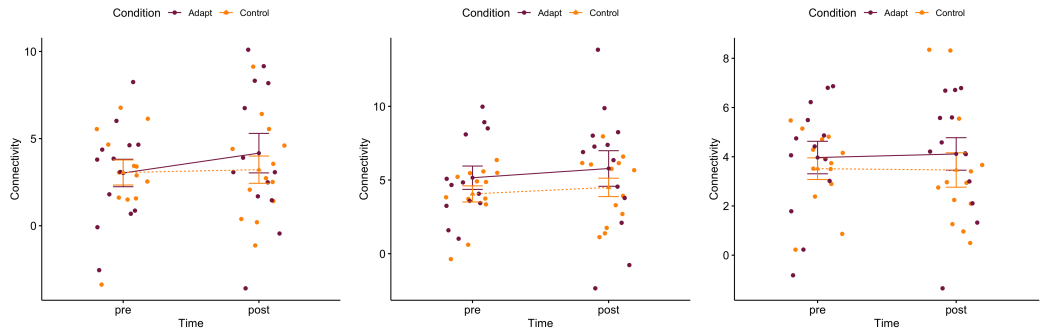
(B) Connectivity change and modelling-based measure of adaptation.

Figure 5.8: Modelling-based results.
Change in cerebellar network connectivity correlates with adaptation, when quantified using the single-state state-space model with generalization.
A. Modelling-free and modelling-based measures of adaptation correlate strongly.
B. Connectivity change correlates with adaptation when quantified by SSM parameter B_{mean}

5.7

5.3.3 Adaptation does not affect connectivity between ROIs.

Adaptation did not significantly affect connectivity between left M1 and the three cerebellar ROIs. As described in section 5.2.4.3, we controlled in our analysis for CSF timecourse in order to account for global signal change. Controlling for CSF timecourse by including connectivity of left M1 with CSF in the model, there was no significant time*condition interaction on connectivity of left M1 with right cerebellum, left cerebellum, or cerebellar Vermis (Right Cerebellum: figure 5.9A; $\chi^2(1) = 0.48$, $p > 0.1$; Left cerebellum: figure 5.9C; $\chi^2(1) = 0.04$, $p > 0.1$); Cerebellar Vermis figure 5.9B; $\chi^2(1) = 0.79$, $p > 0.1$).



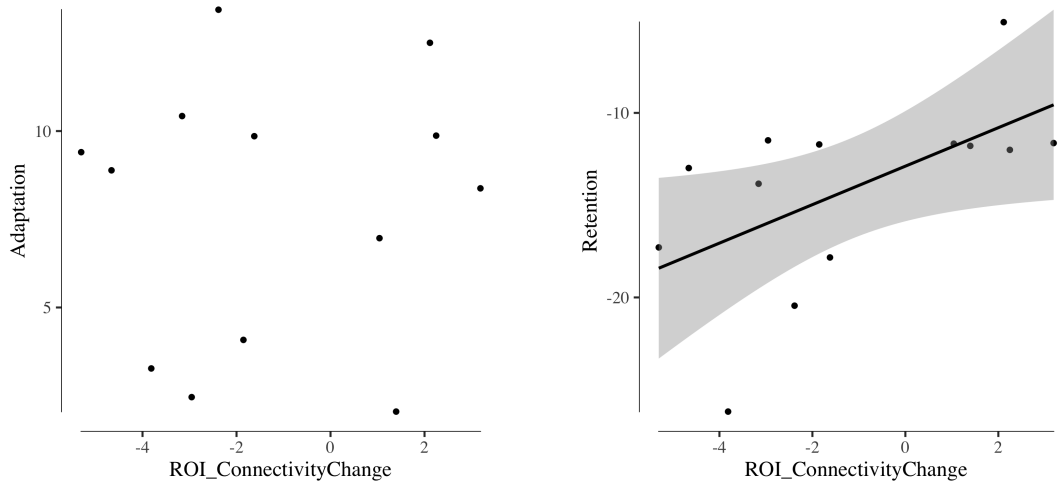
(A) Right Cerebellum (B) Cerebellar Vermis (C) Left Cerebellum

Figure 5.9: Connectivity between left M1 and cerebellar ROIs over time.
Connectivity values shown here are correlation coefficients between mean timecourses within ROIs. Errorbars show group mean ± standard error of the mean.

5.3.4 Retention correlates with connectivity change.

Connectivity change between left M1 and right cerebellum correlated significantly with retention (controlling for left M1-CSF connectivity change in the model: r = .63, p = 0.04; controlling for right Cerebellum-CSF connectivity change in the model: r = .63, p = 0.04; figure 5.10B). The relationship was reduced to a trend when the model did not control for CSF (r = .55, p = 0.07). Participants whose connectivity between left M1 and right cerebellum decreased (negative connectivity change values), showed more retention of the previously learned movement (negative retention values). Connectivity change did not correlate significantly with adaptation (figure 5.10A, r = .11, p = 0.74). Connectivity change also did not correlate significantly with retention in the control condition (r = -.07, p = 0.84). Moreover, change in connectivity between right cerebellum and a control region (right M1) did not correlate with retention (r = -.04, p = 0.90). However, when controlling for CSF by regressing out the CSF timecourse, there was no significant relationship between connectivity change and retention (r = 0.40, p = .17).

Change in connectivity between left M1 and cerebellar Vermis, as well as left M1 and left cerebellum did not correlate significantly with retention (M1 connectivity with cerebellar Vermis controlling for CSF in model: r = .14, p = 0.68; left cerebellum: r = .16, p = 0.62).



(A) Connectivity change and adaptation.

(B) Connectivity change and retention.

Figure 5.10: Connectivity change and Behaviour.
Connectivity change between left M1 and right cerebellum correlates with retention, but not adaptation. Plots show data with variance associated with left M1-CSF connectivity regressed out. Shaded area shows confidence interval.
A. Connectivity change between left M1 and right cerebellum and adaptation did not correlate (r = .11, p = 0.74).
B. Connectivity change between left M1 and right cerebellum and retention correlates when controlling for CSF connectivity in the model (r = .63, p = 0.04).

5.3.5 Connectivity change correlates with baseline GABA

To investigate the involvement of the primary motor cortex in adaptation, we tested whether adaptation changed connectivity between the cerebellum and the primary motor cortex.

In order to ensure that the changes in connectivity strength between the ROIs were not driven by a global signal change, statistical analysis controlled for CSF timecourse in one of two ways. The first way was to include CSF into the model. For this, we added the correlation value of one of the two nodes of interest with the CSF node as a variable. The second way was to regress the CSF timecourse out of the two ROI node timecourses before correlating them. Results are reported for both control strategies.

The resting-state fMRI data described in this chapter was acquired as part of the experiment described in chapter 4. As described in chapter 4, GABA at baseline significantly predicted retention. Since retention also showed a relationship with connectivity change between left M1 and right cerebellum, we tested whether baseline GABA correlated with left M1 - right cerebellar connectivity change.

In the adaptation condition, connectivity change correlated significantly with GABA at baseline, when controlling for GM fraction and CSF connectivity in the model (r = -.64, p = 0.03). This relationship was reduced to a trend when controlling for GM fraction by multiplying the GABA values at baseline with GM percentage (r = -.53, p = 0.07; for details on this GM

correction, see chapter 4). However, in the control condition, there was no significant relationship between connectivity change and GABA baseline (r = .19, p = 0.62). Moreover, when pooling all sessions, there was no significant relationship between connectivity change and GABA baseline (r = -.18, p = 0.41).

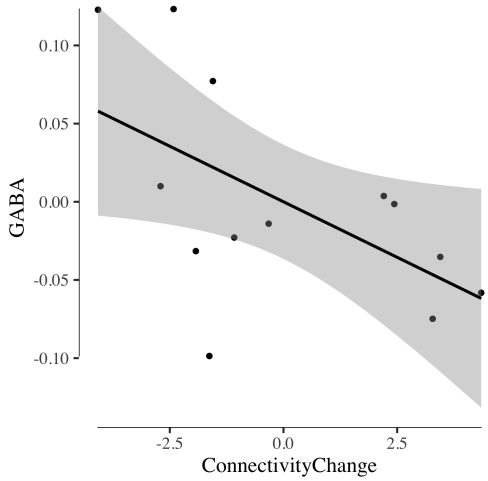


Figure 5.11: Connectivity change and $GABA_{Baseline}$.
Connectivity change between left M1 and right cerebellum correlates with GABA at baseline. Plots show data controlling for right cerebellar - CSF connectivity and GM fraction. Shaded area shows confidence interval.

5.3.6 GABA does not correlate with connectivity in MRS voxel

It has previously been shown that baseline GABA concentration in the motor cortex can be related to the motor-network connectivity strength within the MRS voxel [335]. We therefore tested whether baseline GABA correlated with activity within the MRS voxel during the pre scan. There was no relationship between GABA at baseline and activity within the MRS voxel during the pre scan (r = -0.23, p = .26).

5.4 Discussion

This study investigated the effect of adaptation on resting-state networks with particular focus on resting-state networks involving the cerebellum. I showed a significant increase in cerebellar connectivity after performing a novel adaptation task within a cerebellar resting-state network. Moreover, connectivity change within this network correlated highly with adaptation, such that participants who adapted well showed an increase in connectivity. This effect was specific to adaptation (no correlation with retention), specific to the adaptation condition (no correlation in control session), and specific to the network (no correlation with change in the default mode network as a control network). Additionally, connectivity change correlates with adaptation quantified with a modelling-based approach.

In addition to this network-based connectivity analysis, I investigated connectivity using a Region of Interest (ROI)-based analysis, focussing on connectivity between the hand area of left M1 with cerebellar ROIs defined from the literature. I found that adaptation did not affect connectivity between left M1 and the cerebellar ROIs. However, I showed that connectivity change between left M1 and right cerebellum correlated with retention, such that participants who retained more of the previously learned movement showed a decrease in connectivity. This effect was specific to retention (no correlation with adaptation), specific to the adaptation condition (no correlation in control session), and specific to left M1 (no correlation when testing right M1 - right cerebellar connectivity). Because retention also correlated with baseline GABA (see chapter 4), we tested whether connectivity change correlated with baseline GABA. And indeed, connectivity change correlated with baseline GABA, showing that participants with higher left M1 GABA at baseline showed a decrease in connectivity. However, controlling for CSF by regressing out the CSF timecourse, instead of controlling for CSF in the model, removed the relationship.

Finally, I found no relationship between M1 baseline GABA and activity within the MRS voxel at baseline.

5.4.1 Adaptation affects network connectivity

Adaptation led to stronger connectivity in a cerebellar-basal ganglia resting-state network than movement execution alone. Significantly increased connectivity was evident in the cerebellum after performing the adaptation task, compared to after performing the control task. There was no difference between conditions (adaptation vs. control) in the network before task performance, suggesting that the effect of task condition on connectivity was not driven by baseline differences.

The largest region of increased cerebellar connectivity after adaptation identified in this study was located in the bilateral anterior cerebellum and primarily spans the right and left anterior lobule V. This finding is in line with a recent quantitative meta-analysis of 35 neuroimaging studies involving sensorimotor tasks, which found significant activation in bilateral basal ganglia and in bilateral anterior cerebellar areas for sensorimotor tasks [123]. The region showing increased connectivity after adaptation, but not control, significantly overlaps with converging activity found in this meta-analysis.

Our result is also in line with previous studies highlighting the importance of the anterior cerebellum for adaptation. The anterior cerebellum has been related to motor function in patient studies [310] [311] [309] and it has been shown to contain sensorimotor representations of the body [207] [260] [103] [168] [350].

In a previous study of resting-state connectivity, the right and left anterior cerebellar lobule V were found to be functionally connected at rest to the motor cortex (see figure 1 and table 1 in

[256]). Moreover, increased activation in the right anterior cerebellum in lobule IV/V was found during adaptation [315], specifically during early phases of a visuomotor adaptation task. The same study also found bilateral basal ganglia activation during adaptation, along with previous imaging studies showing basal ganglia activation in early adaptation to a visuomotor rotation [317]. The adaptation-modulated network identified in this study includes not only cerebellar areas, but also basal ganglia regions.

Furthermore, we show that an increase in connectivity of this adaptation-modulated network relates to improved adaptation. This relationship is also present with adaptation quantified using a single-state state-space model. The absence of the adaptation-connectivity relationship in the control session and the absence of a relationship between connectivity change and retention provide compelling evidence for the notion that this network is specific to adaptation.

To our knowledge, we provide first evidence for adaptation-specific changes in a cerebellar resting-state network that relate to adaptation performance.

5.4.2 Retention relates to connectivity change

While adapting a movement is thought to primarily rely on the cerebellum, retaining the compensatory movement is believed to involve M1 [101] [116]. Given that in chapter 4 we link baseline GABA concentration in left M1 to retention, in this chapter we set out to explore the role of left M1 functional connectivity. Importantly, although network strength change correlated with adaptation, this change measure was not derived from left M1. Network strength change was calculated only from values within the group network and the group network does not include M1 (see 5.4). We therefore avoided circularity in our analysis by only considering network connectivity within left M1.

We did not observe a modulation of left M1 - cerebellar connectivity in the adaptation compared to the control condition, but we observed a correlation between left M1 - right cerebellum connectivity change and retention. Participants who showed a decrease in connectivity retained more of the previously learned movement. The relationship was task-specific (no link in control task), regionally specific (no link with right M1) and behaviourally specific (no link with adaptation). These results are in line with the suggested role of M1 for retaining an adapted movement, but the direction of the relationship may seem counter-intuitive. Disrupting left M1 activity using TMS pulses immediately after each adaptation trial, led participants to retain less of the adapted movement, without affecting adaptation [116]. Conversely, stimulating left M1 during adaptation did not influence adaptation, but increased retention [101]. Increased M1 activity has therefore been argued to facilitate the formation of the adaptive motor memory. Along with this, one could expect increased M1-cerebellar connectivity to relate to improved retention. However, it

is important to consider that the results reported in this study pertain to connectivity changes not during task performance, but at rest before and after adaptation. It may be that during adaptation, enhanced activity of M1 supports retention, but that a decrease in connectivity between M1 and cerebellum prevents the new adapted movement from being overridden. Interestingly, the MRS data collected in this experiment shows high GABA at baseline correlated with a decrease in connectivity strength. Previous research has linked high resting GABA with lower connectivity in the motor network and anodal tDCS applied to M1, an intervention known to lead to lower GABA, to an increase in motor network strength [335].

These results may suggest that greater inhibition in left M1 and a decrease in left M1 - right cerebellar connectivity result in more retention, preventing the adapted movement from washing out. However, it is important to note that the described relationships between connectivity and retention as well as GABA at baseline only hold when controlling for CSF in the model. Regressing the contribution of CSF out of the data before calculating connectivity changes removes the correlations discussed here. Given this methodological caveat and the correlational nature of the analysis, we would therefore interpret these results with caution. Although we provide evidence for a potential link between connectivity changes, baseline GABA concentration and behaviour, further research is needed to corroborate these findings and characterise the mechanisms driving them.

5.4.3 Limitations

The novel task paradigm used in this study was sufficient to elicit functional changes in a cerebellar resting-state network and also allowed for quantification of adaptation performance which in turn could be linked to these functional changes. However, a minor limitation of the task used in this study was the sequence in which targets were presented to the participant. Participants were prompted with one of eight targets in a pseudo-randomised fashion. Pseudo-randomised in this context means that all targets on the target circle were shot within a cycle of eight trials, but the sequence in which these targets appeared was random within each cycle. Because of that, every participant experienced a different target sequence over the course of the experiment. Evidence from visuomotor rotation studies indicates that adaptation learning does not generalize beyond a target difference of 45° [343]. Differing target sequences could therefore induce slight differences in task difficulty that add noise to our measurement of adaptation performance. Moreover, modelling adaptation performance with a state-space model can be significantly improved when a generalisation term is introduced into the model that can assume a fixed target sequence. Although the practice of presenting pseudo-randomised target sequences in adaptation studies is still common [100], we choose to fix the target sequence in subsequent adaptation studies. However, given the

large number of adaptation trials used in this study (480 trials), we assume that the effects of an unfixed target sequence are negligible for the interpretation of the results of this study. A second limitation of this adaptation paradigm is the lack of control for cognitive strategies used in compensating the rotation. Recent evidence suggests that adaptation involves different strategies, which may differ in their recruitment of the cerebellum [220]. It is difficult to directly assess strategies used during adaptation without introducing delays between adaptation trials or adding components to the task that are not directly related to adaptation (e.g. verbal report of the target aim). For subsequent studies, we therefore assess awareness of the perturbation and potential strategies used during the task by interviewing participants at the end of the last experimental session.

5.4.4 Conclusions

In this chapter, we provide evidence for a cerebellar resting-state network that is specifically modulated by adaptation and that shows stronger connectivity when participants adapt better. We also find evidence for a potential link between changes in cerebellar-M1 connectivity and retention. Together with the results described in chapter 4, this chapter establishes feasibility and suitability of this novel adaptation task for studying plastic changes in the cerebellum in adaptation.

CHAPTER 6.0

Investigating cerebellar GABA during adaptation using 3T MRSI

Abstract

Neurotransmitter concentrations in human primary motor cortex (M1) have been shown to relate to learning of motor skills. Decreases in GABA in M1 have been observed during model-free motor learning. However, it is not clear if similar changes in GABA concentration are seen in the cerebellum during performance of a model-based adaptation task. Here, we used 3T MRSI to investigate GABA concentration in the cerebellum during adaptation. Because cerebellar activation during motor tasks is lateralized, we hypothesized a GABA decrease ipsilateral to the performing hand, i.e. in the right cerebellar hemisphere.

Methods. MRSI data was acquired in 16 healthy participants (within-subject design) from a 65 x 25 x 15 mm volume containing 7x14 voxels in the cerebellum while participants performed a visuomotor adaptation task using a hand-held joystick with their right hand. During one session (adaptation session) visual feedback was rotated and participants adapted their movements to a stepwise increasing rotation, followed by a washout period (no rotation). In the other session (control session) no rotation was imposed. Resting-state fMRI data was collected before and after participants performed the adaptation and the control task.

Task performance was quantified using mean error. Metabolite concentrations were quantified using LCModel and data was thresholded based on Cramer-Rao bounds, spectral line widths and SNR. Metabolite maps were corrected for tissue composition and internally referenced to total creatine. ROIs of the left and the right cerebellar hemisphere were used to extract mean GABA timecourse during adaptation and control session. To test for changes that pertain to adaptation only, adaptation GABA was normalised to control GABA at each timepoint. A Linear mixed effects model (LME) of normalised GABA was constructed to test for interaction between hemisphere and timepoint. Fixed effects were hemisphere (Right, Left) and timepoint (Baseline,

EarlyAdaptation, LateAdaptation, AfterAdaptation) and hemisphere x acquisition interaction. To test for a relationship between GABA and behaviour, we calculated Spearman's rank-order correlations.

Resting-state fMRI data was cleaned from structured noise using an automatic classifier trained on hand-labelled resting-state data (FIX-based denoising). The resultant cleaned fMRI data was then analysed using a network-level approach by decomposing the concatenated data into 25 components with group-level independent component analysis. A cerebellar network of interest was identified through visual inspection and confirmed through cross-correlating the network's spatial map with regions of interest obtained from a prior study (described in chapter 5). Subject-specific spatial maps were derived through dual regression and tested for a modulation by task condition (adapt vs. control). Network connectivity strength values were obtained by extracting the mean z-value from the subject-specific network maps masked by the group network mask. To test for a relationship between connectivity strength and behaviour, as well as connectivity strength and mean [GABA] in the MRSI volume, we calculated Spearman's rank-order correlations.

Results. Participants adapted to the rotation, with a compensatory movement of $-30.80° \pm 6.16°$ (significant difference between error and imposed rotation during late adaptation t(14) = -21.4, $p < 0.001$). Participants showed a significant aftereffect when visual feedback was removed ($-36.66° \pm 8.39°$; t(14) = -16.77, $p < 0.001$). As hypothesised, right hemispheric GABA decreased during late adaptation (significant interaction term hemisphere (right) x timepoint (LateAdaptation): $\chi^2(1) = 6.53$, $p = 0.04$). The changes were specific to GABA, as glutamate concentration did not show significant changes during adaptation ($\chi^2(1) = 2.62$, $p = 0.27$). Normalised GABA change did not correlate with late or early adaptation. However, GABA concentration during late adaptation correlates with adaptation ($r = 0.52$ $p = 0.046$): Participants with lower GABA concentration adapt better overall.

Cerebellar connectivity was not significantly modulated by adaptation compared to control ($p > 0.1$) and change in connectivity strength of the cerebellar network did not correlate with adaptation (r = -0.12, p = 0.7). Therefore, the effect of task condition on cerebellar connectivity and the link between network strength and adaptation performance demonstrated in chapter 4 did not replicate in this study.

Finally, cerebellar GABA at baseline and cerebellar network strength at baseline correlated significantly ($r = 0.4$ $p = 0.03$).

In summary, we provide first evidence that GABA decreases during adaptation in

the right compared to the left cerebellar hemisphere and that late right hemispheric GABA level relates to adaptation. Moreover, we demonstrate a significant positive relationship between cerebellar network strength and GABA at baseline.

6.1 Introduction

Understanding the changes in the human brain that occur during learning and how these relate to behaviour is fundamental in neuroscience and a vital step in developing effective therapeutic interventions. The cerebellum has been implicated in a wide variety of learning processes of mainly motor learning, though a role in cognitive and emotional learning has more recently been suggested [353]. As such, its role in motor adaptation has been studied widely by using adaptation paradigms that perturb the environment in which participants perform movements. These studies show that the cerebellum is involved in adapting to changes in the environment in a way that suggests the cerebellum learns from sensory prediction errors in particular [308] [347]. However, despite extensive study of the role of the cerebellum in this type of learning, the exact physiological mechanisms that underpin adaptation remain unclear. Here, I combine Magnetic Resonance Spectroscopy Imaging (MRSI), resting-state fMRI and a novel adaptation paradigm to investigate these mechanisms in humans.

In human M1, a decrease in local [GABA] has been observed during motor learning [92] [181]. Moreover, the extent of this decrease has been shown to predict the improvement due to motor learning [181]. Further, when decreasing M1 GABA by applying anodal tDCS over M1 during motor learning, the extent of this decrease correlates with the improvement due to motor learning [332]. In the cerebellum of monkeys, GABAergic Purkinje cells - the sole output neuron of the cerebellar cortex - have been shown to fire more complex spikes after a perturbation is introduced [105]. As monkeys learned to adapt and movement errors got smaller, complex spike firing has been shown to return to baseline [105]. Further, complex spike firing has been to serve as a teaching signal [260] leading to long-term depression (LTD at synapses between parallel fibers and Purkinje cells) [150] [4] [213]. This LTD in turn results in decreased simple spike firing [105] [104] [393] and improved motor performance [224]. Purkinje cells are GABAergic,raising the possibility that a decrease in local [GABA] in the cerebellum is tied to successful adaptation. To date, this has not been investigated in humans.

Identifying adaptation-specific changes in GABAergic signalling may be difficult, as these may be superimposed over other GABA fluctuations. For example, there may be changes in MRS-assessed GABA concentration due to prolonged time in the scanner, as GABA may naturally fluctuate over an extended period of time. GABA may also change during movement. To determine the specificity of changes in [GABA], we therefore included a control task, in which subjects

performed the same movements but in the absence of a rotation.

The cerebellum contains a somatomotor map of the body, and the activation pattern during motor tasks performed with the hand is strongly lateralized [45]. When performing a movement task with the right hand, task-based activation is found predominantly in the right anterior cerebellar hemisphere. We therefore hypothesised that a [GABA] decrease would be evident in the right cerebellar hemisphere compared to the left when participants are learning to adapt to a rotation with their right hand. To assess [GABA] in the right and the left cerebellar hemisphere simultaneously, we employ a newly developed MRSI sequence [338].

Finally, we wanted to relate any changes in cerebellar [GABA] to changes in network connectivity. We therefore recorded resting-state fMRI before and after task performance. The strength of the resting-state motor network has previously been linked to [GABA] in M1 [335]. We therefore hypothesised that cerebellar [GABA] would correlate with strength of a cerebellar resting-state network.

In addition, we explore changes in a cerebellar resting-state network due to adaptation, in line with our previous result showing an adaptation-modulated cerebellar network (reported in chapter 5).

6.2 Methods

6.2.1 Participants

Seventeen healthy, right-handed participants (6 female; 18-34 years; mean age 23 years) participated in this within-subject study. Each participant attended two sessions during which they performed a visuomotor task with either a learning component (adaptation condition) or no learning component (control condition) during MRI. The order of the sessions was counterbalanced across the group.

Participants had no history of neurological or psychiatric conditions and were not taking any medication that affects the central nervous system. All participants gave their written informed consent to participate, in line with central university research ethics committee approval (University of Oxford; R59564/RE002). One participant fell asleep during one scanning session and was therefore excluded from further analysis.

6.2.2 Experimental Protocol

A schematic of the experiment sessions is shown in figure 6.1.

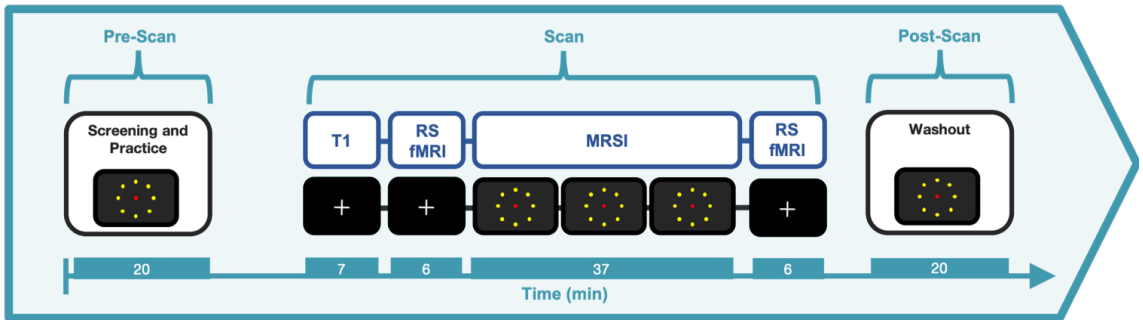


Figure 6.1: Experimental Protocol.

Participants performed a visuomotor task using a hand-held joystick (Nata Technologies, custom-built fMRI joystick, 60 Hz sampling rate) to control a cursor on a screen, which either involved a learning component (adaptation condition) or no learning component (control condition). Participants were instructed to make ballistic movements to 'shoot' with their cursor through one of eight targets. In the adaptation condition, participants had to adapt their movements to a stepwise increasing rotation of the visual feedback, whereas in the control condition there was no rotation. The adaptation task is shown in figure 6.2. This task was similar to that in chapter 4.2.2, but three changes were made. First, the stepwise increasing rotation only went up to 80°, as previously participants only reduced errors up to a rotation of 70° (4.3.1). Second, after the 80° rotation block, visual feedback of the controlled cursor was removed for four blocks ('open loop' blocks), to assess retention of the adapted movement (crossed out eye in figure 6.2). Third, the sequence of target presentation was fixed across participants, to ensure equal task difficulty across subjects. Piloting showed that participants were unable to predict the target sequence when encountering the same sequence of trials twice.

In the control condition, participants performed the task without any rotation imposed for the full duration of the task. To match the open loop phase of the adaptation condition, visual feedback was removed during the last four blocks of the task in the control condition (see figure 6.3).

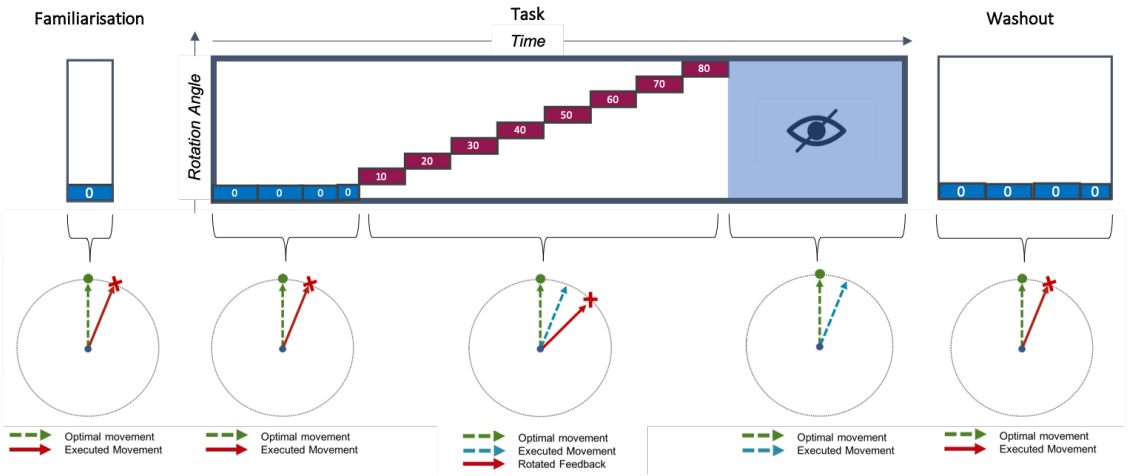


Figure 6.2: Task.
Upper panels. Task Outline. Stepwise increasing rotated feedback required participants to adapt movements to reduce errors (40 trials of 4 seconds duration each). Participants familiarised themselves with the task before the scan (40 trials, no rotation) and performed a washout phase after the main task (144 trials, no rotation). Not depicted: In the control session, participants performed the task without any rotation imposed, but for the same length (616 trials in total for the main task).
Lower panels. Trial Types. During familiarisation, baseline trials of both conditions (control and adapt) and during washout, visual feedback was veridical (Feedback matches executed movement). In the adaptation condition, during adaptation trials visual feedback was rotated (Feedback is rotated compared to executed movement). In control condition, feedback was veridical for all trials apart from the open loop trials. During open loop trials of both conditions, visual feedback was removed (No Feedback). Familiarisation and washout phases took place outside the scanner, whereas the main task (control or adapt) was performed inside the scanner during MRSI acquisition.

6.2.3 Magnetic Resonance Imaging Acquisition

All Magnetic Resonance (MR) data were acquired on a 3T Siemens scanner with a 32-channel head coil. Structural MRI data were acquired using a magnetisation prepared rapid acquisition gradient echo (MPRAGE) sequence (Repetition Time 1900 ms, TE 3.96 ms, slice thickness 1.0 mm, in-plane resolution 1.0 x 1.0 mm^2, GRAPPA factor = 8, flip angle = 8, FOV 256 x 232).

6.2.3.1 Resting-state fMRI.

The resting-state fMRI acquisition was matched to the UK Biobank resting-state fMRI parameters described in [7]. A multiband isotropic EPI acquisition (TR/TE = 735/39 ms, FOV = 210 x 210 mm^2, bandwidth = 2030 Hz/Px, multi-band acceleration factor 8, voxel dimension = 2.4 x 2.4 x 2.4 mm^3, whole brain, acquisition time = 6:10 min for a total of 490 volumes) was performed before and immediately after the task. A separate "single-band reference scan" (SBRef) was acquired before the multiband acquisition [240]. This serves as the reference scan during preprocessing (e.g. during motion correction and registration steps), as it suffers from the same distortions as the multiband data, but has higher contrast [7]. Subjects fixated on a cross-hair image presented centrally on the screen during resting-state fMRI acquisition.

6.2.3.2 MRSI.

Structural images were used to manually place a 65 x 25 x 15 mm MRSI slab in the cerebellum. The slab was positioned to cover anterior and superior areas of the right cerebellum which houses the hand motor representation [19] [244], while avoiding contact with either the dura to minimize significant macromolecule contamination or with brain stem to avoid excess physiological noise [41].

Four MRSI scans were acquired during performance of the visuomotor task (time per scan = 9 min, total acquisition 36 min, TE 32 ms; figure 6.3). MRSI data was acquired using a non-water suppressed semi-LASER semi-DW-CRT sequence with metabolite cycling [338] at 5 x 5 x 15 mm resolution.

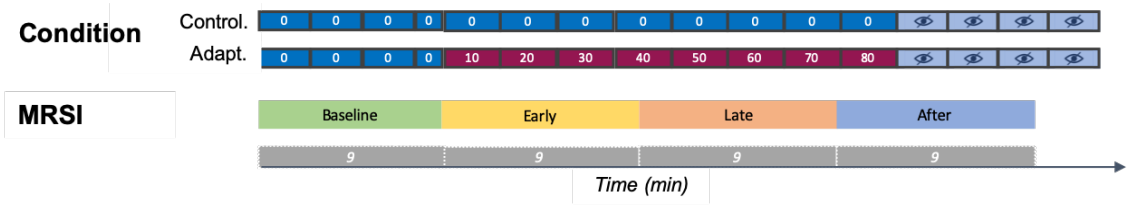


Figure 6.3: MRSI Acquisition and Task Phases.
MRSI was acquired during four phases of the main visuomotor task. The *Base* phase includes all baseline trials of the adaptation condition. The *Early* phase was acquired during early adaptation (and corresponding trials of the control condition). It includes 10°, 20° and 30° rotation blocks of the adaptation condition and the first 16 trials of the 40° block. The *Late* phase corresponds to the late phase of adaptation (and corresponding trials of the control condition). It includes the remaining 24 trials of the 40° block, the 50° and 60° rotation blocks, as well as the first 32 trials of the 70° block. The *After* phase contains primarily the open loop blocks that come after the adaptation phase, but also some of the last adaptation trials. Specifically, it includes the remaining 8 trials of the 70° block and the 80° block. The open loop trials that this last phase includes, are the ones from the first two open loop blocks and the first 8 trials of the third open loop block. After the MRSI acquisition had ended, the task was performed for the remainder of the third open loop block and the fourth and last open loop block.

6.2.4 Behavioural Analysis

Cursor movements were analysed as described in section 3.2.4.1. Adaptation was quantified using modelling-free and modelling-based analysis methods.

6.2.4.1 Modelling-free Analysis

Control Condition. In the control condition, visual feedback was veridical and therefore participants were not required to adapt to a perturbation. However, performance might still change over the course of the experiment. To test for any possible relationship between metabolites and behaviour in the control condition, we calculated indices of control behaviour that matched the MRSI acquisition phases. For the Base phase, we calculated a Control Index (CI) by calculating the mean error of all baseline trials of the control condition (CI_{Base}). Similarly, we calculated a CI_{Early} (blocks 5 - 8.4) and a CI_{Late} (blocks 8.5 - 11) and tested for differences between the CIs at

these time points using paired t-tests.

Adaptation Condition. We grouped every eight consecutive trials into one *epoch*. All blocks (apart from the fourth baseline block) therefore consisted of five epochs. To test for adaptation, we constructed a LME of error during baseline and adaptation trials. We entered epoch and rotation as fixed effects, and an interaction term for epoch x rotation. We allowed intercepts for subjects to vary to account for co-varying residuals within subjects. We allowed intercepts for each of the eight different targets to vary, to account for a target-specific movement bias, meaning subject and target were random effects.

To compare adaptation between participants, we calculated an Adaptation Index. For this, we calculated the mean error across all rotation blocks of the adaptation condition, excluding the first epoch (trials one to eight) of each rotation block [101]. To study relationships between metabolites and adaptation behaviour, we quantified adaptation performance during the early and late phase of the MRSI acquisition (AI_{Early} and AI_{Late}) by calculating the mean of the errors of all trials performed during the scan. We additionally calculated the mean error of all baseline trials of the adaptation condition (AI_{Base}) even though no adaptation was taking place.

To compare retention between participants, we calculated the mean error across all open loop blocks as an index of retention (RI_{Total}).

To compare washout between participants, we calculated the mean error across all the first block of the washout phase as a washout index (WI).

Finally, to determine how performance changed across time, we calculated the response time for each trial, defined as the time between target appearance and movement onset (the point when velocity exceeded 3% of the maximum velocity). Mean response times were calculated for each phase (RT_{Base}, RT_{Early} and RT_{Late}).

6.2.4.2 Modelling-based Analysis

To complement the modelling-free analysis of adaptation behaviour, we modelled adaptation using two types of state-space models described in detail in section 2.5.

We used a single-state state-space model which included a generalization function estimated from the data in order to obtain an overall adaptation rate accounting for different levels of generalization across targets.

Secondly, we used a dual-state state-space model, to obtain adaptation rates of the fast system and of the slow system which we correlated with GABA concentration.

6.2.5 Magnetic Resonance Imaging Analysis

6.2.5.1 Preprocessing

All MRI data processing was carried out using FSL (FMRIB's Software Library, Version 6.00, [162]).

For resting-state functional data, pre-processing steps were largely matched to the UK Biobank processing pipeline [7]. The data was motion corrected using MCFLIRT [161], slice-timing corrected using Fourier-space time-series phase-shifting, distortion-corrected using fieldmaps (B0 unwarping, stripped of non-brain voxels using BET [324], grand-mean intensity normalised and highpass temporally filtered (Gaussian-weighted least-squares straight line fitting, with sigma = 50.0s)).

Single-subject ICA, implemented in MELODIC and the automated classifier FIX, trained on 40 hand-labelled Biobank datasets was used to remove structured noise (chapter 2.1.3.1) [26] [301] [109]. Although these training datasets were matched in acquisition sequence and experimental parameters to the datasets acquired in our experiment, we checked its classification accuracy to ensure the suitability of the Biobank-trained FIX algorithm for our data by manually classifying four datasets and comparing our labels to the FIX-classification. The FIX-classified labels matched our hand classification at 99.8%, which is within the expected range of classification accuracy (98.1-100% as reported in [7]).

Functional data were registered to the MNI-152 template, using the SBref image as an intermediate step. Functional data were first linearly registered to the SBref image using 6 degrees of freedom (FLIRT [163] [161]), then to the structural image using boundary-based registration (BBR; implemented in FLIRT), and finally to the MNI-152 template using non-linear registration (FNIRT [10] [12]).

Finally, spatial smoothing was applied with a 5 mm FWHM Gaussian kernel.

6.2.5.2 Deriving group networks

In order to derive group networks, we applied a group-ICA (described in detail in 2.1.3.2). For this, we concatenated the preprocessed functional data temporally across sessions and across subjects to create a single dataset. We then used the group-ICA to obtain 25 group-level components, as the previously reported cerebellar network we aimed to replicate here had been obtained with a dimensionality of 25.

Subject-and-scan-specific networks were obtained via a dual regression approach, masked by the group mean network and statistical tests performed via randomise [382], using cluster-wise thresholding (z = 2.3, p = 0.05 [387]).

6.2.5.3 Quantifying network strength

As in chapter 5, we quantified network strength for the network of interest by extracting the mean z-value from the subject-and-scan-specific network maps masked by the group network mask.

We aimed to test whether change in connectivity strength correlated with adaptation. We calculated change in network strength by subtracting the strength value of the subject's pre-scan from network strength in the post-scan. Positive change values therefore reflect an increase in network strength. We refer to this difference as connectivity change.

6.2.6 Magnetic Resonance Spectroscopic Imaging Analysis

6.2.6.1 Quality control

MRSI data was preprocessed using in-house scripts and the FID-A toolbox [321]. For each session, raw MRSI data from all blocks were concatenated and corrected for frequency and phase shifts. Residual water signal was removed from the water suppressed MRSI data using HLSVD [48]. LCModel [283] analysis was used to correct the spectrum for each voxel separately for eddy currents and for water using the unsuppressed water signal acquired from the same VOI. Concentration of neurochemicals was quantified within the chemical shift range of 0.5 to 4.2 ppm [283]. Voxels in the metabolite maps were excluded on the basis of CRLB $>$ 60%, water linewidths at FWHM $>$ 20 Hz, or SNR $<$ 20.

MRSI data analysis therefore yielded independent quantification of neurochemical concentrations at four timepoints. All neurochemical concentrations are expressed as to ratio of tCr, a standard reference metabolite acquired from the same spectrum that was chosen for its suitability as an internal reference [250] [17].

6.2.6.2 MRSI alignment to standard space

Metabolite maps were registered to the MNI template, by a linear registrar to the structural scan (FLIRT [163] [161]), and then non-linearly to the MNI template (FNIRT [10] [12]).

Overlap maps of the MRSI slab in MNI space are shown in figure 6.7A.

6.2.6.3 ROI Analysis

As we expected an effect of task on GABA to be evident in the right hemisphere of the cerebellum, as the cerebellum contains mainly lateralised representations of the hand [19] [244], we conducted a ROI-based analysis of the MRSI data by splitting the MRSI maps into left and right hemisphere, separated by 7 mm. We extracted the mean values from all voxels within the hemisphere mask after quality-control thresholding.

6.2.6.4 Normalisation

To study neurochemical changes occurring during adaptation over and above control we normalised Adaptation GABA to Control GABA, to study any changes beyond control condition changes.

The normalisation of the adaptation GABA to the control GABA took the following form:

$$GABA_{Norm}(P) = \frac{GABA_{Adapt}(P)}{GABA_{Adapt\ Baseline}} - \frac{GABA_{Control}(P)}{GABA_{Control\ Baseline}} \tag{6.1}$$

where:

$$GABA_{Norm} = Normalised\ GABA$$
$$P = Acquisition\ Phase$$
$$GABA_{Adapt} = Adaptation\ GABA$$
$$GABA_{Adapt\ Baseline} = Adaptation\ GABA\ at\ baseline$$
$$GABA_{Control} = Control\ GABA$$
$$GABA_{Control\ Baseline} = Control\ GABA\ at\ baseline$$

The GABA data was normalised for each hemisphere separately, resulting in normalised values for left and right cerebellar hemisphere ($GABA_{Right}$ and $GABA_{Left}$ respectively).

6.2.7 Relating adaptation performance to GABA measurements

In order to relate [GABA] to behaviour, we tested for a correlation between [GABA] and measures of adaptation (modelling-free or modelling-based). To ensure that potential relationships are not driven by performance changes that stem from improved movement execution, but are due to better adaptation to the imposed rotation, we tested for relationships between [GABA] and adaptation controlling for improved movement execution shown in the control condition. We control for movement execution by including the error reduction in the control condition (bias reduction) as a control variable in the model. A detailed description of this control analysis is given in section 6.3.3.5.

6.2.8 Statistical Analysis

Statistical analyses of the data were conducted using R [287].

To test whether $GABA_{Right}$ changed significantly compared to $GABA_{Left}$ in the adaptation condition, we constructed a LME of GABA using the R package lme4 [23]. We entered hemisphere (Right, Left) and acquisition (Base, Early, Late, After) and an interaction of condition x acquisition as fixed effects. We hypothesised that during adaptation, right hemispheric GABA should increase

compared to left hemispheric GABA and therefore expected a significant condition x acquisition interaction. To account for covarying residuals within subjects, we allowed intercepts for different subjects to vary, with subject as a random effect in the model. We thereby created a random intercept model.

To test for a possible relationship between GABA and behaviour (adaptation, retention, washout or control behaviour) or GABA and functional connectivity, we calculated Spearman's rank-order correlations (two-tailed, unless otherwise stated). When testing for a relationship between GABA and adaptation behaviour, we included target bias reduction in the control condition as a control variable using a partial correlation.

For paired t-tests, Bonferroni correction was applied to correct for multiple comparisons.

6.3 Results

6.3.1 Control behaviour

6.3.1.1 Error decreases during control condition

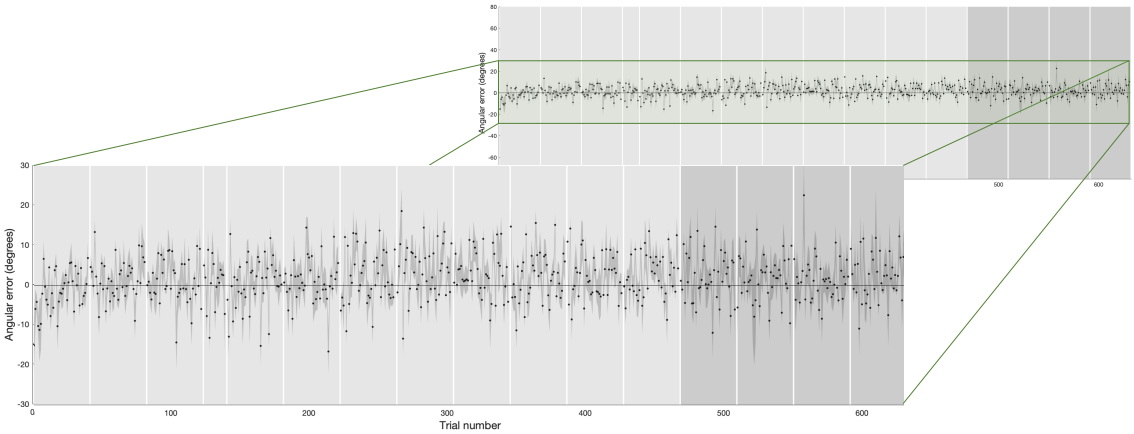


Figure 6.4: Control Behaviour. The small back panel shows control behaviour with the same y-axis scale as the adaptation data in plot 6.2 for visual comparison of the data between conditions. The larger front panel shows the same control behaviour at a larger scale. The mean angular error at each trial averaged across participants is shown. The shaded area represents standard error of the mean. The subject-specific target bias was estimated from the baseline trials and this subject-specific target bias has been removed from the data. Darker shade of the block background indicates no visual feedback.

We first explored whether there were performance changes during the control condition. In the control condition, errors did not change significantly from the baseline phase to the early phase ($t(14) = -1.56$, $p = 0.14$), but decreased significantly from baseline to late phase ($t(14) = -2.69$, $p = 0.02$). On average, participants decreased their angular error by $2.28° \pm 3.58°$ between baseline and late phase. To determine whether this change in error was accompanied by longer response times, which may be a signature of a time-accuracy trade-off, we tested whether response times

increased after baseline. There was no change in response times from baseline to any of the task phases in the control condition (RT_{Base} and RT_{Early}: t(14) = -0.70, p = 0.49; RT_{Base} and RT_{Late}: t(14) = -1.38, p = 0.19). Moreover, response times and errors did not correlate in the control condition (r = 0.02, p = 0.95).

6.3.1.2 Error decrease in the control condition was driven by a reduction in target bias

The error reduction in the control condition seemed to be driven by a reduction in bias. At baseline, participants undershot all targets by a mean of 2.29° ± 3.18° (t(14) = -2.87, p = 0.01), showing on average an anticlockwise bias at baseline. By the late phase, this bias had reduced to zero (One-sample t-test of baseline errors: t(14) = 0.12, p = 0.91). However, the reduction in bias was different for different targets, as revealed by paired t-tests between $Bias_{Base}$ and $Bias_{Late}$ for each target (see table 6.1). Bias only reduced significantly for the two targets that showed the largest bias at baseline: 45° and 270° (45°: t(14) = -4.77, p < 0.01; 270°: t(14) = -4.67, p < 0.01).

Target	$Bias_{Base}$	$Bias_{Late}$
0°	3.88 ± 8.47	4.23 ± 9.13
45°	-14.15 ± 15.36	-9.45 ± 14.02 **
90°	-4.42 ± 23.22	-2.50 ± 20.73
135°	3.10 ± 20.37	3.70 ± 18.90
180°	2.48 ± 10.07	2.64 ± 9.34
225°	-6.69 ± 13.76	-6.19 ± 14.57
270°	-9.81 ± 18.61	-0.85 ± 17.50 **
315°	6.31 ± 25.28	9.46 ± 24.29
Mean	-2.4 ± 19.08	0.12 ± 17.7

Table 6.1: Target Bias in control condition. Target Bias is calculated as mean target-specific error during different phases of the control condition (Base, Late). Paired t-test between $Bias_{Base}$ and $Bias_{Late}$ for each target revealed a significant reduction in error for 45° and 270°. Bonferroni correction was applied to correct for multiple comparisons.
** p-value < 0.01

When visual feedback was removed, participants did not show a bias. Their mean error during these trials was not significantly different from zero (t(14) = -0.26, p = 0.79). The bias for individual targets did not change from the late phase of the control condition when visual feedback was removed (all p > 0.42).

6.3.1.3 Target bias is similar across sessions

We tested whether the target-specific baseline bias in the adaptation session was smaller, if participants had performed the control task in the session before compared to task-naive subjects. There was no difference in target-specific baseline bias for any of the targets (Unpaired t-test between naive subjects' target bias and experienced subjects' target bias (all Bonferroni-adjusted p-values for > 0.24). In addition, the target-specific baseline bias did not differ between first and second session (Paired t-test between subjects' first session target bias and second session target bias (all Bonferroni-adjusted p-values > 0.9).

These results suggested that prior experience with the joystick had no effect on the target-specific baseline bias, and that the target-specific biases might be consistent for every participant. Therefore, in order to be able to quantify specific adaptation above and beyond a reduction of target bias we tested for relationships between GABA and adaptation behaviour controlling for target bias reduction in the model.

6.3.2 Adaptation behaviour.

6.3.2.1 Participants adapted to the rotation.

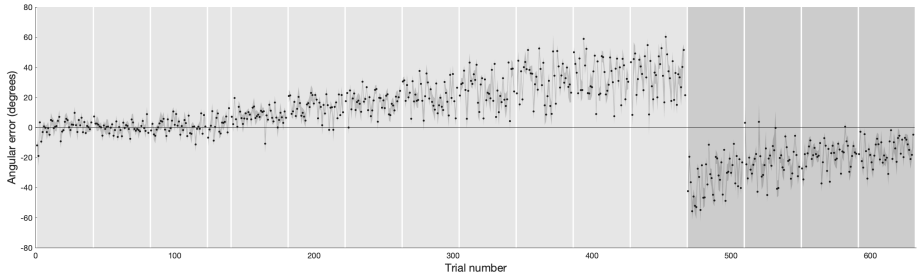


Figure 6.5: Adaptation Behaviour. Shown is angular error at each trial averaged across participants. Shaded area represents standard error of the mean. Subject-specific target bias has been estimated from the baseline trials and this subject-specific target bias has been removed from the data. Darker shade of the block background indicated visual feedback is removed.

Adaptation behaviour is shown in figure 6.5. At baseline, participants did not show a significant bias ($t(14) = -1.09$, $p = 0.29$). Over the course of the adaptation blocks, participants learned to adapt to the perturbation (LME of baseline and adaptation trials shows a highly significant epoch x rotation interaction, ($\chi^2(1)=11.43$, $p < 0.001$)).

When visually comparing adaptation behaviour shown in this chapter to adaptation behaviour in previous chapters, most notably in chapter 4, the stepwise reduction of error within adaptation blocks is less pronounced in the present chapter. This difference is likely because the target sequence in the present experiment was fixed across participants and sessions, whereas the target sequence in experiment 4 differed for each participant and each session. Since each of the eight targets is

associated with a different directional bias, a target-related directional bias is more strongly visible when calculating the mean error across trials that were shot to the same target, as is the case for the adaptation behaviour shown in this chapter. In previous chapters the effect of a target-specific bias averaged out across participants, because of different target sequences for each participant. Although in this chapter the subject-specific target bias has been estimated from the baseline trials and removed from the data that is plotted in figure 6.5, a residual difference between targets remains visible, particularly for trials that come later in the experiment.

After confirming that participants reduced their error over the course of all adaptation blocks, we next tested whether adaptation in the early phase differed from adaptation during the late phase. This was done to determine whether adaptation occurred during both phases to the same extent. The approach taken here is different to the behavioural analysis in previous experimental chapters, where t-tests between start and end error levels of each block were used to identify individual adaptation blocks in which participants showed error reduction. In the present chapter, rather than comparing adaptation performance between individual blocks, we aimed to compare adaptation between early and late phases task, as these phases correspond to different MRSI measurements and could therefore aid interpretation of the MRSI data.

To test whether participants adapted in the early phase, we calculated the difference between mean error and imposed rotation in the early phase ($\text{Delta}_{\text{Early}}$) and showed that it was significantly different from zero, suggesting significant adaptation during the early phase ($t(14) = 11.44$, $p < 0.001$)).

To test whether participants adapted in the late phase, we calculated $\text{Delta}_{\text{Late}}$ in a similar manner and then subtracted $\text{Delta}_{\text{Early}}$ to account for error reduction during the early phase. There was significant adaptation in this late phase measure ($t(14) = -5.55$, $p < 0.001$).

Lastly, we tested whether participants adapted differently in the two phases. We found no significant difference between $\text{Delta}_{\text{Early}}$ and $\text{Delta}_{\text{Late}}$ ($t(14) = 1.62$, $p = 0.49$)

6.3.2.2 Participants retained the adapted movement.

When visual feedback was removed, participants retained the compensatory movement. During the first open loop block, participants showed a significant after-effect of $-36.66° \pm 8.39°$ ($t(14) = -16.77$, $p < 0.001$), which decreased to $-18.11° \pm 10.12°$ in the last open loop block ($t(14) = -6.7$, $p < 0.001$).

6.3.2.3 Participants retained the adapted movement outside the scanner

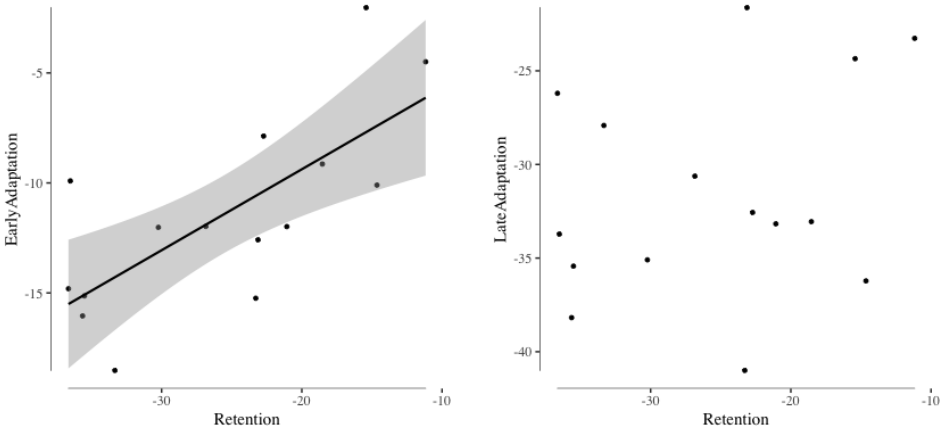
During washout, participants showed a significant compensatory movement of $-11.70° \pm 5.36°$ in the first block ($t(14) = -8.21$, $p < 0.001$). This after-effect was reduced to $-4.86° \pm 5.36°$ in the last 24 trials, suggesting that the adapted movement did not fully wash out over the course of the

washout phase ($t(14) = -3.61$, $p < 0.001$).

6.3.2.4 Early adaptation correlates with retention, but late adaptation does not.

We next wanted to test whether the different phases of the adaptation task were correlated. Early and late adaptation performance did not correlate (no significant correlation between AI_{Early} and AI_{Late}, $r = 0.38$ $p = 0.17$). While early adaptation correlated with retention (AI_{Early} and RI_{Total}, $r = 0.66$ $p < 0.01$; figure 6.6A), late adaptation did not correlate with retention (AI_{Late} and RI_{Total}, $r = 0.24$ $p = 0.38$; see figure 6.6B). To test whether these two correlation coefficients were significantly different, we applied a Fisher z-transformation to the correlation coefficients. We tested for a difference between the z-transformed coefficients and found that early adaptation correlated significantly stronger with retention than late adaptation ($z = -2.74$, $p < 0.01$).

Washout performance did not correlate with early or late adaptation, nor with retention (for all correlations with WI: $p > 0.11$).



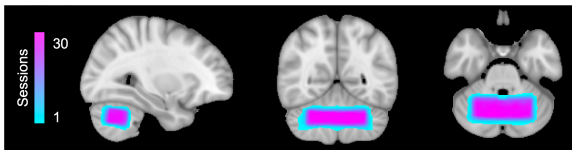
(A) Early adaptation and retention.

(B) Late adaptation and retention.

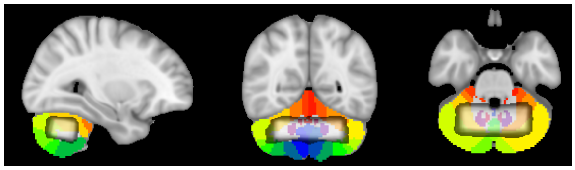
Figure 6.6: Early adaptation correlates with retention while late adaptation does not. Shaded area indicates 95% confidence interval.

6.3.3 MRSI

6.3.3.1 GABA concentration at baseline in adapt and control session is not significantly different



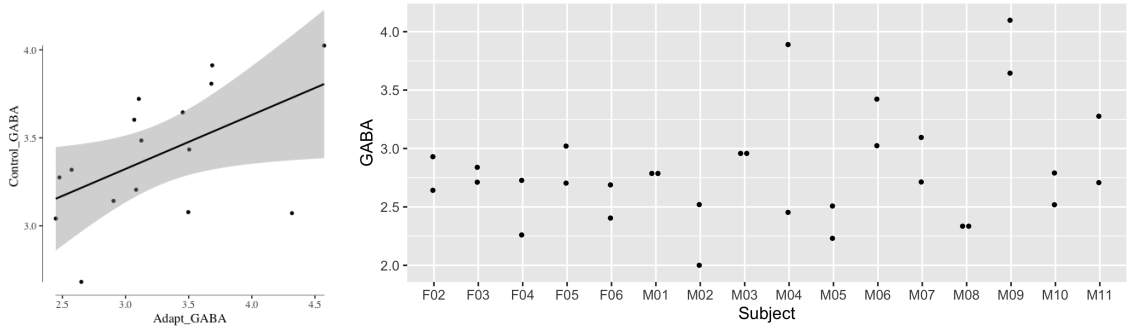
(A) MRSI mask from all sessions.



(B) MRSI mask overlaid on top of cerebellar segmentation atlas.

Figure 6.7: Placement. Overlay mask of all MRSI slabs from all sessions.
A. Overlay mask in magenta-blue in MNI space.
B. Overlay mask in white-grey overlaid on top of segmentation atlas of the cerebellar lobules and deep cerebellar nuclei [69] [67].

MRS-quantified in the cerebrum has previously been shown to be stable over several days [82] [340] [381] and even months [251]. We therefore first tested whether the GABA measurements from the cerebellum were stable across the experimental sessions. GABA concentration was significantly correlated between the first and second sessions (r = 0.45 ; p = 0.03; intra-class correlation = 0.45, p = 0.03; figure 6.8B and figure 6.8A) Baseline GABA in the adaptation session and in the control session were not significantly different (t(15) = -1.08, p = 0.29).

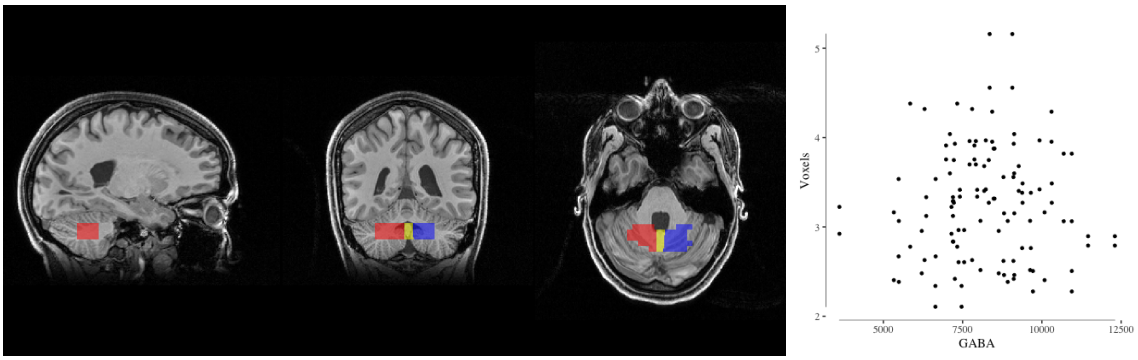


(A) (B)

Figure 6.8: Stability of baseline GABA across sessions.
A. Scatter plot of adaptation session versus control session GABA concentrations at baseline. GABA concentration significantly correlates between the sessions (r = 0.45 ; p = 0.03).
B. Dot plot of intraclass-correlation coefficient. Repeated measurements of GABA acquired at least one week apart strongly resemble each other when between-subject variations are taken into account: The intraclass-correlation coefficient of 0.45 was statistically significant (p = 0.03).

6.3.3.2 GABA does not scale with number of voxels included in ROI

Next, to ensure that differences between left and right GABA were not driven by differently sized ROIs, we tested whether GABA is correlated with number of voxels included in the hemispheric ROIs. There was no significant correlation between GABA and the size of the quality-control thresholded hemispheric ROI mask (r = 0.03 p = 0.77). An overlay map of representative ROI masks is shown in figure 6.9A.



(A) Representative ROI masks

(B) GABA and ROI-Voxels.

Figure 6.9: Hemispheric ROIs.
A. Quality-control thresholded ROI masks are shown for representative subject for left cerebellar hemisphere (blue) and right cerebellar hemisphere (red). All voxels shown in these masks survived quality thresholding and therefore have CRLB $>$ 50%, water linewidths at FWHM $>$ 15 Hz, and SNR $<$ 40. The middle of the slab (yellow) was not considered for analysis.
B. The number of voxels included in the left and right ROI does not correlate with GABA ratio (r = 0.03 p = 0.77).

6.3.3.3 GABA during control task

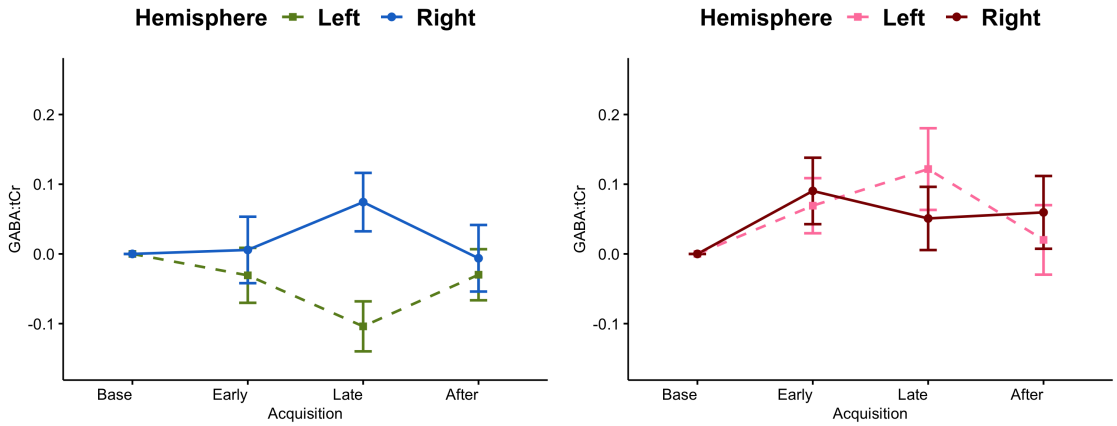
In the control condition, baseline GABA concentration in the right hemisphere was significantly lower than in the left hemisphere (t(14) = -3.24, p $<$ 0.01). We next wanted to test for GABA fluctuations in the two hemispheres during the control task that may occur over an extended period of time or due to movement. In order to investigate whether GABA concentration changes differently in the two hemispheres irrespective of differing baseline concentration in each hemisphere, we normalised left and right hemispheric GABA to their baseline values, shown in figure 6.10A.

Analysis of the control behaviour revealed participants significantly reduced their target bias to the 45° and 270° target. We therefore tested whether this behavioural effect was mirrored by a GABA change (LME with the fixed effects hemisphere (Left, Right) and acquisition (Early, Late, After). There was a significant hemisphere x acquisition interaction driven by significantly increased right hemispheric GABA during the late phase of the control task ($\chi^2(1)$=11.6, p $<$ 0.001).

However, there was no significant relationship between late phase GABA change and target-specific bias on a subject-by-subject basis (r = 0.3 p = 0.93).

In the adaptation condition, right GABA at baseline was significantly lower than left GABA (Paired t-test: t(14) = -3.13, p < 0.01). In order to test whether GABA concentration changed differently in the left compared to the right hemisphere during adaptation after the baseline phase, we normalised left and right hemispheric GABA to their baseline values, shown in figure 6.10B.

We then tested whether GABA changed significantly during the adaptation task using a LME with the fixed effects hemisphere (Left, Right) and acquisition (Early, Late, After). No significant difference in GABA concentration between the hemispheres was observed over the course of the MRSI acquisitions (LME with and without a hemisphere x acquisition interaction term, the interaction term did not make a significant difference for the model fit ($\chi^2(1)$=1.41, p < .71)).



(A) Control GABA.

(B) Adaptation GABA.

Figure 6.10: GABA increases during control condition in right cerebellar hemisphere while decreasing in the left. GABA in the adaptation condition does not change significantly. GABA is normalised to baseline, so values show percentage change from baseline in the respective condition. Error bars represent standard error of the mean.

6.3.3.4 Normalised GABA reveals a significant GABA change during adaptation in right compared to left hemisphere

Given the significant changes in GABA observed in the control condition, we normalised adaptation GABA to control GABA (as described in section 6.2.6.4), to look for adaptation-specific neurochemical changes. We tested for a significant hemisphere x acquisition interaction on these normalised values. There was a significant hemisphere x acquisition interaction, with left hemispheric GABA and right hemispheric GABA diverging over time ($\chi^2(1)$=6.53, p = 0.04; figure 6.11).

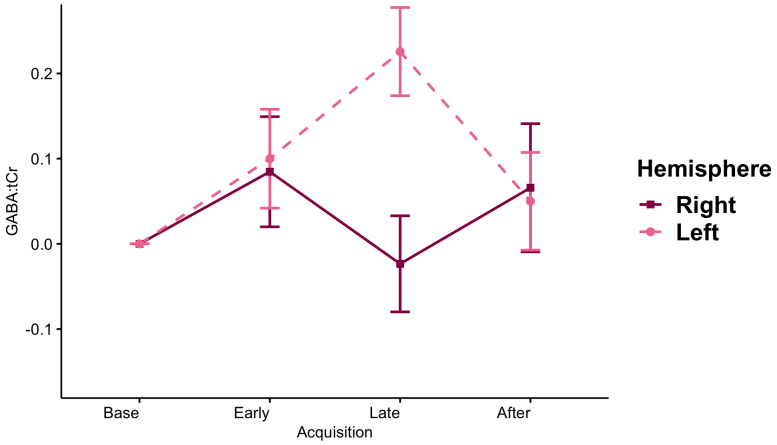


Figure 6.11: Adaptation GABA normalised to control GABA. A significant hemisphere x acquisition interaction is driven by a right hemispheric GABA decrease and left hemispheric GABA increase during late adaptation ($\chi^2(1)$=6.53, p = 0.04). Error bars indicate standard error of the mean.

6.3.3.5 GABA change does not correlate with adaptation.

The significant GABA change from baseline in right compared to left hemispheric [GABA] was found late in the adaptation task. We next wanted to assess whether a direct relationship exists between [GABA] change and adaptation. For this, we tested whether percentage GABA change in the right cerebellar hemisphere related to adaptation performance. In order to control for performance changes that are not directly related to adaptation in this analysis, we included target bias reduction in the model.

There was no relationship of GABA change with either late (r = 0.29 p = 0.3) or early adaptation (r = 0.275 p = 0.32). There was also no relationship between GABA change and adaptation rate obtained from the single-state model (r = 0.03 p = 0.7) nor with the fast and slow adaptation rate from the dual-state model (GABA change vs Adaptation rate fast system: r = 0.06 p = 0.8; GABA change vs Adaptation rate slow system: r = 0.17 p = 0.5;).

Lastly, we explored whether absolute [GABA] reached during the late phase related to overall adaptation performance. We found a significant correlation between absolute [GABA] and overall adaptation, such that participants with lower levels of GABA showed better adaptation overall (r = 0.52 p = 0.046; figure 6.12). However, this relationship was not significant when controlling for bias reduction and control GABA (r = -0.22 p = 0.42).

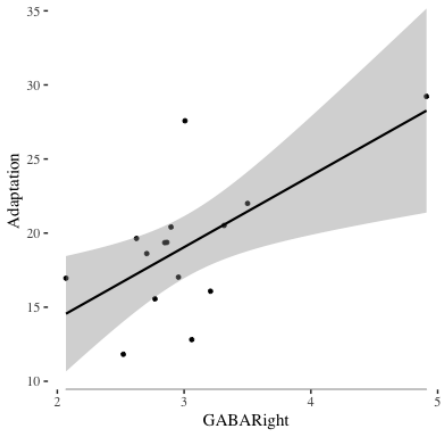
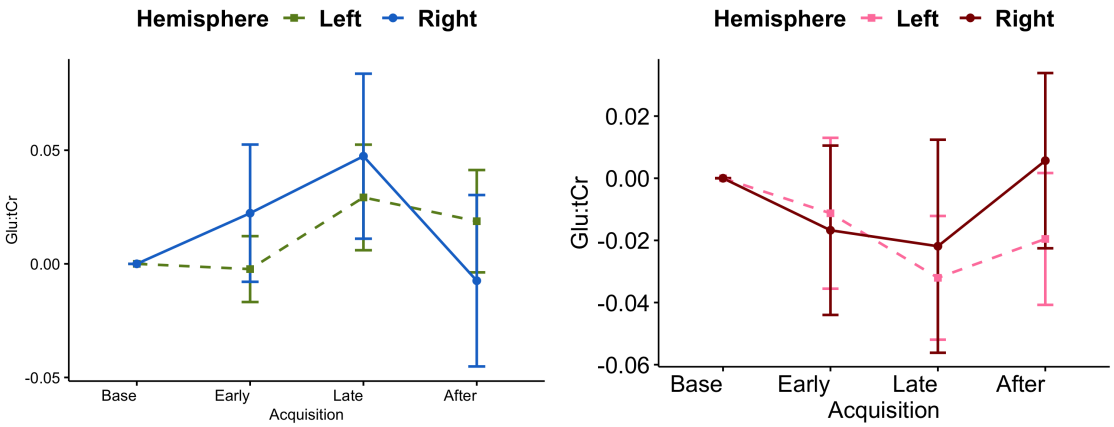


Figure 6.12: Absolute GABA during late phase correlates with overall adaptation performance (r = 0.52 p = 0.046). Participants who show lower GABA adapt better. Shaded area indicates 95% confidence interval.

6.3.3.6 Changes in [GABA] are neurochemically specific.

To determine whether the changes in GABA described above were neurochemically specific, we performed similar analyses for Glutamate. We first tested for changes in right compared to left hemisphere separately for each condition. In the control condition, there was no significant main effect of hemisphere, or hemisphere x acquisition interaction (main effect hemisphere: $\chi^2(1)$=3.96, p = 0.14, hemisphere x acquisition interaction $\chi^2(1)$=2.62, p = 0.27). There was a trend towards a main effect of hemisphere $\chi^2(1)$=3.56, p = 0.06; figure 6.13A).

In the adaptation condition, Glutamate in the right hemisphere was significantly higher than in the left hemisphere (significant main effect hemisphere: $\chi^2(1)$=5.05, p = 0.02). Glutamate did not change across the experiment overall (no significant main effect of acquisition: $\chi^2(1)$=2.35, p = 0.5) and there was no significant Glutamate change in the right hemisphere (no significant hemisphere x acquisition interaction $\chi^2(1)$=0.41, p = 0.93; figure 6.13B).



(A) Control Glutamate.

(B) Adaptation Glutamate.

Figure 6.13: Glutamate does not change differently in right compared to left cerebellar hemisphere in either condition. Glutamate is normalised to baseline, so values show percentage change from baseline in the respective condition. Error bars represent standard error of the mean.

We then investigated Glutamate in the adaptation condition normalised to control condition to control for changes in control Glutamate (see figure 6.14). There was no Glutamate decrease in the right hemisphere during adaptation (no significant hemisphere x acquisition interaction: $\chi^2(1)$=1.71, p = 0.42).

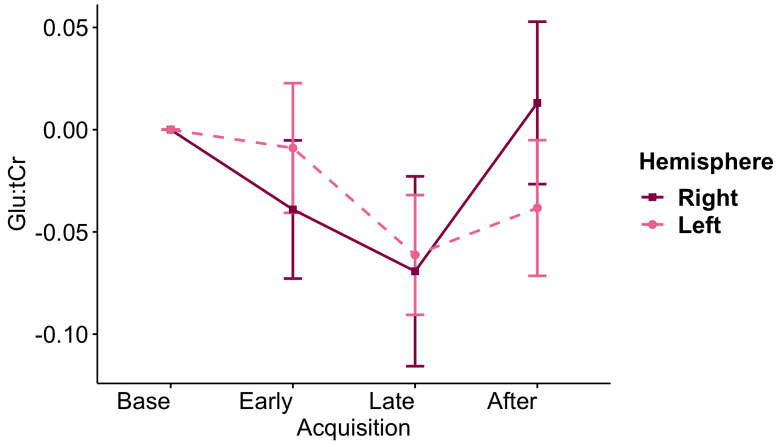


Figure 6.14: Adaptation Glutamate normalised to control Glutamate. No significant hemisphere x acquisition interaction ($\chi^2(1)$=5.9, p = 0.052). Error bars indicate standard error of the mean.

6.3.4 Resting-state Connectivity

6.3.4.1 Relationship between cerebellar GABA and cerebellar connectivity

First, we aimed at testing for a relationship between baseline GABA in the cerebellum and strength of a cerebellar network resting-state network at baseline. From the group networks obtained from the group-ICA run on the resting-state fMRI data as described in section 6.2.5.2, we identified the cerebellar network of interest through visual inspection and cross-correlating the spatial map of the network with the spatial map of the previously identified cerebellar network (figure 6.15).

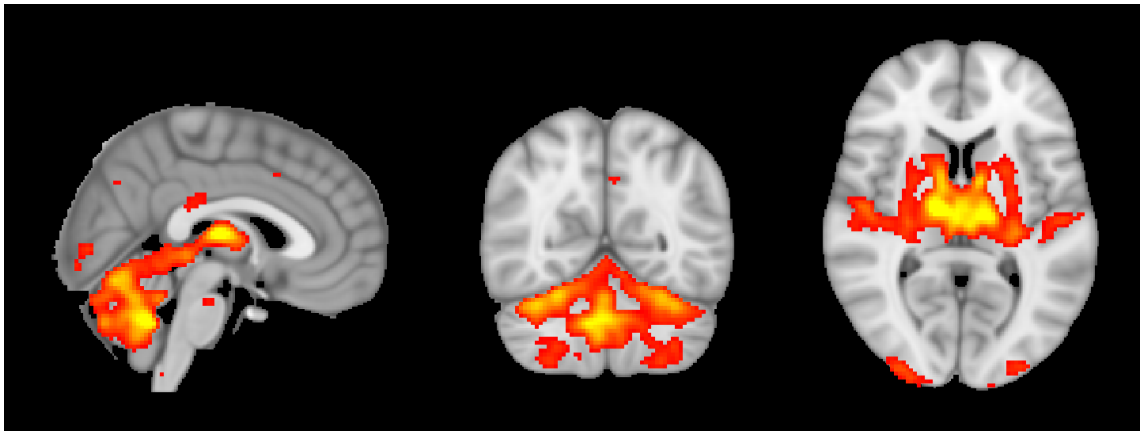
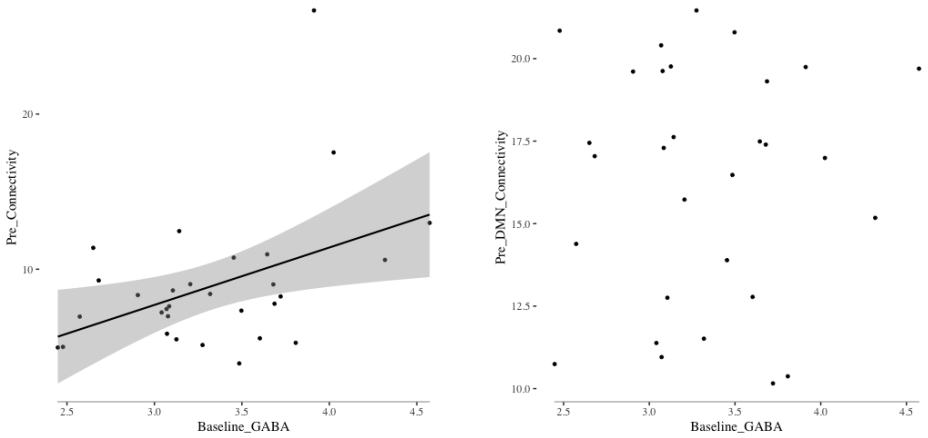


Figure 6.15: Network of interest. This group-level component has been identified through visual inspection as well as cross-correlating its spatial map with the spatial map of the cerebellar network that we aim to replicate. The image shows the z-score map of the network thesholded at z>4.

As in chapter 5, we quantified network strength by extracting the mean z-value from the subject-and-scan-specific network maps masked by the group network mask. There was a significant correlation between mean cerebellar GABA and cerebellar network connectivity strength ($r = 0.4$, $p = 0.03$; figure 6.16A).



(A) Baseline GABA and Cerebellar Network connectivity at timepoint pre.

(B) Baseline GABA and Default Mode Network connectivity at timepoint pre.

Figure 6.16: Cerebellar network connectivity correlates with baseline GABA, while default mode network connectivity strength does not.

Next, in order to ensure that the positive relationship between GABA concentration and connectivity is specific for the cerebellar network, we identified a control network, that did not include the cerebellum. For this, we chose the Default Mode Network as the control network (figure 6.17). Default Mode Network strength at timepoint pre did not correlate with baseline GABA ($r = 0.03$, $p = 0.85$; figure 6.16B). Moreover, the correlation between baseline GABA and cerebellar network strength was significantly different from the correlation between baseline GABA

and Default Mode Network strength (significant difference between z-transformed correlation coefficients z = -1.68, p = 0.05).

We wanted to test whether the relationship between GABA and cerebellar network strength was neurochemically specific and therefore tested for a correlation between baseline Glutamate and cerebellar network strength. Glutamate correlated significantly with cerebellar network strength (r = 0.36 , p = 0.05). Controlling for Glutamate as a control variable in a partial correlation, GABA at baseline and cerebellar network strength did not correlate (r = 0.17, p = 0.37).

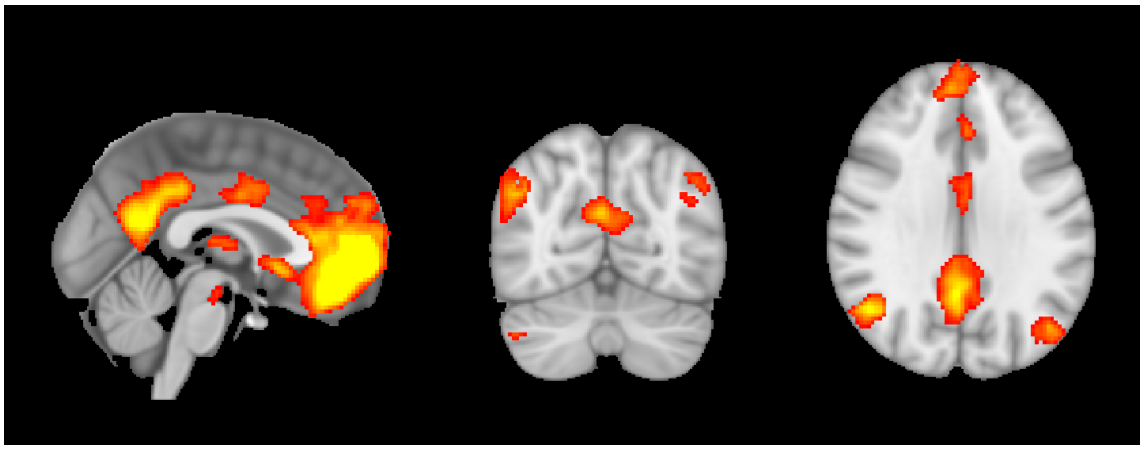


Figure 6.17: Default Mode Network. This group-level component has been identified through visual inspection as the default mode network serves as a control network. The image shows the z-score map of the network thesholded at z>4.

6.3.4.2 Relationship between adaptation and cerebellar connectivity

We aimed to replicate the finding reported in chapter 5 of increased connectivity within a cerebellar resting-state network after adaptation. Further, we wanted to test whether connectivity strength of the cerebellar network correlates with adaptation, as reported in chapter 5.

There was no significant difference between the strength of the cerebellar network at timepoint post after the adaptation task compared to the post-network after the control task (p > 0.1). Therefore, there was no evidence that adaptation modulated the connectivity of the cerebellar resting-state network.

Next, we tested whether the change in strength of the cerebellar resting-state network correlated with adaptation performance. Change in connectivity strength of cerebellar network did not correlate significantly with adaptation (r = -0.19, p = 0.5; figure 6.18).

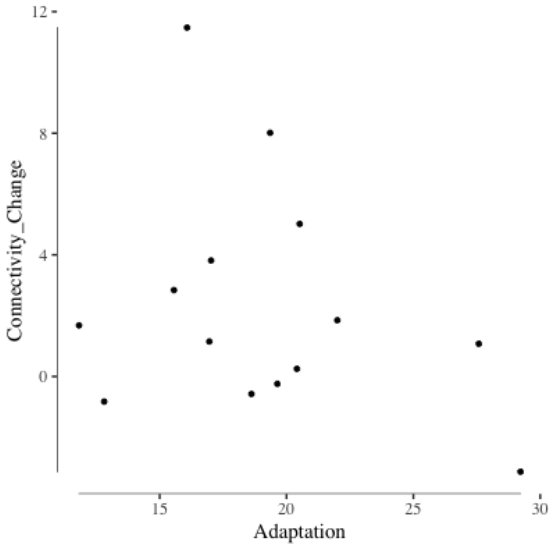


Figure 6.18: Adaptation does not correlate with change in connectivity.

6.3.5 Discussion

In this chapter we aimed to investigate the neurotransmitter changes occurring in the cerebellum during adaptation and link them to adaptation behaviour, as well as network-level connectivity. We used MRS to non-invasively and in vivo quantify [GABA] from a cerebellar slab in participants adapting to an increasing perturbation. We achieved acceptable reliability of GABA measurements, as [GABA] at baseline was not significantly different between sessions and both the Pearson's correlation coefficient and the intraclass-correlation coefficient (ICC) values of [GABA] at baseline from the two sessions were comparable to the values previously reported in the occipital lobe (where $r = 0.53$, $p < 0.05$ and $ICC = 0.52$, $p < 0.05$ in [251]).

Using the MRS-quantified GABA measurements, we show that during adaptation, [GABA] decreases in the right compared to the left cerebellar hemisphere. We show these changes superimposed over cerebellar [GABA] fluctuations that occur in the same participants during movement execution, as evident from GABA measurements taken during performance of a control task without adaptation processes. The right cerebellar [GABA] decrease in comparison to the left cerebellar [GABA] increase observed in the adaptation condition is evident during the late adaptation phase. [GABA] in the right cerebellar hemisphere reached at this late adaptation phase correlates with overall adaptation performance, such that participants with lower [GABA] reached at this stage show greater overall adaptation. The [GABA] change during adaptation is neurotransmitter-specific. This observed change in [GABA] was not mirrored by changes in [Glutamate] in the right cerebellar hemisphere compared to the left.

We also show a relationship between cerebellar [GABA] in the whole MRSI volume at baseline and strength of a cerebellar resting-state network at baseline. Participants with higher cerebellar

[GABA] show stronger cerebellar network connectivity. This relationship is specific to the cerebellar network, as [GABA] does not correlate with strength of the default mode network.

We do not find that adaptation modulates functional connectivity in the cerebellum, as we found in a previous dataset (the results of which are reported in chapter 5). Further, we do not find a relationship between change in cerebellar network strength and adaptation performance (as described in chapter 5).

Taken together, these results suggest that during adaptation, [GABA] decreases in the hemisphere ipsilateral to the adapting hand compared to contralateral [GABA], against a backdrop of GABA fluctuations occurring during simple movement execution. They also suggest that higher baseline levels of [GABA] in the cerebellum relates to stronger cerebellar network. We will discuss the implications and limitations of these results in the following.

6.3.6 [GABA] decreases ipsilaterally during adaptation.

It has previously been shown using MRS that M1 [GABA] decreases during learning of a motor sequence [181]. This decrease in M1 was specific to learning and [GABA], as no change in glutamate was observed. Moreover, early concentrations of GABA correlated with the magnitude of subsequent learning. We provide first evidence here that a similar change in MRS-assessed GABA concentration occurs in the cerebellum during motor adaptation. We find that in the ipsilateral compared to the contralateral cerebellar hemisphere, [GABA] decreases after 9 minutes of adaptation.

Though this finding of an adaptation-related decrease in right cerebellar [GABA] matches the learning-related decrease of [GABA] in M1, the mechanisms underlying this decrease are likely to differ, considering that M1 and the cerebellar cortex differ greatly in their neuronal make up and microcircuitry. For M1, it has been proposed that the MRS-assessed GABA reduction reflects reduced GABAergic signalling of inhibitory interneurons which unmasks latent connections and facilitates plastic changes in M1 [181], a process shown in animals [141] [132] [155] [296].

In the cerebellum, decreased [GABA] could similarly reflect reduced GABAergic signalling of inhibitory interneurons in the cerebellar cortex. However, the [GABA] decrease in the cerebellum could also be a result of altered firing patterns of the major output neuron of the cerebellar cortex, the Purkinje cell. Purkinje cells are GABAergic and exert an inhibitory tone over the deep cerebellar nuclei through tonic firing. In response to perturbing the movements of monkeys, Purkinje cells in the monkeys' cerebellum have been shown to fire more complex spikes driven by input from climbing fibres originating in the inferior olive [105]. When the monkeys adapted their movements, the frequency of complex spikes decreased. However, it should be noted that the initial observation of increased complex spikes in response to large errors and a reduction

of complex spike firing rate when errors get smaller was not replicated in a later study [329]. Further, during saccade adaptation, an inverted relationship between error size and complex spike probability has been shown, where complex spikes firing was decreased when the perturbation was introduced and errors were large and increased as errors got smaller [54]. In response to these conflicting results, complex spikes have been proposed to reflect sensitivity to error rather than error magnitude [212]. Still, complex spikes have a well documented role in error signalling [260] [9] [128] and the prevailing view remains that complex spikes conduct error information in line with the theory of cerebellar learning [4] [150] [269]. Further, this error signalling serves as a teaching signal and results in long-term depression (LTD) at parallel fiber - Purkinje cell synapses [4] [150] [213]. LTD then reduces the firing rate of simple spikes by Purkinje cells and leads to motor performance improving [150]. Evidence supporting this theory of cerebellar learning has been shown in monkeys performing a simple motor learning task [224]. A trial-by-trial analysis of the monkeys' Purkinje cell firing showed complex spikes evident on one trial resulted in reduced firing rates of simple spikes on the following trial accompanied by improved performance due to learning [224]. Decreased Purkinje cell firing as a result of LTD at parallel fibre - Purkinje cell synapses has also been shown in several other animal studies [105] [104] [393].

The significant decrease in ipsilateral cerebellar [GABA] observed in this study could reflect altered Purkinje cell firing caused by LTD at parallel fiber - Purkinje cell synapses in response to adaptation. The decrease here was observed during the late phase of adaptation, after participants had already adapted for 9 minutes. The timing of this decrease is in line with the time course of LTD induced in mice after conjunctive climbing fiber and parallel fiber stimulation [104]. In mice Purkinje cells, a reduced firing rate was detectable after 10 min of stimulation [104].

However, we cannot be certain that the [GABA] measured here reflects altered Purkinje cell activity. MRSI measurement of [GABA] is not able to differentiate between different GABA pools as we are measuring a sum of the three GABA pools present in the central nervous system: GABA in the vesicles within the presynaptic boutons, GABA that is distributed throughout the GABAergic neuron as well as GABA located in extracellular spaces. On the basis of a positive relationship found between TMS measures thought to reflect extracellular GABA and MRS measures of [GABA], it has been suggested that MRS measures of [GABA] are more sensitive to the extracellular pool of GABA [332]. A recent study has failed to replicate the same relationship and the precise contribution of different GABA pools to the overall MRS-assessed GABA signal is an area of ongoing research [78]. Though our results would be in line with a LTD-induced decrease in Purkinje cell firing in response to adaptation, finer spatial and temporal resolution of the GABA measurements would be required to test this interpretation.

Our findings provide insights into the physiological changes that underlie adaptation which

could have implications for therapeutic interventions intended to facilitate adaptation. We find that lower [GABA] during the late adaptation phase is linked to better overall adaptation performance. Local [GABA] can be reduced by applying anodal tDCS [336]. Further, anodal tDCS has been shown to facilitate adaptation when applied to the ipsilateral hemisphere of the cerebellum [101]. Therefore, anodal tDCS applied over the right cerebellum may facilitate adaptation by decreasing local [GABA], a process shown here to occur during adaptation.

6.3.7 [GABA] increases contralaterally during adaptation.

The results of this study suggest changes in [GABA] in the two cerebellar hemispheres that go in opposite directions: while [GABA] decreases ipsilateral to the hand used, contralateral [GABA] increases. Movement execution with no learning component activates only the ipsilateral cerebellum [137] [45], so no activation would be expected for the contralateral hemisphere. However, when executing movements in a task that includes an adaptation component the activation pattern that would be expected for the contralateral cerebellar hemisphere is less clear.

In an early study of adaptation where human participants adapted to a 120° rotation using a computer mouse, cerebellar activation was markedly bilateral in early training sessions [145]. In this study, however, analysis of cerebellar activation did not control for movement execution. Evidence for involvement of the contralateral cerebellum when controlling for the execution of joystick movements comes from a study that studied adaptation-related changes in cerebellar activity. Here, participants adapting their joystick movements to a 90° rotation showed increasing activity in the left posterior cerebellum, controlling for activity evident during joystick movements in the absence of a rotation. In both these fMRI studies the imposed rotation exceeded the extent of rotation applied in commonly used adaptation paradigms that are typically 45° - 80°. It has been argued that abruptly introduced rotations above 80° require corrections that are not based on the adaptation of an existing control policy, i.e. the updating of an internal forward model, but the acquisition of a new control policy, and therefore the nature of the probed adaptation behaviour changes [349] [189] [1]. Although these studies suggest that the left cerebellar hemisphere may be involved during adaptation, the extent to which these findings generalize to adaptation to a relatively small, stepwise increasing rotation, as used in this study, may be limited.

Direct evidence for involvement of the left cerebellar hemisphere in adaptation to a perturbation schedule which is similar to the one used in this study comes from a recent fMRI study [376]. In this experiment, participants adapted to a rotation angle that increased by 2° every 15 trials, resulting in a 60° rotation at the end of the adaptation phase. Contrasting cerebellar activity during adaptation against cerebellar activity in a control condition revealed significant activity in the left dentate nucleus. These studies suggest that adaptation may result in engagement of the cerebellar

hemisphere contralateral to the performing hand, but we cannot be certain about the function of this contralateral involvement. One possible explanation of increased contralateral activity would be that Purkinje cell firing increases in the left cerebellar cortex in order to suppress motor output on the side that is not performing the movement. Our data showing increased [GABA] during late adaptation would match this pattern. It would be interesting to study the effects of non-invasively modulating [GABA] in the contralateral cerebellar hemisphere on adaptation performance, similar to modulation of inter-hemispheric imbalance in M1 [337].

6.3.8 Adaptation does not modulate cerebellar network connectivity.

In the experiment reported in chapter 5, we found increased functional connectivity in a cerebellar network after participants performed the adaptation task. Here, we find no modulation of functional connectivity in the cerebellar network after adaptation.

This null finding may be due to differences in the adaptation task. For the last 10 min and 40 seconds of the task in the present experiment, visual feedback of the movement was removed. This modification of the task was integral to establish that participants showed a signature of adaptation, the aftereffect, and also to probe retention of this aftereffect. However, transient functional connectivity changes may have washed out during this retention probe phase.

Connectivity changes in the cerebellum have previously been shown after 11 minutes of adaptation task performance [3]. Specifically, increased resting-state functional connectivity was shown after participants had adapted their joystick movements to a stepwise increasing rotation compared to the same participants performing a control task. The present study shares several features with the original study by Albert et al. [3]. It is a within-subject, sham-controlled study of resting-state connectivity that used a highly similar joystick task (rotation increasing by 10°, final rotation of 90°) and analysis pipeline (ICA-based decomposition resulting in cerebellar network). It is therefore likely that the changes in functional connectivity that were found in the study by Albert et al. share characteristics with the changes driven by the task used in this experiment and our previous experiment described in chapter 5. Because the changes in the Albert et al. study were driven by only 11 minutes of adaptation, it is also plausible that they are transient changes that are susceptible to washing out over a similarly short period of time. Therefore, the period of removed visual feedback might have sufficed to wash out transient changes in cerebellar connectivity driven by adaptation.

6.3.9 [GABA] relates to cerebellar network connectivity.

Finally, we show a relationship between [GABA] averaged across the entire cerebellar MRSI slab during the baseline phase of the task and cerebellar network strength prior to task performance. This relationship was specific to the cerebellar network, as no relationship was found between

baseline [GABA] and default mode network strength.

Connectivity strength of a resting-state network has been shown to correlate with MRS-assessed [GABA] measured from a major node in the network. Specifically, [GABA] measured from the posteromedial cortex has been linked to default mode network strength [170] and M1 [GABA] has been shown to correlate with motor network strength [335]. In contrast to the correlation found in this experiment, however, both these correlations were negative, such that participants with lower [GABA] exhibited stronger network connectivity.

A positive relationship was recently shown between [GABA] measured from the occipito-temporal cortex and connectivity strength between occipito-temporal cortex and posterior parietal cortex [94]. This relationship, however, was shown with functional connectivity assessed using an ROI-based analysis instead of an ICA-based analysis used in [335] [170] (for a detailed description of both analysis methods see section 2.1.3.2). Moreover, the relationship was reported with [GABA] change and was not driven by baseline [GABA] differences, as revealed by the finding that the correlation remained significant when normalising [GABA] change to baseline [GABA] [94].

The positive correlation between cerebellar [GABA] and cerebellar network strength therefore differs from previously reported negative relationships between baseline [GABA] and connectivity. This finding may be a result of the specific cellular architecture in the cerebellum. In contrast to the excitatory pyramidal cells in the motor cortex, the main output cells of the cerebellum are inhibitory. Increased, synchronous activity of the cerebellum therefore would result in increased GABA release from Purkinje cells. This may explain why higher [GABA] are linked to increased cerebellar network connectivity.

6.3.10 Limitations

Our results demonstrate [GABA] changes in the ipsilateral and contralateral cerebellar hemisphere that develop in opposite directions and occur against a backdrop of GABA fluctuations thought to be driven by movement execution. Previous research has demonstrated that the cerebellum is involved in hand movements [137] [45] and specifically in simple movement execution of a joystick task [107]. To show adaptation-related changes in [GABA], we therefore normalised adaptation [GABA] to control [GABA]. Based on the present data, we cannot rule out the possibility that [GABA] changes occur only during performance of the control task and that the added adaptation components changes the nature of the task such that [GABA] does not change. However, because we have previously shown that the adaptation task used in this experiment drives functional connectivity changes in the cerebellum when compared to performance of the same control task (reported in chapter 5), we argue that the added adaptation component elicits additional changes in the cerebellum. Moreover, because no relationship was shown between control [GABA] and

control task performance, we find no indication that the control [GABA] changes are related to improvements in performance.

In contrast, adaptation [GABA] reached in the ipsilateral hemisphere during the late adaptation phase correlates with overall adaptation performance. When normalised to control [GABA], adaptation [GABA] during late adaptation shows no relationship with adaptation. The lack of correlation found between adaptation and normalised [GABA] may also stem from the coarse temporal resolution of MRSI measurements. Because non-invasive, in vivo GABA assessment through MRSI is technically challenging - particularly in the cerebellum - an acquisition time of several minutes is required to achieve SNR sufficient for reliable GABA quantification. Measurements obtained from this time window might obscure [GABA] changes on a shorter timescale that are driven by fast performance changes and could be linked to those at a finer temporal resolution. Therefore, although the correlation between adaptation and absolute [GABA] may provide corroborating evidence for the [GABA] decrease being linked to adaptation, this result needs to be replicated.

6.3.11 Conclusions

In the present study, we show changes in cerebellar [GABA] during adaptation superimposed over [GABA] fluctuations that occur during a control task. While ipsilateral [GABA] decreases, contralateral [GABA] increases after 10 minutes of adaptation. To our knowledge, this is the first demonstration of cerebellar [GABA] changes assessed non-invasively and in vivo while human participants adapt. We thereby extend findings from motor cortical [GABA] showing a learning-related [GABA] decrease and provide a potential mechanistic explanation for facilitatory effects of cerebellar tDCS on adaptation.

We also relate cerebellar [GABA] to functional connectivity in the cerebellum, in line with previous studies linking local [GABA] and connectivity.

These results give insight into changes at the neurotransmitter level and at the network level that are driven by adaptation and may have implications for interventions targeting the cerebellum.

CHAPTER 7.0

General Discussion

7.1 Summary

In this thesis, I investigated the neural changes tied to motor adaptation by combining a novel adaptation task with imaging (MRS, MRSI and fMRI), brain stimulation (tDCS) and behavioural modelling techniques (SSM). I focused the investigation on understanding changes in the levels of cerebellar GABA during adaptation. Along with this primary aim, I examined the impact of adaptation on functional connectivity and the link between M1 GABA and adaptation. Further, I explored the effects of cerebellar tDCS on adaptation.

The first chapter of this thesis introduced the concept of motor adaptation, defined its features and discussed the neural basis of adaptation. Although much is known about the brain structures involved in adaptation and about the cerebellum's role in particular, interventions aimed at facilitating adaptation produce results of meagre reliability and reproducibility. Studying neural changes that occur when humans adapt to changing physical environments and how these can be facilitated during therapeutic interventions is crucial for our understanding of healthy brain function and for our ability to provide effective interventions following disease or brain damage.

In chapter 2, I reviewed the methods used in this thesis to drive adaptation, measure changes in the brain and stimulate the brain. I used a novel version of the commonly used motor adaptation task, visuomotor rotation, in which participants adapt to a rotation imposed between right-hand joystick movements and a computer cursor. Increasing the imposed rotation stepwise allowed me to drive adaptation over a period of more than 37 minutes while reducing the likelihood of participants becoming aware of the cursor manipulation. Extending the time over which participants adapt enabled measuring changes in the brain with imaging techniques that rely on prolonged acquisition times of several minutes (MRS and MRSI). Reducing the likelihood of participant awareness ensured that adaptation performance was not driven by explicit strategies, which is thought to shift engagement to other brain areas outside the cerebellum. I used tDCS to non-invasively manipulate brain function and fMRI to assess connectivity changes elicited by adaptation. Further, I used single-voxel MRS as well as MRSI to non-invasively measure neurochemical changes associated with adaptation. I discussed the physiological mechanisms that these techniques rely on and outlined

the analysis strategies employed to derive meaningful measures from the data collected with these. Finally, I reviewed modelling approaches developed to quantify adaptation and explained how the state-space models used in this chapter are tailored to the properties of the specific task versions used in each chapter.

In chapter 3, I investigated the changes in adaptation performance induced by anodal tDCS applied to the cerebellum using a within-subject, sham-controlled crossover design. I found no significant facilitatory effect of anodal tDCS on the cerebellum adaptation performance, but evidence of carry-over effects from the first exposure to the adaptation task on the second exposure. A potential effect of stimulation on adaptation of relatively small size may have been masked by a comparatively large effect of task experience (savings) in this crossover study. Within-subject designs for tDCS studies are important to control for the variability in tDCS effects stemming from differences in the individual participants' anatomy and responsiveness to tDCS. However, conducting a within-subject study of adaptation requires elimination or minimisation of the influence of prior task exposure, also known as savings. This study highlights the need to develop effective washout techniques for adaptation paradigms to enable the repeated measurement of adaptation unaffected by task experience. It also establishes the need to study neural changes that take place in the cerebellum during adaptation, in order to develop more effective cerebellar tDCS interventions.

In chapter 4, I examined changes in single-voxel MRS-assessed M1 GABA concentration during adaptation and how concentration levels relate to features of adaptation. As hypothesised, I did not find a change in M1 GABA over the course of the adaptation task compared to the control task. However, in line with the well documented role of M1 in retention of the adapted movement, this study demonstrates for the first time that M1 GABA measured at baseline predicts retention of the compensatory movement. Participants who show high M1 GABA concentration at baseline retain more of the compensatory movement. This relationship was behaviour-specific (no relationship with adaptation), neurotransmitter-specific (no relationship with glutamate) and session-specific (no relationship in control session). The specificity of this result corroborates M1 GABA involvement in retention and suggests that high levels of inhibition may guard a learnt adaptive movement from washing out.

In chapter 5, I investigated the changes in resting-state fMRI that result from adaptation. Connectivity in a cerebellar network is increased after performing the adaptation task compared to the control task. Moreover, the change in strength of this adaptation-modulated network correlates with adaptation performance. That is, participants who adapt better show a greater increase in cerebellar connectivity compared to participants who adapt less well. This study replicates a previously shown change in a cerebellar network through adaptation and extends

this finding to show a relationship with adaptation performance, emphasising that this change is more pronounced the more effectively participants adapt. It also validates the ability of our adaptation task paradigm to evoke plastic changes in the cerebellum and confirms the suitability of this paradigm for investigating adaptation-driven effects on the brain.

Finally, in chapter 6, I applied a novel MRSI technique to investigate the role of cerebellar GABA in adaptation. I found GABA concentration changed differently in the two cerebellar hemispheres during adaptation against non-specific GABA fluctuations present during movement execution: After nine minutes of adaptation, GABA concentration decreases in the ipsilateral (to the right hand performing the task) cerebellar hemisphere and increases in the contralateral hemisphere. Ipsilateral GABA concentration correlates with overall adaptation, such that the lower the GABA level reached at that timepoint, the better participants adapt in total. This finding provides first evidence to my knowledge for an adaptation-related GABA decrease ipsilateral to the adapting hand and suggests a link between concentration levels reached during adaptation and adaptation performance achieved. This effect was specific to GABA (no change in glutamate) and the link between neurotransmitter levels and behaviour was specific to adaptation. These results give insight into the neurochemical changes taking place during adaptation and reveal a potential mechanism that gives rise to the facilitatory effect of cerebellar anodal tDCS on adaptation found in some studies [101] [274]. With this demonstration of the feasibility of investigating cerebellar neurochemistry non-invasively and in vivo while participants adapt, this study provides a potential avenue for further research into how the cerebellum is involved in different types of behaviour.

Further to these findings, in chapter 6 I examined the relationship between resting-state functional connectivity and behaviour, as well as resting-state functional connectivity and cerebellar GABA. I did not replicate the adaptation-related modulation effect described in chapter 4, likely due to task differences. In order to investigate retention of the previously learned movement immediately after adaptation, visual feedback was removed for the last 11 minutes of the task. This alteration may have washed out changes in functional connectivity elicited by adaptation.

Lastly, I showed a link between cerebellar network-level connectivity and mean GABA concentration in the whole cerebellar MRSI volume at baseline. This relationship was positive, such that higher GABA concentration was related to greater cerebellar connectivity strength. As the direction of this correlation stands in contrast to previously shown links between GABA levels within resting-state network nodes and network strength, this finding provides a basis for testing the extent to which the directionality of a link between inhibition and connectivity link varies between brain regions.

7.2 General limitations

The limitations that are specific to each experiment were reviewed in the respective chapters. In the following section, I discuss limitations that pertain to the general approach and rationale of this thesis.

7.2.1 Observational nature of experiments

The results of chapter 6 point towards an important role of cerebellar GABA in adaptation. This study, however, was correlational like all neuroimaging studies, i.e. the cerebellar GABA levels were observed rather than externally manipulated and we can therefore not infer a causal direction of the effect. The direction of the relationship between cerebellar GABA and adaptation therefore remains to be elucidated directly through an intervention study.

Further, the results of chapter 4 suggest that M1 GABA can predict retention. The M1 GABA measurements that predict retention were taken before the assessment of retention. This temporal order can be taken as an indicator of a causal direction, because cause precedes its effect. However, similarly to the study in chapter 6, this study was observational in nature and did not externally manipulate M1 GABA levels, to measure how this manipulation affects retention.

While these studies therefore highlight relationships between neurochemistry and adaptation behaviour, and provide grounds to investigate causality in this relationship, they do not provide conclusive evidence for a causal link.

7.2.2 Generalisability of findings

The visuomotor adaptation paradigm used in this thesis was chosen due to its compatibility with MR experiments, the range of perturbation sequences it allows and its widespread use in the field. While the use of only the visuomotor adaptation paradigm enables us to compare behavioural data obtained from all experiments within this thesis, it limits the generalisability of our findings to other forms of adaptation. There is evidence that the precise brain areas engaged during adaptation depends on the task paradigm used (atrophy of anterior cerebellum correlates with impaired force-field adaptation and atrophy of posterior cerebellum correlates with impaired visuomotor adaptation [288]) and that behavioural features of adaptation are enhanced or diminished in different forms of adaptation (e.g. greater generalisation of aftereffects across space after prism adaptation compared to visuomotor adaptation [185] [27] [28] [294]). Prism adaptation has been proposed as a potential therapy for neglect and it would therefore be of scientific and clinical merit to extend the findings from this thesis to prism adaptation.

7.3 Future research

The experiments reported in this thesis raise important research questions that could be addressed in future studies. These research questions aim to overcome limitations inherent in the design of the experiments in this thesis and to extend our findings to explore the implications of the results.

7.3.1 Driving ipsilateral GABA decrease with tDCS to facilitate adaptation

As shown in chapter 6, adaptation results in reduced cerebellar inhibition ipsilateral to the performing hand. This data raises the question whether driving a reduction in cerebellar GABA using anodal cerebellar tDCS would result in improved adaptation. Using MRSI during sham or real stimulation would allow comparison of the achieved GABA decrease and investigation of a potential link with adaptation performance. Collecting T1-weighted anatomical scans of the participants' heads would furthermore allow modelling of the current flow and estimation of the achieved current distribution within the ipsilateral cerebellar hemisphere. These data could be used to examine differences in the participants' responsiveness to the tDCS intervention due to anatomical differences.

However, as outlined in chapter 3, the task used in this thesis induces large savings that are evident over weeks after initial exposure. Therefore, a prerequisite for this experiment would be extensive piloting of washout paradigms to establish feasibility of a within-subject study of adaptation.

7.3.2 Assessing the effect of tDCS-induced GABA changes on cerebellar connectivity

We show a positive relationship between baseline cerebellar inhibition and connectivity of a cerebellar resting-state network in chapter 6. Previously, a negative relationship between M1 inhibition and connectivity of the motor network has been shown and tDCS applied to M1 has been shown to increase motor network connectivity. First, it would be important to replicate the relationship found between cerebellar inhibition and connectivity at baseline, as this relationship is demonstrated here for the first time and the directionality of the correlation is opposite to relationships between inhibition and network connectivity found in other brain areas. Second, I would propose to investigate the effects of cerebellar tDCS on cerebellar network connectivity, as part of the study outlined in the previous section.

7.3.3 Investigating the changes in cerebellar GABA during force-field and prism adaptation

Finally, a further avenue for future work would be to extend the findings of this thesis to force-field adaptation and prism adaptation. To fully understand the physiological changes the cerebellum undergoes during adaptation and in order to utilise our understanding of these changes in a clinical context, the results shown for visuomotor adaptation need to be replicated using prism and force-field adaptation paradigms. These studies, however, may be constrained by the fact that for a precise replication, the adaptation task would need to be performed inside the scanner, requiring MR-compatible equipment, and the tasks would need to drive adaptation over an extended period of time. However, linking responsiveness of the GABAergic system probed through tDCS to adaptation behaviour shown outside of the scanner might pose a feasible alternative to assessing changes directly during adaptation.

References

1. Abeele, S. & Bock, O. Sensorimotor adaptation to rotated visual input: Different mechanisms for small versus large rotations. *Exp. Brain Res.* **140,** 407–410 (2001).
2. Aguirre, G. K., Zarahn, E. & D'Esposito, M. *The variability of human, BOLD hemodynamic responses* 1998.
3. Albert, N. B., Robertson, E. M. & Miall, R. C. The Resting Human Brain and Motor Learning. *Curr. Biol.* **19,** 1023–1027 (2009).
4. Albus, J. S. *A theory of cerebellar function* 1971.
5. Alexander, G. Parallel Organization of Functionally Segregated Circuits Linking Basal Ganglia and Cortex. *Annu. Rev. Neurosci.* **9,** 357–381 (1986).
6. Alexander, G. E. & Crutcher, M. D. *Preparation for movement: Neural representations of intended direction in three motor areas of the monkey* 1990.
7. Alfaro-Almagro, F. *et al.* Image processing and Quality Control for the first 10,000 brain imaging datasets from UK Biobank. *Neuroimage* **166,** 400–424 (2018).
8. Ambrus, G. G. *et al.* The fade-in - Short stimulation - Fade out approach to sham tDCS - Reliable at 1 mA for naïve and experienced subjects, but not investigators. *Brain Stimul.* **5,** 499–504 (2012).
9. Andersson, G. & Armstrong, D. M. Complex spikes in Purkinje cells in the lateral vermis (b zone) of the cat cerebellum during locomotion. *J. Physiol.* **385,** 107–134 (1987).
10. Andersson, J. L. R., Jenkinson, M. & Smith, S. *Non-linear registration aka spatial normalisation* tech. rep. June (2007), 22.
11. Andersson, J. D., Matuskey, D. & Finnema, S. J. Positron emission tomography imaging of the γ-aminobutyric acid system. *Neurosci. Lett.* **691,** 35–43 (2019).
12. Andersson, J. L. R., Jenkinson, M. & Smith, S. M. Non-linear optimisation. FMRIB technical report TR07JA1. *FMRIB Tech. Rep.* (2007).
13. Anguera, J. A. Contributions of spatial working memory to visuomotor adaptation. *ProQuest Diss. Theses* **22,** 172 (2008).
14. Attwell, D. & Iadecola, C. The neural basis of functional brain imaging signals. *Trends Neurosci.* **25,** 621–625 (2002).
15. Avila, E. *et al.* Cerebellar transcranial direct current stimulation effects on saccade adaptation. *Neural Plast.* **1** (2015).

16. Azevedo, F. A. *et al.* Equal numbers of neuronal and nonneuronal cells make the human brain an isometrically scaled-up primate brain. *J. Comp. Neurol.* **513,** 532–541 (2009).

17. Bachtiar, V. & Stagg, C. J. in *Magn. Reson. Spectrosc. Tools Neurosci. Res. Emerg. Clin. Appl.* 243–253 (2013).

18. Bachtiar, V. & Stagg, C. J. Interindividual Differences in Behavior and Plasticity. *Magn. Reson. Spectrosc.* 243–253 (2014).

19. Barch, D. M. *et al.* Function in the human connectome: Task-fMRI and individual differences in behavior. *Neuroimage* **80,** 169–189 (2013).

20. Barlow, J. S. *The Cerebellum and Adaptive Control* (2002).

21. Barton, J. J., Jama, A. & Sharpe, J. A. Saccadic duration and intrasaccadic fatigue in myasthenic and nonmyasthenic ocular palsies. *Neurology* **45,** 2065–2072 (Nov. 1995).

22. Bassett, D. S. & Bullmore, E. T. Human brain networks in health and disease. *Curr. Opin. Neurol.* **22,** 340–347 (2009).

23. Bates, D., Mächler, M., Bolker, B. M. & Walker, S. C. Fitting linear mixed-effects models using lme4. *J. Stat. Softw.* **67** (2015).

24. Bates, J. F. & Goldman-Rakic, P. S. Prefrontal connections of medial motor areas in the rhesus monkey. *J. Comp. Neurol.* **336,** 211–228 (1993).

25. Beckmann, C. F. Modelling with independent components. *Neuroimage* **62,** 891–901 (2012).

26. Beckmann, C. F. & Smith, S. M. Probabilistic Independent Component Analysis for Functional Magnetic Resonance Imaging. *IEEE Trans. Med. Imaging* **23,** 137–152 (2004).

27. Bedford, F. L. Constraints on Learning New Mappings Between Perceptual Dimensions. *J. Exp. Psychol. Hum. Percept. Perform.* **15,** 232–248 (1989).

28. Bedford, F. L. Perceptual and Cognitive Spatial Learning. *J. Exp. Psychol. Hum. Percept. Perform.* **19,** 517–530 (1993).

29. Berniker, M., Franklin, D. W., Flanagan, J. R., Wolpert, D. M. & Kording, K. Motor learning of novel dynamics is not represented in a single global coordinate system: Evaluation of mixed coordinate representations and local learning. *J. Neurophysiol.* **111,** 1165–1182 (2014).

30. Bindman, L. J., Lippold, O. C. & Redfearn, J. W. The action of brief polarizing currents on the cerebral cortex of the rat (1) during current flow and (2) in the production of long-lasting after-effects. *J. Physiol.* **172,** 369–382 (1964).

31. Biobank, U. K. Protocol for a large-scale prospective epidemiological resource. *City UK Biobank Coord. Cent.* (2006).

32. Bledsoe, J. C., Semrud-Clikeman, M. & Pliszka, S. R. Neuroanatomical and neuropsychological correlates of the cerebellum in children with attention-deficit/hyperactivity disorder-combined type. *J. Am. Acad. Child Adolesc. Psychiatry* **50,** 593–601 (2011).

33. Block, H. & Celnik, P. Stimulating the cerebellum affects visuomotor adaptation but not intermanual transfer of learning. *Cerebellum* **12,** 781–793 (2013).

34. Bock, O. Components of sensorimotor adaptation in young and elderly subjects. *Exp. Brain Res.* **160,** 259–263 (2005).

35. Bogner, W. *et al.* In vivo quantification of intracerebral GABA by single-voxel 1H-MRS-How reproducible are the results? *Eur. J. Radiol.* **73,** 526–531 (2010).

36. Bolt, T., Nomi, J. S., Rubinov, M. & Uddin, L. Q. Correspondence between evoked and intrinsic functional brain network configurations. *Hum. Brain Mapp.* **38,** 1992–2007 (2017).

37. Bond, K. M. & Taylor, J. A. Flexible explicit but rigid implicit learning in a visuomotor adaptation task. *J. Neurophysiol.* **113,** 3836–3849 (2015).

38. Braitenberg, V. Functional interpretation of cerebellar histology. *Nature* (1961).

39. Brayanov, J. B., Press, D. Z. & Smith, M. A. Motor memory is encoded as a gain-field combination of intrinsic and extrinsic action representations. *J. Neurosci.* **32,** 14951–14965 (2012).

40. Brookhart, J. M. A study of corticospinal activation of motor neurons. *Res. Publ. Assoc. Res. Nerv. Ment. Dis.* **30,** 157–173 (1952).

41. Brooks, J. C., Faull, O. K., Pattinson, K. T. & Jenkinson, M. Physiological noise in brainstem fMRI. *Front. Hum. Neurosci.* **7,** 1–13 (2013).

42. Brunoni, A. R. *et al.* A systematic review on reporting and assessment of adverse effects associated with transcranial direct current stimulation. *Int. J. Neuropsychopharmacol.* **14,** 1133–1145 (2011).

43. Brunoni, A. R. *et al.* Clinical research with transcranial direct current stimulation (tDCS): Challenges and future directions. *Brain Stimul.* **5,** 175–195 (2012).

44. Buckner, R. L. Human functional connectivity: New tools, unresolved questions. *Proc. Natl. Acad. Sci. U. S. A.* **107,** 10769–10770 (2010).

45. Buckner, R. L., Krienen, F. M., Castellanos, A., Diaz, J. C. & Thomas Yeo, B. T. The organization of the human cerebellum estimated by intrinsic functional connectivity. *J. Neurophysiol.* **106,** 2322–2345 (2011).

46. Bucy, P. C. A comparative cytoarchitectonic study of the motor and premotor areas in the primate cortex. *J. Comp. Neurol.* **62,** 293–331 (1935).

47. Bucy, P. C. Electrical excitability and cyto-architecture of the premotor cortex in monkeys. *Arch. Neurol. Psychiatry* **30,** 1205–1225 (1933).

48. Cabanes, E., Confort-Gouny, S., Le Fur, Y., Simond, G. & Cozzone, P. J. Optimization of residual water signal removal by HLSVD on simulated short echo time proton MR spectra of the human brain. *J. Magn. Reson.* **150,** 116–125 (2001).

49. Caesar, K., Gold, L. & Lauritzen, M. Context sensitivity of activity-dependent increases in cerebral blood flow. *Proc. Natl. Acad. Sci. U. S. A.* **100,** 4239–4244 (2003).

50. Cantarero, G. *et al.* Cerebellar direct current stimulation enhances on-line motor skill acquisition through an effect on accuracy. *J. Neurosci.* **35,** 3285–3290 (2015).

51. Cassady, K. *et al.* Neural predictors of sensorimotor adaptation rate and savings. *Hum. Brain Mapp.* **39,** 1516–1531 (2018).

52. Castro-Alamancos, M. A., Donoghue, J. P. & Connors, B. W. Different forms of synaptic plasticity in somatosensory and motor areas of the neocortex. *J. Neurosci.* **15,** 5324–5333 (1995).

53. Castro, L. N., Monsen, C. B. & Smith, M. A. The binding of learning to action in motor adaptation. *PLoS Comput. Biol.* **7** (2011).

54. Catz, N., Dicke, P. W. & Thier, P. Cerebellar complex spike firing is suitable to induce as well as to stabilize motor learning. *Curr. Biol.* **15,** 2179–2189 (2005).

55. Cavassila, S., Deval, S., Huegen, C., Van Ormondt, D. & Graveron-Demilly, D. The beneficial influence of prior knowledge on the quantitation of in vivo magnetic resonance spectroscopy signals. *Invest. Radiol.* **34,** 242–246 (1999).

56. Celnik, P. Understanding and Modulating Motor Learning with Cerebellar Stimulation. *Cerebellum* **14,** 171–174 (2015).

57. Chen, B. R., Kozberg, M. G., Bouchard, M. B., Shaik, M. A. & Hillman, E. M. A critical role for the vascular endothelium in functional neurovascular coupling in the brain. *J. Am. Heart Assoc.* **3,** 1–14 (2014).

58. Chen, J. E. & Glover, G. H. BOLD fractional contribution to resting-state functional connectivity above 0.1Hz. *Neuroimage* **107,** 207–218 (2015).

59. Cheng, S. & Sabes, P. N. Modeling Sensorimotor Learning with Linear Dynamical Systems. *Neural Comput.* **18,** 760–793 (2006).

60. Chow, B. W. *et al.* Caveolae in CNS arterioles mediate neurovascular coupling. *Nature* **579,** 106–110 (2020).

61. Crutcher, M. D. & Alexander, G. E. Movement-related neuronal activity selectively coding either direction or muscle pattern in three motor areas of the monkey. *J. Neurophysiol.* **64,** 151–163 (1990).

62. Cunningham, H. A. Aiming Error Under Transformed Spatial Mappings Suggests a Structure for Visual-Motor Maps. *J. Exp. Psychol. Hum. Percept. Perform.* **15,** 493–506 (1989).

63. D'Mello, A. M., Turkeltaub, P. E. & Stoodley, C. J. Cerebellar tdcs modulates neural circuits during semantic prediction: A combined tDCS-fMRI study. *J. Neurosci.* **37,** 1604–1613 (2017).

64. Della-Maggiore, V., Malfait, N., Ostry, D. J. & Paus, T. Stimulation of the posterior parietal cortex interferes with arm trajectory adjustments during the learning of new dynamics. *J. Neurosci.* **24,** 9971–9976 (2004).

65. Della-Maggiore, V. & McIntosh, A. R. Time course of changes in brain activity and functional connectivity associated with long-term adaptation to a rotational transformation. *J. Neurophysiol.* **93,** 2254–2262 (2005).

66. Della-Maggiore, V., Villalta, J. I., Kovacevic, N. & McIntosh, A. R. Functional Evidence for Memory Stabilization in Sensorimotor Adaptation: A 24-h Resting-State fMRI Study. *Cereb. Cortex* **27,** 1748–1757 (2017).

67. Diedrichsen, J. *et al.* Imaging the deep cerebellar nuclei: A probabilistic atlas and normalization procedure. *Neuroimage* **54,** 1786–1794 (2011).

68. Diedrichsen, J. A spatially unbiased atlas template of the human cerebellum. *Neuroimage* **33,** 127–138 (2006).

69. Diedrichsen, J., Balsters, J. H., Flavell, J., Cussans, E. & Ramnani, N. A probabilistic MR atlas of the human cerebellum. *Neuroimage* **46,** 39–46 (2009).

70. Diedrichsen, J., King, M., Hernandez-Castillo, C., Sereno, M. & Ivry, R. B. Universal Transform or Multiple Functionality? Understanding the Contribution of the Human Cerebellum across Task Domains. *Neuron* **102,** 918–928 (2019).

71. Donchin, O., Francis, J. T. & Shadmehr, R. Quantifying generalization from trial-by-trial behavior of adaptive systems that learn with basis functions: Theory and experiments in human motor control. *J. Neurosci.* **23,** 9032–9045 (2003).

72. Donoghue, J. P., Leibovic, S. & Sanes, J. N. Organization of the forelimb area in squirrel monkey motor cortex: representation of digit, wrist, and elbow muscles. *Exp. Brain Res.* **89,** 1–19 (1992).

73. Dreher, W. & Leibfritz, D. New method for the simultaneous detection of metabolites and water in localized in vivo1H nuclear magnetic resonance spectroscopy. *Magn. Reson. Med.* **54,** 190–195 (2005).

74. Dum, R. P. & Strick, P. L. The origin of corticospinal projections from the premotor areas in the frontal lobe. *J. Neurosci.* **11,** 667–689 (1991).

75. Dum, R. P. & Strick, P. L. An unfolded map of the cerebellar dentate nucleus and its projections to the cerebral cortex. *J. Neurophysiol.* **89,** 634–639 (2003).

76. Dum, R. P. & Strick, P. L. Frontal lobe inputs to the digit representations of the motor areas on the lateral surface of the hemisphere. *J. Neurosci.* **25,** 1375–1386 (2005).

77. Dum, R. & Strick, P. Motor Areas in the Frontal Lobe. **77,** 677–682 (2004).

78. Dyke, K. *et al.* Comparing GABA-dependent physiological measures of inhibition with proton magnetic resonance spectroscopy measurement of GABA using ultra-high-field MRI. *Neuroimage* **152,** 360–370 (2017).

79. Eccles, J. C. *The Cerebellum as a Neuronal Machine* (Springer-Verlag, Berlin).

80. Elster, A. D. *MRIquestions.com* 2019.

81. Emir, U. E. *et al.* Regional neurochemical profiles in the human brain measured by 1H MRS at 7T using local B 1 shimming. *NMR Biomed.* **25,** 152–160 (2012).

82. Evans, C. J., McGonigle, D. J. & Edden, R. A. E. Diurnal stability of γ-aminobutyric acid concentration in visual and sensorimotor cortex. *J. Magn. Reson. Imaging* **31,** 204–209 (2010).

83. Evarts, E. V. Relation of pyramidal tract activity to force exerted during voluntary movement. *J. Neurophysiol.* **31,** 14–27 (1968).

84. Fendrich, D. W., Healy, A. F. & Bourne, L. E. Long-Term Repetition Effects for Motoric and Perceptual Procedures. *J. Exp. Psychol. Learn. Mem. Cogn.* **17,** 137–151 (1991).

85. Fernandez-Ruiz, J., Wong, W., Armstrong, I. T. & Flanagan, J. R. Relation between reaction time and reach errors during visuomotor adaptation. *Behav. Brain Res.* **219,** 8–14 (2011).

86. Ferrier, D. Experimental researches in cerebral physiology and pathology. *Br. Med. J.* **1,** 457 (1873).

87. Ferrucci, R. *et al.* Cerebellar transcranial direct current stimulation impairs the practice-dependent proficiency increase in working memory. *J. Cogn. Neurosci.* **20,** 1687–1697 (2008).

88. Ferrucci, R., Bocci, T. & Priori, A. in *Transcranial Direct Curr. Stimul. Neuropsychiatr. Disord. Clin. Princ. Manag.* 223–229 (2016).

89. Ferrucci, R. & Priori, A. Transcranial cerebellar direct current stimulation (tcDCS): Motor control, cognition, learning and emotions. *Neuroimage* **85,** 918–923 (2014).

90. Ferrucci, R. *et al.* Cerebellum and processing of negative facial emotions: Cerebellar transcranial DC stimulation specifically enhances the emotional recognition of facial anger and sadness. *Cogn. Emot.* **26,** 786–799 (2012).

91. Floyer-Lea, A., Wylezinska, M., Kincses, T. & Matthews, P. M. Rapid modulation of GABA concentration in human sensorimotor cortex during motor learning. *J. Neurophysiol.* **95,** 1639–1644 (2006).

92. Floyer-Lea, A., Wylezinska, M., Kincses, T. & Matthews, P. M. Rapid modulation of GABA concentration in human sensorimotor cortex during motor learning. *J. Neurophysiol.* **95,** 1639–1644 (2006).

93. Fox, M. D. & Raichle, M. E. Spontaneous fluctuations in brain activity observed with functional magnetic resonance imaging. *Nat. Rev. Neurosci.* **8,** 700–711 (2007).

94. Frangou, P. *et al.* Learning to optimize perceptual decisions through suppressive interactions in the human brain. *Nat. Commun.* **10,** 474 (2019).

95. Friston, K. J. *et al.* Event-related fMRI: Characterizing differential responses. *Neuroimage* **7,** 30–40 (1998).

96. Fritsch, G. & Hitzig, E. Electric excitability of the cerebrum (Über die elektrische Erregbarkeit des Grosshirns). *Epilepsy Behav.* **15,** 123–130 (2009).

97. Fujita, M. Adaptive filter model of the cerebellum. *Biol. Cybern.* **45,** 195–206 (1982).

98. Gaffin-Cahn, E., Hudson, T. E. & Landy, M. S. Did I do that? Detecting a perturbation to visual feedback in a reaching task. *J. Vis.* **19,** 1–18 (2019).

99. Galea, J. M., Jayaram, G., Ajagbe, L. & Celnik, P. Modulation of cerebellar excitability by polarity-specific noninvasive direct current stimulation. *J. Neurosci.* **29,** 9115–9122 (July 2009).

100. Galea, J. M., Mallia, E., Rothwell, J. & Diedrichsen, J. The dissociable effects of punishment and reward on motor learning. *Nat. Neurosci.* **18,** 597–602 (2015).

101. Galea, J. M., Vazquez, A., Pasricha, N., Orban De Xivry, J. J. & Celnik, P. Dissociating the roles of the cerebellum and motor cortex during adaptive learning: The motor cortex retains what the cerebellum learns. *Cereb. Cortex* **21,** 1761–1770 (2011).

102. Gandiga, P. C., Hummel, F. C. & Cohen, L. G. Transcranial DC stimulation (tDCS): A tool for double-blind sham-controlled clinical studies in brain stimulation. *Clin. Neurophysiol.* **117,** 845–850 (2006).

103. Gao, J. H. *et al.* Cerebellum implicated in sensory acquisition and discrimination rather than motor control. *Science (80-.).* **272,** 545–547 (1996).

104. Gao, W. *et al.* Optical imaging of long-term depression in the mouse cerebellar cortex in vivo. *J. Neurosci.* **23,** 1859–1866 (2003).

105. Gilbert, P. F. & Thach, W. T. Purkinje cell activity during motor learning. *Brain Res.* **128,** 309–328 (1977).

106. Gonzalez Castro, L. N., Hadjiosif, A. M., Hemphill, M. A. & Smith, M. A. Environmental consistency determines the rate of motor adaptation. *Curr. Biol.* **24,** 1050–1061 (2014).

107. Graydon, F. X., Friston, K. J., Thomas, C. G., Brooks, V. B. & Menon, R. S. Learning-related fMRI activation associated with a rotational visuo-motor transformation. *Cogn. Brain Res.* **22,** 373–383 (2005).

108. Griffanti, L. *et al.* Hand classification of fMRI ICA noise components. *Neuroimage* **154,** 188–205 (2017).

109. Griffanti, L. *et al.* ICA-based artefact removal and accelerated fMRI acquisition for improved resting state network imaging. *Neuroimage* **95,** 232–247 (2014).

110. Griffen, T. C. & Maffei, A. GABAergic synapses: Their plasticity and role in sensory cortex. *Front. Cell. Neurosci.* **8,** 1–22 (2014).

111. Grimaldi, G., Taib, N. O. B., Manto, M. & Bodranghien, F. Marked reduction of cerebellar deficits in upper limbs following transcranial cerebello-cerebral DC stimulation: Tremor reduction and re-programming of the timing of antagonist commands. *Front. Syst. Neurosci.* **8,** 9 (2014).

112. Grimaldi, G. *et al.* Cerebellar Transcranial Direct Current Stimulation (ctDCS): A Novel Approach to Understanding Cerebellar Function in Health and Disease. *Neuroscientist* **22,** 83–97 (2016).

113. Gupta, T. *et al.* Cerebellar transcranial direct current stimulation improves procedural learning in nonclinical psychosis: A double-blind crossover study. *Schizophr. Bull.* **44,** 1373–1380 (2018).

114. Haas, K. F. & Macdonald, R. L. GABA(A) receptor subunit $\gamma 2$ and δ subtypes confer unique kinetic properties on recombinant GABA(A) receptor currents in mouse fibroblasts. *J. Physiol.* **514,** 27–45 (1999).

115. Haase, A., Frahm, J., Hanicke, W. & Matthaei, D. 1H NMR chemical shift selective (CHESS) imaging. *Phys. Med. Biol.* **30,** 341–344 (1985).

116. Hadipour-Niktarash, A., Lee, C. K., Desmond, J. E. & Shadmehr, R. Impairment of retention but not acquisition of a visuomotor skill through time-dependent disruption of primary motor cortex. *J. Neurosci.* **27,** 13413–13419 (2007).

117. Haibach, P. S., Reid, G. & Collier, D. H. *Motor Learning and Development* Second, 4–119 (Human Kinetics, Champaign, IL, 2011).

118. Haith, A. M., Huberdeau, D. M. & Krakauer, J. W. The influence of movement preparation time on the expression of visuomotor learning and savings. *J. Neurosci.* **35,** 5109–5117 (2015).

119. Halsband, U., Matsuzaka, Y. & Tanji, J. Neuronal activity in the primate supplementary, pre-supplementary and premotor cortex during externally and internally instructed sequential movements. *Neurosci. Res.* **20,** 149–155 (1994).

120. Handwerker, D. A., Gonzalez-Castillo, J., D'Esposito, M. & Bandettini, P. A. The continuing challenge of understanding and modeling hemodynamic variation in fMRI. *Neuroimage* **62,** 1017–1023 (2012).

121. Handwerker, D. A., Ollinger, J. M. & D'Esposito, M. Variation of BOLD hemodynamic responses across subjects and brain regions and their effects on statistical analyses. *Neuroimage* **21,** 1639–1651 (2004).

122. Hardwick, R. M. & Celnik, P. A. Cerebellar direct current stimulation enhances motor learning inolder adults. *Neurobiol. Aging* **35,** 2217–2221 (2014).

123. Hardwick, R. M., Rottschy, C., Miall, R. C. & Eickhoff, S. B. A quantitative meta-analysis and review of motor learning in the human brain. *Neuroimage* **67,** 283–297 (2013).

124. He, Q. *et al.* Interneuron- and GABAA receptor-specific inhibitory synaptic plasticity in cerebellar Purkinje cells. *Nat. Commun.* **6** (2015).

125. He, S. Q., Dum, R. P. & Strick, P. L. Topographic organization of corticospinal projections from the frontal lobe: Motor areas on the lateral surface of the hemisphere. *J. Neurosci.* **13,** 952–980 (1993).

126. He, S. Q., Dum, R. P. & Strick, P. L. Topographic organization of corticospinal projections from the frontal lobe: Motor areas on the medial surface of the hemisphere. *J. Neurosci.* **15,** 3284–3306 (1995).

127. Hegele, M. & Heuer, H. Implicit and explicit components of dual adaptation to visuomotor rotations. *Conscious. Cogn.* **19,** 906–917 (2010).

128. Herzfeld, D. J., Kojima, Y., Soetedjo, R. & Shadmehr, R. Encoding of error and learning to correct that error by the Purkinje cells of the cerebellum. *Nat. Neurosci.* **21,** 736–743 (2018).

129. Herzfeld, D. J., Vaswani, P. A., Marko, M. K. & Shadmehr, R. A memory of errors in sensorimotor learning. *Science* **345,** 1349–1353 (2014).

130. Herzfeld, D. J. *et al.* Contributions of the cerebellum and the motor cortex to acquisition and retention of motor memories. *Neuroimage* **98,** 147–158 (2014).

131. Hess, G. & Donoghue, J. P. Long-term depression of horizontal connections in rat motor cortex. *Eur. J. Neurosci.* **8,** 658–665 (1996).

132. Hess, G. & Donoghue, J. P. Long-term potentiation of horizontal connections provides a mechanism to reorganize cortical motor maps. *J. Neurophysiol.* **71,** 2543–2547 (1994).

133. Hess, G., Aizenman, C. D. & Donoghue, J. P. Conditions for the induction of long-term potentiation in layer II/III horizontal connections of the rat motor cortex. *J. Neurophysiol.* **75,** 1765–1778 (1996).

134. Heuer, H. & Hegele, M. Adaptation to Visuomotor Rotations in Younger and Older Adults. *Psychol. Aging* **23,** 190–202 (2008).

135. Hinder, M. R., Walk, L., Woolley, D. G., Riek, S. & Carson, R. G. The interference effects of non-rotated versus counter-rotated trials in visuomotor adaptation. *Exp. Brain Res.* **180,** 629–640 (2007).

136. Howarth, C., Peppiatt-Wildman, C. M. & Attwell, D. The energy use associated with neural computation in the cerebellum. *J. Cereb. Blood Flow Metab.* **30,** 403–414 (2010).

137. Hu, D., Shen, H. & Zhou, Z. Functional asymmetry in the cerebellum: A brief review. *Cerebellum* **7,** 304–313 (2008).

138. Huang, V. S., Haith, A., Mazzoni, P. & Krakauer, J. W. Rethinking Motor Learning and Savings in Adaptation Paradigms: Model-Free Memory for Successful Actions Combines with Internal Models. *Neuron* **70,** 787–801 (2011).

139. Hulst, T. *et al.* Cerebellar patients do not benefit from cerebellar or M1 transcranial direct current stimulation during force-field reaching adaptation. *J. Neurophysiol.* **118,** 732–748 (2017).

140. Hunter, T., Sacco, P., Nitsche, M. A. & Turner, D. L. Modulation of internal model formation during force field-induced motor learning by anodal transcranial direct current stimulation of primary motor cortex. *J. Physiol.* **587,** 2949–2961 (2009).

141. Huntley, G. W. Correlation between patterns of horizontal connectivity and the extent of short-term representational plasticity in rat motor cortex. *Cereb. Cortex* **7,** 143–156 (1997).

142. Iadecola, C. The Neurovascular Unit Coming of Age: A Journey through Neurovascular Coupling in Health and Disease. *Neuron* **96,** 17–42 (2017).

143. Ichise, T. *et al.* mGluR1 in cerebellar Purkinje cells essential for long-term depression, synapse elimination, and motor coordination. *Science (80-.).* **288,** 1832–1835 (2000).

144. Imamizu, H., Kuroda, T., Miyauchi, S., Yoshioka, T. & Kawato, M. Modular organization of internal models of tools in the human cerebellum. *Proc. Natl. Acad. Sci. U. S. A.* **100,** 5461–5466 (2003).

145. Imamizu, H. *et al.* Human cerebellar activity reflecting an acquired internal model of a new tool. *Nature* **403,** 192–195 (2000).

146. Ito, M. in *Encycl. Neurosci.* 723–728 (2009).

147. Ito, M. Control of mental activities by internal models in the cerebellum. *Nat. Rev. Neurosci.* **9,** 304–313 (2008).

148. Ito, M. Error detection and representation in the olivo-cerebellar system. *Front. Neural Circuits* **7,** 1–8 (2013).

149. Itō, M. *The cerebellum and neural control* (Raven Press, New York, 1984).

150. Ito, M. & Kano, M. Long-lasting depression of parallel fiber-Purkinje cell transmission induced by conjunctive stimulation of parallel fibers and climbing fibers in the cerebellar cortex. *Neurosci. Lett.* **33,** 253–258 (1982).

151. Ivachtchenko, A., Ivanenkov, Y. & Veselov, M. Preclinical evaluation of AVN-322, novel and highly selective 5-HT6 receptor antagonist, for the treatment of Alzheimer's disease. *Curr. Alzheimer Res.* **13,** 1–1 (2016).

152. Izawa, J. & Shadmehr, R. Learning from sensory and reward prediction errors during motor adaptation. *PLoS Comput. Biol.* **7,** 1–11 (2011).

153. Jackson, S. R. & Husain, M. Visuomotor functions of the posterior parietal cortex. *Neuropsychologia* **44,** 2589–2593 (2006).

154. Jackson, S. R., Newport, R., Mort, D. & Husain, M. Where the eye looks, the hand follows: Limb-dependent magnetic misreaching in optic ataxia. *Curr. Biol.* **15,** 42–46 (2005).

155. Jacobs, K. & Donoghue, J. Reshaping the cortical motor map by unmasking latent intracortical connections. *Science (80-.).* **251,** 944–947 (1991).

156. Jacobson, G. A. *et al.* Subthreshold voltage noise of rat neocortical pyramidal neurones. *J. Physiol.* **564,** 145–160 (2005).

157. Jalali, R., Chowdhury, A., Wilson, M., Miall, R. C. & Galea, J. M. Neural changes associated with cerebellar tDCS studied using MR spectroscopy. *Exp. Brain Res.* **236,** 997–1006 (2018).

158. Jalali, R., Miall, R. C. & Galea, J. M. No consistent effect of cerebellar transcranial direct current stimulation on visuomotor adaptation. *J. Neurophysiol.* **118,** 655–665 (2017).

159. Jayaram, G. *et al.* Modulating locomotor adaptation with cerebellar stimulation. *J. Neurophysiol.* **107,** 2950–2957 (2012).

160. Jefferys, J. G. Influence of electric fields on the excitability of granule cells in guinea-pig hippocampal slices. *J. Physiol.* **319,** 143–152 (1981).

161. Jenkinson, M., Bannister, P., Brady, M. & Smith, S. Improved Optimization for the Robust and Accurate Linear Registration and Motion Correction of Brain Images. *Neuroimage* **17,** 825–841 (2002).

162. Jenkinson, M., Beckmann, C. F., Behrens, T. E. J., Woolrich, M. W. & Smith, S. M. Review FSL. *Neuroimage* **62,** 782–790 (2012).

163. Jenkinson, M. & Smith, S. A global optimisation method for robust affine registration of brain images. *Med. Image Anal.* **5,** 143–156 (2001).

164. Johnson, J. F., Belyk, M., Schwartze, M., Pinheiro, A. P. & Kotz, S. A. The role of the cerebellum in adaptation: ALE meta-analyses on sensory feedback error. *Hum. Brain Mapp.* **40,** 3966–3981 (2019).

165. Jordan, M. I. & Rumelhart, D. E. Forward Models: Supervised Learning with a Distal Teacher. *Cogn. Sci.* **16,** 307–354 (1992).

166. Jörntell, H. & Ekerot, C. F. Reciprocal bidirectional plasticity of parallel fiber receptive fields in cerebellar Purkinje cells and their afferent interneurons. *Neuron* **34,** 797–806 (2002).

167. Juchem, C. & Rothman, D. L. Basis of Magnetic Resonance. *Magn. Reson. Spectrosc. Tools Neurosci. Res. Emerg. Clin. Appl.* 3–14 (2013).

168. Jueptner, M. *et al.* The relevance of sensory input for the cerebellar control of movements. *Neuroimage* **5,** 41–48 (1997).

169. Kagerer, F. A., Contreras-Vidal, J. L. & Stelmach, G. E. Adaptation to gradual as compared with sudden visuo-motor distortions. *Exp. Brain Res.* **115,** 557–561 (1997).

170. Kapogiannis, D., Reiter, D. A., Willette, A. A. & Mattson, M. P. Posteromedial cortex glutamate and GABA predict intrinsic functional connectivity of the default mode network. *Neuroimage* **64,** 112–119 (2013).

171. Kawai, R. *et al.* Motor Cortex Is Required for Learning but Not for Executing a Motor Skill. *Neuron* **86,** 800–812 (2015).

172. Kawato, M., Furukawa, K. & Suzuki, R. A hierarchical neural-network model for control and learning of voluntary movement. *Biol. Cybern.* (1987).

173. Kelly, R. E. *et al.* Visual inspection of independent components: Defining a procedure for artifact removal from fMRI data. *J. Neurosci. Methods* **189,** 233–245 (2010).

174. Kelly, R. M. & Strick, P. L. Cerebellar loops with motor cortex and prefrontal cortex of a nonhuman primate. *J. Neurosci.* **23,** 8432–8444 (2003).

175. Kim, H. E., Parvin, D. E. & Ivry, R. B. The influence of task outcome on implicit motor learning. *Elife* **8,** 1–28 (2019).

176. Kim, S., Stephenson, M. C., Morris, P. G. & Jackson, S. R. TDCS-induced alterations in GABA concentration within primary motor cortex predict motor learning and motor memory: A 7T magnetic resonance spectroscopy study. *Neuroimage* **99,** 237–243 (2014).

177. Kim, S., Stephenson, M. C., Morris, P. G. & Jackson, S. R. TDCS-induced alterations in GABA concentration within primary motor cortex predict motor learning and motor memory: A 7T magnetic resonance spectroscopy study. *Neuroimage* **99,** 237–243 (2014).

178. Kitago, T., Ryan, S. L., Mazzoni, P., Krakauer, J. W. & Haith, A. M. Unlearning versus savings in visuomotor adaptation: Comparing effects of washout, passage of time and removal of errors on motor memory. *Front. Hum. Neurosci.* **7,** 1–7 (2013).

179. Klassen, J., Tong, C. & Flanagan, J. R. Learning and recall of incremental kinematic and dynamic sensorimotor transformations. *Exp. Brain Res.* **164,** 250–259 (2005).

180. Kluzik, J. A., Diedrichsen, J., Shadmehr, R. & Bastian, A. J. Reach adaptation: What determines whether we learn an internal model of the tool or adapt the model of our arm? *J. Neurophysiol.* **100,** 1455–1464 (2008).

181. Kolasinski, J. *et al.* The dynamics of cortical GABA in human motor learning. *J. Physiol.* **597,** 271–282 (2019).

182. Koolschijn, R., Emir, U., Pantelides, A., Behrens, T. & Barron, H. The hippocampus and neocortical inhibitory engrams protect against memory interference. *bioRxiv,* 366377 (2018).

183. Kording, K. P., Tenenbaum, J. B. & Shadmehr, R. The dynamics of memory as a consequence of optimal adaptation to a changing body. *Nat. Neurosci.* **10,** 779–786 (2007).

184. Körding, K. P. & Wolpert, D. M. Bayesian decision theory in sensorimotor control. *Trends Cogn. Sci.* **10,** 319–326 (2006).

185. Krakauer, J. W., Pine, Z. M., Ghilardi, M. F. & Ghez, C. Learning of visuomotor transformations for vectorial planning of reaching trajectories. *J. Neurosci.* **20,** 8916–8924 (2000).

186. Krakauer, J. W. Motor learning and consolidation: The case of visuomotor rotation. *Adv. Exp. Med. Biol.* **629,** 405–421 (2009).

187. Krakauer, J. W., Ghez, C. & Ghilardi, M. F. Adaptation to visuomotor transformations: Consolidation, interference, and forgetting. *J. Neurosci.* **25,** 473–478 (2005).

188. Krakauer, J. W., Ghilardi, M. F. & Ghez, C. Independent learning of internal models for kinematic and dynamic control of reaching. *Nat. Neurosci.* **2,** 1026–1031 (1999).

189. Krakauer, J. W., Hadjiosif, A. M., Xu, J., Wong, A. L. & Haith, A. M. Motor learning. *Compr. Physiol.* **9,** 613–663 (Mar. 2019).

190. Kreis, R. Issues of spectral quality in clinical 1H-magnetic resonance spectroscopy and a gallery of artifacts. *NMR Biomed.* **17,** 361–381 (2004).

191. Kreis, R. The trouble with quality filtering based on relative Cramér-Rao lower bounds. *Magn. Reson. Med.* **75,** 15–18 (2016).

192. Küper, M. *et al.* Activation of the cerebellar cortex and the dentate nucleus in a prism adaptation fMRI study. *Hum. Brain Mapp.* **35,** 1574–1586 (2014).

193. Kurt A., T. & Reza, S. Learning of action through adaptive combination of motor primitives. *Nature* **407,** 742–747 (2000).

194. Le, T. D. *et al.* Lipid signaling in cytosolic phospholipase A2α- cyclooxygenase-2 cascade mediates cerebellar longterm depression and motor learning. *Proc. Natl. Acad. Sci. U. S. A.* **107,** 3198–3203 (2010).

195. Leow, L. A., de Rugy, A., Marinovic, W., Riek, S. & Carroll, T. J. Savings for visuomotor adaptation require prior history of error, not prior repetition of successful actions. *J. Neurophysiol.* **116,** 1603–1614 (2016).

196. Leow, L. A., Loftus, A. M. & Hammond, G. R. Impaired savings despite intact initial learning of motor adaptation in Parkinson's disease. *Exp. Brain Res.* **218,** 295–304 (2012).

197. Leow, L. A., Marinovic, W., Riek, S. & Carroll, T. J. Cerebellar anodal tDCS increases implicit learning when strategic re-aiming is suppressed in sensorimotor adaptation. *PLoS One* **12,** 1–18 (2017).

198. Lewis, C. M., Baldassarre, A., Committeri, G., Romani, G. L. & Corbetta, M. Learning sculpts the spontaneous activity of the resting human brain. *Proc. Natl. Acad. Sci. U. S. A.* **106,** 17558–17563 (2009).

199. Li, C. S. R., Padoa-Schioppa, C. & Bizzi, E. Neuronal correlates of motor performance and motor learning in the primary motor cortex of monkeys adapting to an external force field. *Neuron* **30,** 593–607 (2001).

200. Logothetis, N. K., Pauls, J., Augath, M., Trinath, T. & Oeltermann, A. Neurophysiological investigation of the basis of the fMRI signal. *Nature* **412,** 150–157 (2001).

201. Longden, T. A. *et al.* Capillary K+-sensing initiates retrograde hyperpolarization to increase local cerebral blood flow. *Nat. Neurosci.* **20,** 717–726 (2017).

202. Lowe, M. J., Mock, B. J. & Sorenson, J. A. Functional connectivity in single and multislice echoplanar imaging using resting-state fluctuations. *Neuroimage* **7,** 119–132 (1998).

203. Lu, M., Preston, J. B. & Strick, P. L. Interconnections between the prefrontal cortex and the premotor areas in the frontal lobe. *J. Comp. Neurol.* **341,** 375–392 (1994).

204. Luauté, J. *et al.* Functional anatomy of the therapeutic effects of prism adaptation on left neglect. *Neurology* **66,** 1859–1867 (2006).

205. Luppino, G., Matelli, M., Camarda, R. & Rizzolatti, G. Corticocortical connections of area F3 (SMA-proper) and area F6 (pre-SMA) in the macaque monkey. *J. Comp. Neurol.* **338,** 114–140 (1993).

206. Ma, Y. *et al.* Resting-state hemodynamics are spatiotemporally coupled to synchronized and symmetric neural activity in excitatory neurons. *Proc. Natl. Acad. Sci. U. S. A.* **113,** E8463–E8471 (2016).

207. MacKay, W. A. & Murphy, J. T. Activation of anterior interpositus neurons by forelimb muscle stretch. *Brain Res.* **56,** 335–339 (1973).

208. Maier, M. A., Bennett, K. M., Hepp-Reymond, M. C. & Lemon, R. N. Contribution of the monkey corticomotoneuronal system to the control of force in precision grip. *J. Neurophysiol.* **69,** 772–785 (1993).

209. Mamlins, A., Hulst, T., Donchin, O., Timmann, D. & Claassen, J. No effects of cerebellar transcranial direct current stimulation on force field and visuomotor reach adaptation in young and healthy subjects. *J. Neurophysiol.* **121,** 2112–2125 (2019).

210. Margulies, D. S. *et al.* Precuneus shares intrinsic functional architecture in humans and monkeys. *Proc. Natl. Acad. Sci. U. S. A.* **106,** 20069–20074 (2009).

211. Marinelli, L. *et al.* Learning and consolidation of visuo-motor adaptation in Parkinson's disease. *Park. Relat. Disord.* **15,** 6–11 (2009).

212. Marko, M. K., Haith, A. M., Harran, M. D. & Shadmehr, R. Sensitivity to prediction error in reach adaptation. *J. Neurophysiol.* **108,** 1752–1763 (2012).

213. Marr, J. E. A Theory of Cerebellar Cortex. *J. Physiol.* **202,** 437–470 (1969).

214. Martin, D. L. & Barke, K. E. Are GAD65 and GAD67 associated with specific pools of GABA in brain? *Perspect. Dev. Neurobiol.* **5,** 119–129 (1998).

215. Mathiesen, C., Caesar, K. & Lauritzen, M. Temporal coupling between neuronal activity and blood flow in rat cerebellar cortex as indicated by field potential analysis. *J. Physiol.* **523,** 235–246 (2000).

216. Mathis, M. W., Mathis, A. & Uchida, N. Somatosensory Cortex Plays an Essential Role in Forelimb Motor Adaptation in Mice. *Neuron* **93,** 1493–1503.e6 (2017).

217. Mazzoni, P. & Bracewell, M. The persistent mystery of the basal ganglia's contribution to motor control. *Adv. Clin. Neurosci. Rehabil.* **10,** 22–24 (2010).

218. Mazzoni, P. & Krakauer, J. W. An implicit plan overrides an explicit strategy during visuomotor adaptation. *J. Neurosci.* **26,** 3642–3645 (2006).

219. McDonnell, M. N., Orekhov, Y. & Ziemann, U. Suppression of LTP-like plasticity in human motor cortex by the GABA B receptor agonist baclofen. *Exp. Brain Res.* **180,** 181–186 (2007).

220. McDougle, S. D., Bond, K. M. & Taylor, J. A. Explicit and implicit processes constitute the fast and slow processes of sensorimotor learning. *J. Neurosci.* **35,** 9568–9579 (2015).

221. McDougle, S. D. & Taylor, J. A. Dissociable cognitive strategies for sensorimotor learning. *Nat. Commun.* **10** (2019).

222. McIlwain, H. Biochemistry and the central nervous system (1985).

223. McKeown, M. J. *et al.* Analysis of fMRI data by blind separation into independent spatial components. *Hum. Brain Mapp.* **6,** 160–188 (1998).

224. Medina, J. F. & Lisberger, S. G. Links from complex spikes to local plasticity and motor learning in the cerebellum of awake-behaving monkeys. *Nat. Neurosci.* **11,** 1185–1192 (2008).

225. Medina, J. F., Nores, W. L. & Mauk, M. D. Inhibition of climbing fibres is a signal for the extinction of conditioned eyelid responses. *Nature* **416,** 330–333 (2002).

226. Mescher, M., Merkle, H., Kirsch, J., Garwood, M. & Gruetter, R. Simultaneous in vivo spectral editing and water suppression. *NMR Biomed.* **11,** 266–272 (1998).

227. Miall, R. C. & Jenkinson, E. W. Functional imaging of changes in cerebellar activity related to learning during a novel eye-hand tracking task. *Exp. Brain Res.* **166,** 170–183 (2005).

228. Miall, R. C., Reckess, G. Z. & Imamizu, H. The cerebellum coordinates eye and hand tracking movements. *Nat. Neurosci.* **4,** 638–644 (2001).

229. Miall, R. C., Weir, D. J. & Stein, J. F. Visuomotor tracking with delayed visual feedback. *Neuroscience* **16,** 511–520 (1985).

230. Miall, R. C., Weir, D. J., Wolpert, D. M. & Stein, J. F. Is the cerebellum a smith predictor? *J. Mot. Behav.* (1993).

231. Miall, R. C. & Wolpert, D. M. Forward models for physiological motor control. *Neural Networks* **9,** 1265–1279 (1996).

232. Miall, R. C., Christensen, L. O., Cain, O. & Stanley, J. Disruption of state estimation in the human lateral cerebellum. *PLoS Biol.* **5,** 2733–2744 (2007).

233. Miall, R. C., Jenkinson, N. & Kulkarni, K. Adaptation to rotated visual feedback: A re-examination of motor interference. *Exp. Brain Res.* **154,** 201–210 (2004).

234. Middleton, F. A. & Strick, P. L. Basal ganglia and cerebellar loops: Motor and cognitive circuits. *Brain Res. Rev.* **31,** 236–250 (2000).

235. Miezin, F. M., Maccotta, L., Ollinger, J. M., Petersen, S. E. & Buckner, R. L. Characterizing the hemodynamic response: Effects of presentation rate, sampling procedure, and the possibility of ordering brain activity based on relative timing. *Neuroimage* **11,** 735–759 (2000).

236. Minarik, T. *et al.* The importance of sample size for reproducibility of tDCS effects. *Front. Hum. Neurosci.* **10,** 1–5 (2016).

237. Mink, J. W. The basal ganglia: Focused selection and inhibition of competing motor programs. *Prog. Neurobiol.* **50,** 381–425 (1996).

238. Miranda, P. C., Lomarev, M. & Hallett, M. Modeling the current distribution during transcranial direct current stimulation. *Clin. Neurophysiol.* **117,** 1623–1629 (2006).

239. Moberget, T. *et al.* Cerebellar volume and cerebellocerebral structural covariance in schizophrenia: A multisite mega-analysis of 983 patients and 1349 healthy controls. *Mol. Psychiatry* **23,** 1512–1520 (2018).

240. Moeller, S. *et al.* Multiband multislice GE-EPI at 7 tesla, with 16-fold acceleration using partial parallel imaging with application to high spatial and temporal whole-brain FMRI. *Magn. Reson. Med.* **63,** 1144–1153 (2010).

241. Montague, P. R., Dayan, P. & Sejnowski, T. J. A framework for mesencephalic dopamine systems based on predictive Hebbian learning. *J. Neurosci.* **16,** 1936–1947 (1996).

242. Morgan, P. T. *et al.* Cortical GABA Levels in Primary Insomnia. *Sleep* **35,** 807–814 (2012).

243. Moritz, C. H., Rogers, B. P. & Meyerand, M. E. Power spectrum ranked independent component analysis of a periodic fMRI complex motor paradigm. *Hum. Brain Mapp.* **18,** 111–122 (2003).

244. Mottolese, C. *et al.* Mapping motor representations in the human cerebellum. *Brain* **136,** 330–342 (2013).

245. Mulkey, R. M. & Malenka, R. C. Mechanisms underlying induction of homosynaptic long-term depression in area CA1 of the hippocampus. *Neuron* **9,** 967–975 (1992).

246. Murayama, Y. *et al.* Relationship between neural and hemodynamic signals during spontaneous activity studied with temporal kernel CCA. *Magn. Reson. Imaging* **28,** 1095–1103 (2010).

247. Murphy, K., Birn, R. M. & Bandettini, P. A. Resting-state fMRI confounds and cleanup. *Neuroimage* **80,** 349–359 (2013).

248. Mutha, P. K., Sainburg, R. L. & Haaland, K. Y. Left parietal regions are critical for adaptive visuomotor control. *J. Neurosci.* **31,** 6972–6981 (2011).

249. Myers, L. & Sirois, M. J. Spearman Correlation Coefficients, Differences between. *Wiley StatsRef Stat. Ref. Online,* 1–2 (2014).

250. Near, J. in *Magn. Reson. Spectrosc. Tools Neurosci. Res. Emerg. Clin. Appl.* 49–67 (Elsevier Inc., 2013).

251. Near, J., Ho, Y. C. L., Sandberg, K., Kumaragamage, C. & Blicher, J. U. Long-term reproducibility of GABA magnetic resonance spectroscopy. *Neuroimage* **99,** 191–196 (2014).

252. Near, J., Simpson, R., Cowen, P. & Jezzard, P. Efficient γ-aminobutyric acid editing at 3T without macromolecule contamination: MEGA-SPECIAL. *NMR Biomed.* **24,** 1277–1285 (2011).

253. Near, J. *et al.* in *NMR Biomed.* 11, 1353–1362 (2013).

254. Nitsche, M. A. *et al.* Pharmacological modulation of cortical excitability shifts induced by transcranial direct current stimulation in humans. *J. Physiol.* **553,** 293–301 (2003).

255. Nitsche, M. A. *et al. Chapter 27 Modulation of cortical excitability by weak direct current stimulation - technical, safety and functional aspects* **C,** 255–276 (Elsevier B.V., 2003).

256. O'Reilly, J. X., Beckmann, C. F., Tomassini, V., Ramnani, N. & Johansen-Berg, H. Distinct and overlapping functional zones in the cerebellum defined by resting state functional connectivity. *Cereb. Cortex* **20,** 953–965 (2010).

257. O'Shea, J. *et al.* Induced sensorimotor cortex plasticity remediates chronic treatment-resistant visual neglect. *Elife* **6** (2017).

258. O'Shea, J. *et al.* Predicting behavioural response to TDCS in chronic motor stroke. *Neuroimage* **85,** 924–933 (2014).

259. Ogawa, S., Lee, T. M., Kay, A. R. & Tank, D. W. Brain magnetic resonance imaging with contrast dependent on blood oxygenation. *Proc. Natl. Acad. Sci. U. S. A.* **87,** 9868–9872 (1990).

260. Ojakangas, C. L. & Ebner, T. J. Purkinje cell complex spike activity during voluntary motor learning: Relationship to kinematics. *J. Neurophysiol.* **72,** 2617–2630 (1994).

261. Oldfield, R. C. The assessment and analysis of handedness: The Edinburgh inventory. *Neuropsychologia* **9,** 97–113 (1971).

262. Oldrati, V. & Schutter, D. J. Targeting the Human Cerebellum with Transcranial Direct Current Stimulation to Modulate Behavior: a Meta-Analysis. *Cerebellum* **17,** 228–236 (2018).

263. Omrani, M., Kaufman, M. T., Hatsopoulos, N. G. & Cheney, P. D. Perspectives on classical controversies about the motor cortex. *J. Neurophysiol.* **118,** 1828–1848 (2017).

264. Öngür, D., Prescot, A. P., Jensen, J. E., Cohen, B. M. & Renshaw, P. F. Creatine abnormalities in schizophrenia and bipolar disorder. *Psychiatry Res. - Neuroimaging* **172,** 44–48 (2009).

265. Opitz, A., Paulus, W., Will, S., Antunes, A. & Thielscher, A. Determinants of the electric field during transcranial direct current stimulation. *Neuroimage* **109,** 140–150 (2015).

266. Opitz, A. *et al.* Spatiotemporal structure of intracranial electric fields induced by transcranial electric stimulation in humans and nonhuman primates. *Sci. Rep.* **6,** 1–11 (2016).

267. Orban De Xivry, J. J. & Lefèvre, P. Formation of model-free motor memories during motor adaptation depends on perturbation schedule. *J. Neurophysiol.* **113,** 2733–2741 (2015).

268. Orts-Del'Immagine, A. & Pugh, J. R. Activity-dependent plasticity of presynaptic GABAB receptors at parallel fiber synapses. *Synapse* **72,** 1–12 (2018).

269. Oscarsson, O., Courville, J., de Montigney, C. & Lamarre, Y. in (Raven Press, New York, 1980).

270. Öz, G. *et al.* Proton MRS of the unilateral substantia nigra in the human brain at 4 tesla: Detection of high GABA concentrations. *Magn. Reson. Med.* **55,** 296–301 (2006).

271. Padoa-Schioppa, C., Li, C. S. R. & Bizzi, E. Neuronal Activity in the Supplementary Motor Area of Monkeys Adapting to A New Dynamic Environment. *J. Neurophysiol.* **91,** 449–473 (2004).

272. Palesi, F. *et al.* Contralateral cortico-ponto-cerebellar pathways reconstruction in humans in vivo: Implications for reciprocal cerebro-cerebellar structural connectivity in motor and non-motor areas. *Sci. Rep.* **7,** 1–13 (2017).

273. Panouillères, M. T., Joundi, R. A., Brittain, J. S. & Jenkinson, N. Reversing motor adaptation deficits in the ageing brain using non-invasive stimulation. *J. Physiol.* **593,** 3645–3655 (2015).

274. Panouillères, M. T., Miall, R. C. & Jenkinson, N. The role of the posterior cerebellum in saccadic adaptation: A transcranial direct current stimulation study. *J. Neurosci.* **35,** 5471–5479 (2015).

275. Panouillères, M. T. *et al.* Sensorimotor adaptation as a behavioural biomarker of early spinocerebellar ataxia type. *Sci. Rep.* **7,** 2366 (2017).

276. Parazzini, M. *et al.* Modelling the electric field and the current density generated by cerebellar transcranial DC stimulation in humans. *Clin. Neurophysiol.* **125,** 577–584 (2014).

277. Paz, R., Boraud, T., Natan, C., Bergman, H. & Vaadia, E. Preparatory activity in motor cortex reflects learning of local visuomotor skills. *Nat. Neurosci.* **6,** 882–890 (2003).

278. Paz, R., Natan, C., Boraud, T., Bergman, H. & Vaadia, E. Emerging patterns of neuronal responses in supplementary and primary motor areas during sensorimotor adaptation. *J. Neurosci.* **25,** 10941–10951 (2005).

279. Penfield, W. & Boldrey, E. Somatic motor and sensory representation in the cerebral cortex of man as studied by electrical stimulation. *Brain* **60,** 389–443 (1937).

280. Perich, M. G., Gallego, J. A. & Miller, L. E. A Neural Population Mechanism for Rapid Learning. *Neuron* **100,** 964–976.e7 (2018).

281. Petitet, P., O'Reilly, J. X. & O'Shea, J. Towards a neuro-computational account of prism adaptation. *Neuropsychologia* **115,** 188–203 (2018).

282. Pijnappel, W. W., van den Boogaart, A., de Beer, R. & van Ormondt, D. SVD-based quantification of magnetic resonance signals. *J. Magn. Reson.* **97,** 122–134 (1992).

283. Provencher, S. W. Automatic quantitation of localized in vivo 1H spectra with LCModel. *NMR Biomed.* **14,** 260–264 (2001).

284. Provencher, S. W. Estimation of metabolite concentrations from localized in vivo proton NMR spectra. *Magn. Reson. Med.* **30,** 672–679 (Dec. 1993).

285. Purpura, D. P. & McMurtry, J. G. Intracellular Activities and Evoked Potential Changes During Polarization of Motor Cortex. *J. Neurophysiol.* **28,** 166–185 (1965).

286. Purves, D. *et al. Neuroscience. 2nd edition: Autonomic Regulation of Cardiovascular Function* 109–12 (2001).

287. R Development Core Team 3.0.1. *A Language and Environment for Statistical Computing* R Foundation for Statistical Computing (Vienna, Austria, 2013), https://www.R–project.org.

288. Rabe, K. *et al.* Adaptation to visuomotor rotation and force field perturbation is correlated to different brain areas in patients with cerebellar degeneration. *J. Neurophysiol.* **101,** 1961–1971 (2009).

289. Rampersad, S. M. *et al.* Simulating transcranial direct current stimulation with a detailed anisotropic human head model. *IEEE Trans. Neural Syst. Rehabil. Eng.* **22,** 441–452 (2014).

290. Rangaprakash, D., Wu, G. R., Marinazzo, D., Hu, X. & Deshpande, G. Hemodynamic response function (HRF) variability confounds resting-state fMRI functional connectivity. *Magn. Reson. Med.* **80,** 1697–1713 (2018).

291. Rathelot, J. A. & Strick, P. L. Muscle representation in the macaque motor cortex: An anatomical perspective. *Proc. Natl. Acad. Sci. U. S. A.* **103,** 8257–8262 (2006).

292. Rathelot, J. A. & Strick, P. L. Subdivisions of primary motor cortex based on cortico-motoneuronal cells. *Proc. Natl. Acad. Sci. U. S. A.* **106,** 918–923 (2009).

293. Redding, G. M. & Wallace, B. Adaptive coordination and alignment of eye and hand. *J. Mot. Behav.* **25,** 75–88 (1993).

294. Redding, G. M. & Wallace, B. Prism adaptation and unilateral neglect: Review and analysis. *Neuropsychologia* **44,** 1–20 (2006).

295. Richardson, A. G. *et al.* Disruption of primary motor cortex before learning impairs memory of movement dynamics. *J. Neurosci.* **26,** 12466–12470 (2006).

296. Rioult-Pedotti, M. S., Friedman, D., Hess, G. & Donoghue, J. P. Strengthening of horizontal cortical connections following skill learning. *Nat. Neurosci.* **1,** 230–234 (1998).

297. Romo, R. & Schultz, W. Dopamine neurons of the monkey midbrain: Contingencies of responses to active touch during self-initiated arm movements. *J. Neurophysiol.* **63,** 592–606 (1990).

298. Rothman, D. L. in *NMR Physiol. Biomed.* 353–372 (1994).

299. Rothman, D. L., Petroff, O. A., Behar, K. L. & Mattson, R. H. Localized 1H NMR measurements of γ-aminobutyric acid in human brain in vivo. *Proc. Natl. Acad. Sci. U. S. A.* **90,** 5662–5666 (1993).

300. Rubia, K. Cognitive neuroscience of attention deficit hyperactivity disorder (ADHD) and its clinical translation. *Front. Hum. Neurosci.* **12,** 1–23 (2018).

301. Salimi-Khorshidi, G. *et al.* Automatic denoising of functional MRI data: Combining independent component analysis and hierarchical fusion of classifiers. *Neuroimage* **90,** 449–468 (2014).

302. Sami, S., Robertson, E. M. & Chris Miall, R. The time course of task-specific memory consolidation effects in resting state networks. *J. Neurosci.* **34,** 3982–3992 (2014).

303. Sanes, J. N. & Donoghue, J. P. Plasticity and Primary Motor Cortex. *Annu. Rev. Neurosci.* **23,** 393–415 (2000).

304. Sarmiento, C. I., San-Juan, D. & Prasath, V. B. Letter to the Editor: Brief history of transcranial direct current stimulation (tDCS): From electric fishes to microcontrollers. *Psychol. Med.* **46,** 3259–3261 (2016).

305. Scheenen, T. W., Klomp, D. W., Wijnen, J. P. & Heerschap, A. Short echo time 1H-MRSI of the human brain at 3T with minimal chemical shift displacement errors using adiabatic refocusing pulses. *Magn. Reson. Med.* **59,** 1–6 (2008).

306. Schlerf, J. E., Galea, J. M., Bastian, A. J. & Celnik, P. A. Dynamic modulation of cerebellar excitability for abrupt, but not gradual, visuomotor adaptation. *J. Neurosci.* **32,** 11610–11617 (2012).

307. Schlerf, J. E., Xu, J., Klemfuss, N. M., Griffiths, T. L. & Ivry, R. B. Individuals with cerebellar degeneration show similar adaptation deficits with large and small visuomotor errors. *J. Neurophysiol.* **109,** 1164–1173 (2013).

308. Schlerf, J., Ivry, R. B. & Diedrichsen, J. Encoding of sensory prediction errors in the human cerebellum. *J. Neurosci.* **32,** 4913–4922 (2012).

309. Schmahmann, J. D. Disorders of the Cerebellum: Ataxia, Dysmetria of Thought, and the Cerebellar Cognitive Affective Syndrome. *J. Neuropsychiatr.* **16,** 367–378 (2004).

310. Schmahmann, J. D. From movement to thought: Anatomic substrates of the cerebellar contribution to cognitive processing. *Hum. Brain Mapp.* **4,** 174–198 (1996).

311. Schmahmann, J. D. & Sherman, J. C. The cerebellar cognitive affective syndrome. *Brain* **121,** 561–579 (1998).

312. Schultz, W., Dayan, P. & Montague, P. R. *A neural substrate of prediction and reward* 1997.

313. Schweighofer, N., Arbib, M. A. & Dominey, P. F. A model of the cerebellum in adaptive control of saccadic gain. *Biol. Cybern.* (1996).

314. Sebastian, R. *et al.* Cerebellar tDCS: A novel approach to augment language treatment post-stroke. *Front. Hum. Neurosci.* **10,** 1–8 (2017).

315. Seidler, R. D., Noll, D. C. & Chintalapati, P. Bilateral basal ganglia activation associated with sensorimotor adaptation. *Exp. Brain Res.* **175,** 544–555 (2006).

316. Shadmehr, R. & Moussavi, Z. M. Spatial generalization from learning dynamics of reaching movements. *J. Neurosci.* **20,** 7807–7815 (2000).

317. Shadmehr, R. & Holcomb, H. H. Neural correlates of motor memory consolidation. *Sciences (New. York).* **277,** 821–825 (Aug. 1997).

318. Shadmehr, R. & Mussa-Ivaldi, F. A. Adaptive Task of Dynamics during Learning of a Motor. *J. Neurosci.* **14,** 3208–3224 (1994).

319. Shadmehr, R., Smith, M. A. & Krakauer, J. W. Error Correction, Sensory Prediction, and Adaptation in Motor Control. *Annu. Rev. Neurosci.* **33,** 89–108 (2010).

320. Shibata, K. *et al.* Overlearning hyperstabilizes a skill by rapidly making neurochemical processing inhibitory-dominant. *Nat. Neurosci.* **20,** 470–475 (2017).

321. Simpson, R., Devenyi, G. A., Jezzard, P., Hennessy, T. J. & Near, J. Advanced processing and simulation of MRS data using the FID appliance (FID-A)—An open source, MATLAB-based toolkit. *Magn. Reson. Med.* **77,** 23–33 (2017).

322. Sing, G. C. & Smith, M. A. Reduction in learning rates associated with anterograde interference results from interactions between different timescales in motor adaptation. *PLoS Comput. Biol.* **6** (2010).

323. Smith, A. M., Hepp-Reymond, M. C. & Wyss, U. R. Relation of activity in precentral cortical neurons to force and rate of force change during isometric contractions of finger muscles. *Exp. Brain Res.* **23,** 315–332 (1975).

324. Smith, J. K., Londono, A., Castillo, M. & Kwock, L. Proton magnetic resonance spectroscopy of brain-stem lesions. *Neuroradiology* **44,** 825–829 (2002).

325. Smith, M. A., Ghazizadeh, A. & Shadmehr, R. Interacting adaptive processes with different timescales underlie short-term motor learning. *PLoS Biol.* **4,** 1035–1043 (2006).

326. Smith, S. M. *et al.* Advances in functional and structural MR image analysis and implementation as FSL. *Neuroimage* **23,** S208–S219 (2004).

327. Smith, S. M. *et al.* Correspondence of the brain's functional architecture during activation and rest. *Proc. Natl. Acad. Sci. U. S. A.* **106,** 13040–13045 (2009).

328. Smith, S. M. *et al.* Network modelling methods for FMRI. *Neuroimage* **54,** 875–891 (2011).

329. Soetedjo, R., Kojima, Y. & Fuchs, A. F. Complex spike activity in the oculomotor vermis of the cerebellum: A vectorial error signal for saccade motor learning? *J. Neurophysiol.* **100,** 1949–1966 (Oct. 2008).

330. Stagg, C. J. *et al.* Relationship between physiological measures of excitability and levels of glutamate and GABA in the human motor cortex. *J. Physiol.* **589,** 5845–5855 (2011).

331. Stagg, C. J., Antal, A. & Nitsche, M. A. Physiology of Transcranial Direct Current Stimulation. *J. ECT* **34,** 144–152 (2018).

332. Stagg, C. J., Bachtiar, V. & Johansen-Berg, H. The role of GABA in human motor learning. *Curr. Biol.* **21,** 480–484 (2011).

333. Stagg, C. J., Bachtiar, V. & Johansen-Berg, H. What are we measuring with GABA Magnetic Resonance Spectroscopy? *Commun. Integr. Biol.* **4,** 573–575 (2011).

334. Stagg, C. J. & Nitsche, M. A. Physiological basis of transcranial direct current stimulation. *Neuroscientist* **17,** 37–53 (2011).

335. Stagg, C. J. *et al.* Local GABA concentration is related to network-level resting functional connectivity. *Elife* **2014,** 1–9 (2014).

336. Stagg, C. J. *et al.* Polarity-sensitive modulation of cortical neurotransmitters by transcranial stimulation. *J. Neurosci.* **29,** 5202–5206 (2009).

337. Stagg, C. J. *et al.* Cortical activation changes underlying stimulation-induced behavioural gains in chronic stroke. *Brain* **135,** 276–284 (2012).

338. Steel, A. *et al.* Metabolite-cycled density-weighted concentric rings k-space trajectory (DW-CRT) enables high-resolution 1 H magnetic resonance spectroscopic imaging at 3-Tesla. *Sci. Rep.* **8,** 1–10 (2018).

339. Stehling, M. K., Ordidge, R. J., Coxon, R. & Mansfield, P. Inversion-recovery echo-planar imaging (IR-EPI) at 0.5 T. *Magn. Reson. Med.* **13,** 514 (1990).

340. Stephenson, M. C. Applications of multi-nuclear magnetic resonance spectroscopy at 7T. *World J. Radiol.* **3,** 105 (2011).

341. Stoodley, C. J. *et al.* Author Correction: Altered cerebellar connectivity in autism and cerebellar-mediated rescue of autism-related behaviors in mice. *Nat. Neurosci.* **21,** 1016 (2018).

342. Sutton, R. S. & Barto, A. G. Reinforcement Learning: An Introduction at http://incompleteideas.net (2015).

343. Tanaka, H., Krakauer, J. W. & Sejnowski, T. J. Generalization and multirate models of motor adaptation. *Neural Comput.* **24,** 939–966 (2012).

344. Tanaka, H., Sejnowski, T. J. & Krakauer, J. W. Adaptation to visuomotor rotation through interaction between posterior parietal and motor cortical areas. *J. Neurophysiol.* **102,** 2921–2932 (2009).

345. Taylor, J. A. & Ivry, R. B. Flexible cognitive strategies during motor learning. *PLoS Comput. Biol.* **7** (2011).

346. Taylor, J. A. & Ivry, R. B. The role of strategies in motor learning. *Ann. N. Y. Acad. Sci.* **1251,** 1–12 (2012).

347. Taylor, J. A., Klemfuss, N. M. & Ivry, R. B. An explicit strategy prevails when the cerebellum fails to compute movement errors. *Cerebellum* **9,** 580–586 (2010).

348. Taylor, J. A., Krakauer, J. W. & Ivry, R. B. Explicit and implicit contributions to learning in a sensorimotor adaptation task. *J. Neurosci.* **34,** 3023–3032 (2014).

349. Telgen, S., Parvin, D. & Diedrichsen, J. Mirror reversal and visual rotation are learned and consolidated via separate mechanisms: Recalibrating or learning de novo? *J. Neurosci.* **34,** 13768–13779 (2014).

350. Thickbroom, G. W., Byrnes, M. L. & Mastaglia, F. L. Dual representation of the hand in the cerebellum: Activation with voluntary and passive finger movement. *Neuroimage* **18,** 670–674 (2003).

351. Thomsen, K., Offenhauser, N. & Lauritzen, M. Principal neuron spiking: Neither necessary nor sufficient for cerebral blood flow in rat cerebellum. *J. Physiol.* **560,** 181–189 (2004).

352. Thomsen, K., Piilgaard, H., Gjedde, A., Bonvento, G. & Lauritzen, M. Principal cell spiking, postsynaptic excitation, and oxygen consumption in the rat cerebellar cortex. *J. Neurophysiol.* **102,** 1503–1512 (2009).

353. Timmann, D. *et al.* The human cerebellum contributes to motor, emotional and cognitive associative learning. A review. *Cortex* **46,** 845–857 (2010).

354. Tkáč, I., Starčuk, Z., Choi, I. Y. & Gruetter, R. In vivo 1H NMR spectroscopy of rat brain at 1 ms echo time. *Magn. Reson. Med.* **41,** 649–656 (1999).

355. Tkach, D., Reimer, J. & Hatsopoulos, N. G. Congruent activity during action and action observation in motor cortex. *J. Neurosci.* **27,** 13241–13250 (2007).

356. Tomasch, J. The numerical capacity of the human cortico-pontocerebellar system. *Brain Res.* **13,** 476–484 (1969).

357. Trepel, C. & Racine, R. J. GABAergic modulation of neocortical long-term potentiation in the freely moving rat. *Synapse* **35,** 120–128 (2000).

358. Tseng, Y. W., Diedrichsen, J., Krakauer, J. W., Shadmehr, R. & Bastian, A. J. Sensory prediction errors drive cerebellum-dependent adaptation of reaching. *J. Neurophysiol.* **98,** 54–62 (2007).

359. Turnham, E. J., Braun, D. A. & Wolpert, D. M. Facilitation of learning induced by both random and gradual visuomotor task variation. *J. Neurophysiol.* **107,** 1111–1122 (2012).

360. Ugawa, Y., Uesaka, Y., Terao, Y., Hanajima, R. & Kanazawa, I. Magnetic stimulation over the cerebellum in humans. *Ann. Neurol.* **37,** 703–713 (1995).

361. Vaishnavi, S. N. *et al.* Regional aerobic glycolysis in the human brain. *Proc. Natl. Acad. Sci. U. S. A.* **107,** 17757–17762 (2010).

362. Van Der Kooij, K., Brenner, E., Van Beers, R. J. & Smeets, J. B. Visuomotor adaptation: How forgetting keeps us conservative. *PLoS One* **10,** 1–13 (2015).

363. Van Dijk, K. R. *et al.* Intrinsic functional connectivity as a tool for human connectomics: Theory, properties, and optimization. *J. Neurophysiol.* **103,** 297–321 (2010).

364. Van Baarsen, K. M. *et al.* A probabilistic atlas of the cerebellar white matter. *Neuroimage* **124,** 724–732 (2016).

365. Van Dun, K., Bodranghien, F. C., Mariën, P. & Manto, M. U. TDCS of the cerebellum: Where do we stand in 2016? Technical issues and critical review of the literature. *Front. Hum. Neurosci.* **10,** 199 (2016).

366. Vaswani, P. A. & Shadmehr, R. Decay of motor memories in the absence of error. *J. Neurosci.* **33,** 7700–7709 (2013).

367. Vinet, L. & Zhedanov, A. A 'missing' family of classical orthogonal polynomials. *J. Phys. A Math. Theor.* **44,** 633–9 (2011).

368. Von Helmholtz, H. *Handbuch der physiologischen Optik.* **4,** 416–420 (Voss, 1898).

369. Waddell, K. W. *et al.* Anterior cingulate and cerebellar GABA and Glu correlations measured by 1H J-difference spectroscopy. *Magn. Reson. Imaging* **29,** 19–24 (2011).

370. Wagner, T., Valero-Cabre, A. & Pascual-Leone, A. Noninvasive Human Brain Stimulation. *Annu. Rev. Biomed. Eng.* **9,** 527–565 (2007).

371. Wang, J. & Sainburg, R. L. Limitations in interlimb transfer of visuomotor rotations. *Exp. Brain Res.* **155,** 1–8 (2004).

372. Wang, S. S., Kloth, A. D. & Badura, A. The Cerebellum, Sensitive Periods, and Autism. *Neuron* **83,** 518–532 (2014).

373. Weightman, M., Brittain, J. S., Punt, D., Miall, R. C. & Jenkinson, N. Targeted tDCS selectively improves motor adaptation with the proximal and distal upper limb. *Brain Stimul.* **13,** 707–716 (2020).

374. Weinrich, M. & Wise, S. P. The premotor cortex of the monkey. *J. Neurosci.* **2,** 1329–1345 (1982).

375. Werner, S., Bock, O., Gizewski, E. R., Schoch, B. & Timmann, D. Visuomotor adaptive improvement and aftereffects are impaired differentially following cerebellar lesions in SCA and PICA territory. *Exp. Brain Res.* **201,** 429–439 (2010).

376. Werner, S., Schorn, C. F., Bock, O., Theysohn, N. & Timmann, D. Neural correlates of adaptation to gradual and to sudden visuomotor distortions in humans. *Exp. Brain Res.* **232,** 1145–1156 (2014).

377. Wessel, M. J. & Hummel, F. C. Non-invasive Cerebellar Stimulation: a Promising Approach for Stroke Recovery? *Cerebellum* **17,** 359–371 (2018).

378. Widrow, B., Griffiths, L. J., Mantey, P. E. & Goode, B. B. Adaptive Antenna Systems. *Proc. IEEE* (1967).

379. Wiethoff, S., Hamada, M. & Rothwell, J. C. Variability in response to transcranial direct current stimulation of the motor cortex. *Brain Stimul.* **7,** 468–475 (2014).

380. Wigmore, V., Tong, C. & Flanagan, J. R. Visuomotor rotations of varying size and direction compete for a single internal model in motor working memory. *J. Exp. Psychol. Hum. Percept. Perform.* **28,** 447–457 (2002).

381. Wijtenburg, S. A., Rowland, L. M., Edden, R. A. & Barker, P. B. Reproducibility of brain spectroscopy at 7T using conventional localization and spectral editing techniques. *J. Magn. Reson. Imaging* **38,** 460–467 (2013).

382. Winkler, A. M., Ridgway, G. R., Webster, M. A., Smith, S. M. & Nichols, T. E. Permutation inference for the general linear model. *Neuroimage* **92,** 381–397 (2014).

383. Wolpert, D. M., Diedrichsen, J. & Flanagan, J. R. Principles of sensorimotor learning. *Nat. Rev. Neurosci.* **12,** 739–751 (2011).

384. Wolpert, D. M. & Ghahramani, Z. Computational principles of movement neuroscience. *Nat. Neurosci.* **3,** 1212–1217 (2000).

385. Wolpert, D. M., Miall, R. C. & Kawato, M. Internal models in the cerebellum. *Trends Cogn. Sci.* **2,** 338–347 (1998).

386. Wolpert, D. M., Ghahramani, Z., Jordan, M. I., Series, N. & Sep, N. An Internal Model for Sensorimotor Integration An Internal Model for Sensorimotor Integration. *Science (80-.).* (2007).

387. Woo, Krishan & Wager. Cluster-extent based thresholding in fMRI analyses. *Neuroimage* **100,** 130–134 (2012).

388. Woods, A. J. *et al. A technical guide to tDCS, and related non-invasive brain stimulation tools* 2016.

389. Wu, G. R., Deshpande, G., Laureys, S. & Marinazzo, D. Retrieving the Hemodynamic Response Function in resting state fMRI: Methodology and application. *Proc. Annu. Int. Conf. IEEE Eng. Med. Biol. Soc. EMBS* **15,** 6050–6053 (2015).

390. Wu, G. R. & Marinazzo, D. Sensitivity of the resting-state haemodynamic response function estimation to autonomic nervous system fluctuations. *Philos. Trans. R. Soc. A Math. Phys. Eng. Sci.* **374** (2016).

391. Yamada, C., Itaguchi, Y. & Fukuzawa, K. Effects of the amount of practice and time interval between practice sessions on the retention of internal models. *PLoS One* **14,** 1–17 (2019).

392. Yamazakia, T., Nagao, S., Lennon, W. & Tanaka, S. Modeling memory consolidation during posttraining periods in cerebellovestibular learning. *Proc. Natl. Acad. Sci. U. S. A.* **112,** 3541–3546 (2015).

393. Yang, Y. & Lisberger, S. G. Role of plasticity at different sites across the time course of cerebellar motor learning. *J. Neurosci.* **34,** 7077–7090 (2014).

394. Yavari, F., Towhidkhah, F. & Ahmadi-Pajouh, M. A. Are fast/slow process in motor adaptation and forward/inverse internal model two sides of the same coin? *Med. Hypotheses* **81,** 592–600 (2013).

395. Yavari, F. *et al.* Cerebellum as a forward but not inverse model in visuomotor adaptation task: a tDCS-based and modeling study. *Exp. Brain Res.* **234,** 997–1012 (2016).

396. Yousry, T. A. *et al.* Localization of the motor hand area to a knob on the precentral gyrus. A new landmark. *Brain* **120,** 141–157 (1997).

397. Yuzaki, M. Cerebellar LTD vs. motor learning-Lessons learned from studying GluD2. *Neural Networks* **47,** 36–41 (2013).

398. Zarahn, E., Weston, G. D., Liang, J., Mazzoni, P. & Krakauer, J. W. Explaining savings for visuomotor adaptation: Linear time-invariant state-space models are not sufficient. *J. Neurophysiol.* **100,** 2537–2548 (2008).

399. Zhang, Y., Brady, M. & Smith, S. Segmentation of brain MR images through a hidden Markov random field model and the expectation-maximization algorithm. *IEEE Trans. Med. Imaging* **20,** 45–57 (2001).

400. Zhu, H. & Barker, P. B. in *Methods Mol. Biol.* 711, 203–226 (2011).

401. Zhu, L., Scelfo, B., Tempia, F., Sacchetti, B. & Strata, P. Membrane excitability and fear conditioning in cerebellar Purkinje cell. *Neuroscience* **140,** 801–810 (2006).

402. Ziemann, U. Modulation of practice-dependent plasticity in human motor cortex. *Brain* **124,** 1171–1181 (2001).